



National Library
of Canada

Acquisitions and
Bibliographic Services Branch

395 Wellington Street
Ottawa, Ontario
K1A 0N4

Bibliothèque nationale
du Canada

Direction des acquisitions et
des services bibliographiques

395, rue Wellington
Ottawa (Ontario)
K1A 0N4

Veuillez noter - *Your reference*

Outlets - *Note reference*

NOTICE

The quality of this microform is heavily dependent upon the quality of the original thesis submitted for microfilming. Every effort has been made to ensure the highest quality of reproduction possible.

If pages are missing, contact the university which granted the degree.

Some pages may have indistinct print especially if the original pages were typed with a poor typewriter ribbon or if the university sent us an inferior photocopy.

Reproduction in full or in part of this microform is governed by the Canadian Copyright Act, R.S.C. 1970, c. C-30, and subsequent amendments.

AVIS

La qualité de cette microforme dépend grandement de la qualité de la thèse soumise au microfilmage. Nous avons tout fait pour assurer une qualité supérieure de reproduction.

S'il manque des pages, veuillez communiquer avec l'université qui a conféré le grade.

La qualité d'impression de certaines pages peut laisser à désirer, surtout si les pages originales ont été dactylographiées à l'aide d'un ruban usé ou si l'université nous a fait parvenir une photocopie de qualité inférieure.

La reproduction, même partielle, de cette microforme est soumise à la Loi canadienne sur le droit d'auteur, SRC 1970, c. C-30, et ses amendements subséquents.

SEISMIC DESIGN AND RETROFIT OF COUPLED WALLS USING STRUCTURAL STEEL

by

Kent A. Harries

May 1995



Department of Civil Engineering and Applied Mechanics
McGill University
Montréal, Canada

a thesis submitted to the Faculty of Graduate Studies and Research in partial fulfilment of
the requirements for the degree of Doctor of Philosophy

© Kent A. Harries, 1995



National Library
of Canada

Acquisitions and
Bibliographic Services Branch

395 Wellington Street
Ottawa, Ontario
K1A 0N4

Bibliothèque nationale
du Canada

Direction des acquisitions et
des services bibliographiques

395, rue Wellington
Ottawa (Ontario)
K1A 0N4

Your file - Votre référence

Our file - Notre référence

The author has granted an irrevocable non-exclusive licence allowing the National Library of Canada to reproduce, loan, distribute or sell copies of his/her thesis by any means and in any form or format, making this thesis available to interested persons.

L'auteur a accordé une licence irrévocable et non exclusive permettant à la Bibliothèque nationale du Canada de reproduire, prêter, distribuer ou vendre des copies de sa thèse de quelque manière et sous quelque forme que ce soit pour mettre des exemplaires de cette thèse à la disposition des personnes intéressées.

The author retains ownership of the copyright in his/her thesis. Neither the thesis nor substantial extracts from it may be printed or otherwise reproduced without his/her permission.

L'auteur conserve la propriété du droit d'auteur qui protège sa thèse. Ni la thèse ni des extraits substantiels de celle-ci ne doivent être imprimés ou autrement reproduits sans son autorisation.

ISBN 0-612-08109-5

Canada

Abstract

The reversed cyclic loading responses of reinforced concrete walls coupled with steel beams are investigated. Four full-scale segments of coupled walls having both "shear critical" and "flexure critical" steel coupling beams with their ends embedded in the walls were tested. The reversed cyclic loading responses of these specimens are compared with those of conventionally reinforced and diagonally reinforced concrete coupling beams. Design and detailing guidelines are proposed for both the steel coupling beams and the reinforced concrete embedment regions. Non-linear dynamic analyses of prototype coupled wall structures, comparing conventional and diagonal reinforcement details with the proposed flexure and shear critical steel coupling beams are presented.

Four full-scale reversed cyclic loading tests of shear deficient reinforced concrete coupling beams were conducted to study efficient ways of retrofitting these beams. An unretrofitted control specimen and three specimens with different retrofit details were tested. The retrofit procedure investigated involved applying steel plates to one side of the coupling beams to determine ways of increasing the shear strength of the beams such that the nominal flexural capacity may be attained. Different methods of attaching the retrofit plates using structural epoxy and mechanical anchor bolts are investigated. A method for determining the influence of the steel plate retrofit on the shear capacity of the beam is developed. Non-linear dynamic analyses comparing the structural responses of unretrofitted and retrofitted prototype structures are also presented.

Résumé

L'auteur présente d'abord une étude du comportement sous charges cycliques inversées de murs en béton armé couplés, connectés de façon non conventionnelle à l'aide de linteaux en acier. Des essais ont été effectués sur quatre segments grandeur nature de murs connectés avec linteaux critiques en cisaillement et linteaux critiques en flexion, dont les extrémités sont encastrées dans les segments de murs. Des analyses dynamiques non linéaires ont permis de comparer le comportement des spécimens testés à celui de murs connectés à l'aide de linteaux en béton armé avec armature de flexion conventionnelle et avec armature diagonale. En conclusion de cette étude, l'auteur suggère des directives pour le dimensionnement et la conception détaillée des linteaux en acier ainsi que des zones d'encastrement dans les murs connectés.

Le renfort de linteaux en béton armé conventionnels, critiques en cisaillement, a également fait l'objet d'une étude expérimentale où quatre autres prototypes grandeur nature ont été soumis à des charges cycliques inversées. Un spécimen de contrôle, non renforcé, et trois spécimens avec différents types de renforts ont été testés. La procédure de renfort étudiée consiste à connecter des plaques en acier à la face extrême des linteaux afin d'augmenter la résistance en cisaillement des poutres tout en permettant d'atteindre leur résistance nominale en flexion. Deux types de connexions ont été considérées pour l'attache des plaques en acier aux poutres en béton armé, soit l'utilisation d'époxyde structurale et les boulons d'ancrage. Des analyses dynamiques non linéaires ont également été utilisées pour comparer le comportement des linteaux non renforcés avec les spécimens renforcés avec plaques en acier. En conclusion, l'auteur propose une méthode pour évaluer l'influence des renforts en acier sur la résistance en cisaillement des linteaux.



Acknowledgements

The author gratefully acknowledges Professors D. Mitchell and R.G Redwood for their guidance and encouragement with this research programme. Furthermore, the author would like to thank Dr. W.D. Cook for his particular brand of support and encouragement.

Thanks are extended to the staff and "lab-slaves" of the Jamieson Structures Laboratory at McGill University: Ron Sheppard, John Bartczak, Marek Przykorski, Damon Kiperchuk, Jamie Mitchell, Nick Vannelli, Glenn Marquis, Jay McHarg, Isabelle Villemure, Stuart Bristowe and Albert Wallrap as well as all the staff of the Mechanical Engineering shops.

Thanks are also extended to the following individuals who have helped this work along in some way: Professors B. Stafford-Smith and G. McClure at McGill, Professor P. Leger at Ecole Polytechnique, Andrew Greizic and Sanda Koboevic.

The financial support of the Natural Sciences and Engineering Research Council of Canada is gratefully acknowledged.

Finally, special thanks are extended to all those whose patience I surely tried over the years.

Kent A. Harries
May, 1995

Table of Contents

Abstract	i
Resumé	ii
Acknowledgements	iii
Table of Contents	iv
List of Figures	viii
List of Tables	x
List of Symbols	xi
Introduction and Literature Review	1
1.1 Coupled Wall Structures	1
1.1.1 Behaviour of Coupled Wall Structures	2
1.1.2 Seismic Behaviour of Coupling Beams	2
1.1.3 Ductile Behaviour of Coupled Walls	3
1.2 Analysis of Coupled Walls	4
1.2.1 Continuous Medium Method	4
1.2.2 Equivalent Frame Method	5
1.2.3 Finite Element Methods	5
1.3 Reinforced Concrete Coupled Wall Systems	5
1.3.1 Walls Coupled with Floor Slabs	7
1.4 Steel Link Beams in Eccentrically Braced Frames	7
1.5 Composite Steel and Reinforced Concrete Construction	8
1.5.1 Reinforced Concrete Coupling Beams Containing Encased Steel Members	8
1.5.2 Reinforced Concrete Wall Systems Encasing Steel Frames	9
1.5.3 Embedded Plate Connections	9
1.5.4. Embedded Connections of Structural Steel Members in Precast Concrete	10
1.5.5. Composite Frame Structures	11
1.5.6 Reinforced Concrete Wall Coupled with Embedded Steel Beams	12
1.6 Seismic Retrofit of Reinforced Concrete Coupling Beams	13
1.6.1 Bonded Steel Plate Retrofit Measures	13
1.7 Objectives of Research Programme	15
1.7.1 Steel Coupling Beams Coupling Reinforced Concrete Walls	15
1.7.2 Retrofitted Reinforced Concrete Coupling Beams	16
1.8 Overview of Research Programme	17
Steel Coupling Beam Experimental Programme	30
2.1 Design of the Steel Coupling Beams	30
2.2 Design of the Reinforced Concrete Embedment Region	32
2.3 Description of Specimens	33
2.3.1 Specimen S1	33
2.3.2 Specimen S2	34
2.3.3 Specimen S3	34
2.3.4 Specimen S4	35

2.4 Design and Detailing Wall Reinforcement	35
2.5 Material Properties	37
2.5.1 Coupling Beam Steel	37
2.5.2 Reinforcing Steel	38
2.5.3 Concrete	38
2.6 McGill University Coupled Wall Testing Apparatus	39
2.7 Instrumentation	40
2.8 Load Histories	41
Steel Coupling Beam Experimental Results	50
3.1 Specimen S1	52
3.1.1 Coupling Beam Response	53
3.1.2 Reinforced Concrete Embedment Response	54
3.1.3 Hysteretic Response	55
3.2 Specimen S2	57
3.2.1 Coupling Beam Response	58
3.2.2 Reinforced Concrete Embedment Response	59
3.2.3 Hysteretic Response	60
3.3 Specimen S3	61
3.3.1 Coupling Beam Response	62
3.3.2 Reinforced Concrete Embedment Response	63
3.3.3 Hysteretic Response	64
3.4 Specimen S4	65
3.4.1 Coupling Beam Response	66
3.4.2 Reinforced Concrete Embedment Response	67
3.4.3 Hysteretic Response	68
Response Comparisons of Steel Coupling Beam Specimens	78
4.1 Comparison of Predicted and Experimental Results	78
4.2 Hysteretic Response	80
4.3 Energy Absorption	82
4.4 Response of Coupling Beams	83
4.5 Response of Reinforced Concrete Embedment Region	84
4.6 Comparisons with Reinforced Concrete Coupling Beams	84
4.7 Comparisons with Steel Link Beams in Eccentrically Braced Frames	85
Design and Modelling of Prototype Structures	92
5.1 Design of Prototype Structures	92
5.1.1 Gravity Loading	93
5.1.2 Equivalent Lateral Base Shear	93
5.1.3 Force Modification Factor, R and the Degree of Coupling	94
5.1.4 Load Combinations for Seismic Design	95
5.1.5 NBCC Equivalent Static Elastic Analysis of Prototype Structure	95
5.2 Elastic Analysis of Prototype Structures	96
5.2.1 Criteria for the Selection of a Prototype Model	97
5.2.2 Results of Elastic Analysis of the Prototype Models	97
5.2.3 Force Reduction Coefficients	98
5.3 Design of Prototype Coupling Beams	99
5.3.1 Reinforced Concrete Coupling Beams for Partially Coupled Prototype Structure PC	99

5.3.2	Steel Coupling Beams for Partially Coupled Prototype Structure PS	100
5.3.3	Reinforced Concrete Coupling Beams for Fully Coupled Prototype Structure FC	100
5.3.4	Steel Coupling Beams for Fully Coupled Prototype Structure FS	101
5.3.5	Design of the Reinforced Concrete Walls	101
5.4	Modelling Prototype Structures for Non-linear Dynamic Analysis	103
5.4.1	Conventionally Reinforced Coupling Beams of Prototype PC	105
5.4.2	Steel Coupling Beams of Prototype PS	105
5.4.3	Diagonally Reinforced Coupling Beams of Prototype FC	105
5.4.4	Steel Coupling Beams of Prototype FS	106
5.5	Selection Criteria for Input Ground Acceleration Records	106
5.5.1	Selected Ground Acceleration Records	107
Results of Non-linear Dynamic Analyses of Prototype Structures		116
6.1	Non-linear Dynamic Response of Partially Coupled Prototypes PC and PS	116
6.1.1	Response of Partially Coupled Prototype PC	117
6.1.2	Response of Partially Coupled Prototype PS	118
6.2	Non-linear Dynamic Response of Coupled Prototypes FC and FS	119
6.2.1	Response of Fully Coupled Prototype FC	120
6.2.2	Response of Fully Coupled Prototype FS	120
6.3	Estimating Damage Levels	121
6.4	Evaluation of Prototype Behaviour	124
6.5	Behaviour of Coupled Walls Subjected to "Eastern" Ground Motions	125
6.6	Evaluation of Steel Coupling Beams	126
Experimental Programme for Retrofitting Reinforced Concrete Coupling Beams		141
7.1	Design of the Reinforced Concrete Coupling Beam and Walls	141
7.2	Design of the Steel Plate Retrofit	142
7.3	Description of Specimens	144
7.3.1	Specimen R0	144
7.3.2	Specimen R1	144
7.3.3	Specimen R2	144
7.3.4	Specimen R3	145
7.4	Material Properties	145
7.4.1	Retrofit Plate Steel	146
7.4.2	Structural Epoxy	147
7.4.3	Anchor Bolts	147
7.4.4	Reinforcing Steel	147
7.4.5	Concrete	147
7.5	Experimental Set-up	148
7.6	Instrumentation	149
7.7	Load Histories	149
Behaviour of Retrofitted Reinforced Concrete Coupling Beams		157
8.1	Specimen R0	157
8.1.1	Hysteretic Response	159
8.2	Specimen R1	159
8.2.1	Response of Retrofit Plate	161
8.2.2	Hysteretic Response	162
8.3	Specimen R2	162

8.3.1 Response of Retrofit Plate	163
8.3.2 Hysteretic Response	164
8.4 Specimen R3	164
8.4.1 Response of Retrofit Plate	166
8.4.2 Hysteretic Response	167
Response Comparisons of Retrofitted Reinforced Concrete Coupling Beams	179
9.1 Comparison of Predicted and Experimental Results	179
9.1.1 RESPONSE Model for Specimen R0	181
9.1.2 RESPONSE Model for Retrofitted Specimen R3	181
9.2 Hysteretic Responses	182
9.3 Energy Absorption	183
9.4 Response of Retrofit Plates	183
9.5 Assessment of Retrofit Performance	184
Non-Linear Dynamic Analyses of Unretrofitted and Retrofitted Prototype Structures	192
10.1 Shear Deficient Prototype Structure	192
10.2 Retrofitted Prototype Structure	194
10.3 Modelling Unretrofitted and Retrofitted Prototypes	195
10.3.1 Ground Acceleration Records	196
10.4 Non-linear Dynamic Response of Unretrofitted and Retrofitted Prototypes	196
10.5 Evaluation of Retrofit Procedure	198
Design Recommendations and Conclusions	204
11.1 Behaviour and Design of Steel Beams Coupling Reinforced Concrete Walls	204
11.2 Retrofitting Reinforced Concrete Coupling Beams with Steel Plates	206
11.3 Areas for Future Investigation	207
Statement of Originality	208
References	209
Appendix A - Design of Steel Coupling Beam Specimens	216
Appendix B - Design of Retrofitted Reinforced Concrete Coupling Beam Specimens	225

List of Figures

Figure 1.1 Stress Distribution at the base of coupled wall structures	19
Figure 1.2 Components of coupled wall behaviour	20
Figure 1.3 Diagonally reinforced concrete coupling beam	21
Figure 1.4 Conventionally and diagonally reinforced concrete beams tested by Shiu	22
Figure 1.5 Steel link beam in an eccentrically braced frame	23
Figure 1.6 Steel coupling beam and frame embedded in reinforced concrete wall	24
Figure 1.7 Embedded plate connection	25
Figure 1.8 Structural section embedded in precast concrete	26
Figure 1.9 Components of response of joints in composite frames	27
Figure 1.10 Response components of bearing resistance portion of frame joint behaviour	28
Figure 1.11 Separation of bonded steel plate and concrete	29
Figure 2.1 Parameters of embedment design	42
Figure 2.2 Coupling beam details for Specimens S1 through S4	43
Figure 2.3 Reinforced concrete wall details for Specimens S1 through S4	44
Figure 2.4 Material characteristics of steel coupling beam specimens	45
Figure 2.5 Method of simulating actual coupled wall behaviour	46
Figure 2.6 Coupled Wall Testing Apparatus with steel coupling beam specimen mounted	47
Figure 2.7 Instrumentation of Specimens S1 through S4	48
Figure 2.8 Load histories of Specimens S1 through S4	49
Figure 3.1 Hysteretic response of Specimen S1	69
Figure 3.2 Specimen S1 at the completion of testing	70
Figure 3.3 Coupling beam of Specimen S1 after removal from concrete	70
Figure 3.4 Hysteretic response of Specimen S2	71
Figure 3.5 Specimen S2 at the completion of testing	72
Figure 3.6 Coupling beam of Specimen S2 after removal from concrete	72
Figure 3.7 Hysteretic response of Specimen S3	73
Figure 3.8 Specimen S3 at the completion of testing	74
Figure 3.9 Coupling beam of Specimen S3 at the completion of testing	74
Figure 3.10 Coupling beam of Specimen S3 after removal from concrete	75
Figure 3.11 Hysteretic response of Specimen S4	76
Figure 3.12 Specimen S4 at the completion of testing	77
Figure 3.13 Extent of hinging at the ends of Specimen S4	77
Figure 4.1 Hysteretic responses of Specimens S1 through S4	86
Figure 4.2 Peak-to-peak stiffnesses of Specimens S1 through S4	87
Figure 4.3 Cumulative energy absorption of Specimens S1 through S4	88
Figure 4.4 Equivalent elastic damping coefficients of Specimens S1 through S4	89
Figure 4.5 Coupling beams of Specimens S1 and S2 after testing	89
Figure 4.6 Strains in vertical reinforcement at face of wall in Specimens S1 through S4	90
Figure 4.7 Equivalent elastic damping coefficients for reinforced concrete coupling beams	91
Figure 4.8 Equivalent elastic damping coefficients for shear link in EBF	91
Figure 5.1 Prototype structures	109
Figure 5.2 Prototype coupling beam details	110
Figure 5.3 DRAIN-2DX model of prototype structures	111
Figure 5.4 Development of "pinched" hysteretic model for concrete coupling beams	112
Figure 5.5 Verification of DRAIN-2DX element model for diagonally reinforced beams	113
Figure 5.6 Verification of DRAIN-2DX element model for shear critical steel beam	114

Figure 5.7 Accelerograms used for DRAIN-2DX analyses	115
Figure 6.1 Roof displacement-time history of prototype PC	128
Figure 6.2 Roof displacement-time history of prototype PS	129
Figure 6.3 Hysteretic behaviour of critical coupling beams of prototype PC	130
Figure 6.4 Hysteretic behaviour of critical coupling beams of prototype PS	131
Figure 6.5 Maximum inter-storey drift values for prototypes PC and PS	132
Figure 6.6 Sequence of yielding in prototype PC and PS analyses	133
Figure 6.7 Roof displacement-time history of prototype FC	134
Figure 6.8 Roof displacement-time history of prototype FS	135
Figure 6.9 Hysteretic behaviour of critical coupling beams of prototype FC	136
Figure 6.10 Hysteretic behaviour of critical coupling beams of prototype FS	137
Figure 6.11 Maximum inter-storey drift values for prototypes FC and FS	138
Figure 6.12 Sequence of yielding in prototype FC and FS analyses	139
Figure 6.13 Comparisons of roof displacement-time histories	140
Figure 7.1 Coupling beam and wall reinforcement details for Specimens R0 through R3	151
Figure 7.2 Retrofit details for Specimens R1 through R3	152
Figure 7.3 Material characteristics of retrofit coupling beam specimens	153
Figure 7.4 Coupled Wall Testing Apparatus with concrete coupling beam mounted	154
Figure 7.5 Instrumentation of Specimens R0 through R3	155
Figure 7.6 Load histories of Specimens R0 through R3	156
Figure 8.1 Hysteretic response of Specimen R0	168
Figure 8.2 Specimen R0 at ductility level of $-2.5\delta_y$	169
Figure 8.3 Specimen R0 at the completion of testing	169
Figure 8.4 Hysteretic response of Specimen R1	170
Figure 8.5 Specimen R1 at ductility level of $-2.5\delta_y$	170
Figure 8.6 Specimen R1 at the completion of testing	171
Figure 8.7 Vertical strains in concrete beam and retrofit plate of Specimen R1	172
Figure 8.8 Hysteretic response of Specimen R2	173
Figure 8.9 Specimen R2 at ductility level of $-2.5\delta_y$	173
Figure 8.10 Specimen R2 at the completion of testing	174
Figure 8.11 Vertical strains in concrete beam and retrofit plate of Specimen R2	175
Figure 8.12 Hysteretic response of Specimen R3	176
Figure 8.13 Specimen R3 at ductility level of $-2.5\delta_y$	176
Figure 8.14 Specimen R3 at the completion of testing	177
Figure 8.15 Vertical strains in concrete beam and retrofit plate of Specimen R3	178
Figure 9.1 RESPONSE models for predicting behaviour of Specimens R0 through R3	186
Figure 9.2 Hysteretic responses of Specimens R0 through R3	187
Figure 9.3 Peak-to-peak stiffnesses of Specimens R0 through R3	188
Figure 9.4 Cumulative energy absorption of Specimens R0 through R3	189
Figure 9.5 Principal shear strains in retrofit plates of Specimens R1 through R3	190
Figure 9.6 Hysteretic envelopes of Specimens R0 through R3	191
Figure 10.1 Unretrofitted and retrofitted prototype coupling beam details	199
Figure 10.2 Determination of coupling beam response for DRAIN-2DX models	200
Figure 10.3 Roof displacement-time history of (un)retrofitted prototypes	201
Figure 10.4 Hysteretic behaviour of coupling beams of (un)retrofitted prototypes	202
Figure 10.5 External energy absorbed by unretrofitted and retrofitted prototypes	203

List of Tables

Table 1.1 Summary of specimens reported	18
Table 2.1 Material properties of steel coupling beam specimens	37
Table 2.2 Specified concrete composition and properties	38
Table 2.3 Summary of load histories of Specimens S1 through S4	41
Table 3.1 Response of steel coupling beam specimens	51
Table 3.2 Load stage peaks for Specimen S1	52
Table 3.3 Load stage peaks for Specimen S2	57
Table 3.4 Load stage peaks for Specimen S3	61
Table 3.5 Load stage peaks for Specimen S4	65
Table 4.1 Response of steel coupling beam specimens	79
Table 4.2 Observed and predicted elastic stiffnesses of Specimens S1 through S4 . . .	81
Table 5.1 Summary of NBCC equivalent lateral load parameters	96
Table 5.2 Summary of elastic analysis prototype criteria	98
Table 5.3 Reinforcing details at the base of the prototype core walls	102
Table 5.4 Prototype DRAIN-2DX model properties	104
Table 5.5 Ground motion parameters for locations of prototype structures	107
Table 5.6 Parameters of selected input ground motion	108
Table 6.1 Summary of global and local ductility demands for PC and PS	117
Table 6.2 Summary of global and local ductility demands for FC and FS	119
Table 6.3 Damage ratios for the prototype structures	123
Table 6.4 Comparison of values obtained from non-linear dynamic analyses and those obtained from NBCC equivalent static analysis El Centro record	124
Table 6.5 Summary of global and local ductility demands for prototype PC, located in Montréal	126
Table 7.1 Material properties of retrofitted concrete specimens	146
Table 7.2 Properties of candidate retrofit plates	147
Table 7.3 Specified concrete composition and properties	148
Table 7.4 Summary of load histories of Specimens R0 through R3	150
Table 8.1 Load stage peaks for Specimen R0	158
Table 8.2 Load stage peaks for Specimen R1	160
Table 8.3 Load stage peaks for Specimen R2	162
Table 8.4 Load stage peaks for Specimen R3	165
Table 9.1 Response of retrofitted reinforced concrete coupling beam specimens	180
Table 9.2 Ratio of response parameters of retrofitted specimens to those of R0	184
Table 10.1 Transverse reinforcement spacing requirements of older Canadian concrete design standards	193
Table 10.2 Summary of global and local ductility demands for (un)retrofitted prototypes	197
Table 11.1 Design and detailing criteria for reinforced concrete and steel coupling beams	206

List of Symbols

A_1	area within observed hysteresis loop	f'_c	compressive strength of concrete
A_2	area within equivalent elastic hysteretic loop	f_u	ultimate strength of steel reinforcement
A_p	area of vertical strip of retrofit plate	f_y	yield strength of steel reinforcement
A_s	area of longitudinal or diagonal reinforcing steel	G	shear modulus
$A_{s,eq}$	equivalent area of longitudinal reinforcing steel	h	overall depth of diagonally reinforced coupling beam
A_{sc}	required area of concentrated reinforcement	h	height of steel beam web
A_v	area of transverse reinforcement	h_b	vertical spacing of anchor bolts
$A_{v,eq}$	equivalent area of transverse reinforcement	J	global force reduction coefficient (NBCC §4.1.9.1.(20))
$A_{v,req}$	required area of transverse reinforcement at spacing = s	J_x	force reduction coefficient at level x (NBCC §4.1.9.1.(21))
A_w	area of steel beam web	I	moment of inertia
b'	effective width of embedment	I	seismic importance factor (NBCC §4.1.9.1.(10))
b	width of steel beam flange	I_{eff}	moment of inertia accounting for shear distortion and local plasticity
c	depth of concrete cover	I_{eq}	equivalent moment of inertia accounting for shear distortion
D	specified dead load (A23.3 §8.3.2)	I_g	gross moment of inertia
DR	damage ratio	K_e	elastic stiffness
DR_c	damage threshold of 50%	k	reduction factor for moment of inertia accounting for shear distortion
DR_t	damage threshold of 0.5%		
DR_w	damage ratio for windows	$k\alpha$	measure of relative stiffness of coupling beams and walls
d	distance from extreme compression fibre to centroid of tension steel	L	specified live load (A23.3 §8.3.2)
d_{bh}	diameter of transverse reinforcement	ℓ	length of coupling beam
d_{bl}	diameter of longitudinal reinforcement	ℓ_{cr}	maximum unsupported length of beam
d_{bolt}	diameter of anchor bolt	ℓ_e	embedment length
d_v	shear depth of reinforced concrete, typically 0.9d	ℓ_{eff}	effective length of coupling beam
E	specified earthquake load (A23.3 §8.3.2)	ℓ_h	flexural hinge length (Specimen S4)
E	Young's modulus	ℓ_u	unsupported span of beam
e	eccentricity from centre of embedment to midspan of coupling beam	M	external moment applied to structure
F	foundation factor (NBCC §4.1.9.1.(11))	M_r	factored moment resistance
F_t	concentrated load at top of structure (NBCC §4.1.9.1.(13)(a))	n	number of bolts developing retrofit plate
F_u	ultimate strength of structural steel and retrofit plates	R	force modification factor (NBCC §4.1.9.1.(8) and (9))
F_y	yield strength of structural steel and retrofit plates	S	seismic response factor (NBCC §4.1.9.1.(6))
		s	spacing of transverse reinforcement
		s_b	longitudinal spacing of anchor bolts
		T	fundamental period of structure (NBCC §4.1.9.1.(6))

t	thickness of steel beam flange	ϵ_b	strain at back of embedment (Fig. 1.8)
t_p	thickness of retrofit plate	ϵ_f	strain at face of embedment, assumed to be 0.003 (Fig. 1.8)
V	equivalent static base shear (NBCC §4.1.9.1.(4) and (5))	ϵ_o	concrete strain at peak stress, typically assumed to be 0.002
V_b	shear capacity of anchor bolt	ϵ_{st}	strain at onset of strain hardening of structural or reinforcing steel
V_c	shear capacity of embedment (Chapter 2)	ϵ_{ult}	strain at ultimate stress of structural or reinforcing steel
V_c	concrete contribution to shear capacity (Chapter 9)	λ	cross section shape factor
V_f	factored shear capacity requirement	λ	importance factor (A23.3 §8.3.2)
V_n	ultimate shear applied to coupling beam (Eq. 1.2)	λ_b	beam overstrength factor (A23.3 §21.5)
V_r	factored shear resistance	λ_p	principal shear strain
V_{re}	factored shear resistance of embedded web	λ_w	wall overstrength factor (A23.3 §21.5)
V_s	reinforcing steel contribution to shear capacity	ϕ	material resistance factor for structural steel (0.90)
v	zonal velocity ratio (NBCC §4.1.9.1.(5))	ϕ_c	material resistance factor for concrete (0.60)
W	weight of structure (NBCC §4.1.9.1.(12))	ϕ_s	material resistance factor for reinforcing steel (0.85)
w	thickness of steel beam web	ϕ_u	beam curvature at ultimate strength
w_e	thickness of embedded steel beam web	μ_{drift}	ductility level determined from interstorey drift
x	reduction factor for moment of inertia accounting for local plasticity in walls	μ_{global}	global ductility demand
x_b	length of back compression block in embedment (Fig. 1.8)	μ_{local}	local ductility demand
x_f	length of front compression block in embedment (Fig. 1.8)	μ_{roof}	ductility level determined from roof displacements
Z	section modulus		
α	angle of inclination of diagonal reinforcement		
α	stress block factor for parabolic stress distribution		
β	equivalent elastic damping coefficient (Chapter 4)		
β	stress block factor for parabolic stress distribution		
β_1	stress block factor		
Δ	interstorey drift ratio		
Δ_c	interstorey drift ratio corresponding to DR_c		
Δ_t	interstorey drift ratio corresponding to DR_t		
Δ_{ult}	roof displacement at ultimate		
Δ_y	roof displacement at yield		
δ_{ult}	coupling beam displacement at ultimate		
δ_y	coupling beam displacement at yield		

Chapter 1

Introduction and Literature Review

This thesis investigates the behaviour of reinforced concrete coupled wall systems. Two experimental programmes were conducted. The first investigates the use of steel beams to couple reinforced concrete walls. The second programme investigates the seismic upgrading of existing, shear deficient, reinforced concrete coupling beams retrofitted with attached steel plates. Each programme involved the testing of four full-scale specimens. Analyses of coupled wall structural systems involving both steel and retrofitted concrete beams were also conducted. The suitability of each system is discussed in context with their intended use.

This chapter will outline relevant previous research from which the current study has been developed. The structural response and modelling of coupled wall structures is discussed, followed by a summary of existing research involving reinforced concrete coupled wall systems. Other structural systems with aspects relevant to this thesis programme are discussed, such as; the response of steel link beams in eccentrically braced frames and the behaviour of various forms of composite steel-reinforced concrete construction. An overview of seismic retrofit of coupling beams is presented along with an overview and the objectives of this research programme.

1.1 Coupled Wall Structures

In the last three decades, coupled flexural walls have, increasingly, become recognised as efficient lateral load resisting systems for tall buildings. Coupled walls exhibit considerable lateral stiffness and strength as well as providing an architecturally practical structural system.

Coupled wall systems consist of two or more in-plane walls inter-connected with coupling beams. The presence of moment resistant connections between the beams and the walls serve to stiffen the wall system laterally. Under lateral loads, each wall behaves as a

cantilever as well as resisting the external moment with a couple formed by opposing axial loads in the walls.

1.1.1 Behaviour of Coupled Wall Structures

If a series of fixed base, in-plane walls are connected with pin-ended links, capable of transmitting only axial forces, external moments can only be resisted by the individual cantilever actions of each wall. Therefore, stresses in the walls are linearly distributed across, and have zero magnitude at the centroid of each wall (see Fig. 1.1(a)). Conversely, if rigid coupling beams have rigid moment connections at their ends, the wall system will behave as a wide cantilever. In this case the external moment will be resisted by a linear stress distribution across the width of the entire wall system (see Fig. 1.1(b)) with the 'tension walls' and 'compression walls' forming a couple which helps to resist the external moment. The actual behaviour of coupled wall systems lies between these two extremes, where the external moment is resisted partially by flexural response of the individual walls and partially by the wall couple (see Fig. 1.1(c)).

The coupling of walls also reduces the overall lateral deflection of the wall system. Individual walls behave as vertical cantilevers, deforming in a flexural manner (see Fig. 1.2.(a)). Coupling beams introduce moments into the walls opposing those induced by the cantilever bending of the walls (see Fig. 1.2(b)). The coupling beams, therefore, reduce the moments in the walls by causing a portion of the external moment to be resisted by opposing axial forces in the walls. In this manner, the coupling beams help to restrain the flexural deformation of the walls (see Fig. 1.2(c)).

1.1.2 Seismic Behaviour of Coupling Beams

In order to resist seismic loads, coupling beams must be sufficiently stiff, strong and possess a stable load-deflection hysteretic response. Overly stiff coupling beams result in an over coupling of the wall system. This leads to an undesirable failure mechanism where the wall system behaves as a single pierced wall. The failure mechanism, in this case, will be the formation of plastic hinges, having large ductility demands, at the base of the walls. If the wall system is sufficiently slender or has a relatively light gravity loading, the tension in the 'tension walls' can overcome the compressive gravity effects resulting in net tensile stresses on the wall, reducing the wall's flexural capacity. Overly stiff coupling beams can also lead to shear failures at the base of the walls.

If, on the other hand, the coupling beams are not stiff or strong enough, they will yield prematurely and will be unable to dissipate significant amounts of energy. In this case the

overall resistance of the system is significantly reduced as the walls behave as individual cantilevers.

For optimal performance, the energy dissipating mechanism should involve the formation of hinges in most of the coupling beams and at the base of each wall (Paulay, 1986). This mechanism is similar to that of the weak girder-strong column design philosophy for moment resisting frames. A well-proportioned coupled wall system will minimise the ductility demands on both the beams and at the bases of the walls.

1.1.3 Ductile Behaviour of Coupled Walls

Coupled wall structures are recognised as efficient seismic load resisting systems. Modern seismic design codes (e.g., NBCC, 1995 and SEAOC, 1988) allow a reduction of the pseudo-static base shear to reflect the ability of the structure to dissipate energy through inelastic behaviour. This reduction (the force modification factor, R , in the 1995 NBCC) reflects the overall ductility requirement of the structure. With appropriate design details, coupled walls may be designed using force modification factors of 3.5 to 4. (NBCC, 1995)

Achieving the desired progressive hinging behaviour of the coupling beams requires that the beams be designed for very high levels of ductility. It was shown by Paulay (1970) that, in a specific coupled wall structure, for the top floor deflection to attain a displacement ductility of 4, the rotational capacity of the individual coupling beams can be required to achieve ductility levels of the order of 25.

Saatcioglu et al. (1981) showed that, for more generalised coupled wall structures, for wall ductilities in the range of 4, coupling beam ductilities will range between about 6 and 16. Saatcioglu et al. conducted a number of analyses of coupled walls having different degrees of coupling, beam-to-wall stiffness ratios and imposed ground motions. It was found that coupling beam ductility requirements are inversely proportional to both the capacity of the individual walls and the degree of coupling, that is the ratio of the beam capacity to wall capacity.

Furthermore, the effect of axial forces in the walls will result in a redistribution of moment from the "tension wall" to the "compression wall". This too will effect the overall ductility of the system and the rotational capacity of the coupling beams at their connection to the walls.

1.2 Analysis of Coupled Walls

1.2.1 Continuous Medium Method

Considerable research has been devoted to numerical analysis of coupled shear walls. A simplified analysis, replacing the discrete coupling beams with an equivalent continuous medium, was first used in relation to the 'dowelled cantilever' problem by Chitty (1947). Chitty and Wan (1948) applied the continuous medium method to building frames subjected to wind loads.

Subsequent work by Beck (1962), Eriksson (1961) and Rosman (1964) extended the analysis to account for the finite width of the wall, wall systems with multiple bands of openings and wall systems with different (ie: non-rigid) foundation conditions. Beck, who solved the problem assuming the shear forces in the continuum were indeterminate, produced graphical solutions for deflection, bending moments and axial forces in the walls. Other researchers (such as Shultz, 1961 and Magnus, 1968) selected different force variables as indeterminate and have produced response curves with these assumptions.

Winokur and Gluck (1968a) developed methods for dealing with plan asymmetric structures and accounting for torsional effects. They (1968b) also developed expressions for the ultimate strength of coupled wall systems. Although the solution approaches have differed, all continuous medium solutions are essentially the same, being based on the same differential equations. The continuous medium method remains a fast and efficient manual method for estimating coupled wall behaviour and continues to be used in analytical research (for example: Coull and Bensmail, 1991 and Subedi, 1991a and b).

The continuous medium method assumes that the coupling beams have a point of contraflexure at midspan and do not experience axial deformations. With these assumptions, the behaviour of the system reduces to a single fourth order differential equation, enabling a general closed form of the solution to be obtained. The governing equation for coupled walls expressed in terms of the lateral deflection, y , with respect to the height above the base of the structure, z , is given as (Stafford-Smith and Coull, 1991):

$$\frac{d^4 y}{dz^4} - (k\alpha)^2 \frac{d^2 y}{dz^2} = \frac{1}{EI} \left[\frac{d^2 M}{dz^2} - (k\alpha)^2 \frac{k^2 - 1}{k^2} M \right] \quad (1.1)$$

where M = external moment applied to structure,
 EI = flexural rigidity of walls, and,
 $k\alpha$ is a measure of the relative stiffness of the coupling beams and walls.

1.2.2 Equivalent Frame Method

While the continuous medium method is appropriate for relatively simple coupled wall systems, it is impractical for more complex coupled wall systems. An equivalent frame analysis (MacLeod, 1967 and Schwaighofer, 1969) provides a more practical and versatile approach for analysing coupled wall systems. The equivalent frame method reduces the coupled wall system to a series of equivalent "wide columns", located at the centroid of each wall. Coupling beams are modelled with moments of inertia reduced to account for shear deformations in the beams and rigid ends accounting for the widths of the walls. The equivalent frame method has the additional advantage that the coupled wall system can be linked with the rest of the structure, enabling structural interaction to be determined.

Michael (1967) and Bhatt (1973) developed methods of accounting for local inelastic deformations at the coupling beam-wall interface. These methods involve further adjustments to the stiffness of the coupling beam through the definition of an effective span for the coupling beam.

For most practical applications and analytical research, variations of the equivalent frame method are used for the analysis of coupled walls (for example: Saatcioglu et al., 1980, 1981 and 1983 and Shiu et al., 1984). Coull and Stafford-Smith (1967) provide an extensive historical summary of the development of methods of analysis for shear walls.

1.2.3 Finite Element Methods

With the advent of computer-based structural analysis packages, the number of methods for analysing coupled walls have increased many fold. Plate or shell elements have been shown to model wall structures quite well (for example: Bolander and Wight, 1991 and Remmetter et al, 1992). There are a number of details that must be addressed in order to carry out detailed analyses of coupled wall structures. Specifically, the connection of the coupling beam to the wall, and the modelling of cracked regions. Elements embedded into other elements and contact elements are some of the specialised tools necessary. Furthermore, due to the nature of the response of coupled wall systems, nonlinear analysis provides a better understanding of the force resisting mechanisms within the system.

1.3 Reinforced Concrete Coupled Wall Systems

Following the 1964 Alaskan Earthquake (Berg and Stratta, 1964), considerable attention was devoted to improving the response of reinforced concrete coupling beams in coupled wall systems. Extensive experimental work, under the direction of Paulay at the University of Canterbury, led to the development of design guidelines for reinforced concrete coupling beams.

Tests conducted by Paulay (1969 and 1971) led to design guidelines for coupling beams with relatively large span-to-depth ratios and relatively low shear stress levels. The design philosophy developed for these members avoids brittle shear failures by providing shear resistances large enough to develop flexural hinging in the beams (Park and Paulay, 1975).

Conventionally reinforced beams with relatively small span-to-depth ratios and/or high shear stress levels were shown to exhibit sliding-shear failures at the wall interfaces (Paulay and Binney, 1974 and Park and Paulay, 1975). Because the sliding-shear plane is perpendicular to the beam span, conventional transverse reinforcement has no effect in controlling this mode of failure.

To prevent sliding-shear failures, Paulay and Binney (1974) introduced the concept of using diagonal reinforcement in the coupling beams (see Fig 1.3). Diagonally reinforced coupling beams offer improved ductility and energy absorption over conventionally reinforced coupling beams. Santhakumar (1974) and Paulay conducted quarter-scale model tests on seven-storey coupled walls having coupling beams with a span-to-depth ratio of 1.25. These tests confirmed the superior performance of diagonally reinforced coupling beams, with the attainment of larger displacement ductilities and energy absorption compared with conventionally reinforced coupling beams. With the diagonally reinforced beams, displacement ductilities of the wall system of 8 to 13 were achieved without significant loss of strength.

The University of Canterbury research forms the basis for the design criteria for coupling beams in ductile coupled flexural walls given in the New Zealand (NZS, 1984) and the Canadian Standard (CSA, 1984 and 1994).

Research conducted at the Portland Cement Association (PCA) examined the response of relatively slender coupling beams, having span-to-depth ratios of 2.5 and 5 (Shiu, et al, 1978). These tests confirmed the improved behaviour of diagonally reinforced beams over conventionally reinforced beams. Figure 1.4 shows the hysteretic behaviour of a conventionally reinforced and a diagonally reinforced coupling beam tested by Shiu et al. These tests demonstrated that for larger span-to-depth ratios, the diagonal reinforcement is not as efficient due to its lower angle of inclination. These tests also confirmed the need for closely spaced hoops or spiral reinforcement confining the diagonal bars, both in the coupling beam and along its wall embedments (shown in Fig 1.3). If adequate confinement is not provided, buckling of the diagonal bars may severely effect the response of the beam.

1.3.1 Walls Coupled with Floor Slabs

Flat plate floors coupling structural walls are a common form of construction. Often low storey heights will preclude the use of coupling beams, resulting in the coupling action being supplied by the floor slab only. These systems will typically have a low degree of coupling.

Paulay and Taylor (1981) have shown that the behaviour of slab-coupled walls can be significantly limited by punching shear at the wall toe and the loss of stiffness of the slab due to torsional effects. Furthermore, the stiffness which can be supplied by the slab is typically insufficient to result in optimal behaviour of the coupled wall system (Coull and Wong, 1981).

An extensive research programme conducted at McGill University (Malyszko, 1986, Khan, 1989 and Lim, 1989) investigated the design and detailing of the region of the slab adjacent the shear wall in slab coupled structures. Design recommendations enabling ductile response of the coupling slab were presented. Although punching shear at the wall toe remained a problem, provisions were suggested that will delay such a failure (Lim, 1989).

1.4 Steel Link Beams in Eccentrically Braced Frames

Analogous to coupling beams in reinforced concrete coupled wall systems, steel link beams in eccentrically braced frames serve as the primary ductile energy absorbing elements for these systems (see Fig. 1.5). Recent research has shown that steel link beams in eccentrically braced frames can be detailed to provide excellent ductility and energy dissipating characteristics.

A number of research programmes, under the direction of Popov, have been carried out at the University of California, Berkeley (Roeder and Popov, 1978, Malley and Popov, 1983a and 1983b, and Kasai and Popov, 1986). The results of these programs have led to design recommendations for achieving large ductility and energy absorption characteristics from link beams. Engelhardt and Popov (1989) provide an excellent summary of design and detailing considerations for achieving ductile response from steel link beams of varying spans.

This research clearly indicates the superior hysteretic response of steel beams, particularly when they are designed to yield in shear while remaining elastic in flexure. Malley and Popov (1983b) demonstrated the necessity for detailing link beams to control web and/or flange instability with the provision of stiffeners.

This work has led to the design and detailing requirements for link beams in eccentrically braced frames that form the basis of the provisions of most modern steel design codes (CSA, 1989 and 1994, AISC, 1988 and SEAOC, 1988).

1.5 Composite Steel and Reinforced Concrete Construction

1.5.1 Reinforced Concrete Coupling Beams Containing Encased Steel Members

Although few structures use steel beams to couple reinforced concrete walls, it is interesting to note that many older reinforced concrete coupled wall systems have steel members encased in the reinforced concrete coupling beams. These members often served as erection steel and were not typically accounted for in design.

Paparoni (1972) reported on a study of a reinforced concrete coupling beam containing an encased structural I-section tested at the Laboratorio Nacional de Engenharia Civil in Lisbon. This study investigated the reversed cyclic loading response of a 130 mm wide by 230 mm deep reinforced concrete coupling beam spanning 450 mm containing conventional longitudinal and transverse reinforcement and a 140 mm deep structural I-section. The test specimen was a model of coupling beams in the Parque Central buildings in Caracas, Venezuela. The testing programme also investigated the reversed cyclic loading response of coupling beams reinforced with a combination of longitudinal and inclined reinforcing bars together with closed stirrups. The details of the special inclined reinforcement, different than those suggested by Paulay, provided hinge regions near the ends of the longer beams. The results of these tests suggested that reinforced concrete coupling beams having encased structural steel members and those reinforced with the special inclined reinforcement exhibited ductilities and energy absorption characteristics superior to those of conventionally reinforced coupling beams. The responses, however were not as good as those of Paulay's diagonally reinforced coupling beams. It should be noted that this research report did not specify the end conditions of the embedded section, which would significantly influence the overall response.

Research conducted at McGill University by Mitchell and Cook (1989) investigated the reversed cyclic loading response of a reinforced concrete coupling beam containing a structural steel channel. The encased channel is representative of erection steel used in some older structures. The 280 mm wide by 610 mm deep coupling beam spanning 1525 mm, contained longitudinal reinforcing bars and closely spaced closed stirrups as well as a 150 mm deep structural channel. The results of this test showed some improvement in ductility and hysteretic behaviour over conventionally reinforced coupling beams.

Wakabayashi (1986) summarises a collection of Japanese research investigating the seismic behaviour of concrete encased steel columns in composite frames. The column specimens, subjected to reversed cyclic loading, were bent in double curvature with high shear-to-moment ratios. The nature of the applied loading is very similar to the loading conditions found in coupling beams. The Japanese design approach is to have the encased steel member resist all of the loads. The surrounding concrete provides only stability and fire

protection. All of the tests reported illustrate behaviour typical of steel columns, with only small improvements in stiffness and ultimate capacity. Often the concrete is not sufficiently confined to contribute significantly to the post-peak behaviour of the composite system.

Another research programme which involved composite coupling beams was carried out at the University of Dundee by Subedi (1989). This programme involved replacing conventional shear reinforcement with encased steel plates. The results of this preliminary testing programme indicated that premature shear failure may result if the plate has inadequate anchorage to the concrete. Several different methods were investigated in an attempt to provide horizontal shear resistance between the encased steel plate and the longitudinal reinforcing bars. The specimens of this test series were subjected to monotonic loading only and it is doubtful if the details proposed would perform well under reversed cyclic loading.

1.5.2 Reinforced Concrete Wall Systems Encasing Steel Frames

Another form of composite construction involves steel coupling beams, attached at their ends to erection columns which are in turn embedded in reinforced concrete walls. Fig. 1.6 shows the typical connection detail for this type of construction (Taranath, 1982 and 1988). The beam-to-embedded column connection is a bolted shear connection. The moment capacity required at the face of the wall is developed by means of shear transfer between shear studs on the beam flanges and the surrounding concrete. Taranath (1982) reports on the use of this type of composite coupled wall system in the core of the First City Tower in Houston, Texas, completed in 1982. In the design of the First City Tower beam-wall moment resisting connections, only shear transfer was considered, no allowance was made for the couple developed in the flanges of the embedded member. (see Section 1.5.4)

No analytical or experimental data is available for this type of connection although the redundancy of moment resistance suggests that these structures should behave well in seismic conditions.

1.5.3 Embedded Plate Connections

A common form of composite construction in low rise structures involves connecting steel coupling beams to steel plates embedded in the concrete walls or columns (see Fig 1.7). The heavy steel plates have headed studs embedded in the reinforced concrete walls. Roeder and Hawkins (1981) showed that generally the full moment capacity of the attached steel section could not be attained before failure of the embedment. As such, the connection is recommended for shear transfer only. Although this type of connection is often used in slip form construction, there is some concern over the quality of the field welds used to connect

the coupling beam and the effects of the heat generated by the welding on of the concrete in the vicinity of the embedded plate.

1.5.4. Embedded Connections of Structural Steel Members in Precast Concrete

Structural steel members with their ends embedded in concrete, serving as haunches or brackets, have been used to provide connections in precast and cast-in-place construction. Rath (1974) developed simplified expressions for determining the strength of these embedments. Rath developed further expressions for determining the increased strength of the embedments in cases where reinforcing steel is welded to the embedded section.

Marcakis and Mitchell (1980) investigated the response of different types of structural steel members embedded in reinforced concrete and proposed a design procedure for determining the embedment strength of such connections. This study investigated the effects of axial load on the reinforced concrete elements as well as different combinations of shear and moment applied to the embedded sections. An effective bearing width of the embedded member was determined to be equal to the width of the confined concrete (limited to 2.5 times the width of the embedded member). The tests demonstrated that the embedded connection can be designed to develop the full capacity of the embedded structural steel member. This approach forms the basis of current design recommendations for these type of connections (PCI, 1985 and CPCI, 1987).

The design approach of Marcakis and Mitchell was used as the basis for the embedment design of the S-series of specimens reported in Chapter 2. Figure 1.8 shows the assumed strain and stress distributions within the embedment used to determine its capacity.

For a given loading configuration, the ultimate applied shear, V_n , and the depth of the compression block at the face of the embedment, x_f , can be determined by simultaneously solving the equilibrium equations for shear and moment at the face of the embedment:

$$V_n = 0.85f'_c b \beta_1 x_f - \alpha \beta f'_c b x_b \quad (1.2)$$

$$V_n a = (\alpha \beta f'_c b x_b)(\ell_e - \beta x_b / 2) - 0.85f'_c b \beta_1 x_f (\beta_1 x_f / 2) \quad (1.3)$$

where b = effective width of the embedment,
 β_1 = stress block factor,
 f'_c = compressive strength of concrete, and
 ϵ_b , x_f , x_b , ℓ_e and a are shown in Fig. 1.8(b).

The rectangular stress block factors, α and β are found by matching the position and magnitude of the resultant compression with those from a parabolic stress distribution:

$$\alpha\beta = \frac{\epsilon_b}{\epsilon_0} - \frac{1}{3} \left(\frac{\epsilon_b}{\epsilon_0} \right)^2 \quad \text{and} \quad \beta = \frac{4 - \frac{\epsilon_b}{\epsilon_0}}{6 - 2\frac{\epsilon_b}{\epsilon_0}} \quad (1.4)$$

where ϵ_0 is the concrete strain at maximum stress, typically assumed to be 0.002.

Marcakis and Mitchell produced design curves for embedded sections and developed a simplified expression for the shear capacity of an embedment, V_c :

$$V_c = \frac{0.85f'_c b \ell_e}{1 + \frac{3.6e}{\ell_e}} \quad (1.5)$$

Mattock and Gaafar (1982) proposed another method for determining the capacity of an embedment using a different stress distribution in the embedment. Of particular note is that this method does not allow an increase in the effective width of the embedded section.

None of these studies considered the effect of cyclic loading, nor did they provide sufficient confinement in the embedment region to adequately resist cyclic loads.

1.5.5. Composite Frame Structures

"Composite frames" are moment resisting frames composed of steel beams and reinforced concrete columns, in which the composite beam-column connections are integral parts of the lateral load resisting system. Composite frames have been extensively used in Japanese construction for the past decade and are referred to as steel reinforced concrete (SRC) construction. An English language summary of Japanese research is provided by Wakabayashi (1985). Much of the Japanese research and construction practice involves composite reinforced concrete columns containing large steel columns (see also Section 1.5.1).

North American composite construction, on the other hand, tends toward the use of only very light steel erection columns embedded in reinforced concrete columns. An extensive experimental programme, investigating the joint behaviour of composite frame structures, has been reported by Sheikh, et al. (1989). This programme investigated the behaviour of interior joints subjected to reversed cyclic loading. Complex behaviour models for interior joint regions were developed (see Fig. 1.9). These models accounted for the contribution of the steel web panel, the confined concrete compression strut (confined within the steel flanges), the concrete compression field and the horizontal force transfer provided by the steel erection column. In

addition, various arrangements of stiffeners and shear studs in the joint region were investigated. Kanno (1993) investigated different joint details and has extended the joint behaviour models to account for different stiffener and shear stud arrangements, as well as the presence of transverse floor beams. This research forms the basis of the ASCE Task Committee *Guidelines for Design of Joints Between Steel Beams and Reinforced Concrete Columns* (ASCE, 1993).

Furthermore, Kanno investigated the effect that various beam and joint reinforcement details have on the bearing capacity at the face of the joint. Analytical models, which assume a sliding shear failure at the face of the joint, were developed (see Fig. 1.10). These models account for sliding shear resistance, lateral confining pressures and confining reinforcing steel in order to determine the bearing capacity at the face of a support.

Thus far, investigations of composite frame construction have considered only interior joints. As reported by Kanno (1993), interior joints derive their strength from steel web panel shear, confined concrete compression struts (i.e., bearing capacity) and compression field action in approximately equal proportions. It is unlikely that this behaviour would be consistent in exterior frame joints, which are more comparable to coupling beam-to-wall connections. Because the applied beam forces in exterior connections are not balanced across the connection, it is unlikely that the steel web shear or the compression field action could be developed to the same extent as in the interior connection. As such, the joint behaviour will be similar to that of embedded precast connections (see Section 1.5.4) and will be governed by the bearing capacity of the concrete.

1.5.6 Reinforced Concrete Wall Coupled with Embedded Steel Beams

This new concept in coupled wall design is currently being pursued at the University of Cincinnati (Remmetter, Qin and Shahrooz, 1992) and at McGill University (Harries, 1992 and Harries et al, 1992 and 1993).

Remmetter et al tested three specimens consisting of the stub of a coupling beam projecting from a segment of wall. The coupling beam was loaded vertically in a reversed cyclic manner. The tests investigated the effects of axial load in the wall and of reinforcing bars being welded to the embedded member. Calculation of the embedment capacity was based on the model presented by Mattock and Gaafar (1982).

The preliminary research for this programme (Harries, 1992) involved the testing of two full-scale segments of a coupled wall (two walls coupled by a beam). The coupling beams were designed as link beams in eccentrically braced frames, to achieve maximum ductility and energy absorption (Engelhardt and Popov, 1989). The embedments were designed based on the

method presented by Marcakis and Mitchell (1980). This programme investigated the effect on the overall response of the wall system of different modes of failure of the coupling beam. Guidelines were presented for detailing such systems such that they would exhibit large levels of ductility and energy absorption while containing the yielding, and subsequent plastic hinges to regions outside the embedment region. The preliminary specimens tested are reported as Specimens S1 and S2 in this report.

Both of these programmes have shown encouraging results in terms of the ductility achievable from steel coupling beams embedded in reinforced concrete walls. Recommendations and concerns presented by each research programme are found to be in general agreement.

1.6 Seismic Retrofit of Reinforced Concrete Coupling Beams

Considerable research has been carried out investigating methods of retrofitting damaged or deficient reinforced concrete structural members. Often retrofit schemes will involve "jacketing" the members with either reinforced concrete or steel jackets. Where global structural strengthening is required or in cases where the retrofit is designed to change the weak link element of the structural system, such retrofits have proven efficient.

Coupling beams, especially those of older structures, are often found to be deficient in shear, unable to resist the forces caused by seismic loading (Berg and Stratta, 1964 and Paulay and Binney, 1974). The retrofit, therefore, is often only required to increase the shear capacity of the coupling beams, the flexural capacity of the beams usually being adequate. Increasing the design capacity of the beams with jacketing-type retrofits, which increase both shear and flexural capacities, would require additional retrofit procedures to be applied to the walls and, subsequently, the foundations.

The retrofit of coupling beams is further complicated by architectural and practical constraints of their location in a structure. Coupling beams often comprise the lintel beams of elevator shafts where bulky jacketing cannot be allowed to encroach into the service shaft. The most accessible face on which to retrofit a coupling beam is the face within the elevator shaft. The other faces of the coupling beam are typically not accessible without significant architectural modifications which would affect the use and occupancy of the building. The retrofit solution required, therefore must be compact and improve the shear capacity of the deficient coupling beam without significantly affecting the beam's flexural capacity.

1.6.1 Bonded Steel Plate Retrofit Measures

Steel plates bonded to reinforced concrete structural members have been used as a retrofit measure for the last three decades. Epoxy-bonded plates were first used in South Africa

in 1964 (McKenna and Erki, 1994) to repair beams in which the main tensile reinforcement had been inadvertently omitted. Epoxy bonded plates have been used extensively in both building and highway bridge repair. McKenna and Erki (1994) provide a thorough review of the use of bonded steel plates as well as providing a number of case studies.

In almost all reported cases, bonded plates are applied to the tension face of the beam (and occasionally the compression face). Such retrofit measures have been shown to increase the flexural and shear capacity of the original reinforced concrete beams (for example: Cusens and Smith, 1980, Jones et al., 1982, Trieu, 1986 and Swamy et al., 1987 and 1989). There is no reference to shear-only steel plate retrofits which could be used to retrofit shear deficient coupling beams.

Early research (e.g. L'Hermite, 1967) indicated that study of shear-only bonded plate retrofit warranted attention. Views differ on the feasibility of such systems however. Priestly and Seible (1991), in reference to highway bridge retrofits state:

It is not felt that bonding steel plates to the sides of joints is likely to be effective in enhancing shear strength [of] a concrete jacket, even if bolted through the joint... This is because the flexibility of the steel plate will localize the shear friction stress to the immediate vicinity of the dowel or prestressing bar with little or no stress midway between the dowels. The resulting shear transfer would appear to be less efficient, as a consequence.

A recent preliminary research programme (Al-Sulaimani et al., 1994) investigating the use of bonded fibreglass plate retrofits has investigated the behaviour of shear only retrofits. Two 150 mm square shear deficient beams specimens (of 16 reported) were retrofit; one with 3 mm fibreglass plates applied to both sides of the beam, the other with 20 mm wide "shear strips" applied to both sides of the beam at a 50 mm spacing. An increase in shear capacity of about 21% was reported for both retrofit details. The increased shear capacity, however was insufficient to develop the flexural capacity of the beams (this would have required an increase of about 36%).

Experimental evidence (Cusens and Smith, 1980, Jones et al., 1984, and Trieu, 1986) clearly indicates that significant shear transfer can be developed under monotonic loading with only the use of a structural epoxy adhesive. Recommendations for the use of bonded steel plate retrofits suggest that thickness of the steel plate be kept as thin as practically possible. Furthermore, since the elastic modulus of epoxy resin is lower than that of steel or concrete, the glue line should also be kept as thin as possible. A thin glue line enhances the shear transfer, by minimising transverse contraction of the epoxy layer. It has also been shown (Cusens and Smith, 1980) that thin layers of epoxy behave more favourably when exposed to heat.

All experimental investigations cited describe a failure of the epoxy bond at the ends of the plate. Jones, et al. (1984) described the mechanism involved in the peeling of the plate away from the reinforced concrete specimen (see Fig. 1.11). The steel plate has an interface shear stress, τ , a thickness, t_p , and a width (or height), b . If small incremental lengths of plate, $d\ell$, are considered, the system reduces to an axial tension in the plate and an out of balance peeling force of $\tau bt_p/2$ at the end of the plate. The out of balance force is applied as a tension to the epoxy layer and the concrete. As separation progresses, the effective end of the plate moves inward.

It is clear from these studies that some provision must be made to arrest the propagation of plate separation. Anchor bolts, acting in tension, provided to resist the out of balance shear force offer a method of reducing the separation of the plate. This solution is investigated in this report.

1.7 Objectives of Research Programme

1.7.1 Steel Coupling Beams Coupling Reinforced Concrete Walls

Several researchers have investigated novel approaches for improving the ductility and energy absorption of reinforced concrete coupling beams. For span-to-depth ratios less than about 2, specially detailed diagonal reinforcement (e.g., Paulay and Binney, 1974) has been shown to significantly improve the reversed cyclic loading response. Structural steel members, fully encased in reinforced concrete coupling beams (e.g., Paparoni, 1972 and Mitchell and Cook, 1989) have resulted in slightly improved responses over conventionally reinforced coupling beams.

Excellent ductility and energy absorption characteristics are exhibited with steel link beams in eccentrically braced frames (Malley and Popov, 1983). It has also been shown that steel link beams can be detailed to dissipate large amounts of energy over significantly greater span-to-depth ratios than are practical for reinforced concrete coupling beams.

The objective of the first part of this research programme is to investigate the feasibility of using structural steel members, having their ends embedded in the walls, to replace reinforced concrete coupling beams. This hybrid structural system combines the efficiency of structural steel lateral force resisting elements into reinforced concrete construction.

The use of steel coupling beams to connect reinforced concrete walls has the following potential advantages:

- i. Properly designed and detailed steel coupling beams can exhibit excellent ductility and energy absorption.

- ii. The prefabrication of steel coupling beams provides improved quality control and eliminates a considerable amount of on-site labour.
- iii. Formwork can be significantly simplified.

The specific objectives of this part of the research programme are:

- i. To test full-scale specimens under reversed cyclic loading to determine the hysteretic response of structural steel coupling beams having their ends embedded in reinforced concrete walls.
- ii. To attempt to achieve a reversed cyclic loading response similar to that exhibited by steel link beams in eccentrically braced frames.
- iii. To investigate factors influencing the reversed cyclic loading response of the coupling beam over its clear span and along its embedments.
- iv. To investigate factors influencing the reversed cyclic loading response of the reinforced concrete embedment regions.
- v. To develop design and detailing guidelines to enable large ductilities and energy absorbing capabilities to be achieved in steel coupling beams used to couple reinforced concrete flexural walls.
- vi. To demonstrate the suitability of steel coupling beams as an alternative to reinforced concrete coupling beams with non-linear analysis of complete coupled wall systems.
- vii. To develop practical methods of modelling walls coupled with steel coupling beams.

1.7.2 Retrofitted Reinforced Concrete Coupling Beams

Many older coupled wall structures are found to be deficient in beam shear because they are not designed to have a shear capacity sufficient to ensure flexural yielding. The retrofit solution used often involves the addition of new frames or walls to the structure in order to reduce the loads on individual lateral force resisting systems. A large number of recent examples and case studies of structural retrofit measures are presented in Chapters 12.1 and 12.2 of the *Proceedings of the Tenth World Conference on Earthquake Engineering* (Madrid, 1992). Little attention has been devoted to repairing existing coupled wall systems.

The objective of the second part of this research programme is to investigate retrofit measures for improving the response of shear deficient coupling beams without significantly increasing the design flexural capacity of the beams. Increasing the design flexural capacity of the beams would require subsequent retrofit to the walls and foundations. The retrofit measures investigated involve the application of steel plates to one side of existing shear-deficient reinforced concrete coupling beams. The retrofit measures proposed are suggested for deficient structures subjected to mild or moderate seismic attack.

The use of bonded steel plates to enhance the shear capacity of reinforced concrete coupling beams has the following potential advantages:

- i. Properly designed and detailed bonded plates can significantly enhance the capacity and improve the ductility of shear deficient reinforced concrete coupling beams.
- ii. The nature of the retrofit will not impede existing mechanical services such as elevators and requires no significant structural modifications.
- iii. Bonded plate retrofits could be installed without effecting the use or occupancy of the structure.

The specific objectives of this part of the research programme are:

- i. To test full-scale specimens under reversed cyclic loading to determine the hysteretic response of shear deficient reinforced concrete coupling beams retrofitted with steel plates applied to one side of the beam.
- ii. To attempt to achieve a reversed cyclic loading response for the beam, equivalent to its nominal flexural capacity, and to ultimately change the mode of failure from a brittle shear failure to the development of ductile flexural hinges.
- iii. To investigate methods of ensuring continuity between the retrofit plate and reinforced concrete beam.
- iv. To develop design and detailing guidelines for the retrofit of shear deficient reinforced concrete coupling beams that enhance the shear capacity without significantly effecting the nominal flexural capacity of the beam.

1.8 Overview of Research Programme

Eight full-scale coupling beam specimens were fabricated and tested in the Jamieson Structures Laboratory at McGill University. Specimens S1 through S4 investigated the behaviour of steel coupling beams with their ends embedded in reinforced concrete walls. Specimen R0 was intentionally designed to as a shear deficient reinforced concrete coupling beam to be used as the control for Specimens R1 through R3. Specimens R1 through R3 were identical to Specimen R0 and were retrofitted with steel plates applied to one side of the beams to enhance their shear capacity. Each of Specimens R1 through R3 investigated different methods of connecting the retrofit plates. Table 1.1 summarises the details of the eight specimens tested. The S-series and R-series of specimens are reported in Chapters 2-4 and Chapters 7-9 of this report, respectively.

Specimen	Date of test	Description of Specimen
Specimen S1	August 1991	Preliminary test: shear critical steel coupling beam
Specimen S2	November 1991	Shear critical steel coupling beam
Specimen S3	April 1994	Shear critical, short span steel coupling beam
Specimen S4	January 1993	Flexure critical steel coupling beam
Specimen R0	July 1993	Unretrofitted concrete coupling beam (control)
Specimen R1	August 1993	Epoxyed steel plate retrofit of coupling beam
Specimen R2	November 1993	Epoxyed and bolted steel plate retrofit of beam
Specimen R3	January 1994	Epoxyed and bolted steel plate retrofit of coupling beam, extending onto walls

Table 1.1 Summary of specimens reported

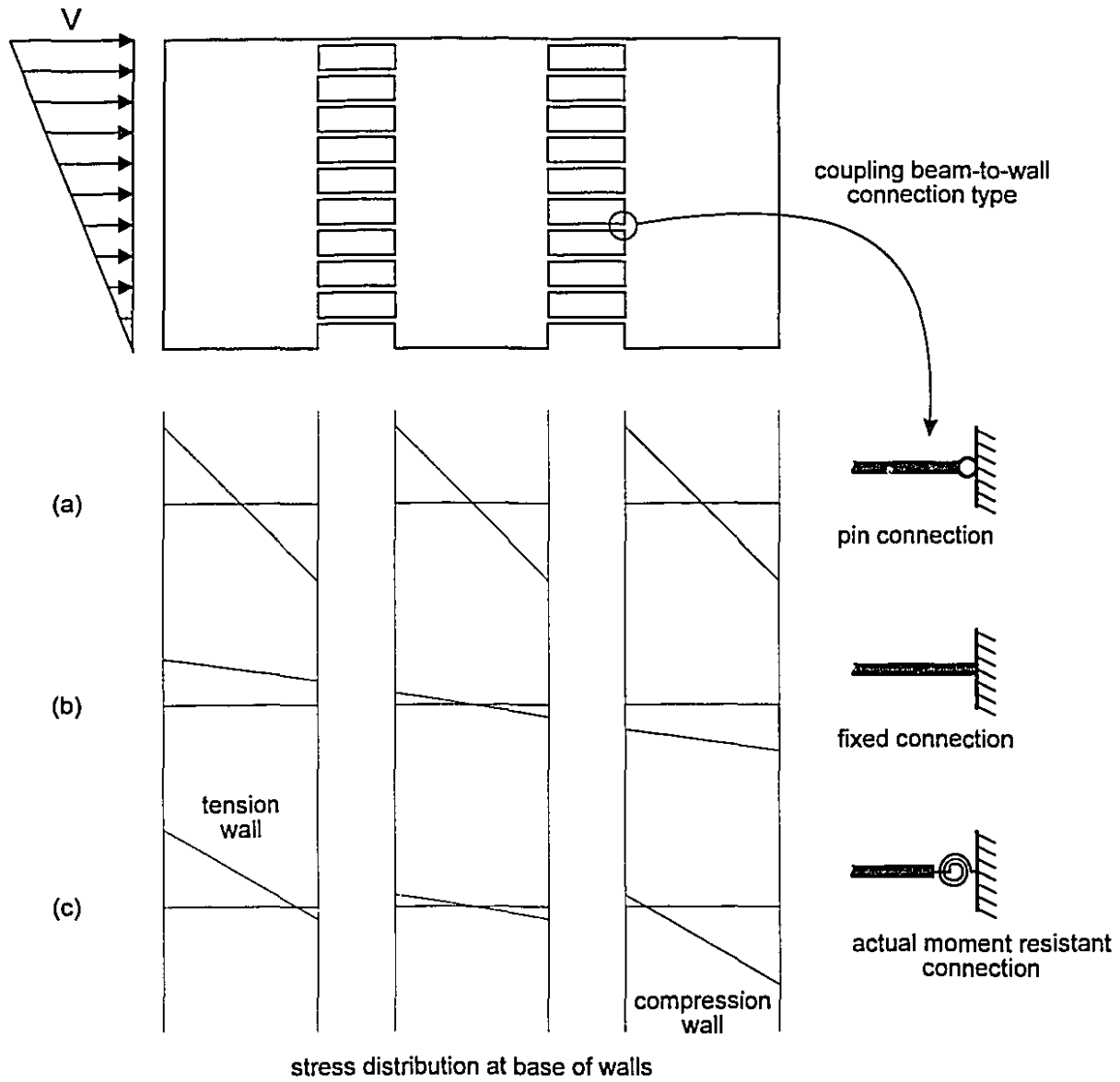
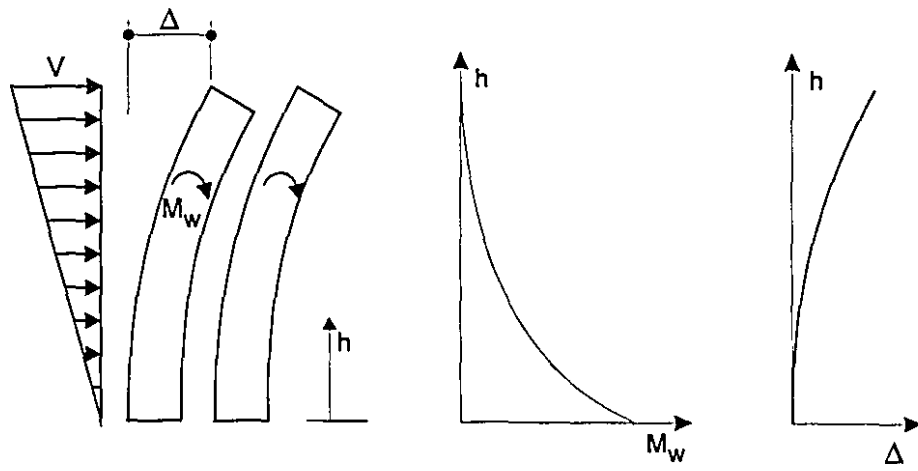
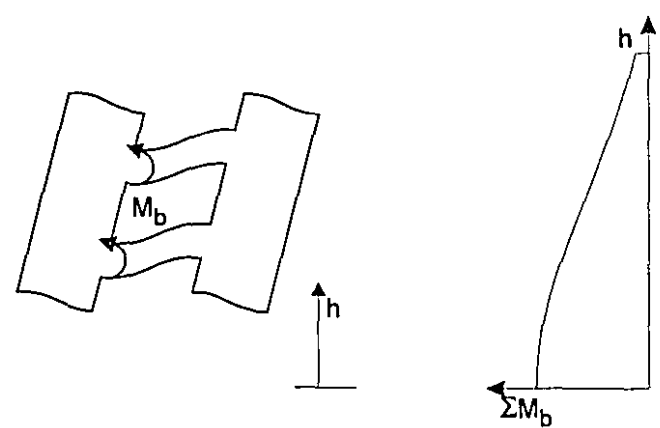


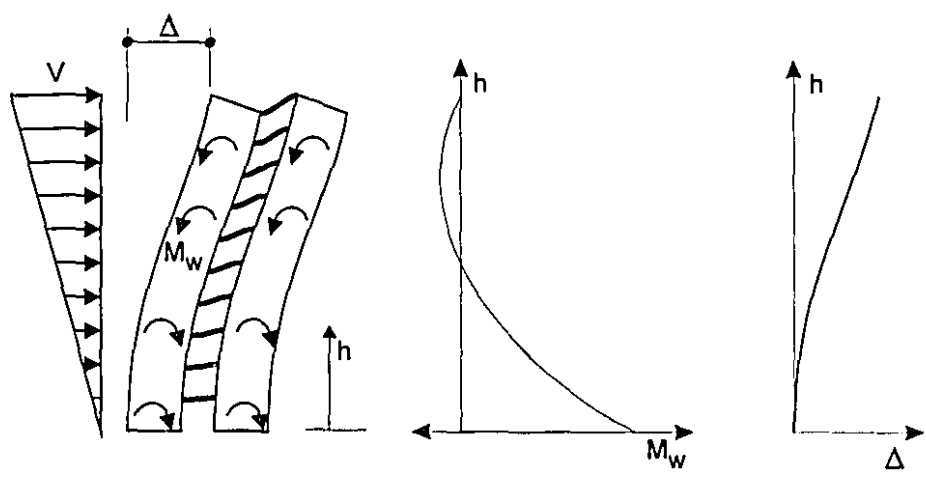
Figure 1.1 Stress distribution at the base of coupled wall structures



(a) individual cantilever walls

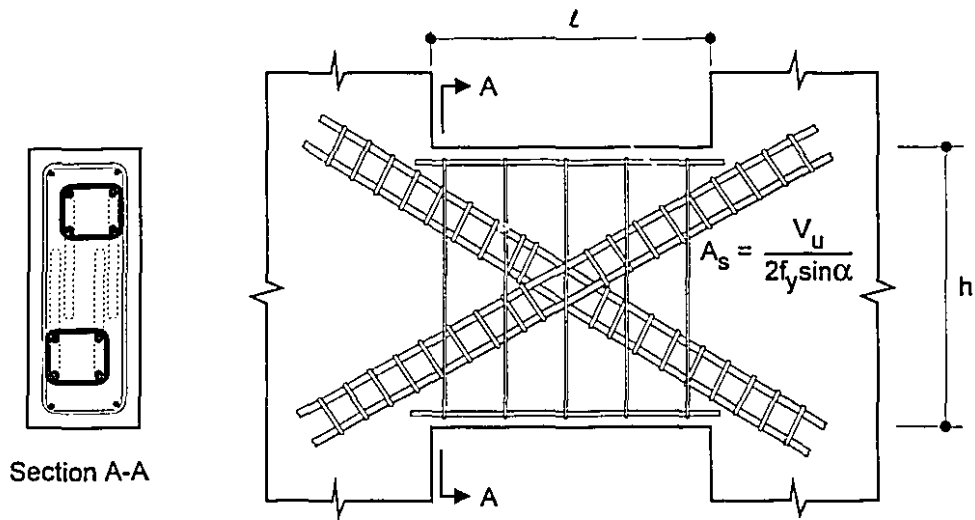


(b) reverse moment introduced by coupling beams

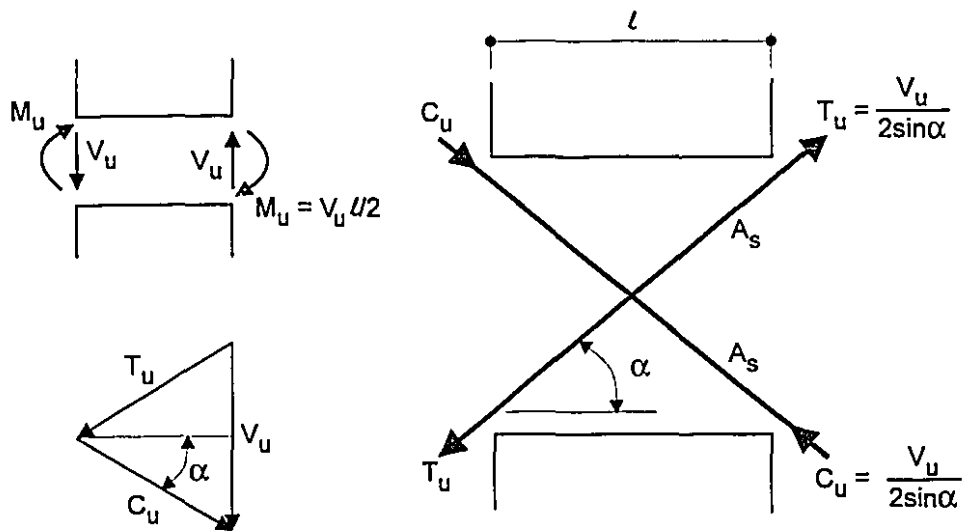


(c) coupled wall behaviour

Figure 1.2 Components of coupled wall behaviour



(a) diagonal coupling beam reinforcement



(b) manner by which diagonal reinforcing resists forces

Figure 1.3 Diagonally reinforced concrete coupling beam (after Park and Paulay, 1975)

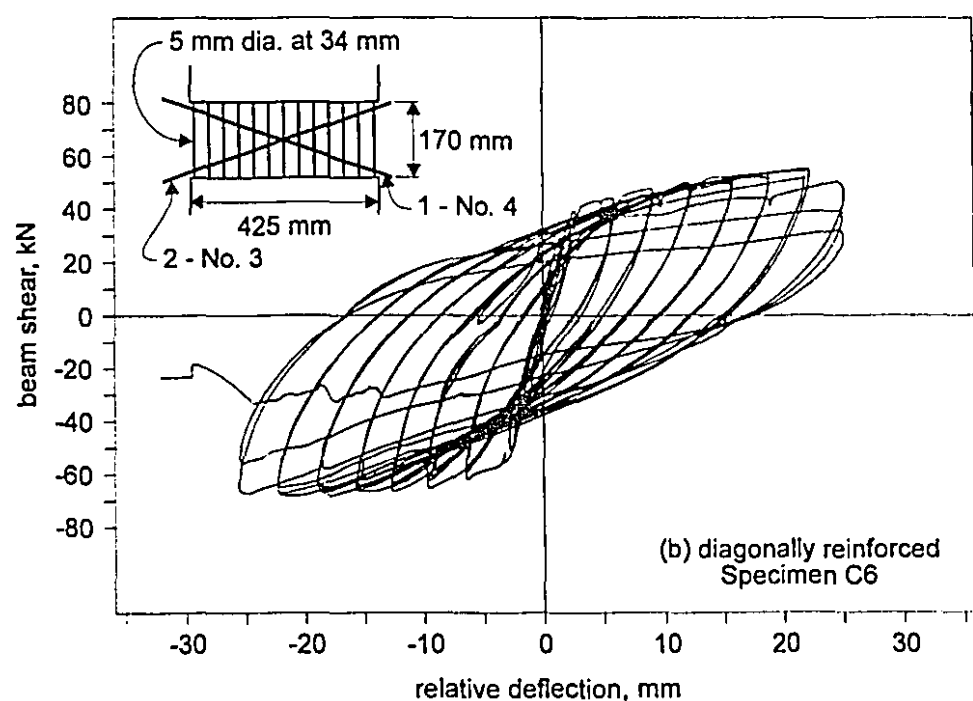
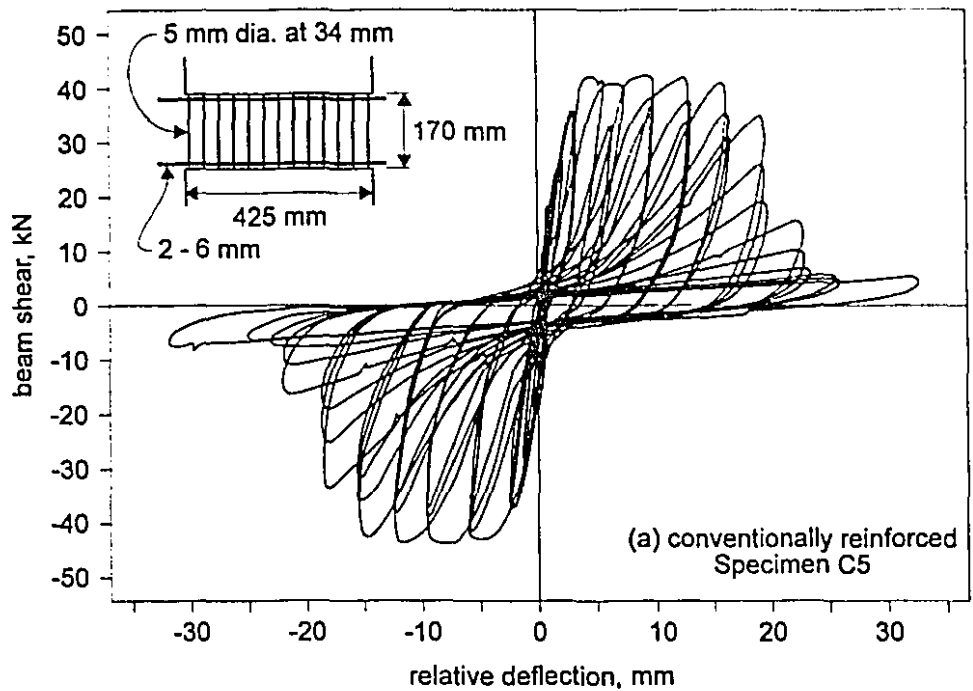


Figure 1.4 Conventionally and diagonally reinforced concrete coupling beams having span-to-depth ratios of 2.5 tested by Shiu et al. (1978)

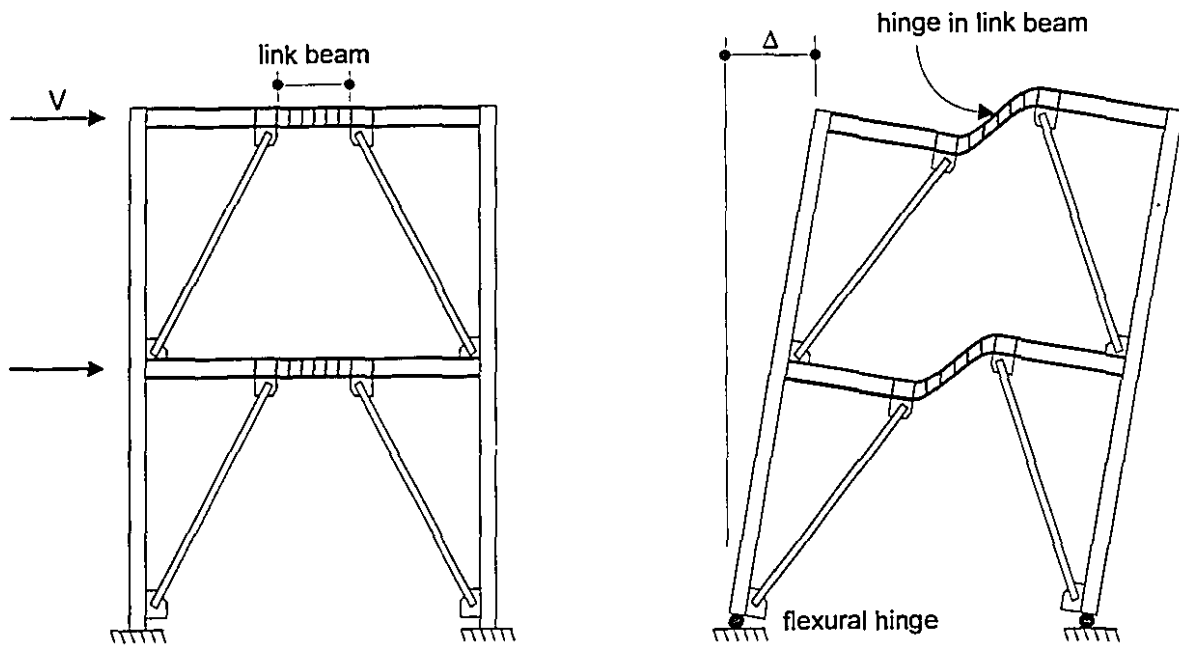


Figure 1.5 Steel link beam in an eccentrically braced frame

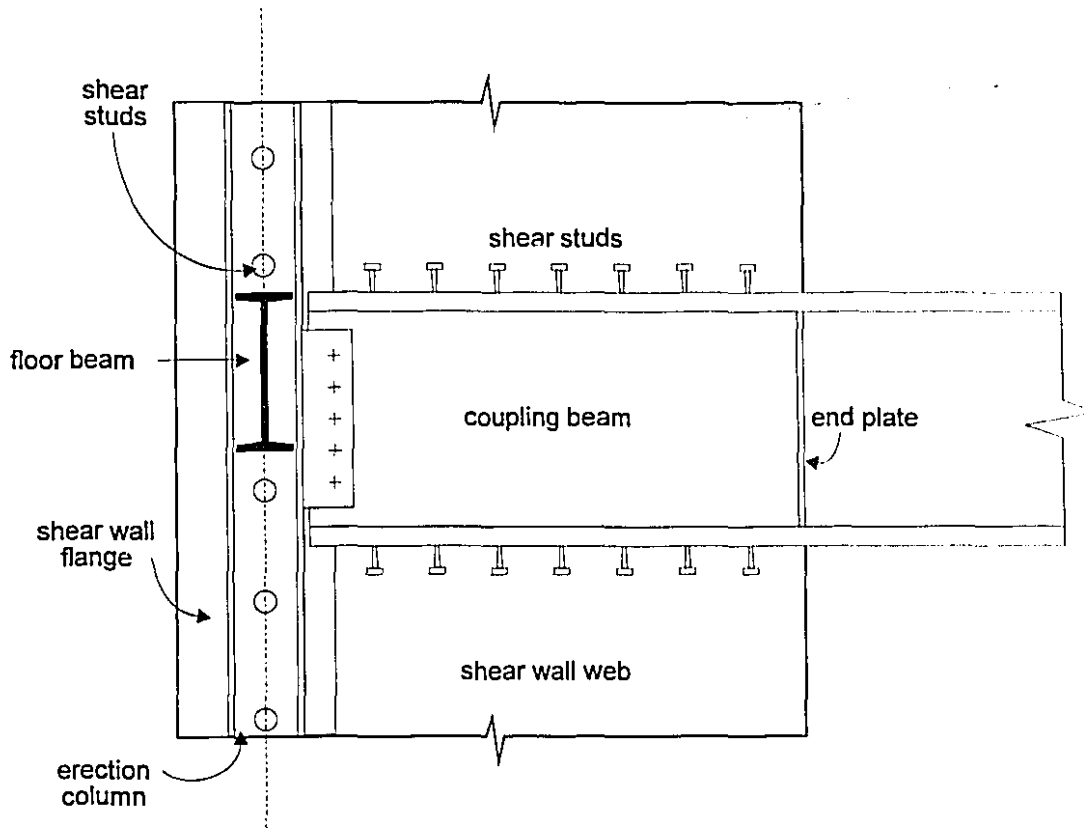


Figure 1.6 Steel coupling beam and frame embedded in reinforced concrete wall
(after Taranath, 1982)

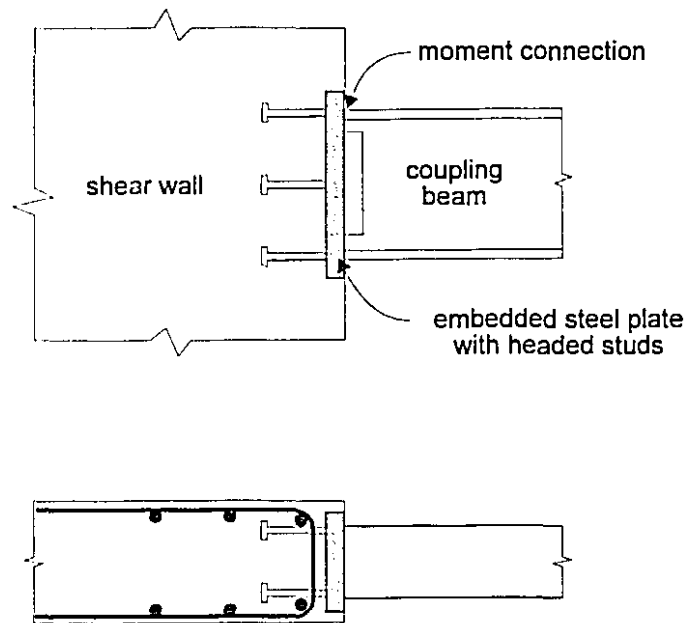
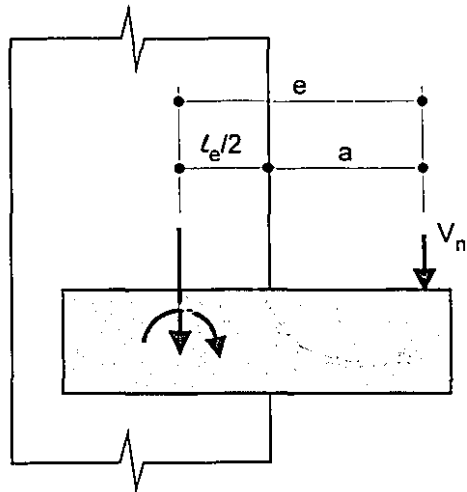
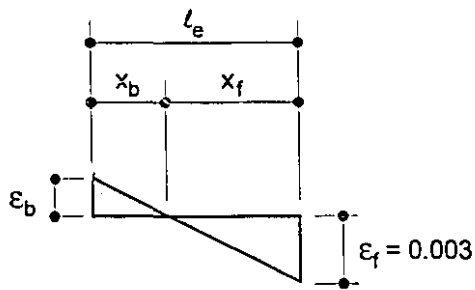


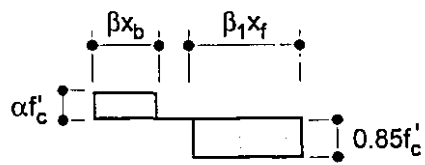
Figure 1.7 Embedded plate connection (after Roeder and Hawkins, 1981)



(a) embedment geometry



(b) assumed strain distribution



(c) assumed stress distribution

Figure 1.8 Structural section embedded in precast concrete
(after Marcakis and Mitchell, 1980)

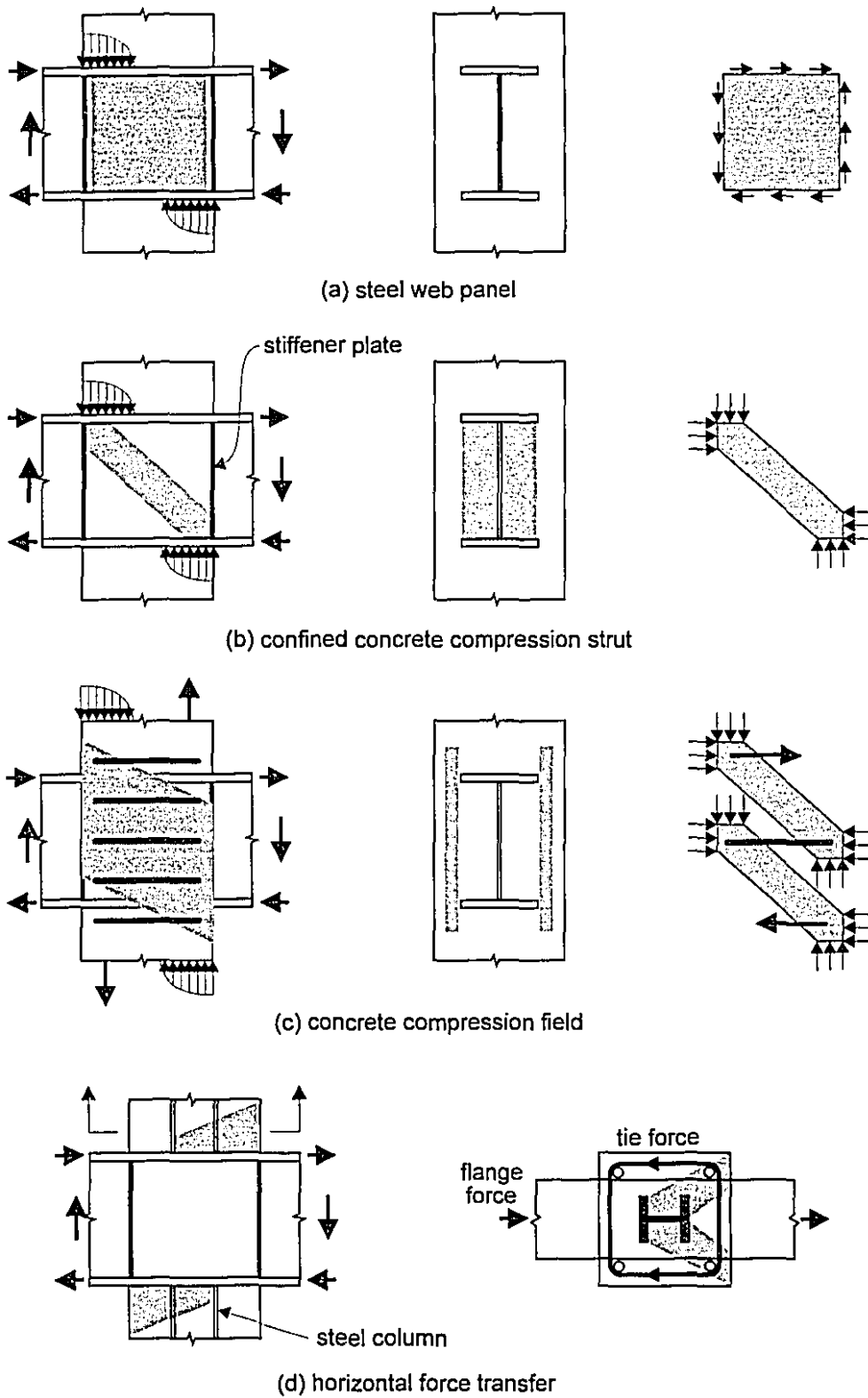


Figure 1.9 Components of response of joints in composite frames (after Sheikh et al, 1989)

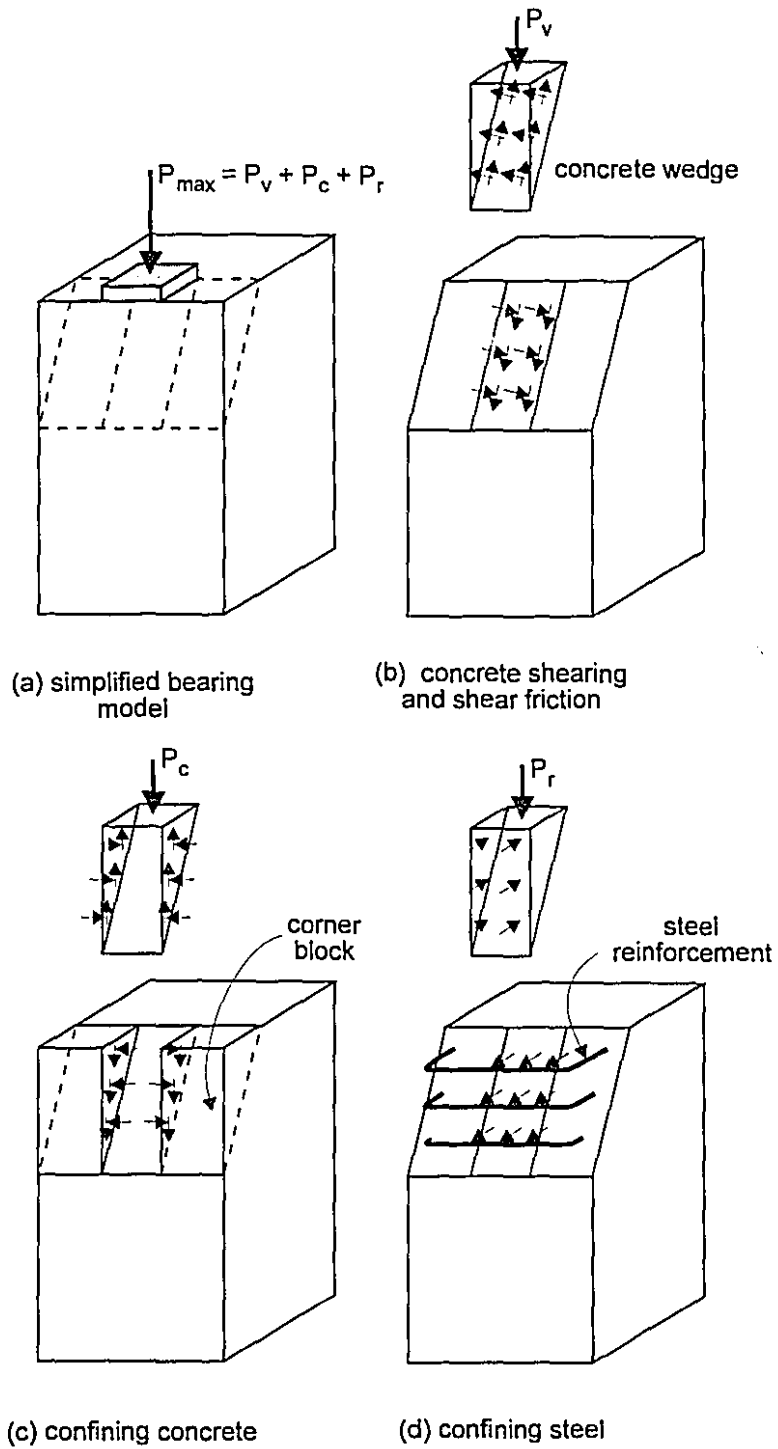


Figure 1.10 Response components of bearing resistance portion of composite frame joint behaviour (after Kanno, 1993)

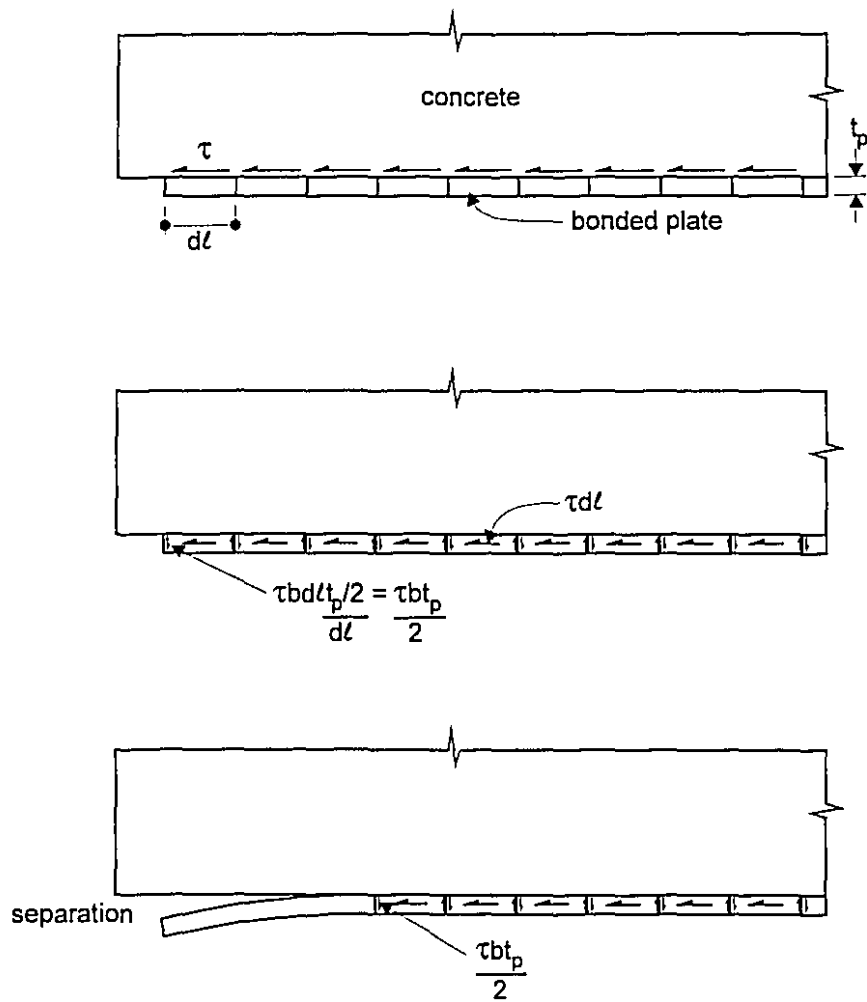


Figure 1.11 Separation of bonded steel plate and concrete
(after Jones et al, 1984)

Chapter 2

Steel Coupling Beam Experimental Programme

2.1 Design of the Steel Coupling Beams

The steel coupling beams were designed in accordance with the seismic design requirements for link beams in eccentrically braced frames of the available Canadian steel design standard. Specimens S1, S2 and S4 were designed in accordance with Appendix D, *Seismic Design Requirements for Eccentrically Braced Frames*, of CAN/CSA S16.1 M89 (CSA, 1989). Specimen S3 was designed in accordance with Clause 27.6, *Ductile Eccentrically Braced Frames*, of CAN/CSA S16.1 M94 (CSA, 1994). Clause 27.6 of the 1994 Standard replaced Appendix D in the 1989 CSA Standard. Furthermore the 1994 Standard incorporates a number of changes from 1989 with respect to beam rotational capacities and intermediate stiffener detailing. These changes reflect design recommendations adopted by SEAOC (1988), NEHRP (1991) and AISC (1992) in the United States. As a result of these changes, the stiffener designs of Specimens S1, S2 and S4 do not exactly conform to the 1994 standard. This lack of conformance did not appear to effect the response of the specimens in any way.

For the desired behaviour of a coupled wall system to be attained, the coupling beams must yield before the walls, behave in a ductile manner and exhibit significant energy absorbing characteristics. Unlike reinforced concrete beams, which must be designed to avoid shear failures, steel coupling beams are ductile and able to absorb significant amounts of energy when detailed to yield in shear rather than flexure. Since the shear-to-moment ratio is typically large for shorter coupling beams, "shear critical" design criteria are attainable.

Specimens S1 through S3 were designed as shear critical coupling beams. The design criteria was to ensure that the ultimate shear capacity of the coupling beam could developed while the beam remained elastic in flexure.

The steps followed for designing and detailing the clear span of the shear critical coupling beams are as follows (Harries et al, 1993). The numbers in brackets refer to clauses of CAN/CSA S16.1 M94.

Step 1: Determine the required area of the web, A_w , to resist the factored shear, V_f , from the expression for plastic shear capacity, V_r (13.4.1.2):

$$V_f \leq V_r = 0.55A_w F_y \quad (2.1)$$

where F_y is the specified minimum yield stress of steel.

Step 2: Determine the required section modulus, Z , such that the section has a moment resistance, M_r , greater than the moment corresponding to the development of strain hardening in shear (13.5). In determining Z , the contribution of the web should be neglected.

$$Z = \frac{M}{\phi F_y} \quad (2.2)$$

where: $M = \frac{\ell_{eff}}{2} \times 1.27V_r$ (2.3)

ℓ_{eff} = the clear span of the coupling beam, ℓ , plus twice the concrete cover, c , to account for cover spalling

ϕ = material resistance factor, typically taken as 0.90, and the factor 1.27 accounts for the development of strain hardening in the web.

Step 3: Ensure that both the web and flanges of the section conform to the limits for Class 1 sections (11.1):

for the web: $\frac{h}{w} \leq \frac{1100}{\sqrt{F_y}}$ (2.4)

where h and w are the height and width of the web, respectively.

for the flanges: $\frac{b}{2t} \leq \frac{145}{\sqrt{F_y}}$ (2.5)

where b and t are the width and thickness of the flange, respectively.

Step 4: In order to control out-of-plane buckling, the effective length of the beam, ℓ_{eff} , must not exceed the maximum unsupported length of the coupling beam, ℓ_{cr} (27.6.9.2):

$$\ell_{eff} \leq \ell_{cr} = \frac{200b}{\sqrt{F_y}} \quad (2.6)$$

Step 5: Provide full-depth stiffeners, with a thickness no less than $0.75w$ nor 10 mm, at the faces of the concrete walls (27.6.5.1). These stiffeners should be flush with the flange tips in order to simplify formwork details.

Step 6: Provide full-depth intermediate stiffeners as required by Clause 27.6.5.

The following steps for designing the embedded portion of a shear critical coupling beam were developed after the testing of Specimen S1 (Harries, 1992). Specimen S2 was designed considering these additional steps.

Step 7: In order to ensure that the coupling beam remain elastic along its embedment, the embedded region is designed for a factored shear resistance, V_{re} , of:

$$V_{re} = \frac{2M_r}{\ell_{eff}} \quad (2.7)$$

thus, the required web thickness in the embedded region, w_e , can be found using Equation 2.1 as:

$$w_e = \frac{V_{re}}{0.55hF_y} \quad (2.8)$$

Step 8: Provide an additional intermediate stiffener on the embedded portion of the coupling beam at a distance equal to the concrete cover from the face of the wall. This stiffener will ensure that the web will not cripple if confinement is lost due to the cover concrete spalling.

In lieu of providing a thicker web over the embedded region of the coupling beam, Specimen S3 was detailed with intermediate stiffeners, conforming to Clause 27.6.5, extending over the length of the embedded portion of the beam as well as the clear span. This detail proved equally as effective in controlling shear yield in the embedded portion of the web.

For the sake of comparison, Specimen S4 was designed as a flexure critical coupling beam. The design criteria being that the beam should remain elastic in shear while developing flexural hinges at either wall face. In this case, a Class 1 rolled section which satisfies the flexural requirements of the beam will invariably satisfy the shear requirements. Once the section is chosen, the same detailing steps are required as for a shear critical section. However, in order to illustrate a design for nominal ductility, intermediate stiffeners (step 6, above) were not included on Specimen S4, otherwise it conforms to CAN/CSA S16.1 M89, Appendix D.

2.2 Design of the Reinforced Concrete Embedment Region

Since the coupling beam is expected to undergo significant inelastic deformation, its embedment must be capable of developing forces corresponding to the plastic capacity of the beam. The design of the concrete embedment is modelled after the design of steel haunches in precast concrete columns developed by Marcakis and Mitchell (1980) and recommended by the design handbooks of the Prestressed Concrete Institute (1985) and the Canadian Prestressed Concrete Institute (1987). This approach is discussed in Section 1.5.4. The shear

and moment in the coupling beam are resisted by the resultants of the two concrete stress blocks over the length of the embedment (see Fig. 1.8). The design criteria is, therefore, to provide an embedment length, adequate to develop the required moment and shear. The required embedment length, ℓ_e , can be determined from the expression for the shear capacity of the embedment, V_c (see Fig. 2.1):

$$V_c = \frac{0.85\phi_c f'_c b' (\ell_e - c)}{1 + \frac{3.6e}{(\ell_e - c)}} \geq 1.27V_r \quad (2.9)$$

where: b' = the effective width of the concrete compression block, defined as the width of the confined wall region measured between the longitudinal wall steel, but not exceeding 2.5 times the width of the embedded flange, b (Fig. 2.1(b))

e = the eccentricity of resultant shear loads from the centre of the embedment assuming that the concrete cover spalls (Fig. 2.1(a)), that is:

$$e = \frac{\ell + \ell_e + c}{2} \quad (2.10)$$

c = depth of concrete cover,

ℓ = clear span of the coupling beam,

f'_c = compressive strength of concrete,

ϕ_c = material resistance factor, typically taken as 0.60, and

$1.27V_r$ is the plastic shear capacity of the coupling beam.

The calculated embedment length, ℓ_e , is a minimum value. It is suggested that, in practice, longer embedment lengths be used. Longer embedments will lower the stress levels in the surrounding concrete and will reduce the tendency of the beam to 'ratchet' itself loose with cycling.

In applying this design procedure to the test specimens, the values of the material resistance factors, ϕ and ϕ_c , were taken as 1.0 and the embedment length chosen was very close to that required.

2.3 Description of Specimens

The details of the four steel coupling beams are shown in Fig. 2.2. Specimens S1 and S2 were tested, by the author, in a preliminary research programme (Harries, 1992). Details of the design and detailing of the specimens are given in Appendix A.

2.3.1 Specimen S1

Specimen S1 was designed as a shear critical coupling beam with an applied factored shear, V_f , of 260 kN. The 347 mm deep section had a clear span of 1200 mm and was

embedded a distance of 600 mm into each wall. The resulting span-to-depth ratio of the coupling beam was 3.46. The moment-to-shear ratio at the face of the wall was 0.60 m. In order to ensure that the section would remain elastic in flexure and that its flange would conform to Class 1 limits, it was necessary to design the specimen as a built-up section. The resulting section (see Fig. 2.2(a)) had 135 x 19 mm flanges and a 5 mm web. Full-depth, 10 mm intermediate stiffeners, spaced at 120 mm, were provided on one side of the web along the clear span. Stiffeners were provided on both sides of the web at the faces of the walls. No additional stiffeners were provided in the embedded region.

2.3.2 Specimen S2

The clear span of Specimen S2 was identical to that of Specimen S1. In order to ensure that the 600 mm embedded portion of the beam remained elastic throughout the test, the thickness of the embedded web, w_e , was increased from 5 mm to 8 mm. The thicker web plate was butt welded to the web in the clear span at a location 30 mm outside the face of each wall (see Fig. 2.2(b)). An additional intermediate stiffener was provided in the embedment at a location 65 mm from the face of the walls, corresponding to the location of the first longitudinal wall reinforcing steel. This stiffener was added in order to protect against web crippling in the embedment after the concrete cover had spalled.

2.3.3 Specimen S3

Specimen S3 was designed as a short shear critical coupling beam, comparable to typical shear links in eccentrically braced frames (Malley and Popov, 1983b). The applied factored shear, V_f , used for the design of Specimen S3 was 360 kN. The 450 mm clear span resulted in a moment-to-shear ratio at the face of the walls of only 0.225 m. This allowed a standard rolled steel section to be used. A W360 x 33 section was chosen, resulting in a span-to-depth ratio for the coupling beam of 1.29. This range of span-to-depth ratio is also more typical of many reinforced concrete coupling beams. The shorter span allowed a shorter embedment length of 500 mm to be used. Full-depth, 10 mm thick intermediate stiffeners, spaced at 150 mm, were provided on one side of the web along the clear span. Stiffeners were provided on both sides of the web at the faces of the walls. In lieu of providing a thicker web in the embedment region, full-depth intermediate stiffeners, spaced at 150 mm, were provided over the length of the embedment. The first of these stiffeners was located 75 mm inside the face of the wall in order to protect against web crippling in the event of cover spalling.

2.3.4 Specimen S4

The 1200 mm clear span of Specimen S4 was designed as a flexure critical coupling beam having a nominal flexural capacity of 163 kNm (corresponding to an applied shear of 270 kN). For the case of a flexure critical coupling beam, most Class 1 rolled sections would satisfy the requirement of remaining elastic in shear while attaining their full plastic flexural capacity. A W360 x 33 rolled section was chosen for Specimen S4. The considerations for detailing this less ductile specimen were to confine the flexural hinges to the clear span of the beam. Stiffeners were provided at the faces of the walls to arrest the development of a flexural hinge into the embedded portion of the beam. Furthermore, 5 mm cover plates were welded to the flanges of the beam over the embedded regions to ensure that the embedments remained elastic.

2.4 Design and Detailing Wall Reinforcement

The reinforced concrete walls were designed in accordance with Clause 21, *Special Provisions for Seismic Design*, of CAN/CSA A23.3-M84 (CSA, 1984). The 300 mm thick, 1500 mm long by 1800 mm high walls, shown in Fig 2.3, were identical for each of the four specimens. The thickness of the walls in the region of the embedment will be partially governed by the width of the embedded beam flange, which must fit within the vertical wall steel. For this reason, it is unlikely that the wall thickness in the region of the embedment could be less than 300 mm for most practical applications. For applications with larger coupling beams, "barbell" shaped walls would become an appropriate design solution.

A region of concentrated reinforcement, consisting of 6 No. 25 reinforcing bars was provided from the inside face of each wall, extending over the length of the embedment. This steel resulted in a reinforcement ratio in the region of concentrated reinforcement of about 1.8%. Due to the nature of seismic loading it is important to provide sufficient steel near the face of the wall to control the flange-concrete interface gap opening. To control this interface opening, concentrated reinforcement, adequate to resist the maximum probable shear resistance of the coupling beam should cross this interface (see Fig. 2.1(b)). Thus the required area of concentrated reinforcement, A_{sc} , in addition to the reinforcement required to resist the wall design forces is:

$$A_{sc} \geq \frac{1.27V_r}{f_y} \quad (2.11)$$

where f_y is the specified minimum yield stress of the reinforcing steel.

In order to effectively control the flange-concrete interface gap opening, it is recommended that two thirds of A_{sc} be provided over the first half of the embedment (Harries et al, 1993).

Beyond the region of concentrated reinforcement, No. 10 vertical bars were located at 300 mm centres, in accordance with the requirements of Clause 21 of CAN/CSA A23.3-M84. Two No. 25 bars were located at the back of the walls to aid the fabrication of the reinforcing cage. All the vertical bars were welded to the loading beam to ensure displacement compatibility between the test frame and the specimen. As can be seen in Fig. 2.3, the spacing of vertical steel in Specimen S3 was slightly adjusted to account for the shorter embedment length.

Two No. 10 horizontal ties were provided immediately above and below the embedded beam. These ties serve to anchor the outwards thrust of the inclined compressive struts radiating from the embedment region. The remaining horizontal ties were placed at 260 mm centres, in accordance with the minimum reinforcement requirements of Clause 21 of CAN/CSA A23.3-M89.

All of the reinforcing steel was fully developed in the region of the embedment.

2.5 Material Properties

Table 2.1 gives the measured material properties for the coupling beams, reinforcing steel and concrete used for Specimens S1 through S4. Figure 2.4 shows the observed material stress-strain curves for the materials used for Specimens S1 through S4.

	S1	S2	S3	S4
Concrete compressive strength, f'_c , at time of test	25.9 MPa (45 days)	43.1 MPa (42 days)	32.9 MPa (16 days)	35.0 MPa (29 days)
Concrete modulus of rupture, f_r	4.84 MPa	data missing	4.65 MPa	4.74 MPa
Concrete splitting tensile strength, f_{sp}	3.83 MPa	4.02 MPa	3.91 MPa	3.92 MPa
No. 10 reinforcing bars	$f_y = 458$ MPa $f_u = 740$ MPa $\epsilon_{ult} = 19\%$		$f_y = 447$ MPa $f_u = 660$ MPa $\epsilon_{ult} = 21\%$	
No. 25 reinforcing bars	$f_y = 410$ MPa $f_u = 676$ MPa $\epsilon_{ult} = 14\%$		$f_y = 437$ MPa $f_u = 658$ MPa $\epsilon_{ult} = 14\%$	
Beam web	$F_y = 320$ $F_u = 468$ $\epsilon_{st} = 3.2\%$ $\epsilon_{ult} = 32\%$	$F_y = 309$ $F_u = 427$ $\epsilon_{st} = 4.0\%$ $\epsilon_{ult} = 37\%$	$F_y = 403$ MPa $F_u = 515$ MPa $\epsilon_{st} = 2.6\%$ $\epsilon_{ult} = 34\%$	
Embedded Web		$F_y = 276$ $F_u = 442$ $\epsilon_{st} = 4.0\%$ $\epsilon_{ult} = 34\%$		
Beam Flange	$F_y = 372$ $F_u = 544$ $\epsilon_{st} = 4.4\%$ $\epsilon_{ult} = 36\%$	$F_y = 295$ $F_u = 499$ $\epsilon_{st} = 2.4\%$ $\epsilon_{ult} = 39\%$	$F_y = 378$ MPa $F_u = 512$ MPa $\epsilon_{st} = 2.5\%$ $\epsilon_{ult} = 35\%$	

Table 2.1 Material properties of steel coupling beam specimens

2.5.1 Coupling Beam Steel

The coupling beams of Specimens S1 and S2 were fabricated with Grade 300W plate material conforming to CSA Standard G40.21. The beams of Specimens S3 and S4 were fabricated from commercially available Grade 300 rolled sections. Additional samples of both the plate stocks and the rolled section were provided by the fabricator for material strength tests. Tension tests were carried out according to the procedure defined in ASTM Standard E8-85a. Applied load and extension over a 50 mm gauge length were recorded up to the onset of strain hardening, ultimate load and extension were also noted. The average results of the

tension tests are summarised in Table 2.1 and Fig. 2.4(c) and (d). The 10 mm, Grade 300W plate stock from which the stiffeners were fabricated was not tested.

2.5.2 Reinforcing Steel

In accordance with Clause 21.2.5.1 of CAN/CSA A23.3-M84, the reinforcing steel used conformed to CSA Standard G30.18. Tension tests were performed on 300 mm lengths of each bar size. Applied load and extension over a 50 mm gauge length were recorded up to the onset of strain hardening. The average results of the tension tests are presented in Table 2.1 and Fig. 2.4(b).

2.5.3 Concrete

Ready-mix concrete with a minimum specified 28 day compressive strength of 30 MPa was used for each of the four specimens. Table 2.2 gives the composition and properties of the concrete mix as specified by the supplier.

Component or Property	Specified quantity
Cement (Type 10)	355 kg/m ³
Water	155 l/m ³
Sand	800 kg/m ³
Course Aggregate (5 - 20 mm)	1035 kg/m ³
Water reducing agent (PDA 25-XL)	1110 mL/m ³
Air entraining agent (Micro-air)	240 mL/m ³
Superplasticiser (SPN) (added on site)	960 mL/m ³
Water-cement ratio	0.44
Slump	150 mm
Entrained air	5 - 8%

Table 2.2 Specified concrete composition and properties

At least 15 150 x 300 mm cylinders and 4 150 x 150 x 600 mm flexural beams were prepared from each concrete batch. Compression, splitting and third point loading flexural tests were conducted to determine the average concrete compressive strength, f'_c , splitting tensile strength, f_{sp} , and the modulus of rupture, f_{cr} . The average concrete strengths at the time of testing are reported in Table 2.1 and the average concrete compressive strengths are shown in Fig. 2.4(a).

2.6 McGill University Coupled Wall Testing Apparatus

Figure 2.5 illustrates the manner by which the test set-up duplicates the loading and boundary conditions of the portion of coupled wall being represented. Each test specimen models a single coupling beam and the portion of wall immediately above and below the beam. The response of typical coupled wall system reveals that the critical coupling beam is usually about one third of the way up the structure. Furthermore, in determining the response of a coupled wall system, it is assumed that the centroidal axes of the walls remain parallel at any level of the structure. Figures 2.5(a) and (b) show the location of the test specimen and its deformation pattern in an actual structure, respectively. Figure 2.5(c) illustrates the manner in which the testing apparatus simulates the applied shear, V , and the relative displacement, δ , of the actual structure. As in the actual structure, the centroidal axes of the walls are maintained parallel throughout testing.

The McGill University Coupled Wall Testing Apparatus is shown in Fig. 2.6. In order to clamp the test specimens to the testing apparatus and to simulate the compressive stresses in the walls due to gravity loads, post-tensioned vertical rods were strapped to the exterior of each wall as shown in Fig. 2.6. Each pair of rods was post-tensioned to a force of 225 kN. The rods were located at 250 mm centres, resulting in a uniform applied compressive stress of 3 MPa on each wall.

The loads and reactions are applied to the walls through the loading beams at the base of each wall. The west, or fixed beam was post-tensioned to the reaction floor of the laboratory with threaded rods. The total tie-down force was determined to be 1.5 times the maximum applied load (assumed to be the capacity of the loading system used). The tie-down closest to the coupling beam was post-tensioned to 1.25 times the maximum applied load, the further tie-down was post-tensioned to about 0.25 times the maximum applied load. For Specimens S1, S2 and S4, these two forces were 670 kN and 130 kN, respectively. For Specimen S3 (whose maximum applied load was notably higher), these forces were 800 kN and 220 kN, respectively.

The east, or loaded beam is loaded vertically in a reversed cyclic manner such that the centroids of the walls remain parallel. The loading is applied by two loading systems, each with their line of action passing through the midspan of the coupling beam. Upwards, or positive loading is applied with a 120 kip (534 kN) hydraulic ram located between the reaction floor and loading beam. Downwards, or negative loading is applied with tension rods and two 60 kip (267 kN) hydraulic rams located beneath the reaction floor. A single hydraulic ram is located at the back of the loaded wall to provide the forces required to balance the dead load of the specimen and keep the walls parallel.

Both walls are restrained from out-of-plane or lateral movement. The fixed wall is braced with heavy steel angles to a reaction frame post-tensioned to the reaction floor. The loaded wall is restrained against lateral movement with heavy duty rollers fixed to a similar frame. The out-of-plane support was designed for a force equal to 6% of the longitudinal flange force in the coupling beam (CSA S16.1, Clause 27.6.6). This value corresponds to 46 kN for Specimens S1 and S2 and 19 kN for Specimens S3 and S4. These forces would only develop if the coupling beams were to buckle laterally, as such the lateral restraint was present only as a safety measure. No significant out-of-plane displacements were observed in any of the tests.

2.7 Instrumentation

Figure 2.7 shows the instrumentation used for Specimens S1 through S4. An array of linear voltage differential transformers (LVDTs) measured the vertical displacements of the walls, allowing the differential displacement and rotations of each wall to be determined.

Electrical resistance strain gauges were located along the flanges of the coupling beams to determine the flexural strains in the beams. Strain gauges were also located at the tips of the flanges near the faces of the walls in order to determine strain variations across the width of the flanges and to give an indication of local flange instabilities.

Strain rosettes (0° - 45° - 90°) were located along the embedded and clear span portions of the coupling beam web (on the side without stiffeners) in order to record shear strains in the web. Strain gauges on the exposed portion of the coupling beam were often backed up with mechanical strain targets punched directly into the steel.

Strain gauges were also located on the reinforcing steel in the region of the embedment. Figure 2.7(b) shows the layout of these gauges which varied from specimen to specimen.

Positive loads were recorded with two 445 kN capacity load cells located between the hydraulic rams and the loading beam. Negative loads were recorded with 334 kN capacity load cells located on each tension rod. An additional load cell was located at the back of each specimen to record the force required to keep the walls parallel. All recorded load values were post-processed to remove the effect of the dead load of the specimen, leaving only the shear applied to the coupling beam.

All load, displacement and strain readings were recorded with a Doric 245 data acquisition system and simultaneously displayed to facilitate ease of test control.

In addition to automatic instrumentation, the exposed portions of the coupling beams were coated with a whitewash. The whitewash begins flaking at a strain equivalent to the yield strain of steel. As such the whitewash allows visual verification of yielding as well as illustrates the "yield lines" at earlier stages of the test.

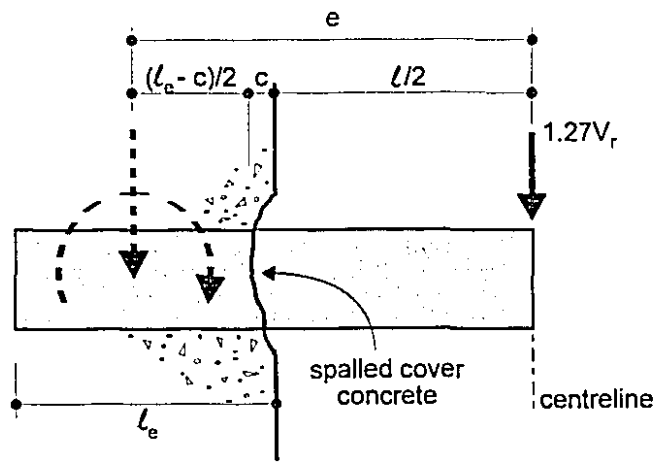
2.8 Load Histories

The loading history for each specimen is shown in Fig. 2.8. In order to control testing, applied shear versus deflection of the loaded walls was plotted as testing progressed. Upwards loads and deflections are considered as positive.

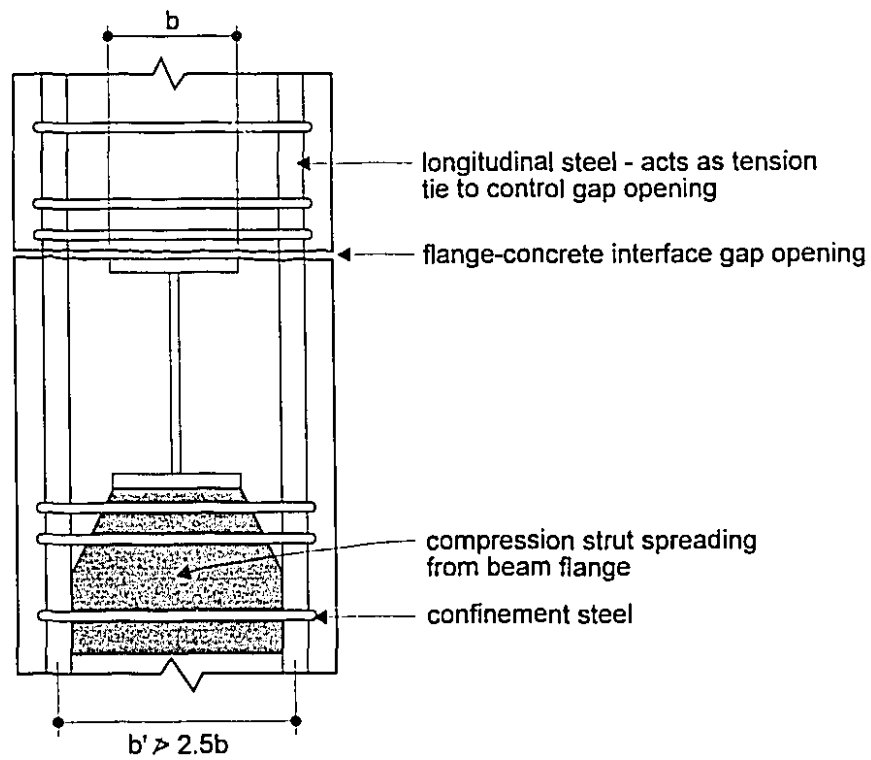
The tests were conducted under "load control" up to the point of general yield and "deflection control" thereafter. The specimens were cycled three times at each load or deflection level. Each full cycle involved a positive and negative peak. Load control involved cycling the specimens at predetermined load levels until general yield was achieved. Multiples of the deflection at general yield, δ_y , were then used as cycle peaks for deflection control. Testing was stopped when a 20% load decay from ultimate was reached or the travel of the testing apparatus was exhausted. At this point a final monotonic loading cycle was carried out to determine the post-peak response of the specimens. Table 2.3 gives the load and deflection peaks, the value used for δ_y and the value of the final monotonic loading cycle for each test. It must be noted that these values were used for test control, the actual experimental results were determined after post-processing.

	Specimen S1	Specimen S2	Specimen S3	Specimen S4
Load Control (3 cycles each)	± 100 kN ± 200 kN ± 250 kN	± 100 kN ± 200 kN	± 200 kN ± 350 kN	± 120 kN ± 240 kN
δ_y	± 12 mm	± 11 mm	± 4 mm	± 13 mm
Deflection Control (3 cycles each)	$\pm 2\delta_y$ $\pm 4\delta_y$ $\pm 6\delta_y$ $\pm 8\delta_y$	$\pm 2\delta_y$ $\pm 4\delta_y$ $\pm 6\delta_y$ $\pm 8\delta_y$ $\pm 10\delta_y$	$\pm 2\delta_y$ $\pm 4\delta_y$ $\pm 6\delta_y$ $\pm 8\delta_y$ $\pm 10\delta_y$	$\pm 1.5\delta_y$ $\pm 2\delta_y$ $\pm 3\delta_y$
Final monotonic	$+10.2\delta_y$	$-13.6\delta_y$	-	$-7\delta_y$

Table 2.3 Summary of load histories of Specimens S1 through S4

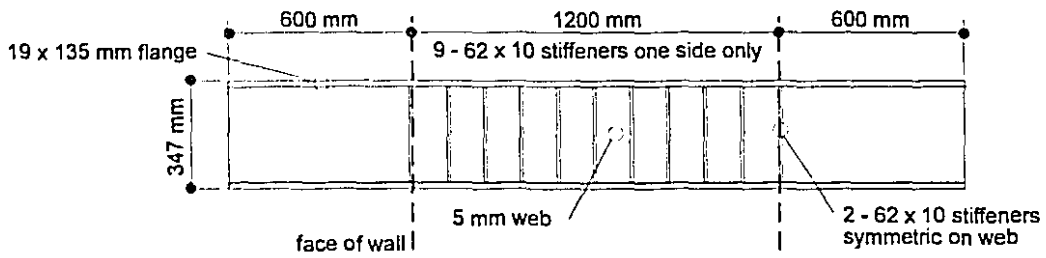


(a) eccentricity of resultant shear

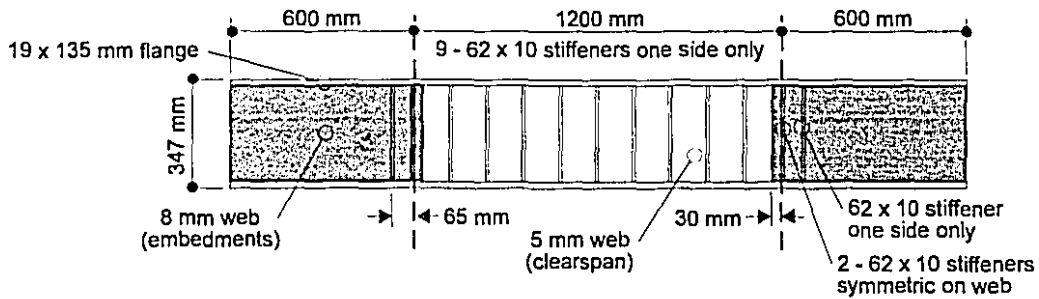


(b) effective width of bearing and tension steel requirement across flange-concrete interface

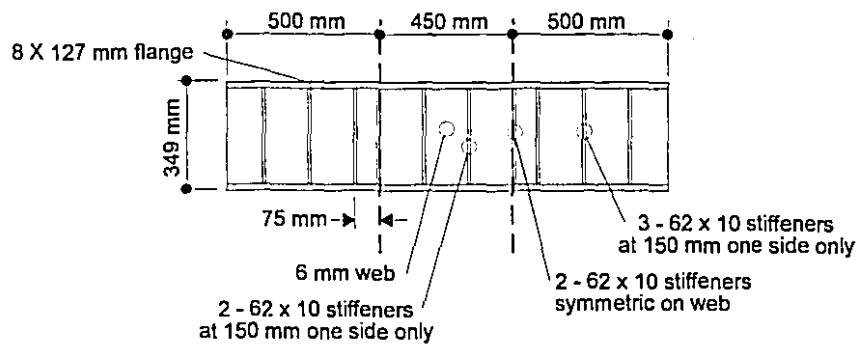
Figure 2.1 Parameters of embedment design



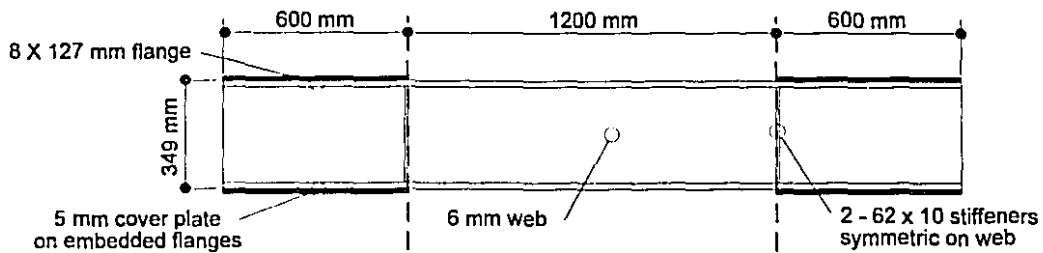
(a) Specimen S1 - shear critical built-up section



(b) Specimen S2 - shear critical built-up section

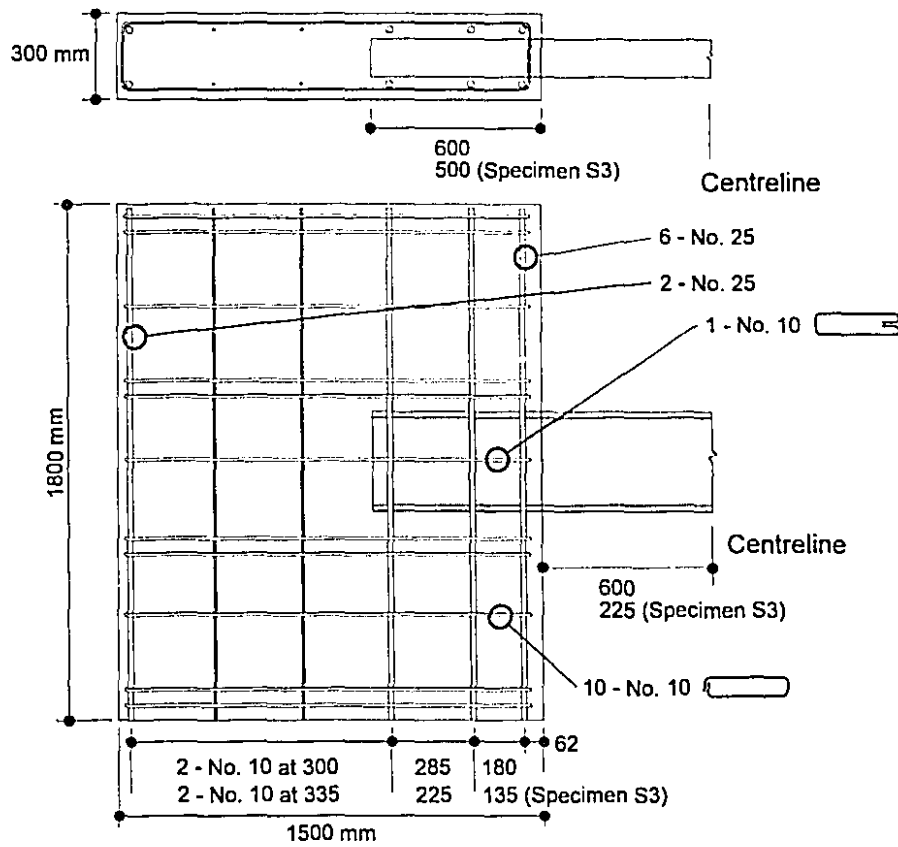


(c) Specimen S3 - shear critical W360 x 33

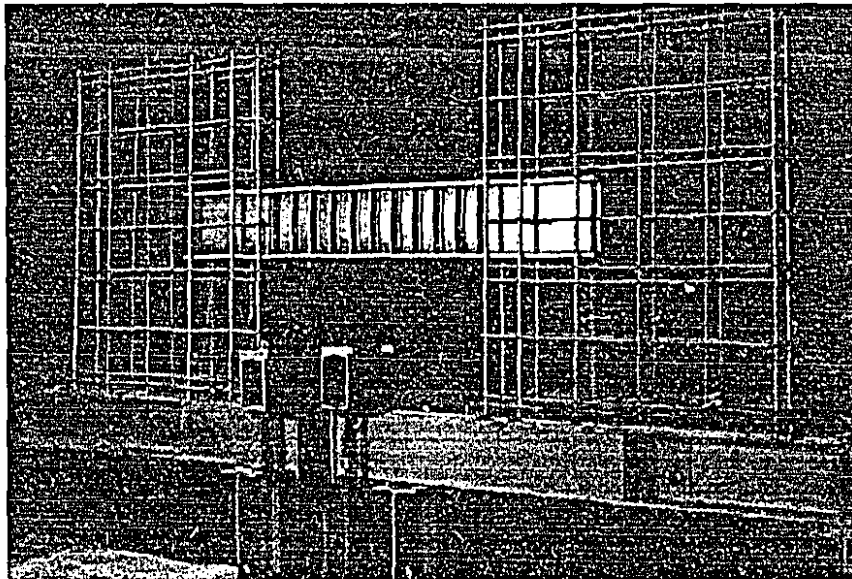


(d) Specimen S4 - flexure critical W360 x 33

Figure 2.2 Coupling beam details for Specimens S1 through S4

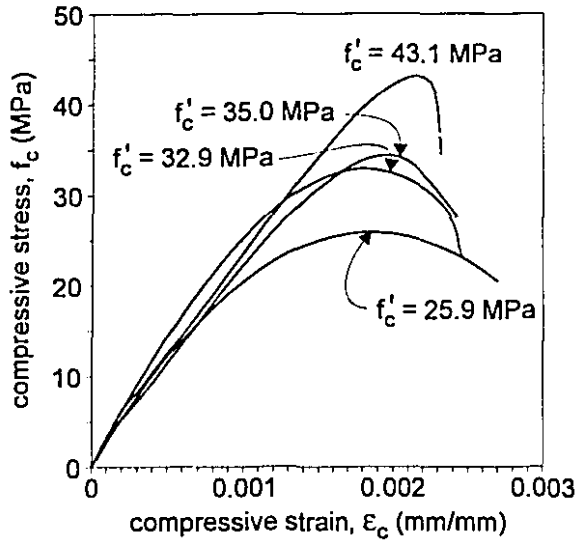


(a) Specimens S1 through S4

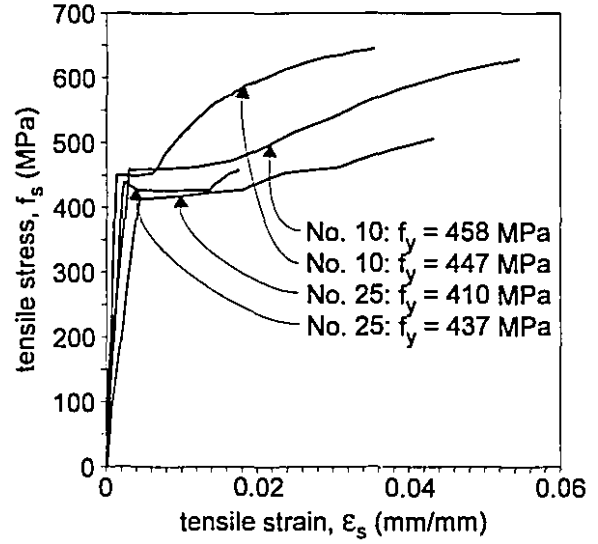


(b) Specimen S1

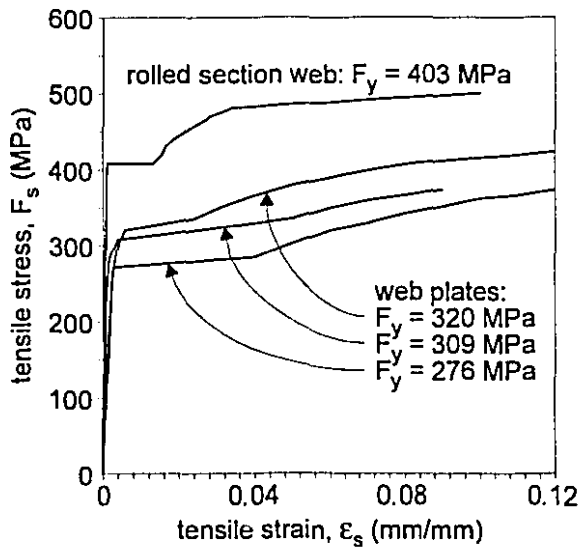
Figure 2.3 Reinforced concrete wall details for Specimens S1 through S4



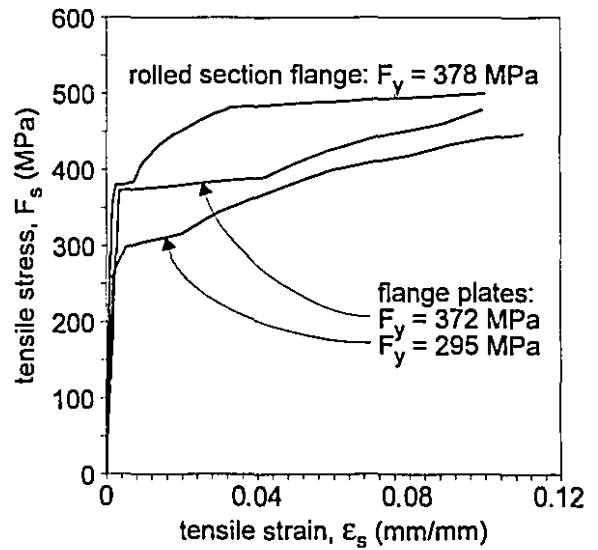
(a) concrete



(b) reinforcing steel



(c) coupling beam webs



(d) coupling beam flanges

Figure 2.4 Material characteristics of steel coupling beam specimens

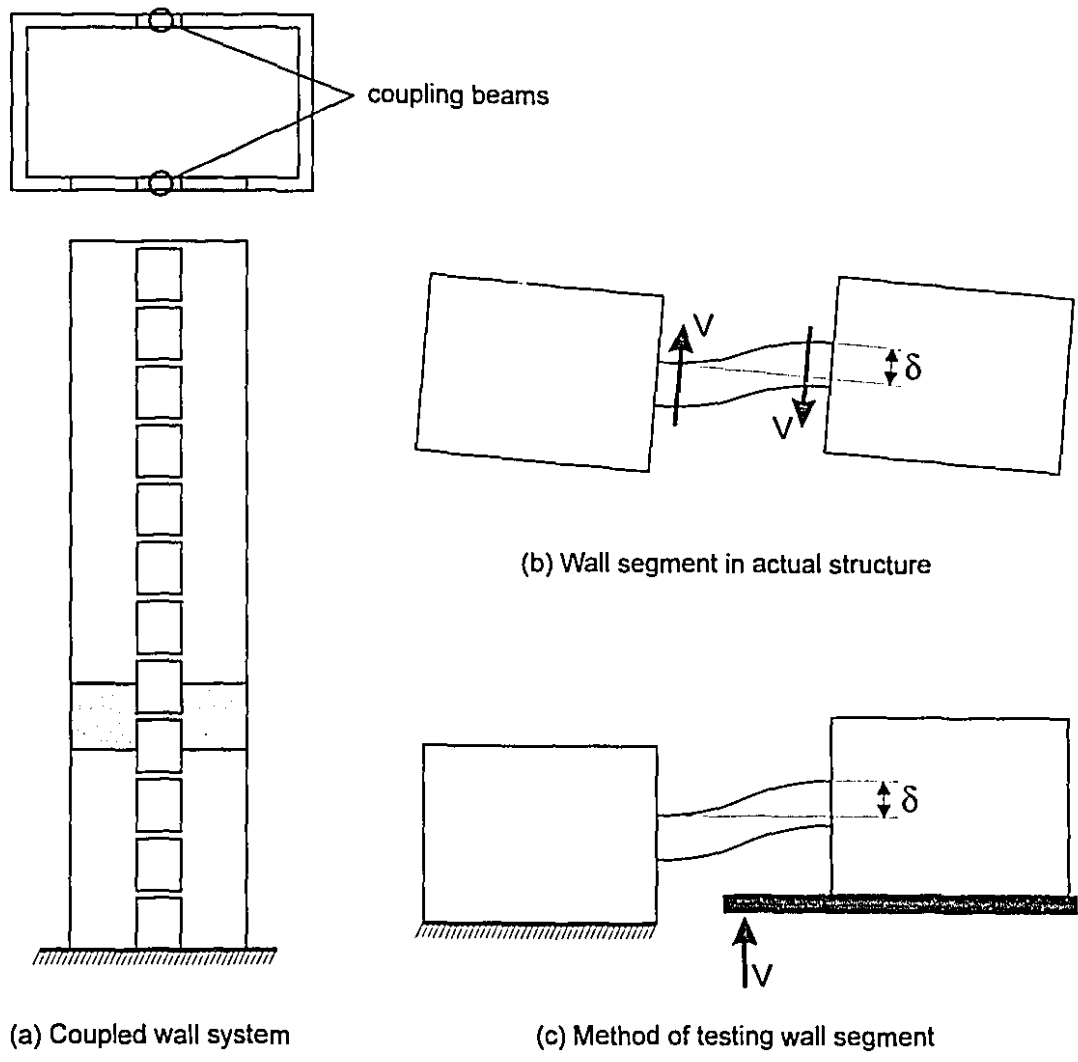


Figure 2.5 Method of simulating actual coupled wall behaviour

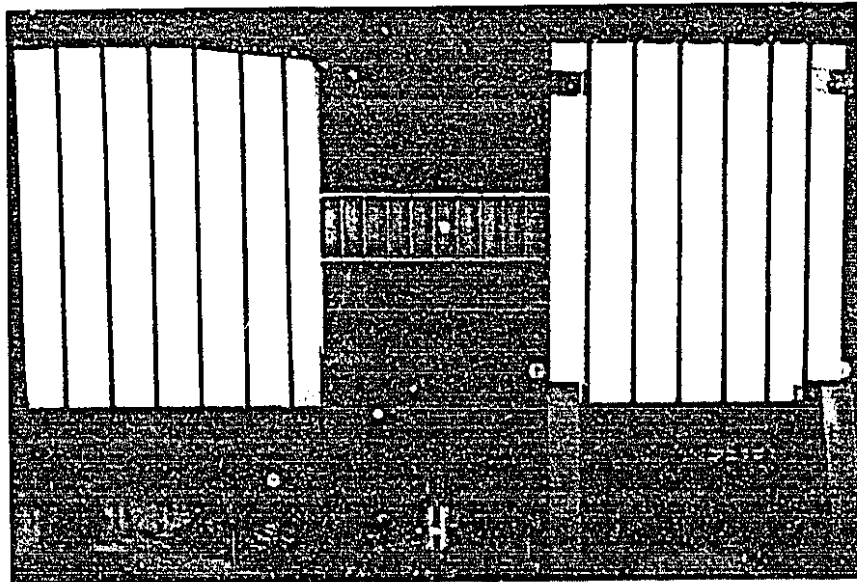
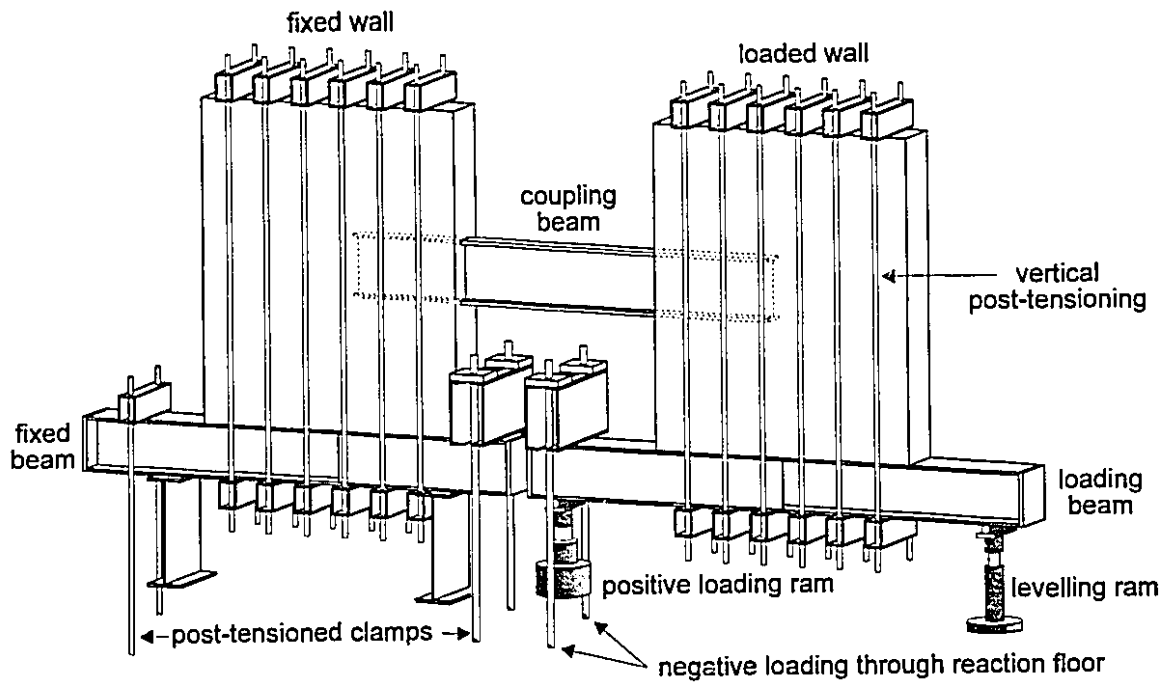
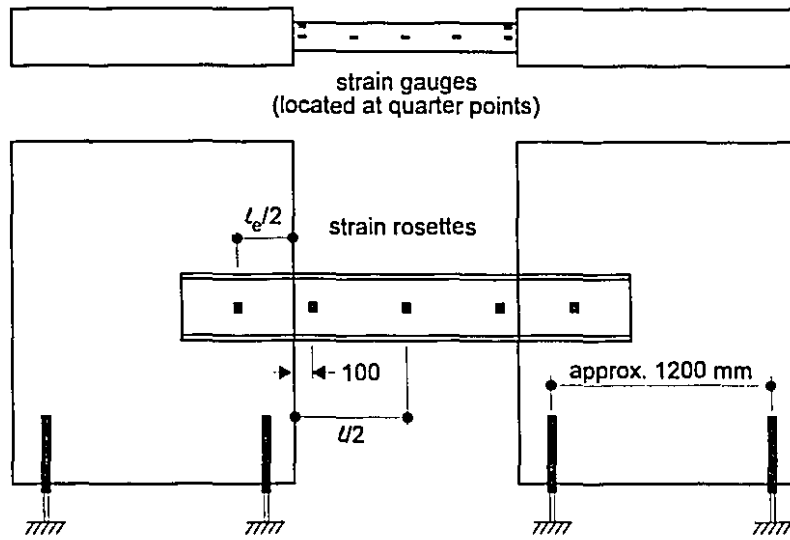
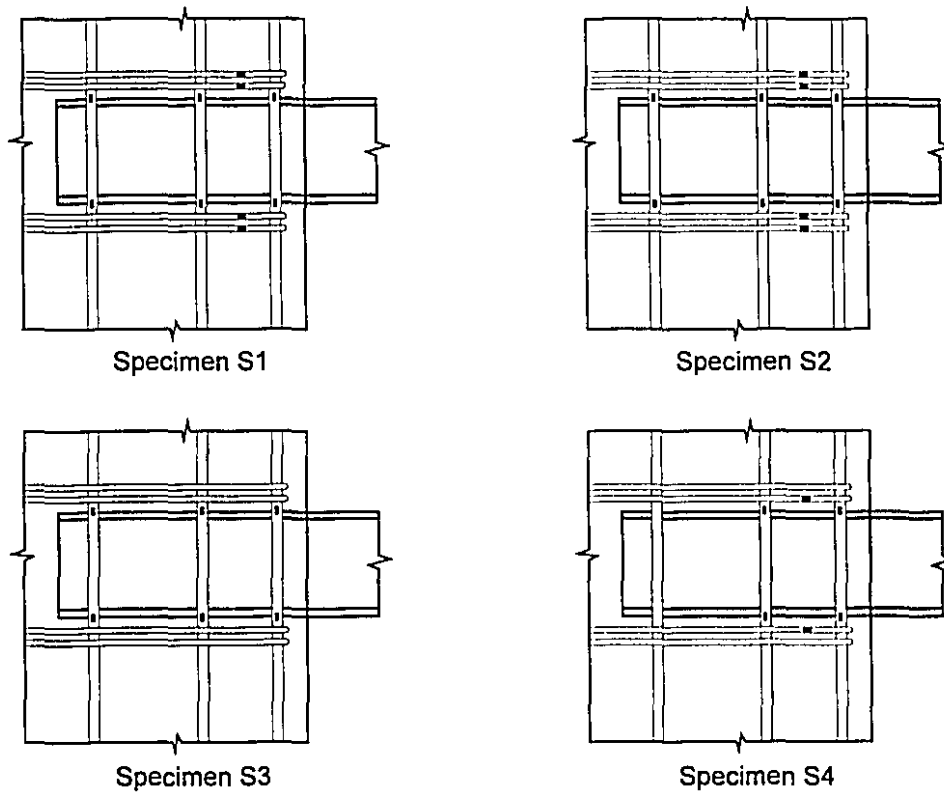


Figure 2.6 Coupled Wall Testing Apparatus with steel coupling beam specimen mounted

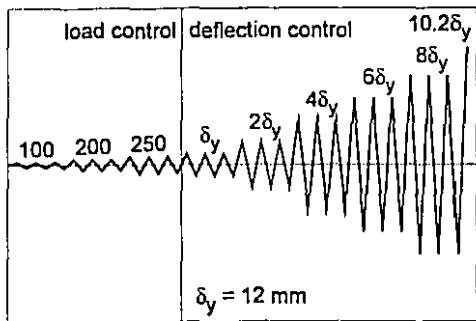


(a) Coupling beam strain gauge and LVDT locations

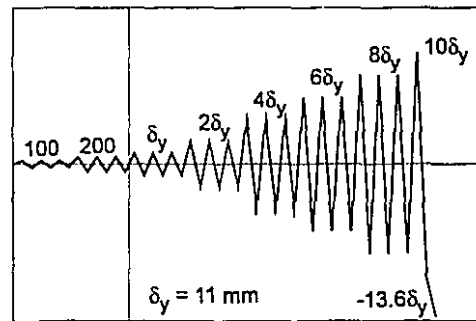


(b) Reinforcing steel strain gauge locations

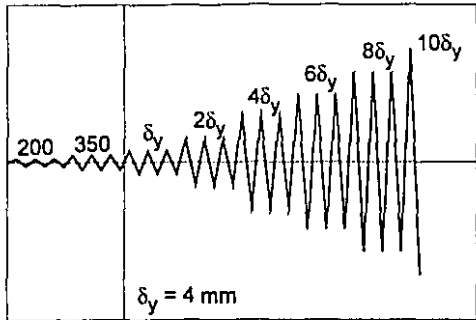
Figure 2.7 Instrumentation of Specimens S1 through S4



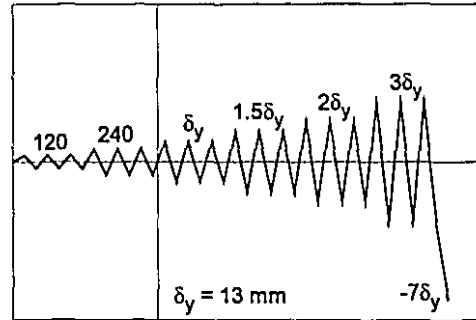
(a) Specimen S1



(b) Specimen S2



(c) Specimen S3



(d) Specimen S4

Figure 2.8 Load histories of Specimens S1 through S4

Chapter 3

Steel Coupling Beam Experimental Results

This chapter presents a detailed description of the observed experimental behaviour of Specimens S1 through S4.

For the load-deflection responses, the load corresponds to the shear transmitted through the coupling beam and the deflection represents the vertical displacement of the loaded (east) wall relative to the fixed (west) wall. The displacements have been corrected to account for measured, differential rotations of the walls. It should be noted that these differential rotations were very small, resulting in only minor corrections to the deflections. Table 3.1 summarises the key behavioural stages in the responses of Specimens S1 through S4. Also presented are the values predicted for each behavioural stage. The predicted values were calculated using the design approach presented in Sections 2.1 and 2.2. Actual material properties and measured dimensions were used in calculating the predicted response of the specimens. Summaries of the load stage peak load and deflections for each specimen are given in Tables 3.2 through 3.5. The loadstep designations A and B represent positive (upwards) and negative (downwards) loading, respectively.

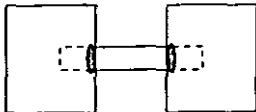
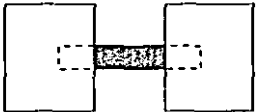
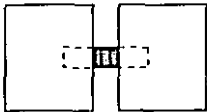
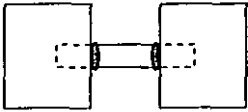
	Specimen S1		Specimen S2		Specimen S3		Specimen S4	
(1) Coupling beam details	shear critical built up section $\ell = 1200$ mm $\ell_e = 600$ mm		shear critical built up section $\ell = 1200$ mm $\ell_e = 600$ mm		shear critical W360 x 33 $\ell = 450$ mm $\ell_e = 500$ mm		flexure critical W360 x 33 $\ell = 1200$ mm $\ell_e = 600$ mm	
	predicted	observed	predicted	observed	predicted	observed	predicted	observed
(2) First shear yield of beam	292 kN	≈ 250 kN	262 kN	≈ 230 kN	411 kN	415 kN	411 kN	local yielding only
(3) General shear yield of beam	321 kN	303 kN	310 kN	274 kN	449 kN	446 kN	449 kN	remained elastic
(4) First flexural yield of beam	494 kN	386 kN due to crippling	391 kN	remained elastic	853 kN	local yielding only	320 kN	314 kN
(5) Ultimate capacity of beam Mode of failure	407 kN shear	409 kN at $6\delta_y$ shear	393 kN shear	446 kN at $8\delta_y$ shear	570 kN shear	- 687 kN at $-8\delta_y$ shear	406 kN flexure	403 kN at $3\delta_y$ flexure
(6) Yield of embedded portion of beam	321 kN shear	≈ 350 kN shear	442 kN shear	yielding at $10\delta_y$	449 kN	remained elastic	444 kN flexure	remained elastic
(7) Capacity of reinforced concrete embedment	357 kN	was not attained	593 kN	was not attained	633 kN	was not attained	482 kN	was not attained
(8) Principal mode of failure Hinge locations	crippling of embedded web causing flange buckling leading to flexural hinge 		controlled shear hinging of clear span; web buckling in all panels 		controlled shear hinging of clear span; web buckling in all panels 		flexural hinging at wall faces causing flange instability 	

Table 3.1 Response of steel coupling beam specimens

3.1 Specimen S1

The applied load versus relative deflection response of Specimen S1 is shown in Fig. 3.1. The load stage peak applied load and relative deflection values are given in Table 3.2.

Load Stage	Positive (A) Cycle		Negative (B) Cycle		Notes
	Applied Shear (kN)	Relative Deflection (mm)	Applied shear (kN)	Relative Deflection (mm)	
1	100.2	1.91	-101.2	-2.06	
2	100.9	2.01	-98.3	-2.35	
3	98.3	1.98	-101.4	-2.30	
4	198.0	4.65	-199.4	-4.56	first interface crack
5	196.0	4.61	-198.0	-4.78	
6	198.4	4.63	-198.0	-4.78	
7	249.3	6.75	-249.5	-6.13	initial yield of web
8	251.4	6.88	-247.4	-6.54	
9	246.9	6.77	-250.9	-6.91	
10	303.3	12.01	-300.1	-11.08	general yield of web, δ_y
11	300.6	11.44	-299.1	-11.59	initial spalling
12	301.7	11.47	-301.1	-10.82	
13	347.5	24.46	-360.3	-24.76	$2\delta_y$
14	358.7	24.17	-369.4	-26.14	
15	352.4	25.11	-359.4	-27.43	
16	375.1	48.78	-386.8	-50.10	$4\delta_y$
17	373.7	50.08	-384.7	-48.26	stiffeners bending
18	374.6	49.29	-385.0	-49.35	
19	388.4	70.34	-409.1	-75.51	$6\delta_y$
20	383.4	69.92	-404.1	-76.01	
21	379.4	69.94	-395.1	-76.06	severe spalling
22	387.7	93.22	-398.9	-102.07	$8\delta_y$
23	371.7	93.50	-373.1	-99.88	
24	358.6	95.24	-327.8	-100.56	first rebars yield
END	344.3	122.84	-	-	

Table 3.2 Load stage peaks for Specimen S1

The first horizontal cracking in the wall, along the coupling beam flange-concrete interface occurred at load stage 4 corresponding to an applied shear of ± 200 kN. First shear yielding at the mid-depth of the web of the coupling beam, as determined from the strain rosettes, occurred at an applied shear of ± 250 kN, at load stage 7. From elastic analysis, based on the measured yield stress of the web material, the predicted initial shear yield was 292 kN.

General yielding of the coupling beam web, occurred at load stage 10A, at a load of 303 kN and a relative vertical displacement of 12.0 mm. At this stage, flaking of the whitewash on the coupling beam web occurred and there was a noticeable change in the load-deflection response. General yielding in the negative direction occurred at load stage 10B, at a load of -300 kN and a displacement of -11.0 mm. The predicted shear yield of the coupling beam was ± 321 kN. The displacement at general yielding, δ_y , was taken as ± 12 mm.

Maximum shear values were recorded at load stages 19A and 19B, with values of 338 kN and -409 kN, respectively. The displacements at these peaks were 70.3 mm and -75.5 mm, respectively, corresponding to about $\pm 6\delta_y$. The predicted value for the ultimate shear capacity of the coupling beams was 407 kN, assuming that a plastic shear capacity equal to 1.27 times the general yield shear can be attained.

After load stage 19 a reduction in stiffness in the load deflection response was observed with cycling and the peak load values began to decline. By the end of load stage 24, corresponding to displacements of $\pm 8\delta_y$, the peak load values had decreased to 359 kN and -328 kN respectively. The recorded displacements were 95.2 mm and -100.6 mm.

The specimen was finally loaded monotonically in the positive direction to a peak load of 344 kN and a peak displacement of 122.8 mm, that is, about $10.2\delta_y$. The test was stopped at this stage due to lack of travel of the loading system. It is important to note that in the latter stages of loading that the peak loads attained did not drop below 80% of the maximum capacity obtained. A photograph of Specimen S1 after testing is shown in Figure 3.2. It can be seen that there is little flexural deformation over the clear span with significant shear deformations along the clear span (see Fig. 3.2). The web crippling that occurred near the end of testing also led to damage of the concrete embedment region (see Fig. 3.3)

3.1.1 Coupling Beam Response

The coupling beam performed very much as predicted at both yield and ultimate loads. The predicted values for shear yield and ultimate were 321 kN and 407 kN, respectively. The measured values were 303 kN at yield and 409 kN at ultimate. The predicted ultimate flexural capacity was 296 kNm, corresponding to an applied shear of 494 kN over the 1200 mm clear span. Local flexural yielding in the flange of the coupling beam, immediately inside the face of

the wall, occurred at a ductility of about $4\delta_y$. Factors contributing to the premature local yielding of the flange were the increase in clear span due to concrete spalling at the face of the wall and outward ratcheting of the coupling beam, and the distress caused by crippling of both the web and flange in the embedment. Apart from the localised yielding of the flange, very little flexural deformation of the coupling beam was observed during the test. Crippling of the web in the embedment was estimated to have occurred at load stage load 17A with noticeable flexural yielding of the last set of stiffeners at the end of the clear span.

Due to web crippling, the overall height of the section decreased 19.8 mm to 327.2 mm at a location about 40 mm into the embedment. The resulting "collapse" of the flanges gave about a 16% decrease in flexural capacity of the beam. Compounding this decrease in capacity, the spalling of concrete cover resulted in an increased effective clear span. This increase in clear span resulted in about a 7% increase in the applied moment at any shear level. The combined effect of flange collapse and the increase in clear span reduced the predicted flexural capacity of the coupling beam to about 249 kNm, corresponding to an applied shear of 389 kN. Local shear yielding occurred at an applied shear of -386 kN.

Investigation of the coupling beam upon removal from the concrete walls showed a pronounced shear deformation at each end of the beam. Figure 3.3 shows the significant distress of the coupling beam web and flanges just inside the embedment. Permanent shear deformation in the embedment resulted in a relative horizontal movement of the top and bottom flanges of 13.2 mm. Tearing of the coupling beam web occurred at the back of each embedment, in the heat affected zone of the web-to-flange weld. This tearing, located at the top and bottom of the web, was due to shear yielding of the embedded web.

3.1.2 Reinforced Concrete Embedment Response

Stresses in the embedment region caused by reversed cyclic loading result in alternating compression zones in the concrete at the top and bottom flanges of the coupling beam near the face of the wall. Similar actions occur near the end of the embedment as shown in Fig. 1.8. The first evidence of cracking at the coupling beam flange-concrete interface was observed at load stage 4, at an applied shear of ± 200 kN. Horizontal cracks located at the flange-concrete interface extended from the flange across the inner face of the wall to the side faces of the walls.

Localised spalling and crushing of the concrete along the top and bottom flanges of the coupling beam, at the front of the compression zone, was first observed at load stage 10A, at an applied shear on the coupling beam of 303 kN. By load stage 13, this distress was evident at all four flange-concrete interfaces. Progressive spalling resulted in a repositioning of the front

compressive zone further into the embedment region. This resulted in an effective increase in the clear span of the coupling beam and a decrease in the embedment length resulting in a larger compressive force at the face of the wall.

Further cycling resulted in the spalling of a semi-circular block of cover concrete at the face of each wall. At load stage 21A, the outer portions of this detached block of concrete spalled off, exposing the sound concrete confined between the coupling beam flanges. This confined concrete served to stiffen the web in this region. Due to the relative movement between the coupling beam and the concrete, delamination of the concrete occurred along a vertical plane delineated by the flange tips of the coupling beam. Although delamination occurred, the outer concrete is reinforced with the vertical and horizontal reinforcing bars and therefore does not spall. The inner concrete is confined by the coupling beam flanges and continues to stiffen the web.

The first vertical crack appeared in the east wall at load stage 16B, at an applied shear of -386 kN. This crack was located 600 mm from the inner face of the wall, the location of the end of the coupling beam embedment. A similar crack appeared in the west wall, 550 mm from the inner face of the wall at load stage 17A.

Vertical and inclined cracks were observed on the east wall at an applied shear in the coupling beam of -385 kN at load stage 17B. These cracks delineate the direction of principal compressive stresses running from the compressive zones at the flange-concrete interfaces to the loading beam. Such cracking was also evident on the back of the west wall.

Severe distress of the embedment region near the faces of the walls extended about 100 mm into each wall by the final stages of the test, resulting in exposure of the first set of reinforcing bars. Despite the complete loss of surrounding concrete, these bars remained elastic throughout the test (see Fig. 4.6(a)) reaching a peak tensile strain of 1150 microstrain (yield strain \approx 2050 microstrain). The confined concrete immediately above and below the coupling beam, however, appeared to remain sound.

It was not until the final load stage, when the wall was pushed to a displacement of $10\delta_y$, that there was evidence of yielding in the reinforcing bars around the embedment region. The horizontal ties above and below the flanges had just begun to yield at this final load stage.

3.1.3 Hysteretic Response

The hysteretic response of Specimen S1 (see Fig. 3.1) shows relatively large, stable hysteresis loops throughout the testing. The hysteresis loops exhibit slight "pinching" as the cracks which form along the top and bottom flanges open and close with the reversed cyclic loading. The loops show very little stiffness degradation until a ductility level of $8\delta_y$ is reached,

at which point the stiffness degradation in the loading cycles becomes more pronounced. The peak loads for the displacements at $\pm 8\delta_y$ also show some decay.

3.2 Specimen S2

The applied load versus relative deflection response of Specimen S2 is shown in Fig. 3.4. The load stage peak applied load and relative deflection values are given in Table 3.3. As described in Section 2.1, this specimen was designed to restrict the inelastic deformations to the clear span of the steel coupling beam.

Load Stage	Positive (A) Cycle		Negative (B) Cycle		Notes
	Applied Shear (kN)	Relative Deflection (mm)	Applied shear (kN)	Relative Deflection (mm)	
1	100.1	2.38	-99.2	-2.39	
2	99.7	2.60	-101.3	-2.35	
3	100.0	2.56	-93.6	-2.38	
4	199.9	4.94	-194.2	-4.59	first interface crack
5	199.8	4.91	-199.2	-5.20	
6	198.2	4.88	-195.4	-5.33	
7	273.9	11.46	-272.9	-9.16	general shear yield, δ_y
8	275.4	10.99	-273.8	-10.54	
9	273.6	11.09	-274.8	-9.63	
10	311.8	22.05	-333.0	-22.24	$2\delta_y$
11	324.4	21.90	-336.6	-22.86	
12	325.4	22.45	-336.9	-23.11	
13	358.5	44.19	-386.5	-44.53	$4\delta_y$
14	358.2	43.96	-396.0	-44.18	
15	377.5	44.09	-393.0	-45.43	
16	390.5	65.97	-429.0	-65.23	$6\delta_y$, initial spalling
17	401.6	66.28	-427.0	-67.07	
18	400.5	66.40	-427.8	-66.83	web buckling
19	409.8	88.01	-445.6	-90.34	$8\delta_y$
20	412.1	88.01	-436.7	-88.83	
21	436.4	88.18	-426.0	-88.79	severe buckling
22	389.7	110.64	-424.2	-110.29	$10\delta_y$
END	-	-	-361.3	-150.28	

Table 3.3 Load stage peaks for Specimen S2

The first horizontal cracking in the wall, along the coupling beam flange-concrete interface occurred at load stage 4 corresponding to an applied shear of ± 200 kN. First shear yielding at the mid-depth of the coupling beam, as determined from the strain rosettes, occurred at an applied shear of about 230 kN. From elastic analysis, based on the measured yield stress of the web material, the predicted initial shear yield was 262 kN.

General yielding of the coupling beam web, occurred at load stage 7A, at a load of 274 kN and a relative vertical displacement of 11.5 mm. At this stage, flaking of the whitewash on the coupling beam web occurred and there was a noticeable change in the load-deflection response. General yielding in the negative direction occurred at load stage 7B, at a load of -273 kN and a displacement of -9.2 mm. The predicted shear yield of the coupling beam was ± 310 kN. The displacement at general yielding, δ_y , was taken as ± 11 mm.

Maximum shear values were recorded at load stages 19B and 21A, with values of -446 kN and 436 kN, respectively. The displacements at these peaks were -90.3 mm and 88.2 mm, respectively, corresponding to about $\pm 8\delta_y$. The predicted value for the ultimate shear capacity of the coupling beams was 393 kN, indicating that more significant strain hardening was occurring than the 27% stress increase assumed for plastic design.

After load stage 21 some reduction in stiffness in the load deflection response was observed with cycling and the peak load values began to decline. By the completion of load stages 22A and 22B, corresponding to displacements of $\pm 10\delta_y$, the peak load values had decreased to 390 kN and -424 kN respectively. The recorded displacements were 110.6 mm and -110.3 mm. The specimen was finally loaded monotonically in the negative direction to a peak load of -361 kN and a peak displacement of -150.3 mm, that is, about $13.6\delta_y$ and 16.3 times the actual displacement at general yield in the negative direction. As was the case with Specimen S1, the peak loads attained did not drop below 80% of the maximum capacity obtained. A photograph of Specimen S2 after testing is shown in Figure 3.5. The double curvature of the stiffeners evident over the clear span of this specimen indicates that shear hinging was distributed over the length of the span.

3.2.1 Coupling Beam Response

The coupling beam performed much as predicted at yield and was found to have considerable reserve capacity before reaching its ultimate load. The predicted values for shear yield and ultimate were 310 kN and 393 kN, respectively. The observed values were 274 kN at yield and 446 kN at ultimate. The predicted ultimate flexural capacity was 235 kNm, corresponding to an applied shear of 391 kN over the 1200 mm clear span. The first signs of flexural yielding of the coupling beam in the clear span occurred at load stage 22, at a relative

deflection of $\pm 10\delta_v$. The flexural capacity of Specimen S2 was not reduced by web crippling at any stage of the test.

The relatively high concrete strength for this specimen and the thicker web in the embedment region resulted in very small rotations of the embedment region. As can be seen in Fig. 3.5, significant shear deformations extend over the clear span of the coupling beam. The double curvature deformation pattern further indicates that the embedments remained relatively rigid.

Controlled web buckling in the clear span was first observed at load stage 18B, and became more pronounced as the test progressed. Figures 3.5 and 3.6 clearly show the degree of web buckling by the end of the test. Tension field action, with the associated buckling, between adjacent stiffeners was clearly evident. The shear distress in the coupling beam was more pronounced by load stage 21B when the web stiffeners began to show signs of flexural yielding in double curvature. Once the stiffeners began to yield, some twisting of both flanges was observed, although this did not progress to the point of inducing buckling in the stocky flanges.

The concrete cover at the inner face of both walls had spalled off by load stage 21A, revealing the thicker web in the embedment regions. Although there was little lateral support provided by the concrete for the embedded webs, no evidence of yielding was observed in this region. In the final cycle at $10\delta_v$, strain rosettes on the west embedded web indicated that the web had just begun to yield. The east embedment remained elastic throughout the test. The predicted shear yield for the embedded webs was 442 kN. Figure 3.6 shows an overall view of the coupling beam after removal from the walls. It is clear that the distress was confined to the clear span as is desired for this structural system.

3.2.2 Reinforced Concrete Embedment Response

The first evidence of cracking in the wall was observed at load stage 4, at an applied shear of ± 200 kN. Horizontal cracks located at the coupling beam flange-concrete interface extended from the flange across the inner face of the wall to the side faces of the walls.

Further cracking resulted in the spalling of a semi-circular block of concrete at the inner face of each wall. At load stage 18A, further spalling occurred revealing the well confined concrete of the wall and the sound concrete confined between the coupling beam flanges.

The first vertical cracks appeared at load stage 8A, at an applied shear in the coupling beam of 275 kN. The cracks were located 480 and 325 mm from the inner face of the east wall and 730 and 445 mm from the face of the west wall. Vertical and inclined cracks, delineating the direction of principal compressive stresses, were observed on the east wall at an applied

shear of -337 kN at load stage 12B. Similar cracks were observed on the west wall at an applied shear of 358 kN at load stage 13A.

Spalling of the embedment region near the inner face of the wall extended about 100 mm into the wall by the final stages of the test, resulting in exposure of the first set of vertical reinforcing bars. Despite the loss of surrounding concrete, these bars remained elastic throughout the test (see Fig. 4.6(b)) reaching a peak tensile strain of 900 microstrain (yield strain \approx 2050 microstrain). There was no evidence of yielding of the horizontal ties in the embedment region and the confined concrete immediately above and below the coupling beam appeared sound.

3.2.3 Hysteretic Response

The response of Specimen S2 (see Fig. 3.4) shows large, stable hysteresis loops, up to a ductility level of $8\delta_y$. The hysteretic response exhibits behaviour typical of that of steel beams designed and detailed to yield in shear. Only slight stiffness degradation was noticed when a ductility level of $8\delta_y$ was reached and no strength degradation was observed. The cycle at $\pm 10\delta_y$ exhibited some decay in stiffness and a 20% drop in the peak load value. As the specimen was loaded monotonically at the end of testing to 16.3 times the deflection at yield in the negative direction, very little load degradation was evident. The final displacement reached was -150 mm, the limit of the test set up.

3.3 Specimen S3

Specimen S3, having a shorter clear span of 450 mm, was designed as a "shear critical" coupling beam. The applied load versus relative deflection response of Specimen S3 is shown in Fig. 3.7. The load stage peak applied load and relative deflection values are given in Table 3.4. The data for the initial load stages 1A through 2A was not properly recorded.

Load Stage	Positive (A) Cycle		Negative (B) Cycle		Notes
	Applied Shear (kN)	Relative Deflection (mm)	Applied shear (kN)	Relative Deflection (mm)	
1	-	-	-	-	
2	-	-	-200.2	-0.85	
3	201.6	1.22	-207.8	-0.95	
4	352.5	2.75	-352.9	-1.69	
5	356.5	2.98	-356.5	-1.67	
6	355.7	3.06	-354.6	-1.63	
7	446.1	4.12	-467.2	-3.51	general shear yield, δ_y
8	431.8	4.11	-468.9	-3.70	
9	429.5	4.14	-466.7	-3.62	
10	459.7	7.67	-507.7	-8.00	$2\delta_y$
11	465.9	7.55	-516.7	-7.77	
12	476.1	7.68	-530.9	-7.82	
13	522.3	15.57	-601.8	-15.96	$4\delta_y$
14	542.4	15.22	-607.2	-15.85	
15	551.6	15.51	-610.6	-15.80	
16	571.9	23.16	-656.8	-23.88	$6\delta_y$
17	588.3	22.66	-659.5	-24.03	
18	591.9	22.80	-665.7	-23.96	flange instability
19	607.5	30.83	-686.7	-31.65	$8\delta_y$, web buckling
20	619.7	30.44	-679.5	-31.97	severe buckling in east panel
21	583.8	30.58	-618.9	-32.14	
22	576.4	38.78	-530.0	-23.59	$10\delta_y$, web rupture
END	-	-	-299.5	-40.18	

Table 3.4 Load stage peaks for Specimen S3

The first horizontal cracking in the wall, along the coupling beam flange-concrete interface occurred at load stage 3B corresponding to an applied shear of -208 kN. First shear yielding at the mid-depth of the coupling beam, as determined from the strain rosettes, occurred at an applied shear of about 415 kN. From elastic analysis, based on the measured yield stress of the web material, the predicted initial shear yield was 411 kN.

General shear yielding of the coupling beam web, occurred at load stage 7A, at a load of 446 kN and a relative vertical displacement of 4.1 mm. At this stage, flaking of the whitewash on the coupling beam web occurred and there was a noticeable change in the load-deflection response. General yielding in the negative direction occurred at load stage 7B, at a load of -467 kN and a displacement of -3.5 mm. The predicted shear yield of the coupling beam was ± 449 kN. The displacement at general yielding, δ_y , was taken as ± 4 mm.

Maximum shear values were recorded at load stages 19B and 20A, with values of -687 kN and 620 kN, respectively. The displacements at these peaks were -31.6 mm and 30.4 mm, respectively, corresponding to about $\pm 8\delta_y$. The predicted value for the ultimate shear capacity of the coupling beams was 571 kN, indicating that significant strain hardening occurred in the web of this specimen.

After load stage 20 some reduction in stiffness in the load deflection response was observed with cycling and the peak load values began to decline. By the completion of load stage 22A, corresponding to a relative displacement of $10\delta_y$, the peak load value had decreased to 576 kN.

As is discussed in the following section, severe web buckling in the east panel of the coupling beam span led to the final rupture of the coupling beam. The failure of the coupling beam occurred after load stage 22A, under negative loading toward load stage 22B, at an applied load of -518 kN and a relative deflection of -36 mm.

Figure 3.8 shows Specimen S3 at the end of testing.

3.3.1 Coupling Beam Response

The coupling beam performed very much as predicted at yield and was found to have considerable reserve capacity. The predicted values for shear yield and ultimate were 449 kN and 571 kN, respectively. The observed values were 446 kN at yield and 686 kN at ultimate. The predicted ultimate flexural capacity was 192 kNm, corresponding to an applied shear of 853 kN over the 450 mm clear span. Only local flexural yielding was observed during testing. This yielding resulted from "collapse" of the flanges brought about by the severe web buckling, especially at the east end of the coupling beam (see Fig. 3.9). By load stage 22A, the overall depth of the beam had "collapsed" to 318 mm from 349 mm. This would result in a 24%

decrease in flexural capacity, lowering the ultimate flexural capacity to 146 kNm, or a shear of 649 kN over the clear span.

Controlled web buckling in the clear span was first observed at load stage 19, and became more pronounced as the test progressed. At load stage 21, all further increases in shear deformation occurred in only the east panel of the beam. From load stage 21A onward, the west and centre panel only accounted for 13 mm of the observed relative deflection. The remaining relative deflection (19 mm and 26 mm for load stages 21 and 22, respectively) occurred in the shear hinge developed in the east panel.

Between load stages 22A and 22B the coupling beam web ruptured. The events culminating in the final failure were as follows:

- i) At load stage 22A the out-of-plane buckling of the east, 333 mm deep by 145 mm wide panel of the coupling beam exceeded 50 mm. The west confining stiffener of this panel was very clearly in double curvature (see Fig. 3.9).
- ii) At a relative deflection of -7.1 mm the weld between the confining stiffener and the coupling beam web failed in tension, allowing the severe buckling to extend into the centre panel of the beam. At this weld failure the applied shear dropped from -529 kN to -487 kN, an 8% decrease.
- iii) After the weld failure, the load carrying capacity again began to increase. At a relative displacement of -23.6 mm the applied load had returned to a peak of -530 kN. At this point, the load carrying ability of the beam began to slowly decay.
- iv) At a relative deflection of -36 mm the coupling beam web experienced a tearing failure along the failed stiffener weld's heat affected zone (see Fig 3.10). At this rupture the applied shear dropped from 518 kN to 332 kN, a 36% decrease.

This form of tearing failure is typical of short shear links in eccentrically braced frames, particularly those with stiffeners on only one side of the web (Malley and Popov, 1983b). Despite the high loads applied to the beam and the sudden failure of the web, all distress to the beam was restricted to the clear span (see Fig 3.10).

3.3.2 Reinforced Concrete Embedment Response

Since the applied loads were significantly higher than in Specimens S1 and S2, horizontal cracking was observed at the first load stage, at an applied shear of ± 200 kN. Horizontal cracks in the concrete located at the coupling beam flange-concrete interface extended from the flange across the inner face of the wall to the side faces of the walls.

Further significant cracking was not observed until load stage 7, at an applied shear of 446 kN when the first vertical cracks began to appear, coinciding with the location of the concentrated vertical reinforcement in the wall.

Further horizontal and vertical cracking was considerably more pronounced on the east wall. By load stage 16, vertical and inclined cracking delineating the flow of forces away from

the embedment had become evident on both walls. Small amounts of spalling occurred on the faces of the walls at the flanges of the coupling beam.

As can be seen in Fig. 3.8, the amount of distress in the wall was notably less than that in Specimens S1 or S2 (see Figs. 3.2 and 3.5). Strains in the vertical reinforcing bars in the wall remained elastic throughout the test (see Fig 4.6(c)), not exceeding 1200 microstrain (yield strain = 2185 microstrain).

3.3.3 Hysteretic Response

The response of Specimen S3 (see Fig. 3.7) shows large, stable hysteresis loops throughout the response history. The hysteretic response exhibited behaviour typical of that of short steel link beams in eccentrically braced frames (Malley and Popov, 1983b). No significant strength or stiffness degradation was noticed through a ductility level of $10\delta_y$. The load drops due to the fracture of the stiffener weld and the eventual fracture of the web are evident in the final negative cycle.

3.4 Specimen S4

Specimen S4, having a clearspan of 1200 mm, was designed and detailed as a nominally ductile, "flexure critical" coupling beam. Because of this, the response of Specimen S4 is notably less stiff than the previous specimens and most of the distress is confined to the unstiffened coupling beam. The applied load versus relative deflection response of Specimen S4 is shown in Fig. 3.11. The load stages, peak applied loads and relative deflections values are given in Table 3.5.

Load Stage	Positive (A) Cycle		Negative (B) Cycle		Notes
	Applied Shear (kN)	Relative Deflection (mm)	Applied shear (kN)	Relative Deflection (mm)	
1	120.3	3.11	-117.8	-3.16	
2	123.6	3.22	-150.6	-4.56	
3	120.3	3.19	-148.5	-3.91	
4	227.0	7.02	-238.9	-7.09	
5	240.7	7.61	-244.6	-7.80	
6	240.4	7.93	-241.0	-7.51	
7	314.1	13.36	-334.6	-13.16	general flexural yield, δ_y
8	320.6	13.37	-323.5	-13.05	
9	310.8	13.52	-323.2	-13.07	
10	337.2	20.22	-361.9	-19.57	$1.5\delta_y$
11	347.4	20.37	-363.1	-19.97	
12	349.8	20.17	-360.1	-19.44	
13	361.3	26.73	-381.8	-25.93	$2\delta_y$
14	366.8	26.78	-383.3	-25.96	flange instability
15	368.0	26.81	-382.9	-25.99	
16	380.3	39.94	-403.6	-39.07	$3\delta_y$, flange buckle
17	386.0	39.93	-402.3	-39.12	
18	385.1	40.02	-396.7	-39.91	local web buckling
END	-	-	-321.8	-91.62	

Table 3.5 Load stage peaks for Specimen S4

The first horizontal cracking in the wall, along the coupling beam flange-concrete interface occurred at load stage 4 corresponding to an applied shear of ± 230 kN. By load stage 5B, twisting of the coupling beam flanges, near the wall faces, was already in evidence. First evidence of flexural yielding occurred at an applied shear of ± 258 kN, (155 kNm at the face of the walls) on the tension flange of the east end of the coupling beam. Yield of the compression flange at the same end of the beam was observed at an applied load of 311 kN (187 kNm). General yielding, as determined by a noticeable decrease in stiffness of the load-deflection response, was determined to be at an applied load of 314 kN (188 kNm), at a deflection of 13.4 mm. General yielding in the negative direction occurred at an applied shear of -335 kN (201 kNm) and a displacement of -13 mm. From elastic analysis, based on the measured yield stress of the flange material, the predicted applied shear at flexural yield was 320 kN (192 kNm). The displacement at general yielding, δ_y , was taken as ± 13 mm.

Maximum applied shear values were recorded at load stages 16B and 17A, with values of -404 kN (242 kNm) and 386 kN (232 kNm), respectively. The displacements at these peaks were -39.1 mm and 39.9 mm, respectively, corresponding to about $\pm 3\delta_y$. The predicted value for the ultimate applied shear capacity of the coupling beams was 406 kN (244 kNm).

Evidence of twisting of the beam was apparent as early in the test as load stage 7. By load stage 14, buckles in the compression flanges, near the face of both walls were apparent. These buckles straightened out when the flanges were cycled into tension. At load stage 18B the coupling beam webs in the vicinity of the flexural hinge buckled out of plane. At this point the specimen was loaded monotonically in the negative direction to a peak load of -321 kN (193 kNm) and a peak displacement of -91.6 mm, that is, about $7\delta_y$. The test was stopped at this stage as it was clear that all deflection was resulting from significant plastic rotations at each end of the coupling beam. A photograph of Specimen S4 after testing is shown in Figure 3.12. The flexural hinges at either end of the beam are clearly evident.

3.4.1 Coupling Beam Response

The coupling beam performed very much as predicted at yield and ultimate capacities. It is noted that flexural responses of steel beams are more predictable than shear responses. The predicted values for applied shear corresponding to flexural yield and ultimate capacities were 320 kN and 406 kN, respectively. The observed applied shears at yield and ultimate were 314 kN and 403 kN, respectively. The predicted shear capacity of the coupling beam was 449 kN. The beam remained elastic in shear throughout the test. Only local crippling of the web in the hinge regions was observed.

Unlike shear yielding, which occurs uniformly over the entire length of a coupling beam, flexural hinging propagates away from the region of critical moment. For the case of an embedded coupling beam, the hinging occurs at the face of the wall and propagates toward the centre of the span. In this specimen, hinging is prevented from entering the embedment region by the provision of the wall-face stiffeners and the flange cover plates. In any event, hinging is not as likely to propagate into an embedment because the region is stiffer than the span and the moment gradient is considerably steeper inside the embedment. Figure 3.13 shows the measured degree of hinge propagation with increased ductility. At a ductility level of $3\delta_y$ the hinges had extended about 160 mm from the faces of the walls.

By load stage 14, the hinges began to show evidence of instability: buckles in the compression flanges, near the face of both walls were apparent. These buckles straightened out when the flanges were cycled into tension. At load stage 18B the coupling beam webs in the vicinity of the flexural hinge crippled and flange support in the hinge region was lost.

In addition to flexural hinging, lateral instability was observed in the clear span of the web. Because the beam was shorter than its maximum unsupported length, l_{cr} , of 1470 mm this instability was controlled and manifested itself in the beam flanges twisting relative to each other. This twisting resulted in the flange tips deflecting about 2 mm toward each other on one side of the beam and 2 mm away from each other on the other side of the beam. This effect was observed over the entire clear span of the beam. Once flexural hinging of the coupling beam was established, this effect, although present, did not appear to get more severe.

3.4.2 Reinforced Concrete Embedment Response

The first evidence of cracking in the walls was observed at load stage 4, at an applied shear of 230 kN. Horizontal cracks located at the coupling beam flange-concrete interface extended from the flange across the inner face of the wall to the side faces of the walls.

Once hinges were established in the beam, at load stage 13, no new cracking was evident in the walls, as all deformations were confined to the hinges. By load stage 18 there was evidence of crushing in the front of the embedment region, although the crushing was less severe than observed in the other specimens.

As can be seen in Fig. 3.12, the amount of distress in the wall was notably less than that in Specimens S1 or S2 (see Figs. 3.2 and 3.5). Strains in vertical wall steel remained elastic throughout the test (see Fig 4.6(d)), not exceeding 600 microstrain (yield strain = 2185 microstrain).

3.4.3 Hysteretic Response

The response of Specimen S4 (see Fig. 3.11) shows relatively large, stable hysteresis loops throughout the response history. The hysteretic response exhibits behaviour typical of that of steel beams with a flexural mode of response. No significant strength or stiffness degradation was noticed through a ductility level of $3\delta_y$. The final monotonic loading curve shows the stable load decay response of the flexural hinges.

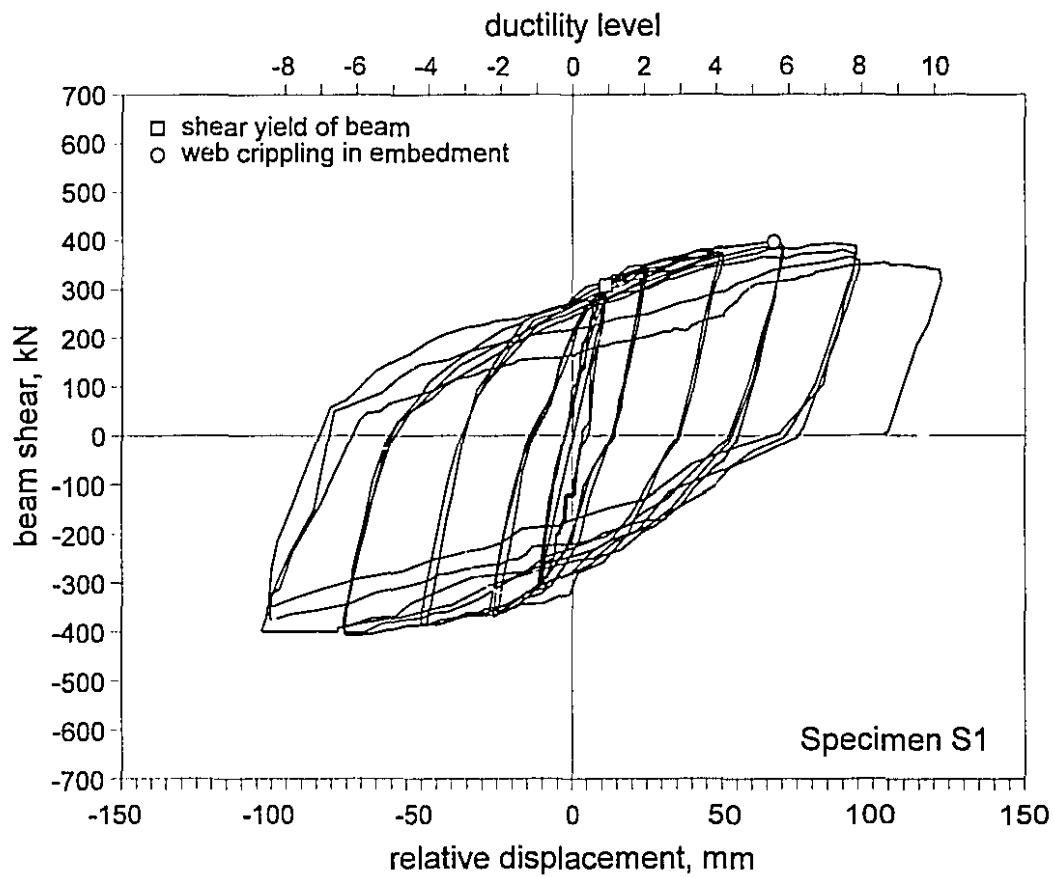


Figure 3.1 Hysteretic response of Specimen S1

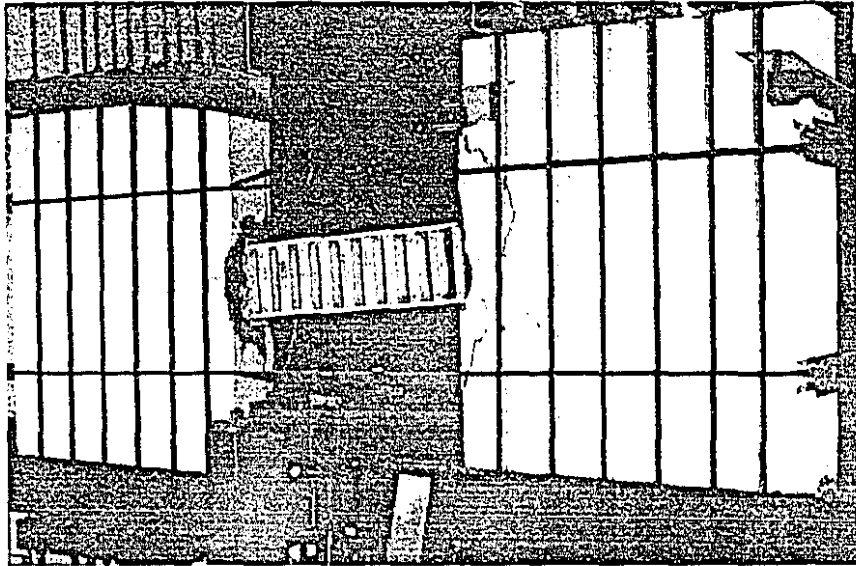


Figure 3.2 Specimen S1 at the completion of testing



Figure 3.3 Coupling beam of Specimen S1 after removal from concrete

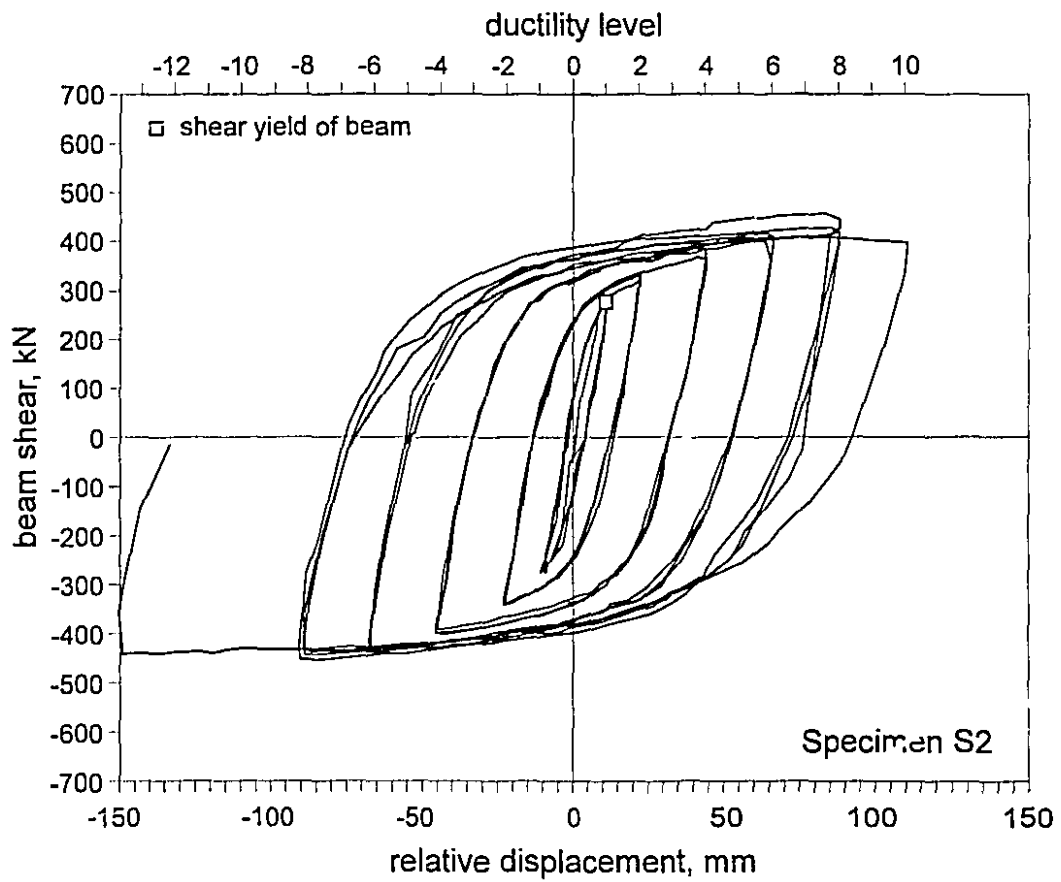


Figure 3.4 Hysteretic response of Specimen S2

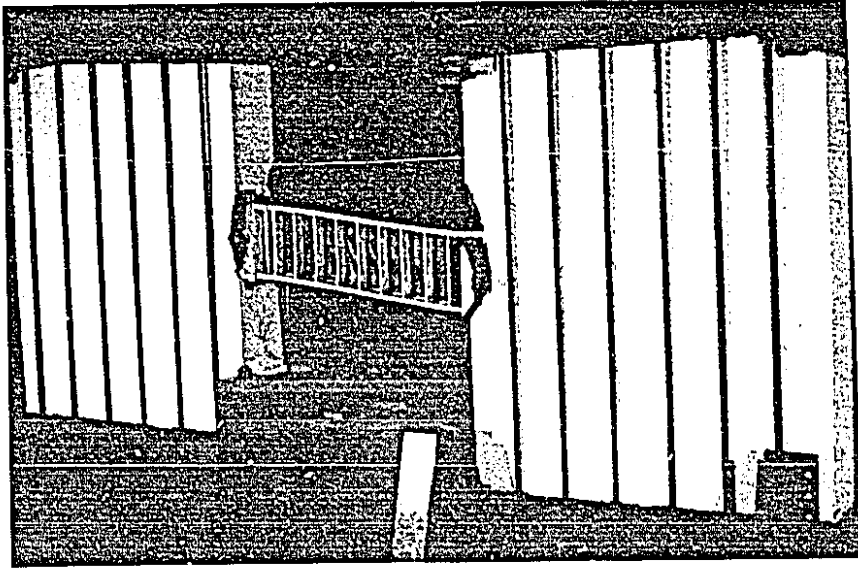


Figure 3.5 Specimen S2 at the completion of testing



Figure 3.6 Coupling beam of Specimen S2 after removal from concrete

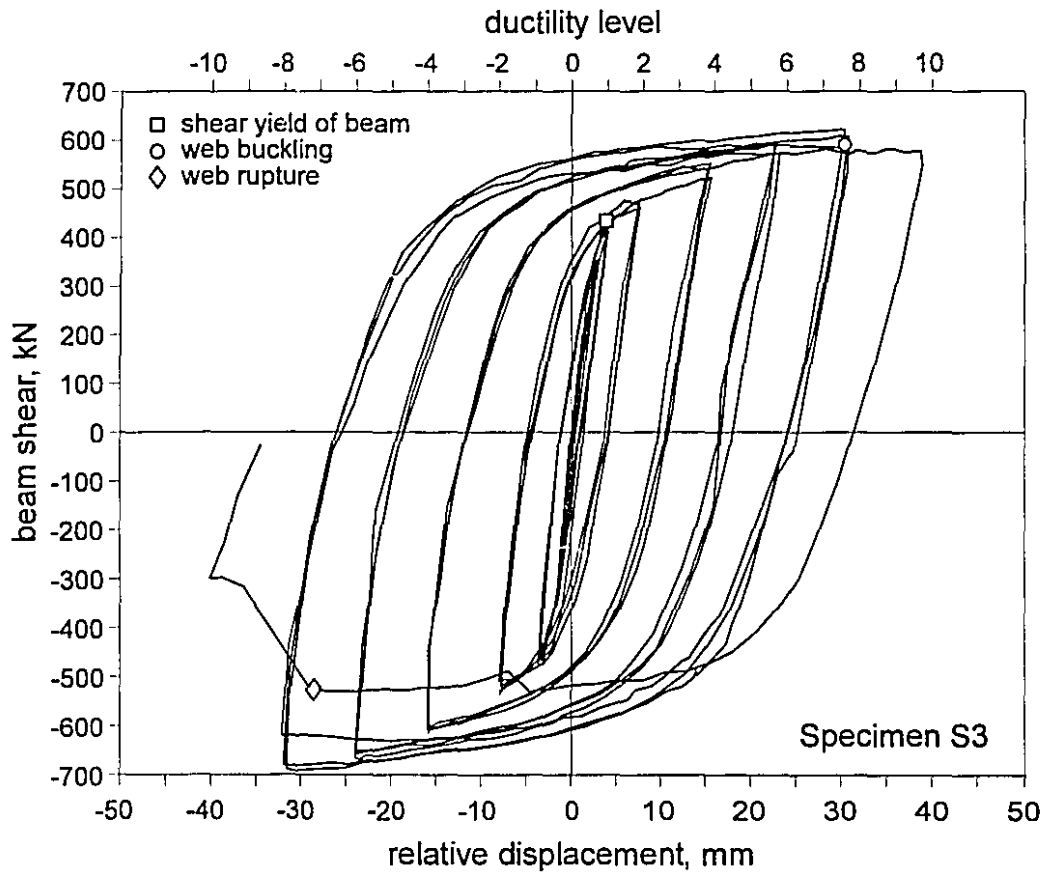


Figure 3.7 Hysteretic response of Specimen S3

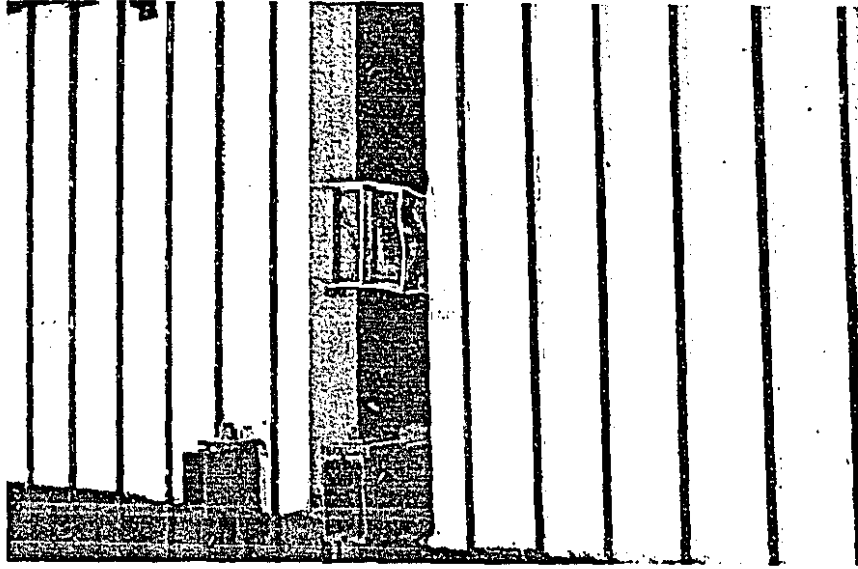


Figure 3.8 Specimen S3 at the completion of testing

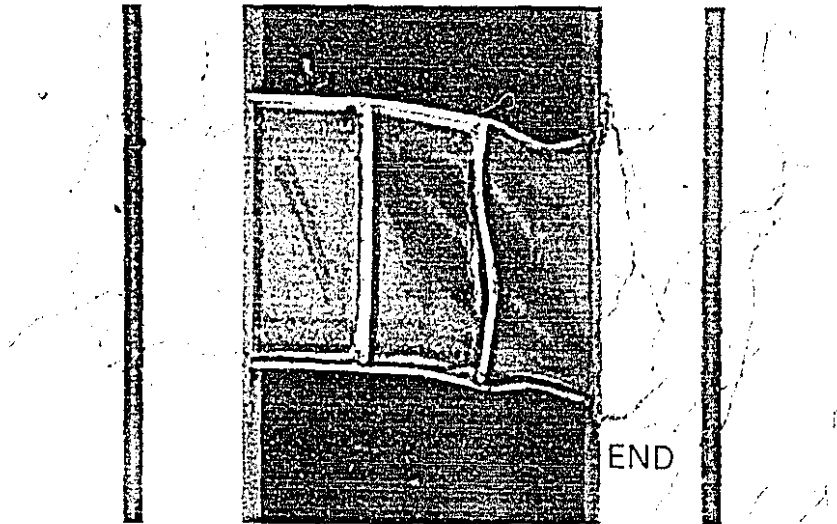


Figure 3.9 Coupling beam of Specimen S3 at completion of testing

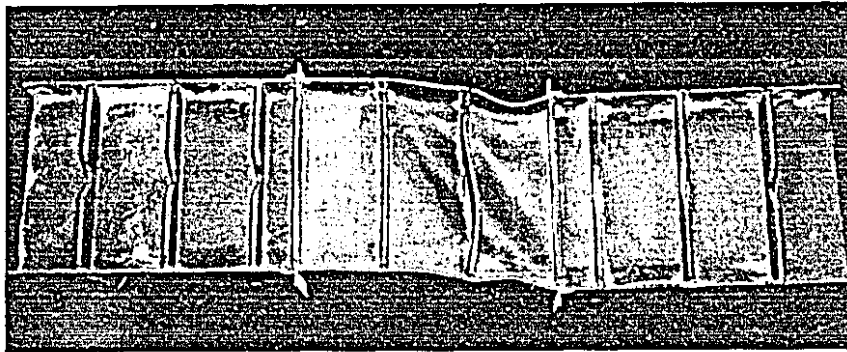


Figure 3.10 Coupling beam of Specimen S3 after removal from concrete

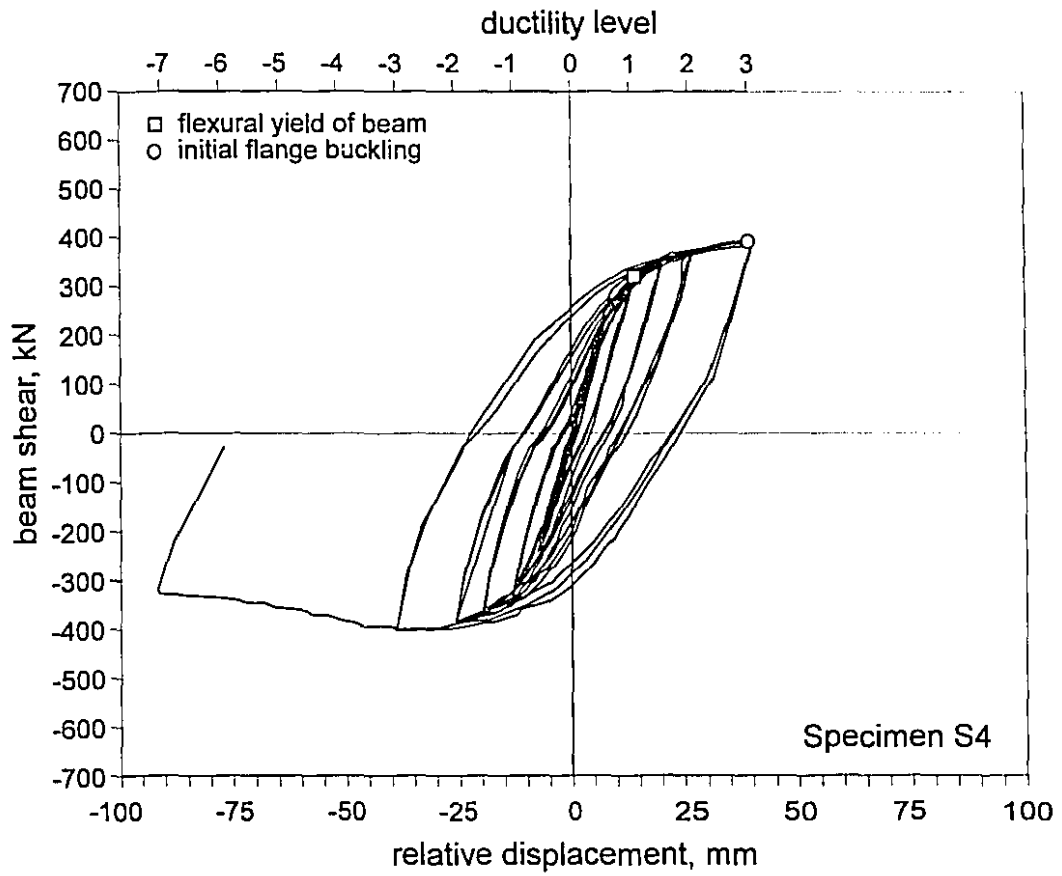


Figure 3.11 Hysteretic response of Specimen S4

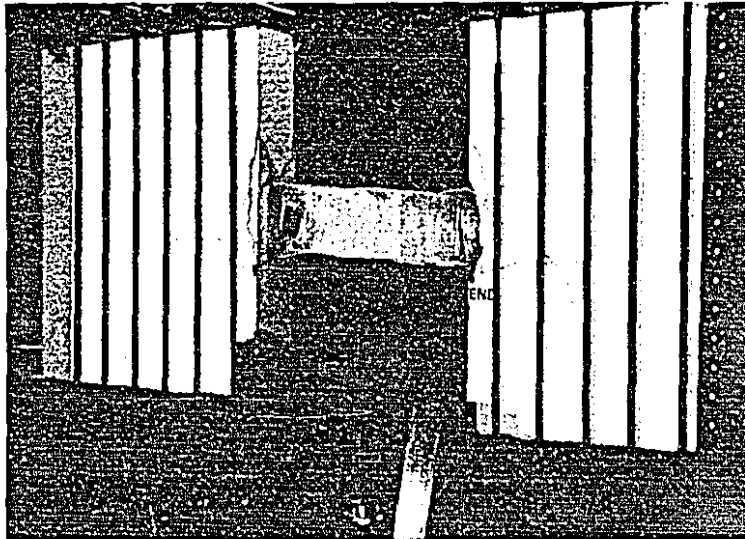


Figure 3.12 Specimen S4 at the completion of testing

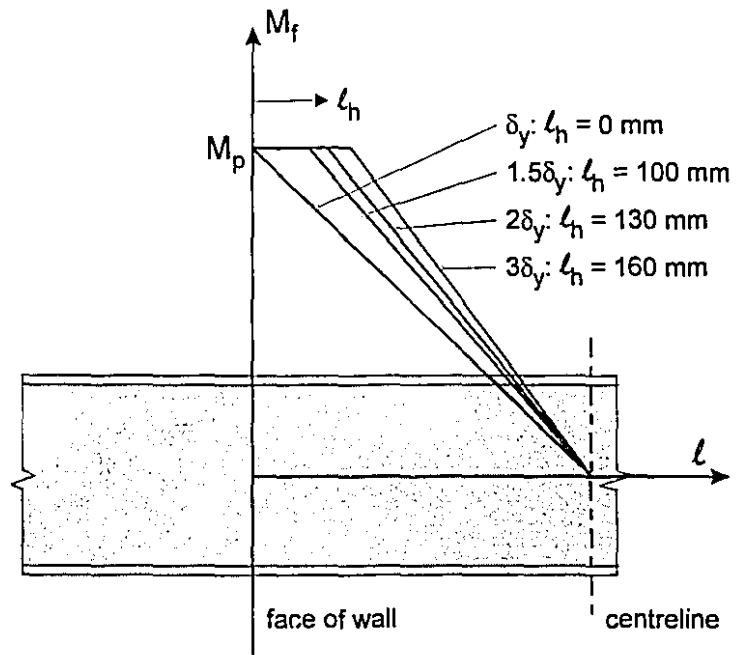


Figure 3.13 Extent of hinging at the ends of Specimen S4

Chapter 4

Response Comparisons of Steel Coupling Beam Specimens

4.1 Comparison of Predicted and Experimental Results

Table 4.1 compares the observed and predicted applied shears corresponding to the key behavioural events of the steel of coupling beam specimens. The predicted values were calculated using the design approach presented in Sections 2.1 and 2.2. Measured material properties and section dimensions were used in determining the predicted capacities of the specimens.

The predicted values for the initial shear yield of the coupling beam (Table 4.1, row (2)) were determined by shear flow calculations at the neutral axis of the beam (ie: vIt/Q). The shape factor used was 3/2.

General shear yield and yield of the embedded portion of the beam (rows 3 and 6) were determined from the equation for plastic shear capacity: $V_r = A_w F_y / \sqrt{3}$.

Flexural yield (row 4) was determined from the design equation: $M_r = Z F_y$, where Z was determined neglecting the contribution of the web (the web was included for 'flexure critical' Specimen S4).

Ultimate capacities (row 5) were determined assuming a strain hardening factor of 1.27 (ie: $F_u = 1.27 F_y$). Measured strain hardening values (see Table 2.1) indicate strain hardening factors of about 1.4 for the materials used.

Embedment capacities (row 7) were determined from Equation 2.9, using a value of $\phi_c = 1$. The large variation of predicted embedment capacities result from the variation of concrete strengths from specimen to specimen (see Table 2.1).

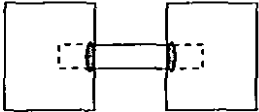
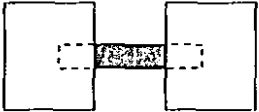
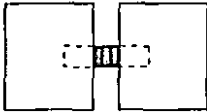
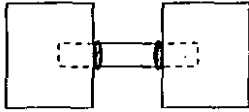
	Specimen S1		Specimen S2		Specimen S3		Specimen S4	
(1) Coupling beam details	shear critical built up section $\ell = 1200$ mm $\ell_e = 600$ mm		shear critical built up section $\ell = 1200$ mm $\ell_e = 600$ mm		shear critical W360 x 33 $\ell = 450$ mm $\ell_e = 500$ mm		flexure critical W360 x 33 $\ell = 1200$ mm $\ell_e = 600$ mm	
	predicted	observed	predicted	observed	predicted	observed	predicted	observed
(2) First shear yield of beam	292 kN	≈ 250 kN	262 kN	≈ 230 kN	411 kN	415 kN	411 kN	local yielding only
(3) General shear yield of beam	321 kN	303 kN	310 kN	274 kN	449 kN	446 kN	449 kN	remained elastic
(4) First flexural yield of beam	494 kN	386 kN due to crippling	391 kN	remained elastic	853 kN	local yielding only	320 kN	314 kN
(5) Ultimate capacity of beam Mode of failure	407 kN shear	409 kN at $6\delta_y$ shear	393 kN shear	446 kN at $8\delta_y$ shear	570 kN shear	- 687 kN at $-8\delta_y$ shear	406 kN flexure	403 kN at $3\delta_y$ flexure
(6) Yield of embedded portion of beam	321 kN shear	≈ 350 kN shear	442 kN shear	yielding at $10\delta_y$	449 kN	remained elastic	444 kN flexure	remained elastic
(7) Capacity of reinforced concrete embedment	357 kN	was not attained	593 kN	was not attained	633 kN	was not attained	482 kN	was not attained
(8) Principal mode of failure Hinge locations	crippling of embedded web causing flange buckling leading to flexural hinge 		controlled shear hinging of clear span; web buckling in all panels 		controlled shear hinging of clear span; web buckling in all panels 		flexural hinging at wall faces causing flange instability 	

Table 4.1 Response of steel coupling beam specimens

Specimens S2 through S4 behaved as predicted and desired. Specimen S1 did not behave as well as desired, with significant yielding and distress penetrating into the embedded regions and some ratchetting-out of the embedded steel member. The response of Specimen S1 did however lead to changes in the design approach (reflected in Sections 2.1 and 2.2) to prevent inelastic action in the steel beam over its embedded region. The predicted mode of failure for all four specimens correspond with the observed failure modes. As was discussed in Section 3.1.1, the observed response of Specimen S1 was not the desired shear hinge over the clear span. The detailing changes made for Specimens S2 and S3 accounted for the observed concrete spalling, resulting in the desired shear hinges.

It is apparent from the response of the embedment region of Specimen S3, that the composite nature of the embedment results in additional load carrying capacity over that predicted. The shear capacity of the embedded region of Specimen S3 was 449 kN, neglecting the effect of the confining concrete and the axial compression in the walls. The maximum capacity attained, 687 kN, was 153% of the predicted, unconfined value.

4.2 Hysteretic Response

The hysteretic responses of Specimens S1 through S4 are presented in Fig. 4.1. Specimens S2 and S3 exhibited very large, stable loops through a ductility level of $10\delta_y$ with little strength or stiffness decay evident. This response is typical of well detailed steel sections behaving in a primarily shear mode of response (see Section 1.4). Specimens S1 and S4 exhibited a more rounded, pinched response, more typical of steel sections yielding in a flexural mode. Strength and stiffness decay was also more evident in Specimens S1 and S4.

Figure 4.2 shows the peak-to-peak hysteretic stiffness plotted against the relative displacement for Specimens S1 through S4. Beyond yield, the stiffnesses of Specimens S1, S2 and S4 are virtually indistinguishable. The three plots illustrate comparable stiffnesses and similar rates of stiffness decay. Specimen S3, having a shorter clear span than the other specimens, exhibits a stiffer response and, due to the nature of the eventual failure, a greater rate of stiffness decay.

Table 4.2 shows the predicted and observed initial elastic stiffnesses of each specimen. The predicted elastic stiffness, K_e , of the beams is determined using the equation for fixed end conditions:

$$K_e = \frac{12EI_{eq}}{\ell^3} \quad (4.1)$$

where I_{eq} is the equivalent moment of inertia of the coupling beam accounting for the effect of shear distortion as determined from the following equation:

$$I_{eq} = \frac{I_b}{1 + \frac{12EI_b\lambda}{\ell^2GA_w}} = kI_b \quad (4.2)$$

where: I_b = moment of inertia of the coupling beam,
 A_w = shear area of coupling beam (excluding flanges),
 E = Young's modulus for coupling beam,
 G = shear modulus for coupling beam,
 ℓ = clear span of coupling beam and,
 λ = cross sectional shape factor for shear (3/2 for I-section).

	Specimen S1	Specimen S2	Specimen S3	Specimen S4
(1) Observed initial stiffness	50.7 kN/mm	41.8 kN/mm	188.7 kN/mm	38.0 kN/mm
(2) Theoretical elastic stiffness	54.7 kN/mm	54.7 kN/mm	215.3 kN/mm	50.3 kN/mm
(3) Effective length of beam = $(12EI_{eq}/K_e)^{1/3}$	1231 mm (1.03 ℓ)	1313 mm (1.09 ℓ)	470 mm (1.04 ℓ)	1317 mm (1.10 ℓ)
(4) I_{eq} accounting for shear (Eq. 4.2)	0.24 I_b	0.24 I_b	0.10 I_b	0.44 I_b
(5) K_e at yield	38.7 kN/mm	26.5 kN/mm	119.7 kN/mm	24.5 kN/mm
(6) Observed I_{eff} = $K_e\ell^3/12E$	0.19 I_b	0.13 I_b	0.06 I_b	0.23 I_b
(7) I_{eff} accounting for embedment inelasticity	0.79 kI_b	0.54 kI_b	0.60 kI_b	0.53 kI_b

Table 4.2 Observed and predicted elastic stiffnesses of Specimens S1 through S4

As can be seen in Table 4.2, there is reasonable correlation between observed and predicted stiffnesses. In all cases the observed stiffness is less than the predicted value due to the fact that the beam ends are not perfectly restrained. This lack of restraint results from cracking near the face of the embedment which has the effect of increasing the effective length of the beam (see Table 4.2, (3)). Often, for elastic analysis of reinforced concrete coupled walls, the effective length of the beams is assumed to extend a distance $d/4$ into each wall, where d is the depth of the beam. (Candy, 1964 and Michael, 1967). In all cases the increase in effective length is considerably smaller than $\ell + d/2$, indicating that the embedment is behaving well.

For seismic lateral load analysis, it is of interest to know the effective member stiffness close to yield of the coupling beam under reversed cyclic loading. Hence it is necessary to include an additional factor, x , in Eq. 4.2 to account for inelasticity occurring in the embedment region. Therefore, the effective moment of inertia, I_{eff} , is determined as:

$$I_{eff} = x I_{eq} = x k I_b \quad (4.3)$$

The value of the factor x was found, from these experiments, to lie between 0.50 and 0.60. It is interesting to note that a typical value of x for reinforced concrete coupling beams is about 0.20 (Paulay and Priestley, 1992). It must be noted that the special design requirements in the embedment region have resulted in the higher values of x . The value of k is a correction for shear distortion which need not be applied if the analysis program accounts for shear deformations.

4.3 Energy Absorption

The primary advantage of the use of steel coupling beams is their ability to absorb significant amounts of energy through large displacements. Figure 4.3(a) shows the cumulative hysteretic energy absorption for Specimens S1 through S4. The real energy absorption of Specimens S1 and S2 are virtually identical. Specimen S3, due its shorter span, was not able to absorb as much energy as Specimens S1 and S2 beyond a ductility of about $4\delta_y$. The flexural hinging of Specimen S4 was able to absorb significant amounts of energy although only through a limited displacement.

Figure 4.3(b) shows the cumulative hysteretic energy absorption normalised by the cumulative energy absorption at general yielding of the coupling beam in order to properly compare the responses of the specimens. Specimen S1 was able to dissipate about 30 times its yield energy through a ductility of $10\delta_y$. The change in failure mode from flexural to shear hinging resulting from the improvements made to Specimen S2, results in a significant increase in energy absorption capacity to about 60 times the specimen's yield energy. Although Specimen S3 is not able to absorb as much energy, its short span makes it very efficient. Specimen S3 was able to absorb about 80 times its yield energy through a ductility of $10\delta_y$. An elastic-perfectly plastic beam tested through the same load history would exhibit a cumulative energy absorption of 90 times its yield energy through a ductility of $10\delta_y$.

The flexural hinging in Specimen S4 was able to dissipate only about 17 times its yield energy through a ductility of $3\delta_y$.

In order to quantify the response of each specimen and allow comparisons with other tests, an equivalent elastic damping coefficient, β , is defined (see Fig. 4.4, inset):

$$\beta = \frac{A_1}{2\pi A_2} \quad (4.4)$$

where A_1 = the area within the hysteresis loop of one half cycle, and,
 A_2 = the area of the triangle defined by an equivalent elastic stiffness to the peak load and corresponding deflection at each half cycle.

A larger damping coefficient reflects a greater ability to dissipate energy. The maximum value of β , representing elasto-perfectly plastic hysteretic behaviour is about $2/2\pi = 31.8\%$.

The equivalent elastic damping coefficients for Specimens S1 through S4 are shown in Fig. 4.4. Once again, the efficiency of the shear critical specimens can be ranked, with the short span of Specimen S3 being the most efficient at dissipating energy. Specimen S4 appears to be as efficient as the shear critical specimens at lower ductility levels, however the efficiency of the flexural hinge would likely decay rapidly with increased deformation. This type of decay can also be seen in Specimen S1, where the flexural hinging in the embedment appears to have begun to effect the energy dissipation capability at ductility levels greater than $4\delta_y$. No such decay is evident in Specimens S2 and S3 which developed well defined shear hinges.

The width of the response band is an indication of the degree of decay in energy absorption ability with cycling at a given ductility level. The upper bound of the response band represents the first half cycle at a ductility level while the bottom bound represents the sixth and final half cycle. A thin band indicates little decay of energy absorption ability with cycling. It can be seen in Fig. 4.4 that the specimens developing shear hinges (S2 and S3) exhibit less decay of energy absorption ability with cycling than Specimens S1 and S4.

4.4 Response of Coupling Beams

Obtaining the desired coupling beam response requires proper detailing of the beams over their clear span and embedded regions. In order to achieve the desired (and predictable) response of the clear span, the embedded region must be detailed to remain elastic and to arrest hinge propagation into the embedded region. Figure 4.5 shows the coupling beams of Specimens S1 (top) and S2 (bottom) after removal from the walls. Although the clear span detailing is identical, the very different failure modes are obvious. The flange collapse in the embedment region of Specimen S1 resulted in the development of flexural hinges. The shear hinge, developed over the entire clear span of Specimen S2 is evident as the controlled web buckling between adjacent stiffeners.

The embedments of Specimens S3 and S4 were both properly detailed. As such hinging was restricted to the clear spans of the coupling beams (see Figs. 3.8 and 3.12). This ensured that the desired and predicted response was achieved.

4.5 Response of Reinforced Concrete Embedment Region

The reinforced concrete embedment regions were designed to resist the maximum expected plastic shear capacity of the coupling beam sections (see Section 2.2). In this respect, all of the specimens behaved well. Despite some cover spalling, the confined concrete above and below the embedded section remained sound throughout testing. In addition the concrete confined between the coupling beam flanges remained sound, providing additional resistance not accounted for in the design of the embedment (Equation 2.9).

The energy absorption ability of a steel coupling beam system can be significantly affected by the development of a horizontal gap along the coupling beam flange-concrete interface. If this gap experienced significant opening and closing, the hysteretic response would have a "pinched" response. In order to control this gap opening, minimum reinforcing steel was provided across the interface (Equation 2.11).

Figure 4.6 shows the vertical strains observed in the first reinforcing bars inside the face of the wall for each specimen. The vertical strains did not exceed 1200 microstrain, or about 60% of the yield strain in any of the specimens. The plots illustrate the degree of distress within the embedment. The hinging within the embedment region of Specimen S1 resulted in tensile strains in the vertical reinforcing which increased with increasing loading. These tensile strains result from the build-up of severe distress in the embedment region. Smaller strains were measured in the longitudinal bars in Specimen S2 where the failure was removed from the embedment region. The gap control in Specimens S3 and S4 was more efficient where the hinging in the clear span was confined to a smaller region, isolated from the embedment.

There was a small initial compression of about 100 microstrain in each specimen resulting from the clamping of the specimen to the reaction beams.

4.6 Comparisons with Reinforced Concrete Coupling Beams

In order to assess the performance of steel beams coupling reinforced concrete walls, the responses of the Specimens S1 through S4 are compared to typical responses of reinforced concrete coupling beams.

A discussion of both conventionally reinforced and diagonally reinforced concrete coupling beams is given in Section 1.3. For ductile systems, conventionally reinforced coupling beams containing longitudinal reinforcement and closed hoops are only permitted where the shear is low and the span-to-depth ratio is relatively high. Diagonally reinforced coupling beams, due to their excellent ductility and energy absorption characteristics, are required in cases where the shear is high. Diagonal reinforcement, however, has been shown to be impractical when the span-to-depth ratio is greater than about 2.

Two specimens, tested by Shiu et al. (1978) were chosen as representative of the response of conventionally and diagonally reinforced concrete coupling beams. Both specimens had a span-to-depth ratio of 2.5 and their capacities were comparable to those of this study.

Figure 4.7 shows the equivalent elastic damping coefficient, β , of each of the S-series of specimens and the specimens tested by Shiu. Despite the larger span-to-depth ratios, Specimens S1, S2 and S4 exhibited greater energy absorption capability than either the diagonally or conventionally reinforced concrete specimens.

The response of diagonally reinforced concrete coupling beams with smaller span-to-depth ratios (Paulay, 1971) show little improvement in hysteretic damping over those with larger ratios. The damping coefficients of Paulay's beams, whose span-to-depth ratios were 1.29 and 1.02, are only marginally higher than Shiu's (span-to-depth = 2.5) beams shown in Fig. 4.7.

Specimen S3, with a span-to-depth ratio of 1.29 exhibited significantly greater energy absorption ability than the comparable diagonally reinforced specimens. The short shear span of Specimen S3 also showed greater energy absorption ability than the other steel specimens tested (see Fig. 4.7).

4.7 Comparisons with Steel Link Beams in Eccentrically Braced Frames

The response of a representative steel "shear link" in an eccentrically braced frame was chosen from the work of Malley and Popov (1983). The shear link selected had similar dimensions to those of Specimens S1 and S2 and a span-to-depth ratio of 3.7.

Figure 4.8 shows the equivalent elastic damping coefficient, β , of the S-series of specimens and that of the steel shear link tested by Malley. It is clear, that in terms of ductility and energy absorption, the response of Specimen S2 closely approaches the response of the steel shear link. The response of Specimen S3 exceeds the response of the shear link, although it has a shorter shear link and therefore would have a marginally better response than the one tested by Malley and Popov.

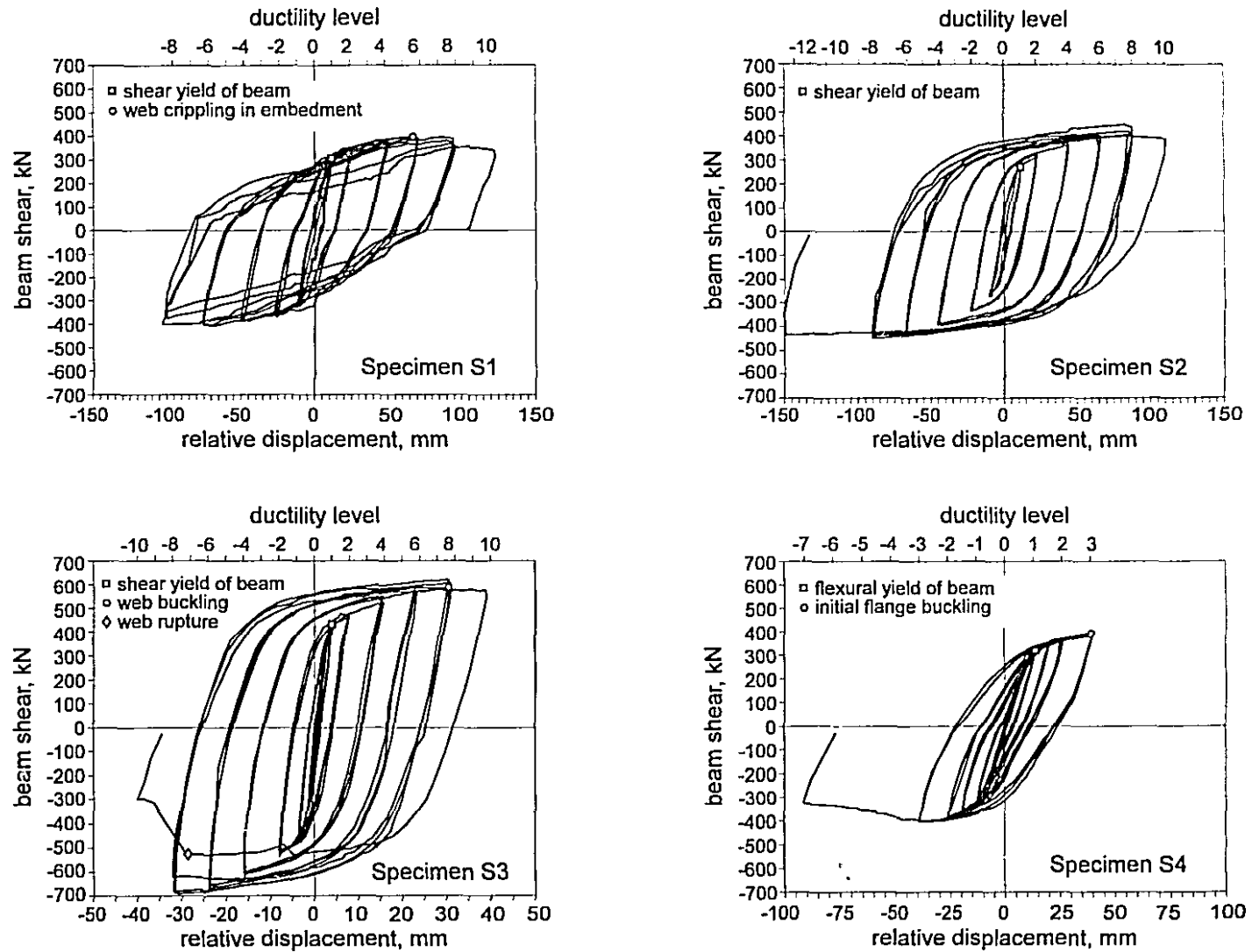


Figure 4.1 Hysteretic responses of Specimens S1 through S4

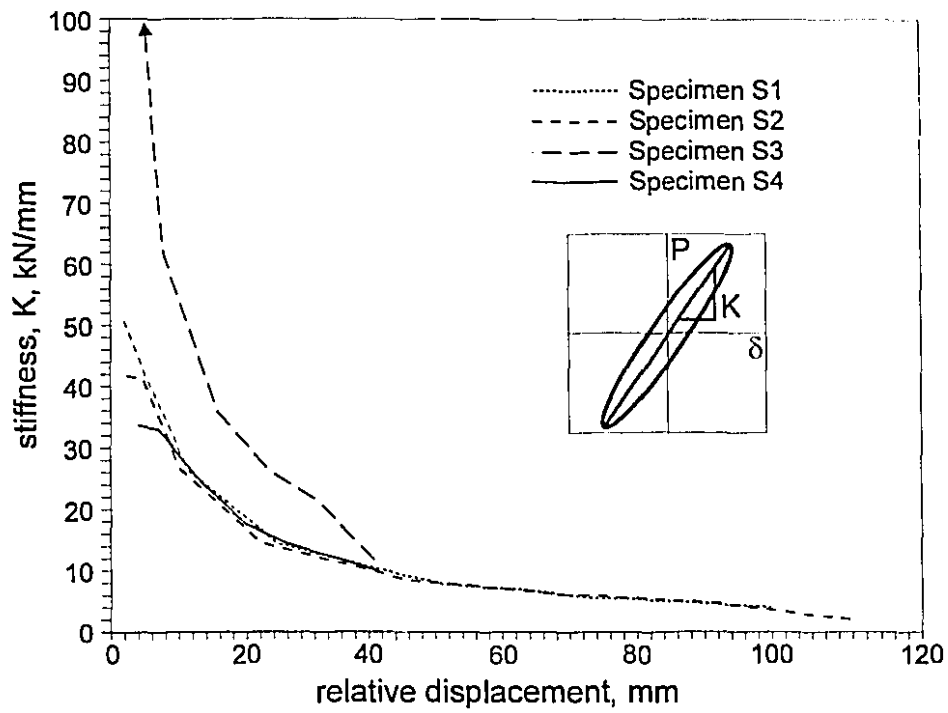


Figure 4.2 Peak-to-peak stiffnesses of Specimens S1 through S4

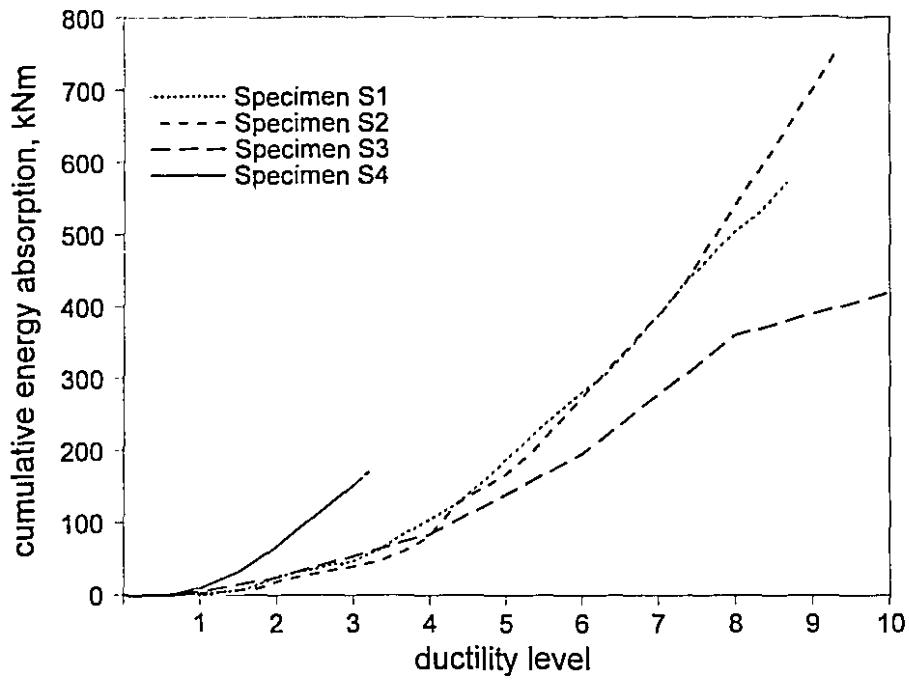


Figure 4.3(a) Cumulative hysteretic energy absorption of Specimens S1 through S4

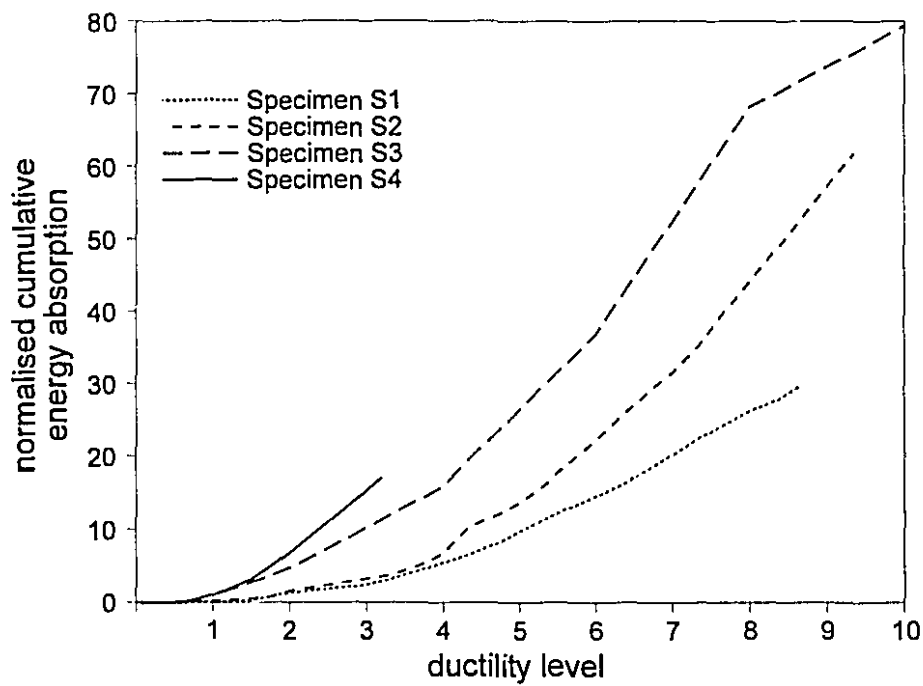


Figure 4.3(b) Normalised cumulative energy absorption of Specimens S1 through S4

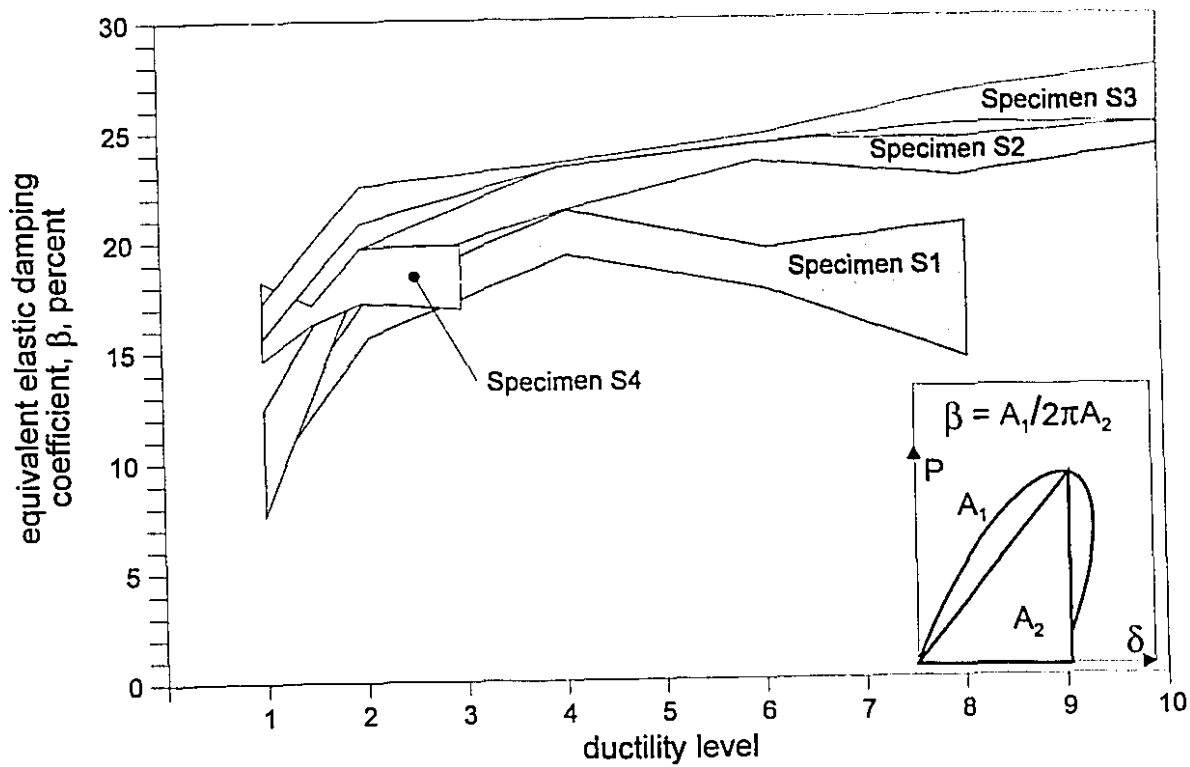


Figure 4.4 Equivalent elastic damping coefficients of Specimens S1 through S4

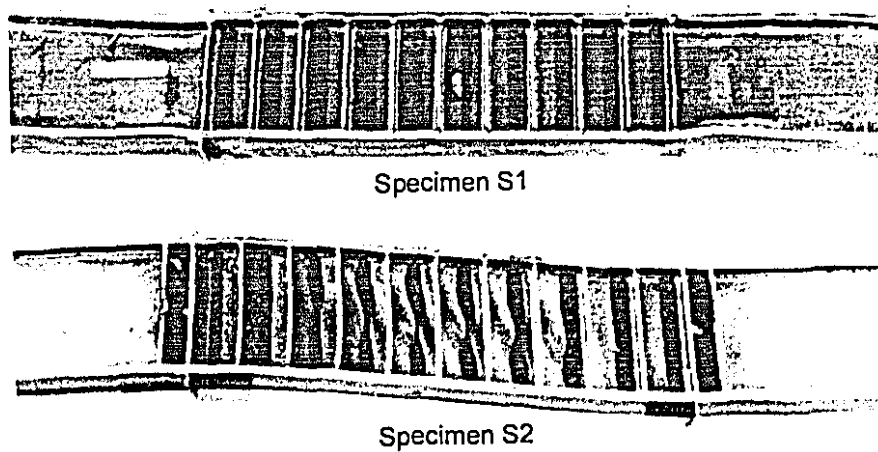


Figure 4.5 Coupling beams of Specimens S1 and S2 after testing

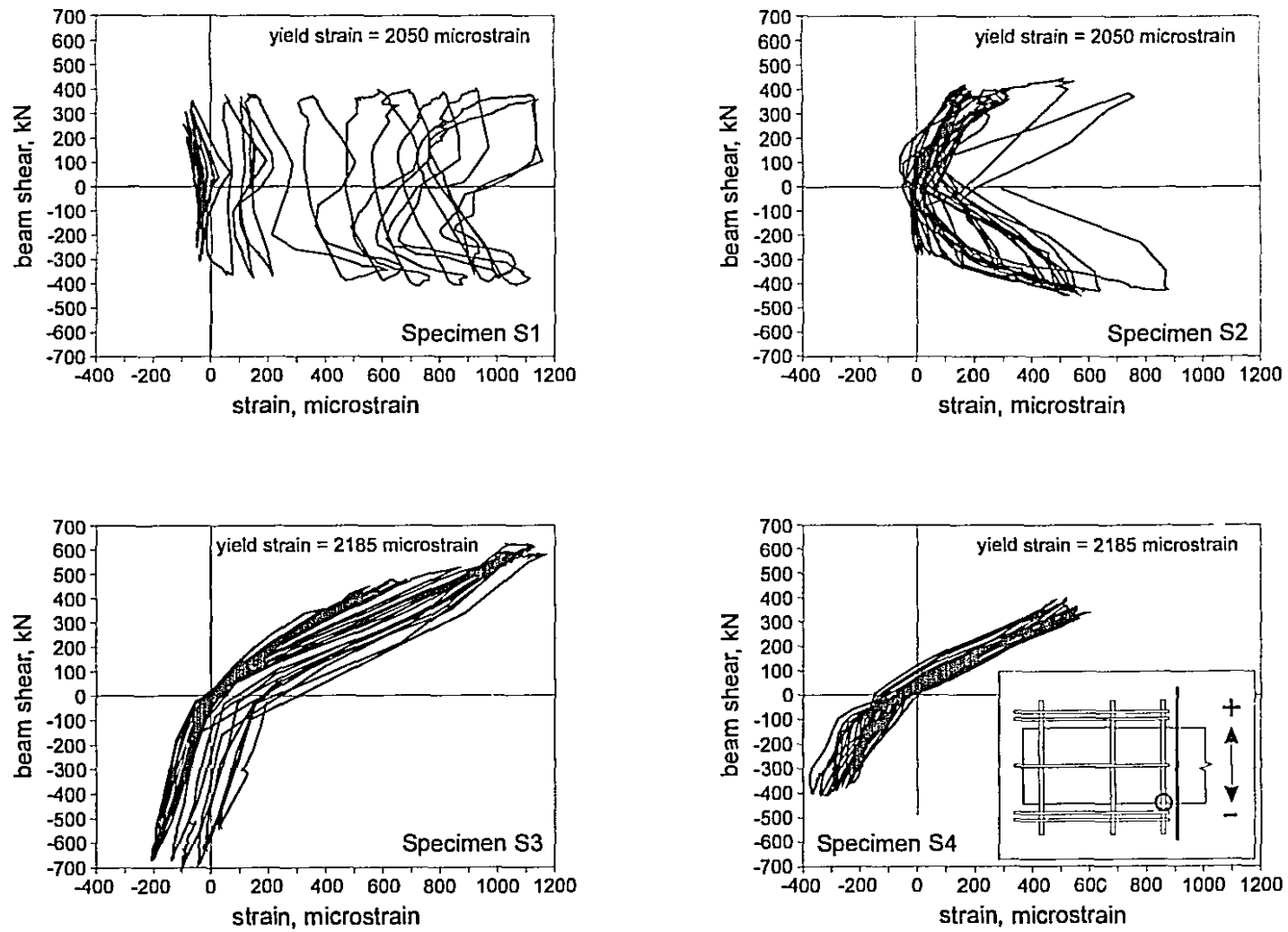


Figure 4.6 Strains in vertical reinforcement at face of wall in Specimens S1 through S4

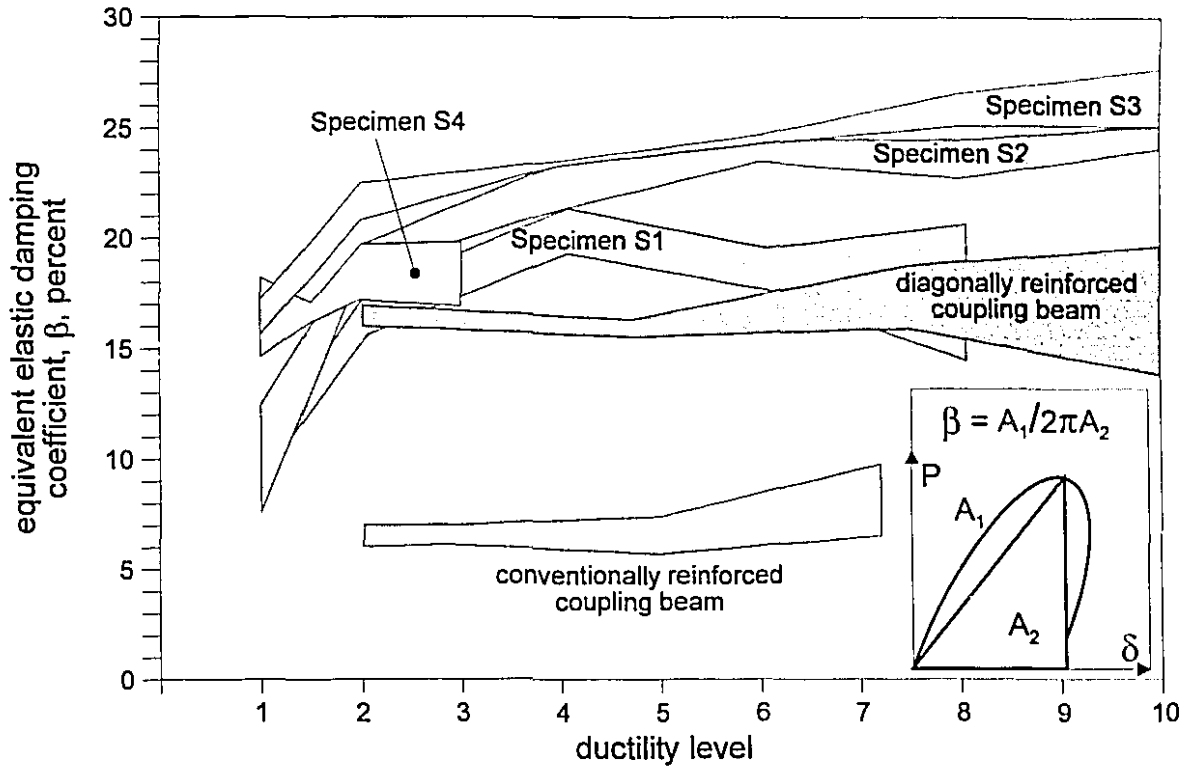


Figure 4.7 Equivalent elastic damping coefficients for Specimens S1 through S4 and reinforced concrete coupling beams (Shiu et al., 1978)

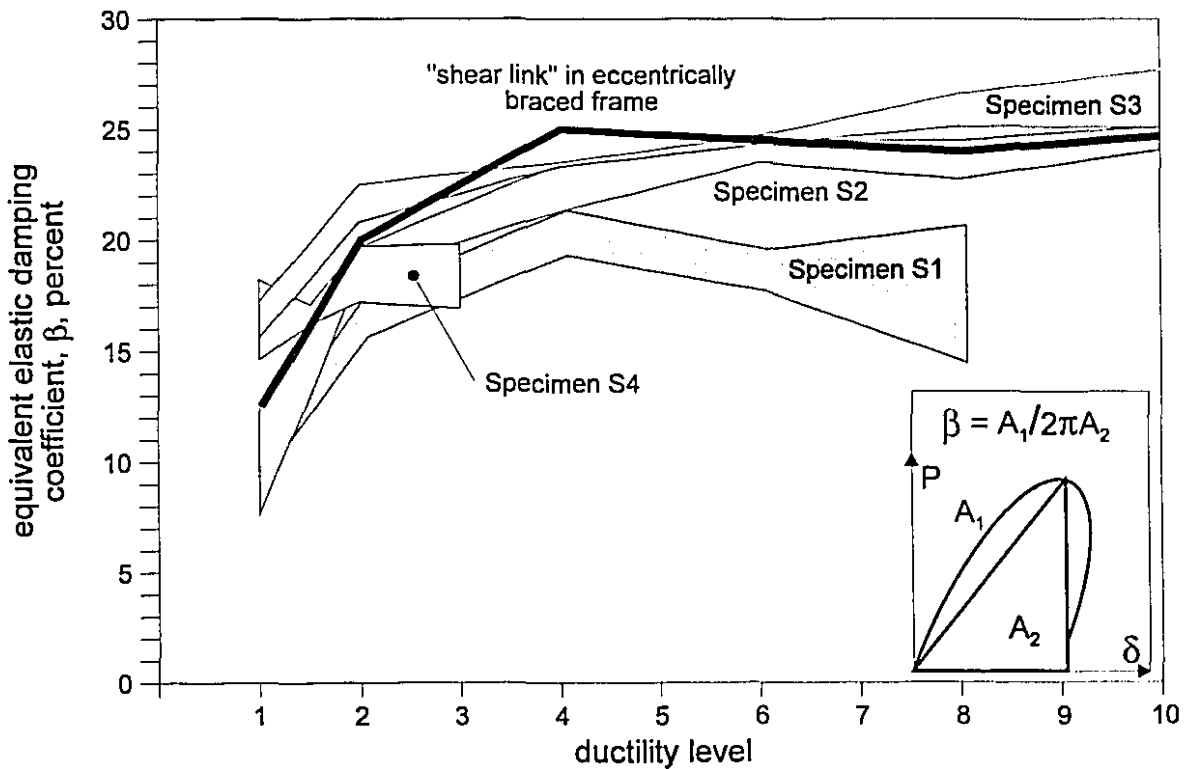


Figure 4.8 Equivalent elastic damping coefficients for Specimens S1 through S4 and steel "shear link" in eccentrically braced frame (Engelhardt and Popov, 1986)

Chapter 5

Design and Modelling of Prototype Structures

In order to investigate the response of embedded steel coupling beams in complete structures, two prototypes were developed. The structures, presented in the following sections, were designed to conform to 1995 National Building Code of Canada (NBCC) requirements.

The prototype structures were designed as fully coupled and partially coupled core wall structures to be located in Vancouver. Clause 4.1.9 of the NBCC was used to determine the design forces for the walls and coupling beams of the structures. The computer program ETABS (1992) was used for the initial elastic analysis. A summary of the development of the prototype models and their initial analyses is presented in Sections 5.1 and 5.2. The design details are discussed in Section 5.3. Section 5.4 reports on the development of non-linear structural models of the prototype structures. The computer program DRAIN-2DX (1992) was used for the non-linear dynamic analyses.

5.1 Design of Prototype Structures

The prototype structures were flat-plate and core-wall structure in which all of the lateral load would be resisted by the core. This conforms with the requirements of both the NBCC and CSA A23.3-94 (hereafter referred to as A23.3).

The 18 storey prototype structures developed are shown in Fig 5.1. The overall structure is 42 m by 30 m, having six 7 m bays in the longitudinal direction (x-direction) and five 6 m bays in the transverse direction (y-direction). A 14 m by 9 m double channel core is located in the centre of the building plan. Coupling beams are located in the middle of the 14 m, longitudinal wall of the core. The resulting structure is symmetric about the centre of the core, thus minimising eccentricities. The floor slabs are 200 mm thick and all of the columns are 600 mm square. The typical storey height is 3.6 m and the ground floor storey height is 4.5 m. The resulting overall height of the structure is 65.7 m.

In order to compare partially and fully coupled wall structures (see Section 5.1.3), two coupling beam dimensions were considered. The coupling beams in the partially coupled structure were 4 m long, while those in the fully coupled structure were 1.3 m long. The reinforced concrete coupling beams, in both cases, were 700 mm deep by 400 mm wide. Prototypes PC and PS are the partially coupled structures having reinforced concrete and steel coupling beams, respectively. Similarly, prototypes FC and FS are the fully coupled structures having reinforced concrete and steel coupling beams, respectively.

Normal density concrete with a compressive strength, f'_c , of 35 MPa was used in the design. The yield stress of reinforcing steel, f_y , was 400 MPa and the yield stress of coupling beam structural steel, F_y , was 300 MPa.

5.1.1 Gravity Loading

The following values were used in determining gravity loads:

mass of concrete	23.5 kN/m ³
floor live load	2.4 kPa
floor mechanical load	0.5 kPa
floor partition (dead) load	1.0 kPa
curtain wall load	0.5 kPa
roof dead load	0.5 kPa
roof mechanical load (over 2 bays)	1.6 kPa
roof snow load (from NBCC 4.1.7)	2.3 kPa

The weight of the structure, W , specified by NBCC 4.1.9.1.(2), was determined as the dead load of the structure plus 25% of the snow load.

5.1.2 Equivalent Lateral Base Shear (NBCC 4.1.9.1)

The minimum equivalent static base shear, V , from clauses 4.1.9.1.(4) and (5) of the NBCC is given by:

$$V = \frac{vSIFW}{R} U \quad (5.1)$$

where: v = zonal velocity ratio, defined as the specified horizontal ground velocity as determined by NBCC 4.1.9.1.(5) and 2.2.1;

S = seismic response factor (4.1.9.1.(6));

I = seismic importance factor (4.1.9.1.(10));

F = foundation factor (4.1.9.1.(11));

W = weight of the structure (4.1.9.1.(12));

R = force modification factor (4.1.9.1.(8) and (9)); and

U = calibration factor, equal to 0.6 (4.1.9.1.(6)).

Vancouver is located in velocity and acceleration zone 4 (ie: $Z_a = Z_v = 4$) and has a zonal velocity ratio, v , of 0.20. In a Canadian context, this is considered to be a significant seismic zone. The seismic response factor, S , is determined as a function of the fundamental period of the structure, T . The relationship used to determine S is given as: $1.5\sqrt{T}$ (4.1.9.1.(6)). The value of the importance factor, I , and foundation factor, F , were taken as 1.0. The selection of the force modification factor is discussed in Section 5.1.3.

The equivalent seismic base shear is distributed over the height of the structure with an inverted triangular distribution as prescribed by NBCC 4.1.9.1.(13)(a). The triangular distribution approximates the response of the fundamental mode shape of the structure. A portion of the load, F_t , is applied at the top of the structure to account for contributions of higher mode shapes to the response of the structure.

The weights of the prototype structures, their fundamental periods, seismic response and force modification factors and their resulting equivalent seismic base shears are given in Table 5.1.

5.1.3 Force Modification Factor, R and the Degree of Coupling

The degree of coupling of a coupled wall structure is the percentage of base overturning moment resisted by the coupled response of the walls; that is axial compression and tension in the walls resulting from shears in the coupling beams. A23.3 Clause 21.1 defines a ductile coupled wall as one "*where at least 66% of the base overturning moment resisted by the wall system is carried by axial tension and compression forces resulting from shear in the coupling beams*". (In the interest of clarity, a ductile coupled wall is referred to as fully coupled in this text.) Similarly, a ductile partially coupled wall is defined as one whose degree of coupling is less than 66%.

Acknowledging the difference in response between coupled and partially coupled walls, A23.3 allows a force modification factor, R , of 4.0 for ductile coupled walls while a force modification factor of 3.5 is permitted for partially coupled walls. For comparison, ductile flexural walls (ie: cantilever walls) are permitted a force modification factor of 3.5. This difference recognises the improved response characteristics of coupled walls with a large degree of coupling.

5.1.4 Load Combinations for Seismic Design

Load combinations for seismic design, for structures without storage loads, are given in the NBCC as:

$$1.0D + \gamma(1.0E) ; \text{ and} \quad (5.2)$$

$$1.0D + \gamma(0.5L + 1.0E) \quad (5.3)$$

where: D = specified dead load;
L = specified live load;
E = specified earthquake loads; and
 γ = importance factor (taken as 1.0).

These prescribed loading conditions represent a considerable simplification from previous versions of the NBCC. It is important to note that in cases where the dead load is counteractive, NBCC 4.1.5.1.(5) requires that the dead load be calculated without including the effect of partition loading. Excluding the partition loading will result in the floor dead loading being only about 85% of the actual specified dead load. One example where the dead load is reduced in this manner is in determining net axial forces in the walls of a coupled wall structure.

5.1.5 NBCC Equivalent Static Elastic Analysis of Prototype Structure

Table 5.1 summarises the analysis parameters for the NBCC equivalent static elastic load analysis for both prototype structures. The design parameters for the ductile flexural wall in the y-direction are given in the last column of Table 5.1. The structural weight, base shear and concentrated load for the y-direction of the fully coupled prototype structure are about 2% greater than those shown for the partially coupled prototype structure. It was determined that the coupled wall response will govern the wall design in both prototypes. It should also be noted that the lateral base shear for wind loading was less than that for seismic loading for each prototype.

	Ductile Coupled Walls FC and FS	Ductile Partially Coupled Walls PC and PS	Ductile Flexural Walls
controlling fundamental period of structure (NBCC 4.1.9.1.(7)(b)(c))	1.58 seconds	1.90 seconds	1.97
seismic response factor, S (4.1.9.1.(6))	1.19	1.09	1.07
degree of coupling (ETABS)	71%	54%	-
force modification factor, R (4.1.9.1.(8) and A23.3 21.1)	4.0	3.5	3.5
weight of structure, W (4.1.9.1.(2))	184783 kN	181448 kN	181448 kN
lateral seismic base shear, V (4.1.9.1.(4))	6615 kN	6776 kN	6647 kN
concentrated load at top of structure, F_t (4.1.9.1.(13)(a))	878 kN	900 kN	1100 kN

Table 5.1 Summary of NBCC equivalent lateral load parameters

5.2 Elastic Analysis of Prototype Structures

The elastic analysis of the prototype structures was carried out using the computer program ETABS (1992). Only the core of the structure was modelled as it was assumed that 100% of the lateral forces would be carried by the core. This assumption allows the higher force modification factors to be used. The remainder of the structure, in this case, need only be capable of *resisting gravity loads under seismically induced deformations* (NBCC 4.1.9.1.(9)(d)). (An ETABS analysis which included the columns predicted that the walls would resist more than 98% of the total lateral loading.)

The core structure is modelled with ETABS as an assemblage of vertical shear walls interconnected by horizontal floor diaphragms which are rigid in their own plane. The panel elements, used to model the core walls, are based on an isoparametric finite element membrane formulation where the in-plane rotational stiffnesses are defined. This formulation provides full continuity of beam elements framed into the panels. ETABS solutions enforce three dimensional displacement compatibility, therefore, torsional and warping effects are accurately modelled.

ETABS also accounts for P- Δ effects in the structural stiffness matrix by using a geometric correction. As such, the effects of the P- Δ phenomenon are reflected in the periods of the structure and are accounted for in the final three dimensional overturning equilibrium.

5.2.1 Criteria for the Selection of a Prototype Model

In developing the prototype structures four principal criteria had to be met:

- (i) The degree of coupling of the system had to allow the intended design to be carried out. That is the partially coupled prototypes, PC and PS, had to have a degree of coupling less than 66%, while the degree of coupling of prototypes FC and FS had to exceed 66%.
- (ii) Under specified loading conditions, there could be no uplift (i.e. net tension) at the base of the tension wall of the coupled wall system. In determining the resultant forces at the base of the wall, the gravity dead loads do not include partition loading as required by NBCC 4.1.5.1.(5) (see Section 5.1.4). Satisfying this criteria justifies the use of fully fixed boundary conditions at the base of the structure.
- (iii) The interstorey drift limits of NBCC 4.1.9.2.(3) had to be respected: The maximum interstorey drift, multiplied by the force modification factor, R, can not exceed 2% of the storey height.
- (iv) The shear in the coupling beams had to respect the limits defined in A23.3 21.5.8.2. For the fully coupled prototype, where diagonal reinforcement was to be used, the shear in the reinforced concrete coupling beam could not exceed:

$$1.0\sqrt{f'_c} \quad (5.4)$$

For the partially coupled prototype, the shear in the reinforced concrete coupling beam is limited to:

$$0.1(\ell_u/d)\sqrt{f'_c} \quad (5.5)$$

where: ℓ_u = the clear span of the coupling beam;
d = distance from the extreme compression fibre to the centroid of the tensile reinforcement; and
 f'_c = the compressive strength of concrete.

Furthermore, for the partially coupled prototypes, the span-to-depth ratio, ℓ_u/d , must exceed 4.0 (A23.3 21.5.8.2 and 21.3.1)

5.2.2 Results of Elastic Analysis of the Prototype Models

The prototypes were modelled with ETABS. Torsional effects were included as specified by NBCC 4.1.9.1.(23). The equivalent lateral loads were applied to the structure with a 10% eccentricity from the coincident shear centre and centre of mass of the structure. This prescribed eccentricity accounts for accidental eccentricities as there is no computed structural eccentricity. The inclusion of torsional effects increases the shear in one coupling beam, simultaneously reducing it in the other. Since torsional effects may be applied in either direction, the larger beam shear is used for design of all coupling beams. The effect of including torsional effects in the analysis was to increase the critical beam shears 16% and 23% in the partially and fully coupled prototypes, respectively.

P- Δ effects were also included in the analysis. Since only the core wall is considered to resist lateral loads, the P- Δ effects were approximated in a conservative manner by

increasing the vertical load on the walls to reflect the entire weight of the structure. These additional loads are not included in the dead load analyses. In order to account for inelastic deformations (NBCC, 1995), the stiffness of the elements were reduced by a factor of 1/R. As coupled walls are relatively stiff structures, the P- Δ effects are relatively small. In the case of the partially coupled prototype, the P- Δ effects increase the wall forces by less than 10%. The P- Δ effects in the stiffer fully coupled prototype structure result in less than a 4% increase in design forces.

In order to account for non-linear effects, the stiffness of the coupling beams was reduced by 50% (this was done by specifying a beam of only one-half its actual width). The stiffness of the walls was not adjusted.

A23.3 allows for up to 20% redistribution of the coupling beam forces. It is likely that this would result in uniform coupling beam details over the height of the prototype structures.

The results of the elastic analysis, in terms of the selection criteria (see Section 5.2.1) are given in Table 5.2. Both prototype structures responded within the NBCC drift limits in the perpendicular, flexural wall direction.

	Ductile Coupled Wall	Ductile Partially Coupled Wall
degree of coupling	71%	54%
tension resultant from coupling action	21780 kN	15603 kN
compression resultant from dead load	22534 kN	21027 kN
maximum allowable interstorey drift (4.1.9.2.(3))	18.0 mm	20.6 mm
maximum observed interstorey drift	2.2 mm	7.1 mm
maximum allowable beam shear (A23.2 21.5.8.2)	1325 kN (Equation 5.4)	842 kN (Equation 5.5)
maximum observed beam shear	1006 kN	603 kN

Table 5.2 Summary of elastic analysis prototype criteria

5.2.3 Force Reduction Coefficients

Design forces for the prototype structures were determined from the elastic ETABS analyses. NBCC 4.1.9.1.(20) allows a force reduction coefficient, J , to be applied to the base overturning moment. Furthermore, NBCC 4.1.9.1.(21) allows a similar coefficient, J_x , to be applied to the overturning moment at each level, x , of the structure. The force reduction

coefficients are used to account for the effect of response modes greater than the fundamental frequency on which the NBCC equivalent static lateral analysis is based.

For the prototype structures considered, J is equal to 0.8 at the base of the structure and J_x ranges from 0.8 in the first storey to 1.0 at the roof level. As the core is considered to act alone in resisting lateral forces, the entire reduction is applied to forces in the core. Overturning moment, shear and axial load in the walls and shear in the coupling beams, determined by elastic analysis, are reduced by the appropriate force reduction coefficients to determine design forces.

5.3 Design of Prototype Coupling Beams

In order to adequately compare the responses of reinforced concrete and steel coupling beams, beams with similar stiffnesses and capacities are required. The design procedure for the prototype structures involved first designing an appropriate reinforced concrete coupling beam according to the requirements of CSA A23.3 Clause 21. A comparable steel beam was then selected based on the criteria discussed in Sections 5.3.2 and 5.3.4 and designed according to the requirements of CSA S16.1 Clause 27. The compatibility of the resulting pairs of prototype structures was verified by additional equivalent static ETABS analyses using as-designed coupling beams.

In order to simplify the modelling procedure and not to introduce additional parameters, the coupling beams are identical over the height of the structure as are the wall thicknesses. This simplification will result in a stiffer structural response, particularly in the upper levels of the structure.

5.3.1 Reinforced Concrete Coupling Beams for Partially Coupled Prototype Structure PC

The details of the conventionally reinforced concrete coupling beam for the ductile partially coupled wall, PC, are shown in Fig. 5.2 (a). The 4 m long, 700 x 400 mm beam has 8 No. 30 longitudinal reinforcing bars, in two layers, at both the top and bottom of the section. Shear reinforcement consists of double-leg, No. 10 seismic hoops spaced at 90 mm. The No. 30 longitudinal bars are embedded 1900 mm into each wall. The coupling beams satisfy the requirements for ductile seismic design of CSA A23.3 Clauses 21.3, 21.5 and 21.7.

The capacity of the coupling beams was determined using the computer program RESPONSE (Collins and Mitchell, 1991). RESPONSE uses an iterative analysis procedure linking a plane sections analysis for flexure and axial load with the Modified Compression Field Theory (Collins and Mitchell, 1991) for shear. The coupling beams were determined to be "flexure critical" and have a flexural capacity of 1230 kNm.

5.3.2 Steel Coupling Beams for Partially Coupled Prototype Structure PS

Selection of a steel coupling beam for the partially coupled prototype structure was made based on matching, as closely as possible, the capacity and stiffness of the designed reinforced concrete beam. The selection criteria for the steel beam were as follows:

- i) The flexural stiffness, EI , of the steel section should be similar to the cracked stiffness of the reinforced concrete beam, assumed to be $0.5EI_g$. The moment of inertia of the steel beam will therefore be $0.5E_c/E_s \approx 7.5\%$ of the gross section moment of inertia, I_g , of the reinforced concrete beam.
- ii) The section must be flexure critical over the given span and conform to the limits of a Class 1 section (CSA S16.1 M94).
- iii) The overall width of the section, b , must fit within the concentrated wall steel. In this case, the allowable width was limited to 270 mm.
- iv) The section should be a rolled section available in Canada.

Satisfying criteria i and ii will ensure that the degree of coupling of the structure, and therefore the elastic response, will remain essentially the same as for the walls with reinforced concrete coupling beams.

A W610 x 140 section was chosen (see Fig. 5.2 (b)). The coupling beam is provided with full depth stiffeners at the face of each wall and does not require any intermediate stiffeners. The required embedment length, determined from Equation 2.9, is 1475 mm. The design of the steel coupling beam satisfies the requirements for flexure critical link beams of CSA S16.1 M94 Clause 27.6.

The capacity of the steel coupling beam is about 7.5% greater than that of the reinforced concrete coupling beam. This results in a slight increase, from 54% to 55%, in the degree of coupling for the steel coupling beam system over the reinforced concrete coupling beam system. This increase translates to a 3.6% decrease in moment at the base of the walls.

5.3.3 Reinforced Concrete Coupling Beams for Fully Coupled Prototype Structure FC

The details of the diagonally reinforced concrete coupling beam for the ductile coupled wall, FC, are shown in Fig. 5.2 (c). The 1.3 m long, 700 x 400 mm beam has diagonal reinforcement consisting of 4 No. 35 bars enclosed with No. 10 hoops, spaced at 100 mm, in each direction. (Alternatively, the diagonal bars may be enclosed in a 150 mm diameter spiral with a 100 mm pitch.) The diagonal steel is embedded 2000 mm into each wall and is confined over its entire length. Conventional No. 15 corner and midside reinforcement, enclosed with No. 10 seismic hoops spaced at 300 mm, is also provided. The coupling beams satisfy the requirements for ductile seismic design of A23.3 Clause 21.5.

The flexural capacity of the prototype coupling beams was determined to be 705 kNm. The design method for diagonally reinforced concrete beams ensures that the member behaves in a ductile flexural manner.

5.3.4 Steel Coupling Beams for Fully Coupled Prototype Structure FS

Selection of a steel coupling beam for the coupled prototype structure was based on matching, as closely as possible, the capacity and stiffness of the designed reinforced concrete beam. The selection criteria for the steel beam were as follows:

- i) The flexural stiffness, EI , of the steel section should be similar to the cracked stiffness of the reinforced concrete beam.
- ii) The section must be shear critical over the given span and, since it will be heavily stiffened, need only conform to the limits of a Class 2 section (CSA S16.1 M94).
- iii) The overall width of the section, b , must fit within the concentrated wall steel. In this case, the allowable width was limited to 300 mm. (In practice, this may prove a difficult criterion to satisfy, particularly where built-up sections are required.)
- iv) The section should be available in Canada.

A WWF700 x 164 section with additional 19 mm flange plates was chosen (see Fig. 5.2 (d)). The coupling beam is provided with full depth stiffeners at the face of each wall and intermediate stiffeners on both sides of the web spaced at 130 mm along its span (CSA S16.1 Clause 27.6.5). The required embedment length, determined from Equation 2.9, is 745 mm. The design of the steel coupling beam satisfies the requirements for shear critical link beams of CSA S16.1 M94 Clause 27.6.

The capacity of the steel coupling beam is about 5% less than that of the diagonally reinforced concrete coupling beam. This results in a decrease, from 71% to 69%, in the degree of coupling for the steel coupling beam system from the reinforced concrete coupling beam system. This decrease translates to a 7.3% increase in moment at the base of the walls.

5.3.5 Design of the Reinforced Concrete Walls

The reinforced concrete walls were designed in accordance with CSA A23.3 Clause 21.5. The walls are required to have a *moment resistance greater than the overturning moment corresponding to the development of the nominal moment resistance of the coupling beams above the level under consideration*. The wall overstrength factor, γ_w , therefore, is determined from the cumulative effect of the individual beam overstrength factors, γ_b . The wall overstrength factor is applied to the wall design forces in addition to the force reduction factor, J_x (see Section 5.2.3).

For simplicity of modelling, the coupling beams are assumed to have the same details over the height of the structure, resulting in slightly larger wall design forces. The wall

overstrength factors for the partially coupled prototypes range from 1.24 to 1.54, indicating that there would be little variance in coupling beam design over the height of the structure. The wall overstrength factors for the coupled prototypes range from 1.54 to 2.71. In the transverse direction (i.e.: the ductile flexural wall), only the force reduction factors are applied.

The core of each prototype structure consists of two channel-shaped walls arranged toe-to-toe, connected with the coupling beams (see Fig. 5.1). The walls have areas of concentrated reinforcement at each beam-wall interface, at the toes of the channel, and at the corners where the "flanges" meet the "web" of the walls. The capacity of the walls under the combined effect of flexure and axial loads was determined with the computer program RESPONSE (Collins and Mitchell, 1991). It should be noted that with the toe-to-toe arrangement, the wall subject to weak direction bending is simultaneously the compression wall of the coupled wall couple. Table 5.3 summarises the reinforcing details at the base of each wall. These details were kept constant over the first three storeys, as required by A23.3 in regions of possible hinging.

	Partially Coupled Walls PC and PS	Coupled Walls FC and FS
concentrated reinforcement at beam-wall interface	10-No. 35 in two rows at 135 mm	4-No. 30
concentrated reinforcement at wall corner	32-No. 35 in two rows at 135 mm	22-No. 35 in two rows at 135 mm
distributed vertical reinforcement in wall flange	26-No. 15 in two curtains at 300 mm	36-No. 15 in two curtains at 300 mm
distributed vertical reinforcement in wall web	30-No. 15 in two curtains at 300 mm	40-No. 15 in two curtains at 300 mm
distributed horizontal reinforcement in wall flange	two curtains No. 15 at 125 mm	two curtains No. 15 at 140 mm
distributed horizontal reinforcement in wall flange	two curtains No. 15 at 450 mm	two curtains No. 15 at 130 mm

Table 5.3 Reinforcing details at the bases of the prototype core walls

5.4 Modelling Prototype Structures for Non-linear Dynamic Analysis

The prototype structures were modelled using the plane frame, non-linear dynamic computer program DRAIN-2DX (1992). The prototype structures are modelled as equivalent frames (see Section 1.2.2). The walls are modelled as equivalent columns located at the centroid of each wall (see Fig. 5.3(a)). The beams have rigid offsets at their ends modelling the width of the walls (see Figs. 5.3(b) through (e)). As one of the design criteria for the prototype structures was that neither wall go into tension (see Section 5.2.1, item (ii)), an assumption of fixed end conditions at the base of the walls was considered appropriate. (DRAIN-2DX actually requires that a stiff support spring, rather than a nodal restraint, be used for degrees of freedom through which dynamic effects are introduced. This essentially means that the node has zero displacement, relative to the ground, rather than zero absolute displacement.) In order to minimise computational demands, the lateral displacements at each storey are constrained, thus axial loads in the coupling beams are neglected.

The walls are modelled with 90% of their gross moment of inertia (Paulay and Priestley, 1992). Because of the large variability of axial load in the walls, it is necessary to define an axial load-moment interaction surface for the wall elements. The axial load-moment interaction envelope is defined in DRAIN-2DX by six points: positive and negative axial and moment capacities (see Table 5.4) and the positive and negative "balance points" defined as the peak moment capacities of the element under compression. At a particular time step, this interaction relationship is used to find the nominal flexural resistance corresponding to the axial load on the wall. This is then used to generate the appropriate moment-rotation response for the wall.

The stiffness of the reinforced concrete coupling beams were taken as 50% of their gross stiffness (Paulay and Priestley, 1992). It should be noted that values for assumed stiffness of reinforced concrete coupling beams are open to a great amount of interpretation and vary considerably in the literature. The initial stiffness of the coupling beams was appropriately reduced to account for shear deformations (see Eq. 4.2). Furthermore, for each steel coupling beam, the initial stiffness used for analysis was calculated considering an effective clearspan of the beam equal to 1.05 times the actual span. This value is consistent with the experimentally observed initial stiffness results presented in Table 4.2. Strain hardening stiffness was taken as 2% of elastic stiffness for the steel coupling beams. No post-yield stiffness was assigned to the reinforced concrete coupling beams.

Elastic stiffness damping was assumed to be 4% of critical damping for the prototypes with reinforced concrete coupling beams and 3% of critical damping for those with steel beams (Paulay and Priestley, 1992).

Horizontal ground accelerations (see Section 5.5) were introduced at the base of the structure. The ground motion records were discretised at 0.02 seconds. The time step used for dynamic analyses was 0.005 seconds. A summary of input parameters of the DRAIN-2DX models is given in Table 5.4.

	PC	PS	FC	FS
	WALL ELEMENTS			
Distance between wall centroids	11072 mm		9984 mm	
Young's modulus	32.5 MPa		32.5 MPa	
Moment of inertia	16.12 x 10 ¹² mm ⁴ (90% I _{gross})		31.28 x 10 ¹² mm ⁴ (90% I _{gross})	
Cross-section area	7.28 x 10 ⁶ mm ²		8.36 x 10 ⁶ mm ²	
Positive moment capacity	125661 kNm		127715 kNm	
Negative moment capacity	52711 kNm		24000 kNm	
Compressive capacity	289548 kN		316252 kN	
Tensile capacity	38080 kN		25920 kN	
	COUPLING BEAM ELEMENTS			
Length of beam	4000 mm		1300 mm	
Young's modulus	32.5 MPa	200000 MPa	200000 MPa	200000 MPa
Moment of inertia	5.71 x 10 ⁹ (50% I _{gross})	1.12 x 10 ⁹	diagonal truss elements	3.18 x 10 ⁹ neglects web
Cross-section area	2.80 x 10 ⁵	1.79 x 10 ⁵	4000 mm ²	3.24 x 10 ⁵
Moment capacity	±1230 kNm	±1245 kNm	±705 kNm (truss capacity: ±1600 kN)	±2587 kNm
Shear capacity	flexure critical, not applicable	flexure critical, not applicable	> 1084 kN	±940 kN stiffness: 485100 kPa
Elastic damping	4%	3%	4%	3%

Table 5.4 Prototype DRAIN-2DX model properties

5.4.1 Conventionally Reinforced Coupling Beams of Prototype PC

The coupling beams of PC were sufficiently long (span-to-depth ratio of 5.7) to be considered typical flexural beams. The DRAIN-2DX beam-column element is, however, unable to model the pinched hysteretic response typical of reinforced concrete in flexure. The method used to model the pinching behaviour involved modelling the coupling beam as a rigid member spanning between rotational springs (see Fig. 5.3(b) and 5.4(a)). The springs available in DRAIN-2DX allow a pinched hysteretic response to be achieved (Fig. 5.4(b)). Using two springs in parallel, one exhibiting pinched (or gap closure) behaviour (Fig. 5.4(c)), the other having inelastic unloading parameters (Fig. 5.4(d)), any degree of pinched response can be achieved. The beam stiffness and capacity is assigned to the springs in the ratio that reflects the degree of pinching. For these models, 90% of the beam stiffness was assigned to the spring with the pinched hysteretic behaviour.

5.4.2 Steel Coupling Beams of Prototype PS

The flexure critical steel coupling beams of PS were modelled using the beam-column element available in DRAIN-2DX. The beams spanned between the centroids of the walls and were provided with rigid offsets at their ends representing the width of the wall (see Fig. 5.3(c)). This arrangement accurately represents the coupling beam behaviour up to the point where flange buckling in the flexural hinges becomes likely. Once flange buckling occurs, significant strength degradation would become apparent. It was felt that ductility levels exceeding 4 would be required before strength degradation would become apparent, as such the simple beam-column element was considered sufficient.

5.4.3 Diagonally Reinforced Coupling Beams of Prototype FC

The method of modelling the short, diagonally reinforced coupling beams of FC is shown in Figure 5.3(d). The diagonal reinforcement is assumed to act as tension and compression resisting truss elements. This model directly reflects the design procedure for diagonally reinforced concrete beams (Paulay and Binney, 1974). In order to verify this model, the results of the diagonal truss model were used to predict the response of Paulay's Beam 317 (see Fig. 5.5). The truss elements are made up of only the diagonal reinforcing steel and are assumed to have the same stiffness and capacity in both compression and tension. A truss model using the steel tensile response and confined concrete compressive response was found to significantly overestimate the beam load-deformation response. As can be seen in Figure 5.5, the diagonal truss model accurately predicts the observed response of the diagonally reinforced Beam 317.

The use of diagonal trusses requires that rigid beam-column elements be used to span from the wall column to the end of the beams (see Fig. 5.3(d)). This model results in significantly greater computational demands and necessitates post-processing to determine coupling beam shears and moments.

5.4.4 Steel Coupling Beams of Prototype FS

Because the coupling beams of FS are shear critical, the DRAIN-2DX beam-column element will not, alone, adequately model the response of the beam. The beam is modelled as an elastic flexural beam with rotational springs at each end to model the shear behaviour (see Fig. 5.3(e)). The span of the beam is modelled as it appears in the prototype, with the moment of inertia calculated neglecting the effect of the web, which is assumed to yield (this is consistent with step 2 of the design method outlined in Section 2.1). The rotational springs at each end of the beam are assigned a capacity equal to the shear capacity of the beam and a stiffness equal to the shear stiffness, GA_w , of the beam (see Fig. 5.6(a)).

In order to verify the appropriateness of this technique, a model of Specimen S3 was subjected to the displacement history shown in Fig. 2.7. The resulting hysteretic behaviour of the model and of Specimen S3 are shown in Fig. 5.6(b). The DRAIN-2DX model closely predicts both the observed stiffness and capacity. The DRAIN-2DX bi-linear model is unable to predict the Bauschinger effect, however this will not significantly effect the response parameters of interest in this study.

5.5 Selection Criteria for Input Ground Acceleration Records

In order to accurately assess the mean maximum response of a structure, non-linear dynamic analysis is typically carried out using a number of different accelerograms. The selection of accelerograms should reflect the expected nature of ground motion. It has been shown (Newmark and Hall, 1982) that strong energy content (related to velocity, rather than peak horizontal ground acceleration), is one of the most important parameters affecting structural damage. As such, most code writing bodies (including NBCC, 1995) use both acceleration and velocity criteria in categorising design ground motion. The peak acceleration to peak velocity ratio, a/v , therefore, becomes an important criteria in selecting representative ground motions. The acceleration records used for this study were selected on the basis of their a/v ratios.

The NBCC gives design values for peak horizontal acceleration (PHA) and peak horizontal velocity (PHV) corresponding to a probability of exceedance of 10% in 50 years (a probability of 0.0021). The maximum accelerations and velocities used for this study were assumed to be 1.5 times the maximum design values. It is felt that such scaling represents the maximum

credible earthquake. It must be noted that it is not possible to accurately estimate the probability of occurrence of such an event in Canada due to a lack of data. Table 5.5 gives the PHA and PHV values for Montréal and Vancouver.

Location	NBCC Design PHA (g)	NBCC Design PHV (m/s)	a/v	Maximum credible PHA (g)	Maximum credible PHV (m/s)
Montréal	0.180	0.097	2	0.270	0.146
Vancouver	0.210	0.210	1	0.315	0.315

Table 5.5 Ground motion parameters for locations of prototype structures

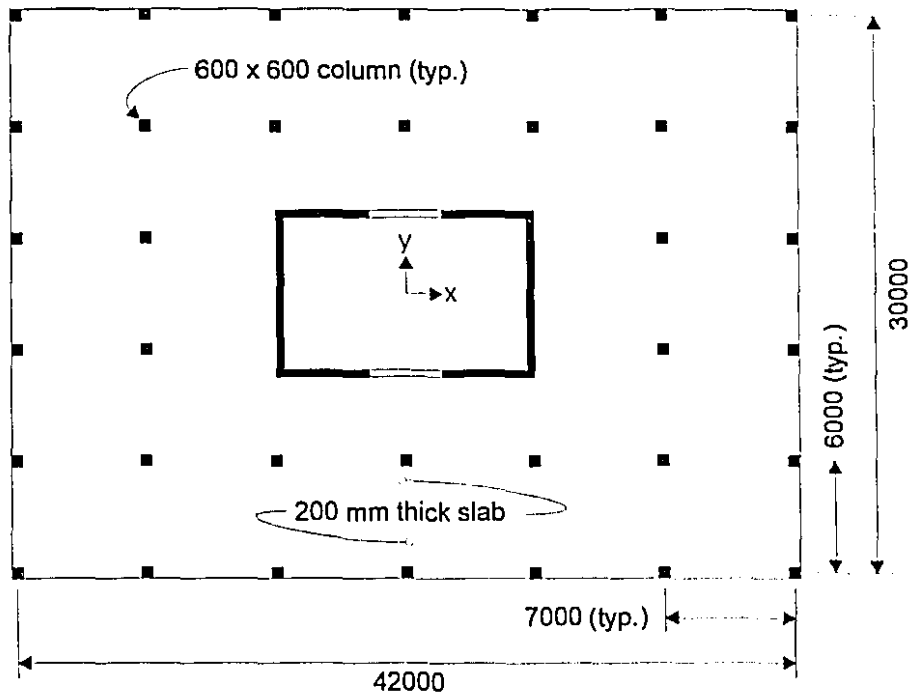
The prototype structures all fall into the category of medium to long period structures whose response is principally controlled by velocity parameters rather than acceleration. Each ground motion record selected was scaled by the ultimate PHV value (see Table 5.5). The resulting scaled accelerograms maintain their characteristic a/v ratios and represent large earthquakes having a low probability of exceedance. It is felt that with these appropriately scaled ground motions, significant non-linear behaviour of the prototype structures would be predicted.

5.5.1 Selected Ground Acceleration Records

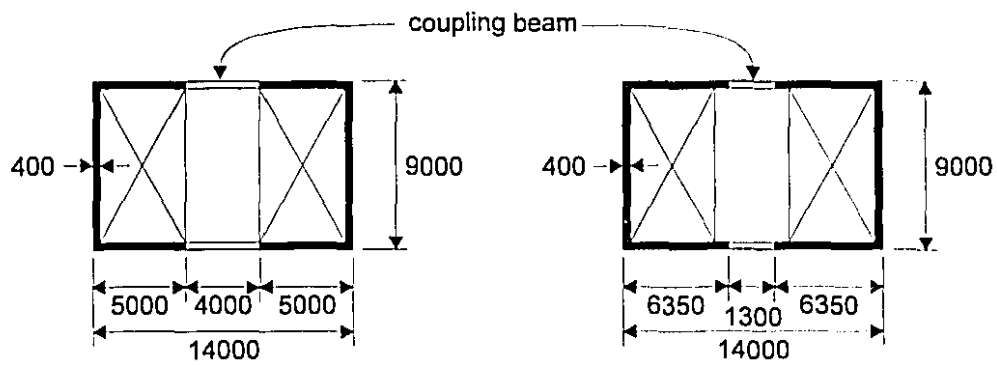
Seven acceleration records were selected, four having characteristics typical of "West coast" earthquakes and three typical of "Eastern" earthquakes. The prototypes structures, located in Vancouver, were subjected to the ground motions from the 1989 Loma Prieta (Maley, et al, 1989), the 1971 San Fernando, (MUSE, 1987), the 1952 Kern County (MUSE, 1987) and the 1940 Imperial Valley earthquakes. These records have a/v ratios of 0.86 to 1.31. In order to investigate the response of coupled wall structures in less severe seismic zones, three "Eastern" records, representative of Montréal, were also selected. The partially coupled prototype, with its beam and wall capacities suitably reduced, was subjected to the ground motions from the 1988 Saguenay, Québec (Munro and Weichert, 1989), the 1985 Nahanni, NWT (MUSE, 1987) and the 1966 Honshu, Japan (MUSE, 1987). These records have a/v ratios ranging from 1.02 to 5.16. Table 5.6 summarises the key parameters of the selected ground motions and their PHA values scaled to give peak horizontal velocities equal to the NBCC PHV. (The names in bold text, are the name by which each record will be referred to hereafter.)

Earthquake Record	Comp.	PHA (g)	PHV (m/s)	a/v	scaled PHA (g)
Vancouver (1.5 x PHV = 0.315 m/s)					
Loma Prieta 3, California, October 17, 1989	0°	0.472	0.361	1.31	0.412
Kern County, (Taft), California, July 21, 1952	111°	0.176	0.177	0.99	0.313
San Fernando (Griffith Park), California, February 9, 1971	0°	0.177	0.205	0.86	0.272
El Centro, Imperial Valley, California, May 18, 1940	0°	0.342	0.334	1.02	0.323
Montréal (1.5 x PHV = 0.146 m/s)					
Saguenay (Chicoutimi Nord), Canada, November 25, 1988	124°	0.129	0.025	5.16	0.753
Nahanni, Canada, December 23, 1985	0°	1.101	0.462	2.38	0.348
Honshu, Japan, April 5, 1966	0°	0.265	0.111	2.39	0.348

Table 5.6 Parameters of selected input ground motion



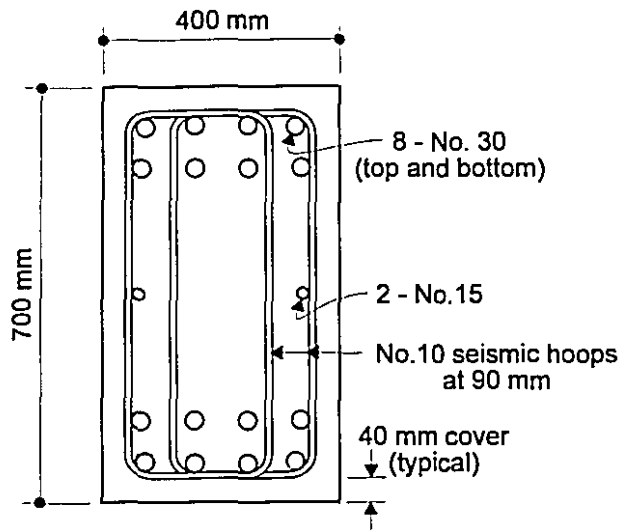
(a) typical floor plan



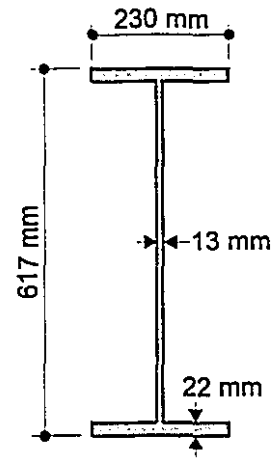
(b) core of partially coupled wall system (prototypes PC and PS)

(c) core of fully coupled wall system (prototypes FC and FS)

Figure 5.1 Prototype structures

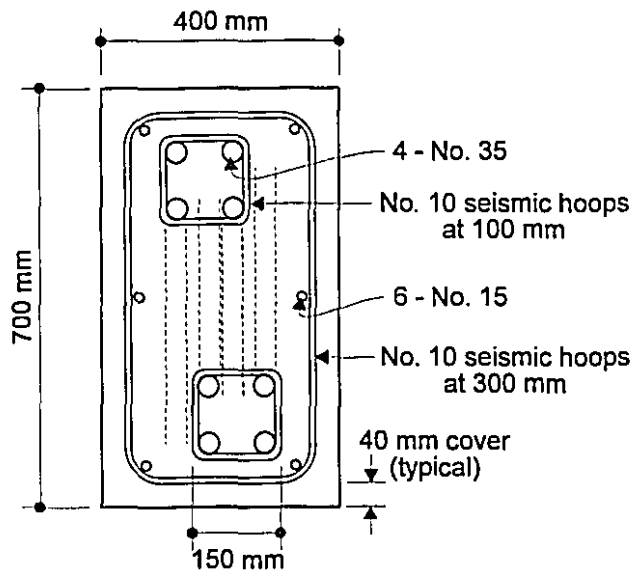


(a) Prototype PC

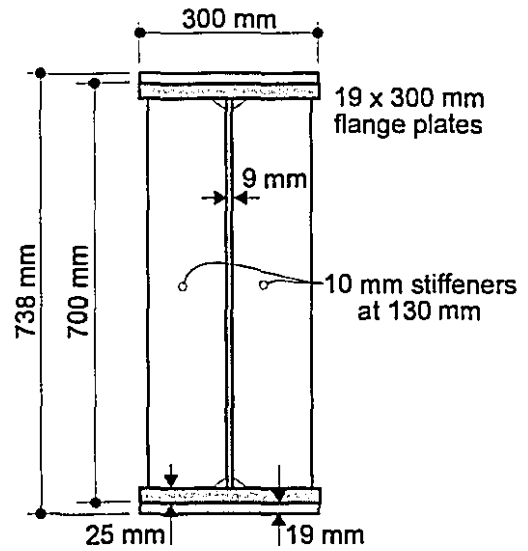


W610 x 140
no intermediate stiffeners required

(b) Prototype PS



(c) Prototype FC



WWF700 x 164

(d) Prototype FS

Figure 5.2 Prototype coupling beam details

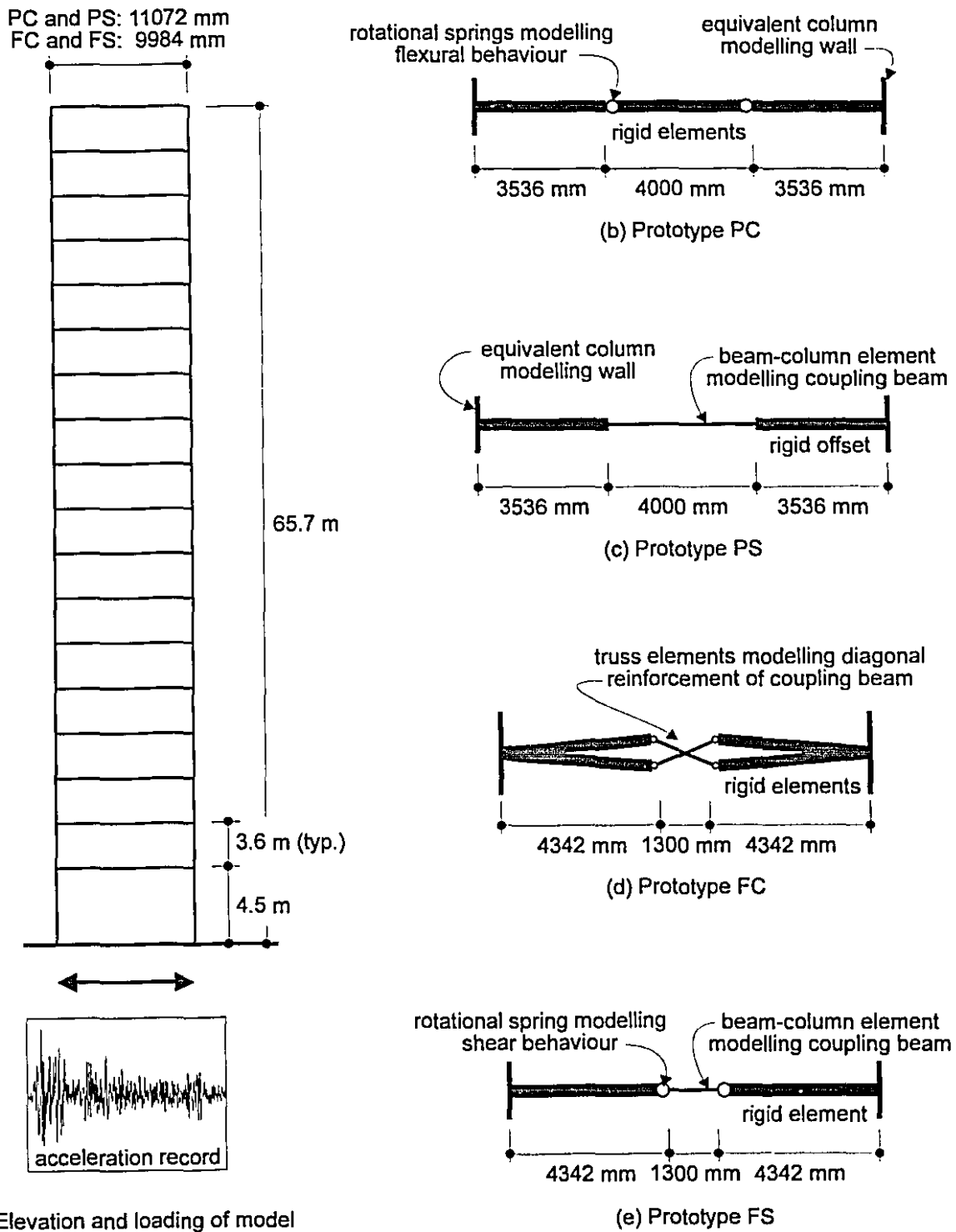
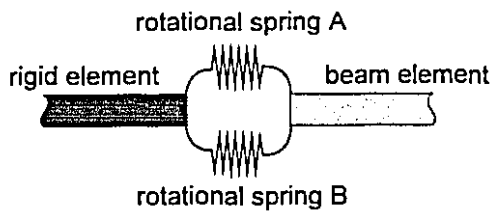
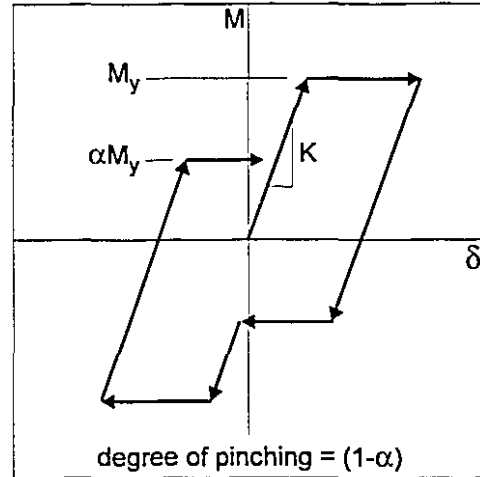


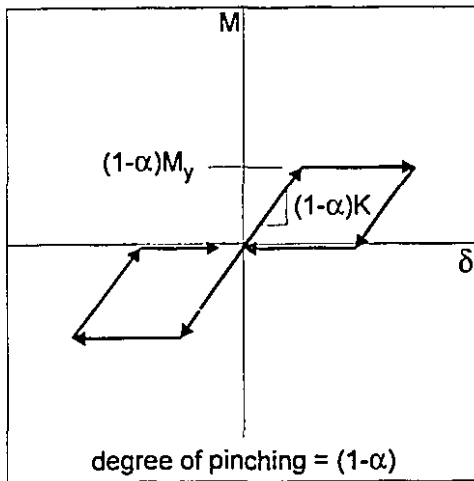
Figure 5.3 DRAIN-2DX model of prototype structures



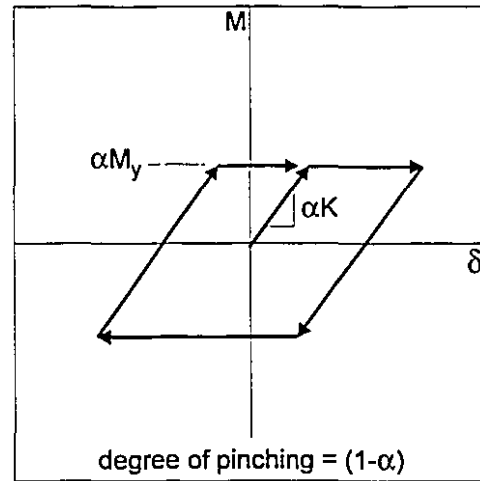
(a) parallel rotational springs modelling "pinched" hysteretic behaviour of reinforced concrete coupling beams



(b) "pinched" hysteretic response of reinforced concrete provided by rotational springs A and B

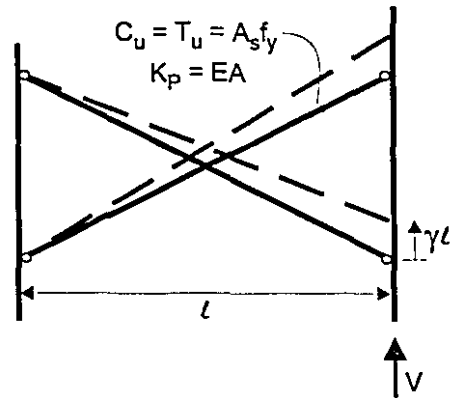


(c) "pinched" behaviour of rotational spring A

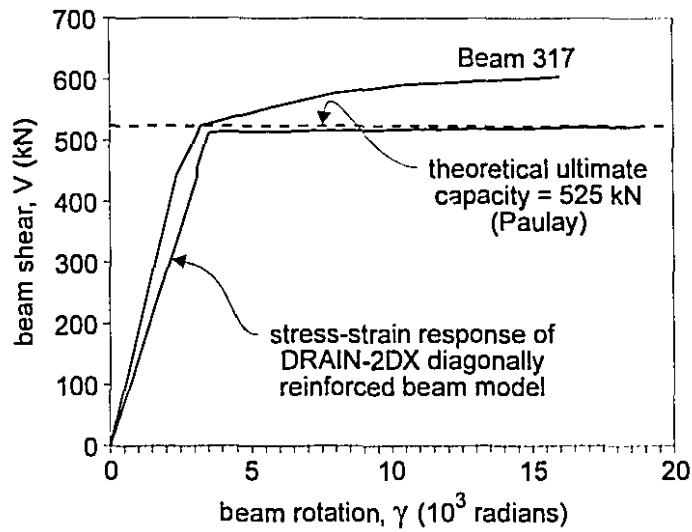


(d) inelastic behaviour of rotational spring B

Figure 5.4 Development of "pinched" hysteretic model for reinforced concrete coupling beams

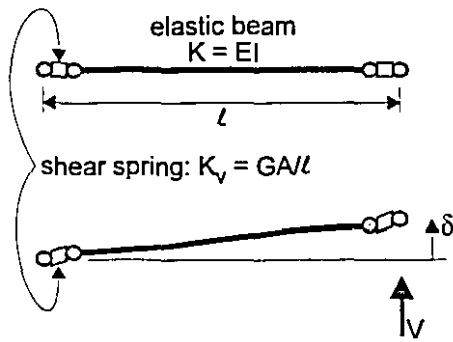


(a) diagonal truss model used to model diagonally reinforced concrete coupling beams

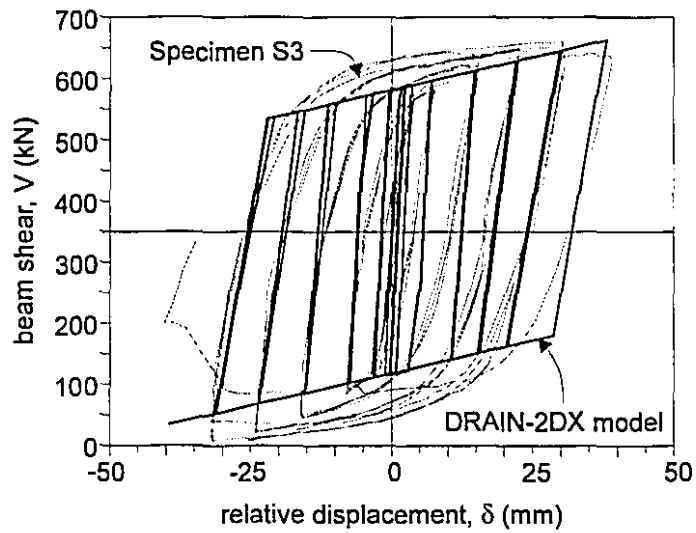


(b) comparison of observed monotonic stress-strain response of Beam 317 (Paulay and Binney, 1974) and diagonal truss model used for DRAIN-2DX modelling of diagonal reinforcement

Figure 5.5 Verification of DRAIN-2DX element models for diagonally reinforced concrete coupling beams



(a) shear beam model used to model shear critical steel coupling beams



(b) comparison of observed hysteretic behaviour of Specimen S3 and that predicted using DRAIN-2DX shear beam model

Figure 5.6 Verification of DRAIN-2DX element model for shear critical steel coupling beam

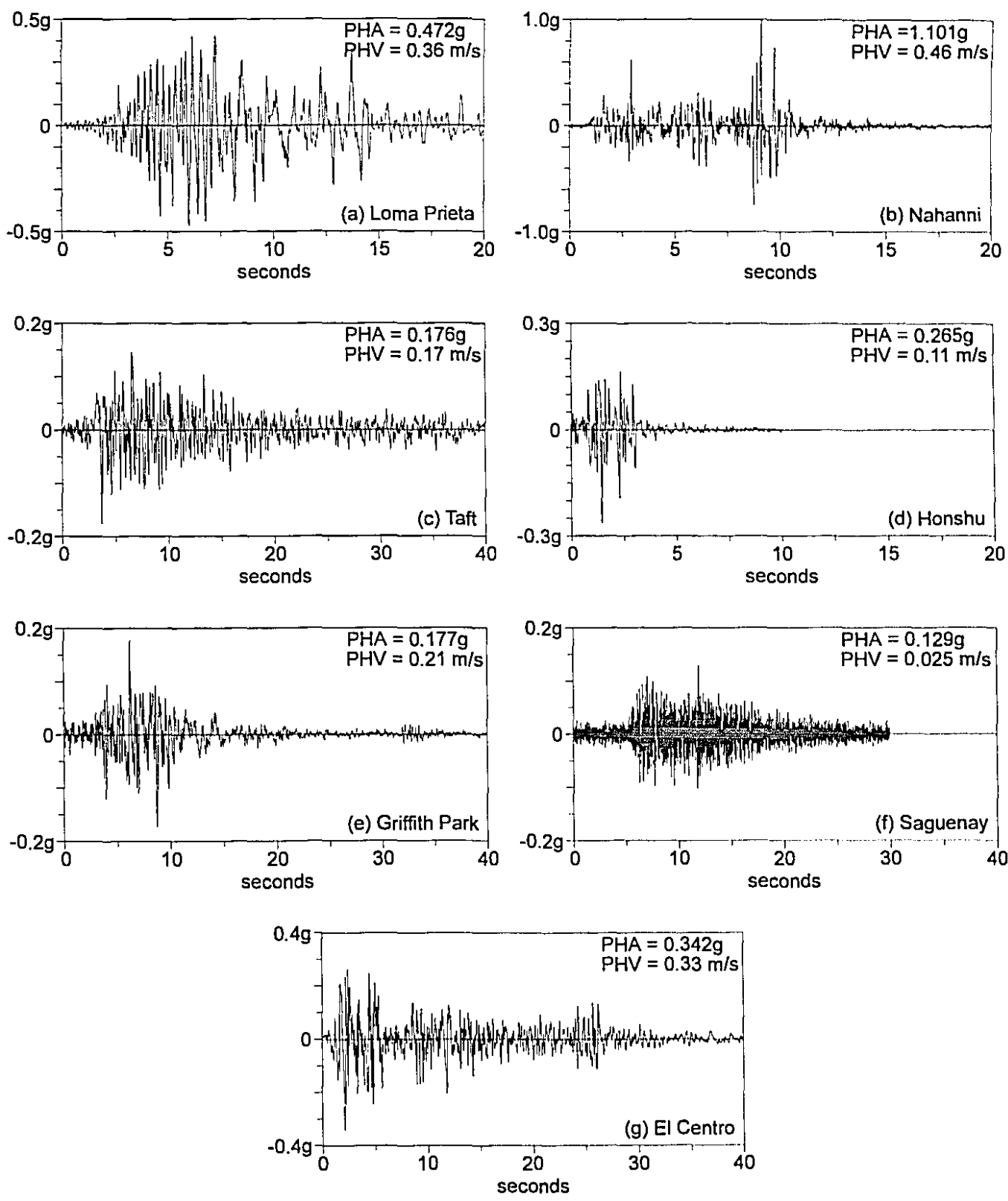


Figure 5.7 Accelerograms used for DRAIN-2DX analyses

Chapter 6

Results of Non-linear Dynamic Analyses of Prototype Structures

The results of the DRAIN-2DX non-linear dynamic analyses performed on the prototype structures are presented in this chapter. Two prototype structures were designed as partially coupled and two as fully coupled, one each with reinforced concrete coupling beams, the other with steel coupling beams. Each prototype was subjected to four ground acceleration records resulting in a total of 16 analyses. Additional analyses, representing the less severe seismic conditions of Montréal were conducted on a modified partially coupled prototype. Very little inelastic behaviour was predicted in these additional analyses, as such only a brief assessment of performance is presented (see Section 6.5). Each analysis considered only the first 20 seconds of response as it was felt that this would be sufficient time to include all critical stages in the structure's response to the earthquake. The duration of significant ground motion for each acceleration record fell well within the first 20 seconds.

6.1 Non-linear Dynamic Response of Partially Coupled Prototypes PC and PS

Prototypes PC and PS, located in Vancouver, were subjected to the scaled acceleration records of all four "West coast" earthquakes considered (see Table 5.6). Figures 6.1 and 6.2 show the roof displacement-time histories for PC and PS, respectively. Figures 6.3 and 6.4 show the critical coupling beam shear versus relative shear deformation for PC and PS, respectively. Figure 6.5 shows the interstorey drifts for the eight analyses conducted. The NBCC specified maximum interstorey drift for the structure is 0.02 times the storey height, or 72 mm (Clause 4.1.9.2.(3)). Figure 6.6 shows the sequence of beam element yielding for the eight analyses conducted.

Table 6.1 summarises the displacement and ductility demands of the partially coupled prototype structures subject to the acceleration records scaled to 1.5 times the PHV. This scaling factor accounts for an increase in ground motion above the 10% in 50 year values and can be thought of as a factor to account for the influence of torsional effects. It must be

pointed out that torsional effects are included in the design while the 2-dimensional analysis procedures cannot account for torsion. As a measure of the relative structural ductility, the global ductility demand of the structural system, μ_{global} , is defined as the maximum displacement of the roof, Δ_{max} , divided by the roof displacement at first yield of the structure, Δ_y . Similarly, the local ductility demand of the coupling beams, μ_{local} , is defined as the maximum relative vertical displacement of the ends of the critical coupling beam, δ_{max} , divided by the relative vertical displacement at yield, δ_y of the coupling beam being considered. The local ductility demand was determined from the critical coupling beam, that is the coupling beam at the floor which experiences the greatest inter-storey drift.

acceleration record	time of first yield	Δ_y (mm)	Δ_{max} (mm)	δ_y (mm)	δ_{max} (mm)	μ_{global}	μ_{local}
prototype PC							
El Centro	1.60 s	75.1	258.4	16.6	61.1	3.4	3.7
Griffith Park	6.32 s	78.3	213.5	16.5	46.2	2.7	2.8
Loma Prieta	5.36 s	79.6	201.0	14.9	62.5	2.5	4.2
Taft	3.44 s	79.3	207.0	16.1	54.1	2.6	3.4
prototype PS							
El Centro	1.56 s	75.8	213.7	19.0	57.2	2.8	3.0
Griffith Park	6.28 s	77.1	181.2	19.0	44.6	2.4	2.4
Loma Prieta	4.68 s	75.8	190.7	17.9	60.6	2.5	3.4
Taft	3.40 s	74.2	204.2	19.2	54.7	2.8	2.9

Table 6.1 Summary of global and local ductility demands for PC and PS

The responses of both PC and PS appear to be quite stable. In all cases the peak response occurred within the time frame considered and was being damped out by the end of the 20 seconds considered.

6.1.1 Response of Partially Coupled Prototype PC

Global ductility demand for this prototype was in the range of 2.5 to 3.4. These values approach to the force modification factor, R , of 3.5 used to design this prototype.

The local ductility demands observed for these prototypes ranged from 2.8 to 3.7, or about 130% of the global structural ductility demand. Extrapolating from predictions of ductility

demand presented by Saatcioglu (1981), a maximum beam ductility demand of about 3 would be expected for this prototype structure.

The hysteretic responses of the critical coupling beams are shown in Fig. 6.3. Large relative displacements in the elastic range allow considerable amounts of energy to be absorbed prior to yielding, reducing the ductility demand over that of a stiffer structural system. In all cases the ductility demand did not exceed levels beyond which strength decay may be expected.

Maximum inter-storey drifts (see Fig. 6.5(a)) reached about 18 mm, corresponding to a drift ratio of 0.005, significantly less than the NBCC limiting drift ratio of 0.02.

The sequence of coupling beam yield is shown in Fig. 6.6(a). In each structure, a block of between 6 and 9 coupling beams experienced inelastic behaviour at approximately the same time. This predicted response would indicate that there is a reasonable degree of force redistribution among the coupling beams. As such, the structure is able to absorb energy in a reasonably efficient manner.

6.1.2 Response of Partially Coupled Prototype PS

Prototype PS behaved in a similar manner to prototype PC. The hysteretic responses of the critical coupling beams are shown in Fig. 6.4. The slightly improved energy absorption capacity exhibited by these beams, has the effect of reducing the energy absorption demands on the walls and thus reducing the displacements somewhat.

Maximum inter-storey drifts (see Fig. 6.5(b)) were about 18 mm, corresponding to a drift ratio of 0.005, significantly less than the NBCC limiting drift ratio of 0.02.

The sequence of coupling beam yield is shown in Fig. 6.6(b). In each structure, a block of between 6 and 13 coupling beams experienced inelastic behaviour. This predicted response, exhibiting greater distribution of inelastic action than prototype PC, suggests a superior energy absorption capacity than PC. The stable hysteretic response of "flexure critical" steel coupling beams through ductility levels of at least 3.0 demonstrates this point (ie: Specimen S4).

6.2 Non-linear Dynamic Response of Coupled Prototypes FC and FS

Prototypes FC and FS, located in Vancouver, were subjected to the scaled acceleration records all four "West coast" earthquakes (see Table 5.6). Figures 6.7 and 6.8 show the roof displacement-time histories for FC and FS, respectively. Figures 6.9 and 6.10 show the critical coupling beam shear versus relative shear deformation for FC and FS, respectively. Figure 6.11 shows the interstorey drifts for the eight analyses conducted. The NBCC specified maximum interstorey drift ratio for the structure is 0.02, or 72 mm of interstorey drift. Figure 6.12 shows the sequence of element yielding for each model analysed. Table 6.2 summarises the displacement and ductility demands of the coupled prototype structures.

acceleration record	time of first yield	Δ_y (mm)	Δ_{max} (mm)	δ_y (mm)	δ_{max} (mm)	μ_{global}	μ_{local}
prototype FC							
El Centro	1.22 s	47.5	146.1	3.82	17.05	3.1	4.5
Griffith Park	6.08 s	46.3	135.7	3.51	15.67	2.9	4.5
Loma Prieta	4.10 s	43.6	129.8	3.43	15.52	3.0	4.5
Taft	3.22 s	42.6	211.5	3.42	28.51	5.0	8.2
prototype FS							
El Centro	1.28 s	48.9	137.8	4.71	29.05	2.8	6.2
Griffith Park	6.08 s	50.2	109.7	4.59	19.43	2.2	4.2
Loma Prieta	4.08 s	48.6	140.7	6.00	39.78	2.9	6.6
Taft	3.24 s	48.2	181.8	5.17	37.63	3.8	7.3

Table 6.2 Summary of global and local ductility demands for FC and FS

The ductility demands on the structures subjected to the scaled Taft record were greater than for the other records. This is due to the relatively long period of sustained ground motion evident in this record.

The responses of both FC and FS appear to be very well controlled. In all cases the peak response occurred well within the time frame considered and was being damped out by the end of the 20 seconds considered.

The inter-storey drifts (see Fig. 6.11) fall well within the NBCC limit of 72 mm, indicating that structural and non-structural damage will likely be relatively minimal outside of the core.

6.2.1 Response of Fully Coupled Prototype FC

Global ductility demand for this prototype was in the range of 3 to 5. These values are similar to the force modification factor, R , of 4.0 used to design this prototype.

The hysteretic response of diagonally reinforced concrete coupling beams (see, for example, Fig. 1.4) has been shown to be quite stable, exhibiting little pinching, through ductility levels of 6 to 8 (Paulay and Binney, 1974, Santhakumar, 1974 and Shiu, et al., 1978). The DRAIN-2DX model, although a bi-linear simplification of the coupling beam response, accurately represents the peak capacity and ductility demands of the beams at the ductility levels predicted.

The local ductility demands observed for these prototypes (see Table 6.2) ranged from 4.5 to 8.3, or about 150% of the global structural ductility demand. This result is consistent with what would be expected for such highly coupled structural systems. Extrapolating from predictions of ductility demand presented by Saatcioglu (1981), a maximum beam ductility demand of about 5 would be expected for this prototype structure.

Maximum interstorey drifts (see Fig. 6.11(a)) ranged from about 9 to 14 mm, corresponding to drift ratios of 0.0025 to 0.004, significantly less than the NBCC limiting drift ratio of 0.02.

The high level of coupling in this prototype structure is evident in the sequence of element yielding shown in Fig. 6.12(a). In most cases, from 9 to 12 coupling beams yield before there is evidence of flexural hinging at the base of, what is in all cases, the "tension wall". Although the "tension wall" appears to yield first when subjected to the Loma Prieta record, seven coupling beams yield virtually simultaneously (within about 0.1 seconds). Once the "tension wall" yields, there is a significant moment redistribution at the base of the structure, resulting, in redistribution of forces to the "compression wall". This important redistribution effect is accounted for by modelling the response of the "tension" and "compression" walls with the appropriate non-linear relationships.

6.2.2 Response of Fully Coupled Prototype FS

Global ductility demand for this prototype was in the range of 2.2 to 3.8. These values are lower than those determined for the diagonally reinforced coupling beam system. Although the ultimate lateral deflections are comparable, the yield deflections are 3% to 13% greater. This increase is likely due to the lower assumed stiffness damping coefficient (see Section 5.4) and the slightly lower degree of coupling (see Section 5.3.4).

The predicted coupling beam hysteretic responses (see Fig. 6.10) closely resemble the observed responses of the shear critical Specimens S2 and S3 (see Figs 3.4 and 3.7). The

DRAIN-2DX model, therefore, appears to accurately model the response of these beams through the ductility levels predicted.

The local ductility demands observed for these prototypes (see Table 6.2) ranged from 4.2 to 7.3, or about 210% of the global structural ductility demand. This result is consistent with what would be expected for this prototype structure, whose degree of coupling is 3% less than that of the diagonally reinforced prototype (see Section 5.3.4).

Maximum interstorey drifts (see Fig. 6.11(a)) ranged from about 8 to 12 mm, corresponding to drift ratios of 0.0022 to 0.0033, again, significantly less than the limit of 72 mm or 0.02.

As the degree of coupling is somewhat less for the steel coupling beams than for the diagonally reinforced coupling beams, there is less distribution of coupling beam yielding before the base of the walls yield (see Fig. 6.12(b)). There is still evidence of shear yielding in 4 to 8 coupling beams before flexural yielding at the base of the "tension wall". The greater flexibility of the steel "shear critical" beams on one hand, and the larger energy absorption on the other, resulted in slightly reduced global ductility demand. However, the fact that fewer beams yielded resulted in a slightly larger local ductility demand.

6.3 Estimating Damage Levels

In order to estimate probable structural and non-structural damage levels in the prototype structures, it is necessary to define a damage index. Hasselman and Wiggins (1982), based on observations of seismic performance during the 1971 San Fernando earthquake, developed a correlation between structural damage and inter-storey drift. Their method determines a damage ratio, defined as the repair cost divided by the replacement cost for a structure with seismic damage. The relationship between the damage ratio, DR, and the inter-storey drift ratio, Δ , is given as:

$$\log DR = \log DR_t + \left(\frac{\log DR_c - \log DR_t}{\log \Delta_c - \log \Delta_t} \right) (\log \Delta - \log \Delta_t) \quad (6.1)$$

where: DR_t = damage threshold of 0.5%;

DR_c = damage threshold of 50%;

Δ_t = inter-storey drift ratio corresponding to DR_t , taken as 0.00085; and

Δ_c = inter-storey drift ratio corresponding to DR_c .

In this relationship, the 50% damage threshold, DR_c , represents significant structural damage, likely resulting in the replacement of the structure. The corresponding drift ratio, Δ_c , depends on the quality of construction and the duration and magnitude of the expected ground motions. For this analysis the value of Δ_c used was 0.0196, corresponding to a well

constructed building in Vancouver (Paultre, 1987). These predicted damage ratios apply to the structure as a whole. The stiff, lateral load resisting core, would experience greater damage levels. The damage levels in the core would be a function of the force levels experienced by the core in addition to the drift ratios. As desired, the inelastic action is concentrated in the coupling beams, which act as the energy dissipators.

Hasselmann and Wiggins also suggest a method of relating inter-storey drift to probable window damage. The damage ratio for windows, DR_w , is defined as:

$$\log DR_w = 2.35 \log \Delta + 6.3 \quad (6.2)$$

The value of DR_w is a function of the interstorey drift only and can be interpreted as the percentage of windows likely to be damaged as the structure deflects.

The maximum inter-storey drift ratios and damage ratios for the prototypes subjected to the maximum credible earthquake are given in Table 6.3.

Earthquake Record	Maximum inter-storey drift ratio	Damage Ratio, DR	Damage Ratio for windows, DR _w
Prototype PC			
El Centro	0.0052	7.13%	8.56%
Griffith Park	0.0041	5.03%	4.90%
Loma Prieta	0.0047	6.15%	6.75%
Taft	0.0053	7.34%	8.95%
Prototype PS			
El Centro	0.0046	5.96%	6.42%
Griffith Park	0.0035	3.99%	3.37%
Loma Prieta	0.0049	6.54%	7.45%
Taft	0.0044	5.58%	5.78%
Prototype FC			
El Centro	0.0026	2.51%	1.61%
Griffith Park	0.0024	2.35%	1.45%
Loma Prieta	0.0025	2.38%	1.48%
Taft	0.0040	4.89%	4.68%
Prototype FS			
El Centro	0.0026	2.55%	1.65%
Griffith Park	0.0021	1.85%	0.98%
Loma Prieta	0.0026	2.61%	1.71%
Taft	0.0034	3.77%	3.08%

Table 6.3 Damage ratios for the prototype structures

The stiff nature of coupled wall response is evident in the low values for the predicted damage ratios. Despite the large ductility demands predicted, the damage ratios remain low, reflecting the small interstorey drift ratios. The damage ratios for all prototypes are similar at the same level of scaled ground acceleration.

For each prototype structure, the improved energy absorption of the steel coupling beams is evident as a reduction in damage ratios.

6.4 Evaluation of Prototype Behaviour

It is important that the criteria and methods used in design of structural systems accurately reflect what can be expected in the actual structure. The NBCC approximates ductile non-linear behaviour with an equivalent static analysis incorporating a force reduction factor, R . Seismic base shears are divided by the R -factor to yield an equivalent seismic base shear to be used in a pseudo-static analysis. The deformations found from this analysis are then multiplied by the R -factor to account for the expected non-linear behaviour of the structure. Thus, the R -factor corresponds to the level of ductility that the structure is expected to be able to attain. Table 6.4 summarises the key deformation results of the pseudo-static NBCC analysis (rows 1-2 and 5-6) (see Section 5.2) and the non-linear dynamic analyses (rows 3-4 and 7-8) (see Section 5.4) for each prototype structure. The values in Table 6.4 correspond to the El Centro ground accelerations scaled to 1.5 times the PHV. The ductility levels, μ_{drift} and μ_{roof} , are defined as the predicted non-linear deformation divided by the deformation predicted by the NBCC pseudo-static analysis. For these analyses the predicted ductility values are in the range of the NBCC prescribed values of R , 3.5 for PC and PS and 4.0 for FC and FS. The predicted non-linear ductilities are close to the design R -values, indicating that the NBCC design criteria are appropriate for these structures.

El Centro ground motion scaled to 1.5 PHV	Maximum Inter-storey Drift		Maximum Roof Deflection	
	mm	μ_{drift}	mm	μ_{roof}
Partially Coupled - $R = 3.5$				
(1) NBCC - PC	7.1 mm		106 mm	
(2) NBCC - PS	6.7 mm		99 mm	
(3) Non-linear - PC	18.7	2.6	258.4	2.4
(4) Non-linear - PS	16.6	2.5	213.7	2.2
Fully Coupled - $R = 4.0$				
(5) NBCC - FC	2.2 mm		33 mm	
(6) NBCC - FS	2.3 mm		35 mm	
(7) Non-linear - FC	9.2	4.2	146.1	4.4
(8) Non-linear - FS	9.3	4.0	137.8	3.9

Table 6.4 Comparison of values obtained from non-linear dynamic analyses and those obtained from NBCC equivalent static analysis for El Centro ground motion record

6.5 Behaviour of Coupled Walls Subjected to "Eastern" Ground Motions

In order to assess the performance of coupled structures subjected to less severe seismic conditions, a partially coupled prototype structure was subjected to the three "Eastern" ground motion records (see Section 5.5.1) appropriately scaled for Montréal. The partially coupled prototype, PC (see Figs 5.1 and 5.2(a)), was redesigned to represent a ductile partially coupled wall structure designed for Montréal. Moving prototype PC from Vancouver to Montréal results in a 50% reduction in the seismic base shear. As such, the design forces for the coupling beams in Montréal are one half of the values for Vancouver. Therefore, the coupling beam longitudinal reinforcement becomes 4 - No. 30 bars, top and bottom, and the hoop spacing will be increased to 160 mm ($d/4 = 158$ mm).

The details of the wall reinforcement for prototype PC, located in Montréal, is governed by minimum steel requirements in both the x and y directions. Whereas the beam capacities were about 50% of their Vancouver values, the wall capacities, because of minimum steel requirements, were about 65% of their Vancouver values. It should be acknowledged that the core design of this prototype is considerably stiffer than would normally be expected for a structure built in Montréal. The plan dimensions were maintained, however, in order that direct comparisons could be made. For instance, a structure having the same architectural dimensions, located in Montréal, would typically have more slender walls, resulting in a considerably decreased degree of coupling. Alternately, such a structure may be designed for nominal ductility (ie: $R = 2.0$), in which case the design details would be similar to those of prototype PC, designed for Vancouver.

The prototype PC, with reduced capacities, was subjected to the three "Eastern" ground motion records (see Section 5.5.1) scaled to 1.5 times the PHV for Montréal. These records have a/v ratios more representative of "Eastern" earthquakes.

Little inelasticity was observed with both the Nahanni and Honshu ground motion records. Furthermore, the response of the structure to the Saguenay ground motion record remained elastic. The maximum elastic beam shear predicted during the Saguenay event was only about 75% of the beam capacity.

The significant effect that the nature of ground motion has on a structure of this type is apparent. As expected, the eighteen storey prototype structure is sensitive to ground motion velocity rather than acceleration (see Section 5.5). As such, ground motions with higher a/v ratios will have less significant effects on the structures. Table 6.5 gives the predicted global and local ductility demands of each prototype subjected to scaled Montréal ground motion records.

acceleration record	a/v	Δ_y (mm)	Δ_{max} (mm)	δ_y (mm)	δ_{max} (mm)	μ_{global}	μ_{local}
Saguenay	5.16	remained elastic					
Nahanni	2.38	45.3	58.1	10.9	13.6	1.3	1.3
Honshu	2.39	45.0	48.0	10.6	13.1	1.1	1.2

Table 6.5 Summary of global and local ductility demands for prototype PC, located in Montréal

The degree of non-linearity evident for these structures subjected to "Eastern" ground motions is easily developed by either steel or concrete coupling beams. At these ductility demands, the increased energy absorption ability of the steel coupling beams is not exploited. The prototype structures designed for Vancouver and subjected to "West coast" ground motions provide a better test of the difference between the steel and reinforced concrete coupling beams.

6.6 Evaluation of Steel Coupling Beams

It is apparent that from these analyses that embedded steel coupling beams replacing reinforced concrete coupling beams represent a viable structural system. For both partially and fully coupled wall systems, steel coupling beams, designed for the same load levels as their concrete counterparts, are able to absorb greater amounts of energy. The effect of this is that the walls are not required to participate as fully in absorbing the earthquake energy. The structures coupled with steel beams exhibit slightly smaller lateral displacements, resulting in less structural damage and a lower overall ductility demand. Figure 6.13 shows roof displacement-time histories for the El Centro ground motion records of all four prototypes located in Vancouver. For both partially and fully coupled walls the effect of the steel beam's improved energy absorption ability is evident as the steel coupled prototypes (PS and FS) exhibit a more controlled response, having smaller peak displacements. The negative shift apparent in the response of prototype FC is indicative of increased inelastic behaviour in the walls.

Comparing Figs 6.13(a) and (b) clearly illustrates the significant effect that the degree of coupling has on the lateral stiffness of the structure. The exceptional lateral stiffness of coupled wall structures, and thus their relatively small drift ratios, make them well suited to severe seismic regions particularly where limitation of non-structural damage is a consideration.

Steel coupling beams have been shown to exhibit large ductilities without significant loss of strength or stiffness (see Chapter 3). Therefore it is likely that a steel coupling beam system would be better able to withstand ground motions of long duration with numerous excursions to near-peak accelerations or velocities.

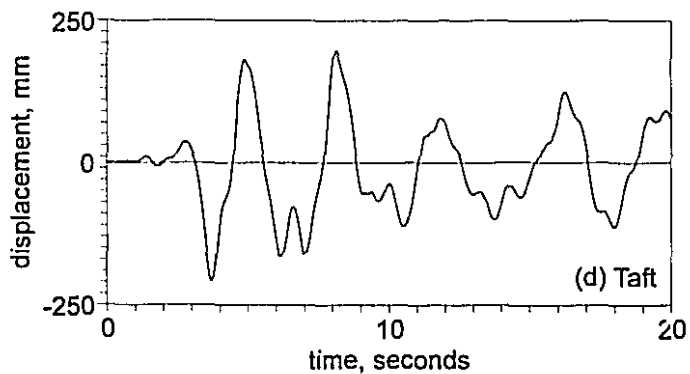
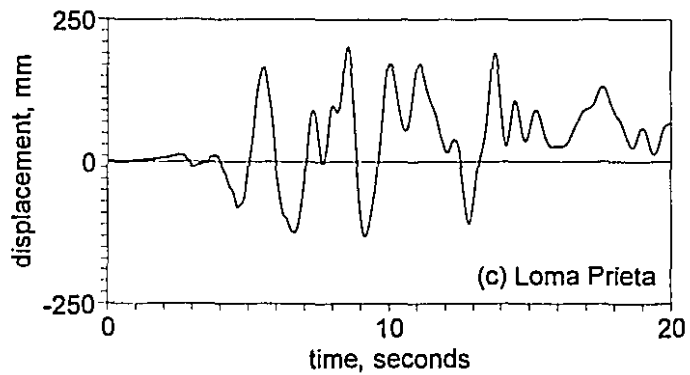
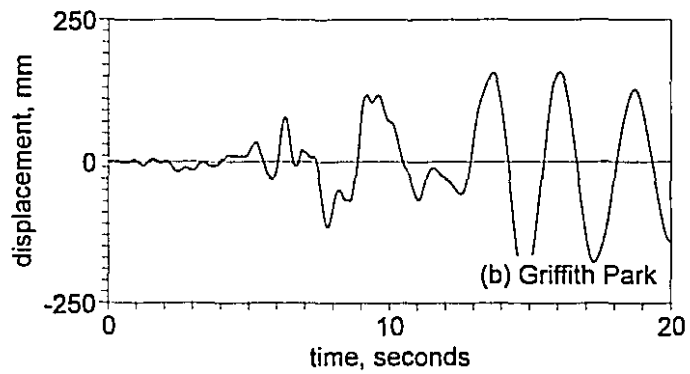
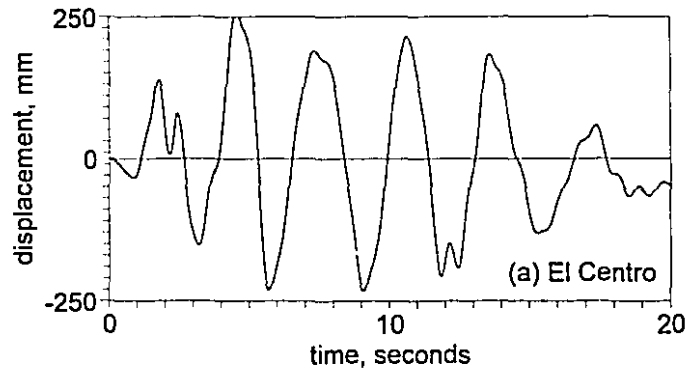


Figure 6.1 Roof displacement - time history for prototype PC

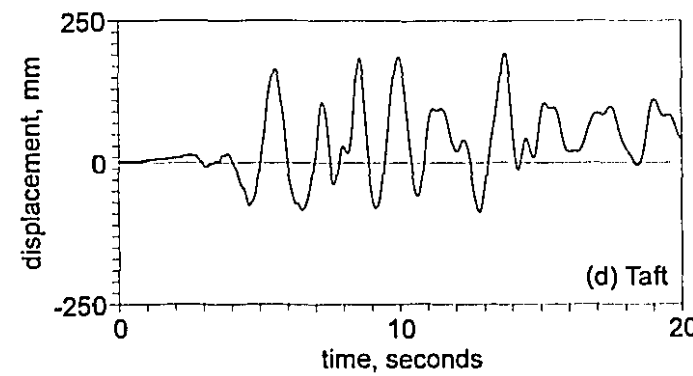
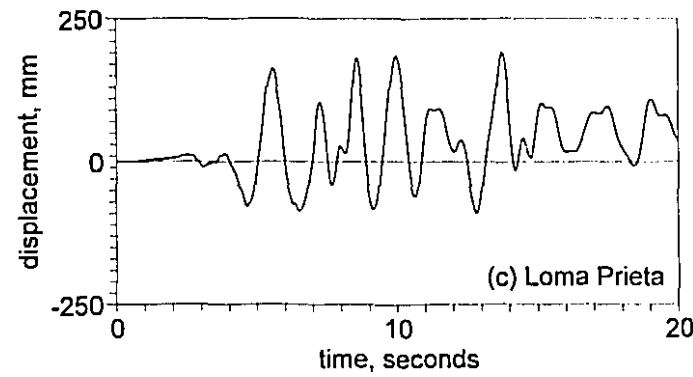
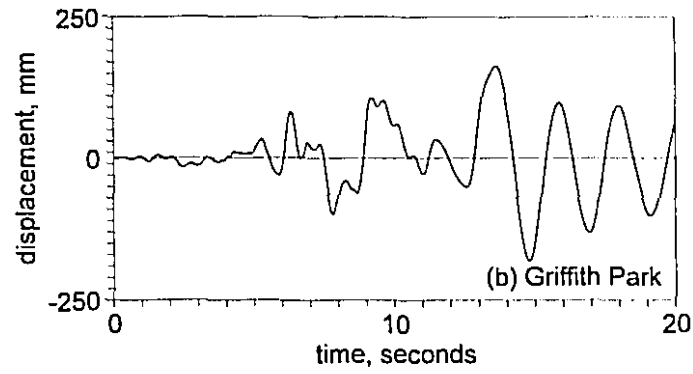
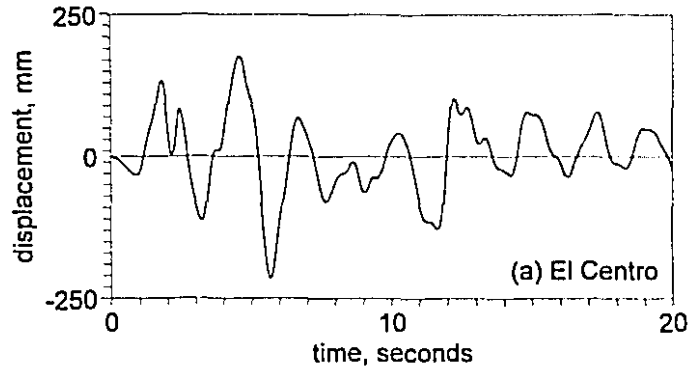


Figure 6.2 Roof displacement - time history of prototype PS

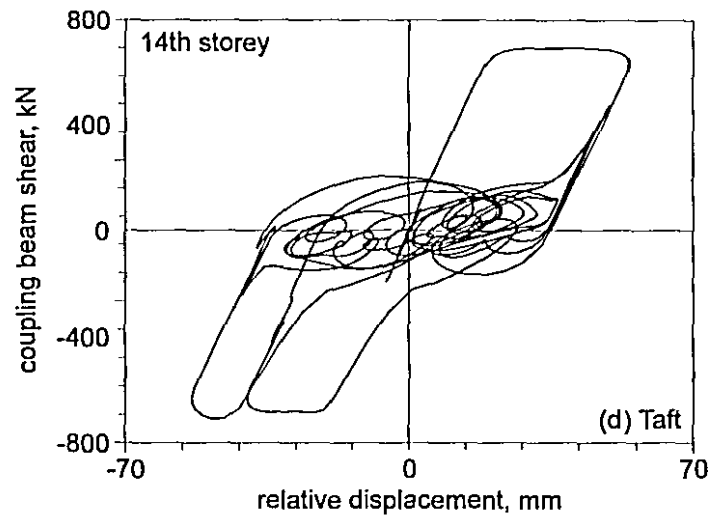
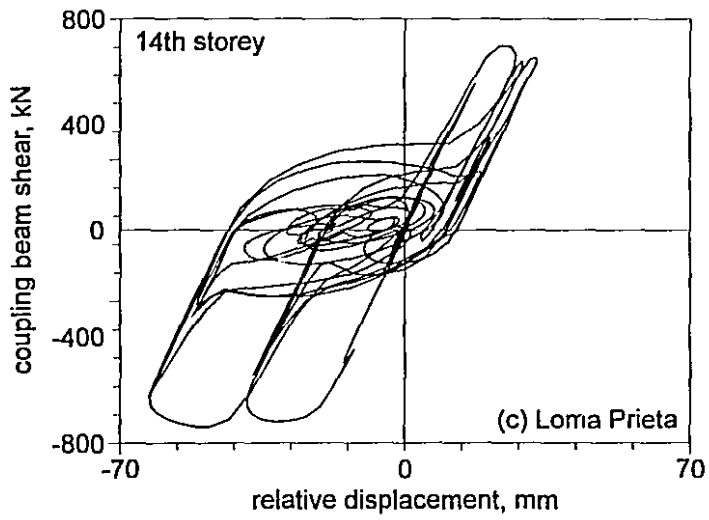
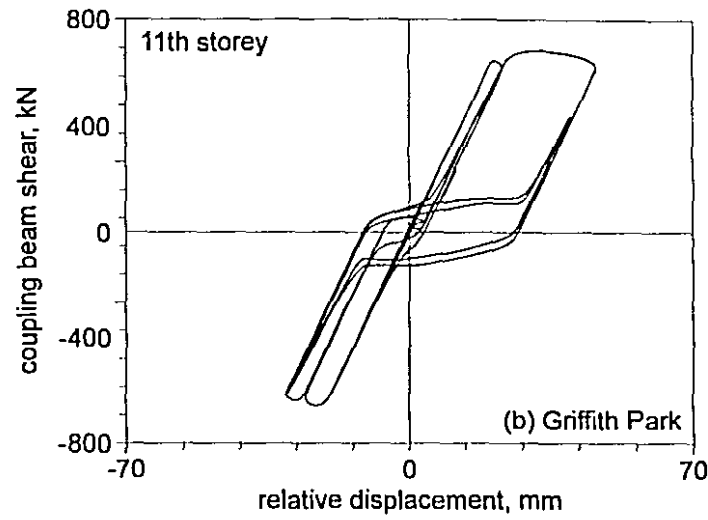


Figure 6.3 Hysteretic behaviour of critical coupling beams of prototype PC

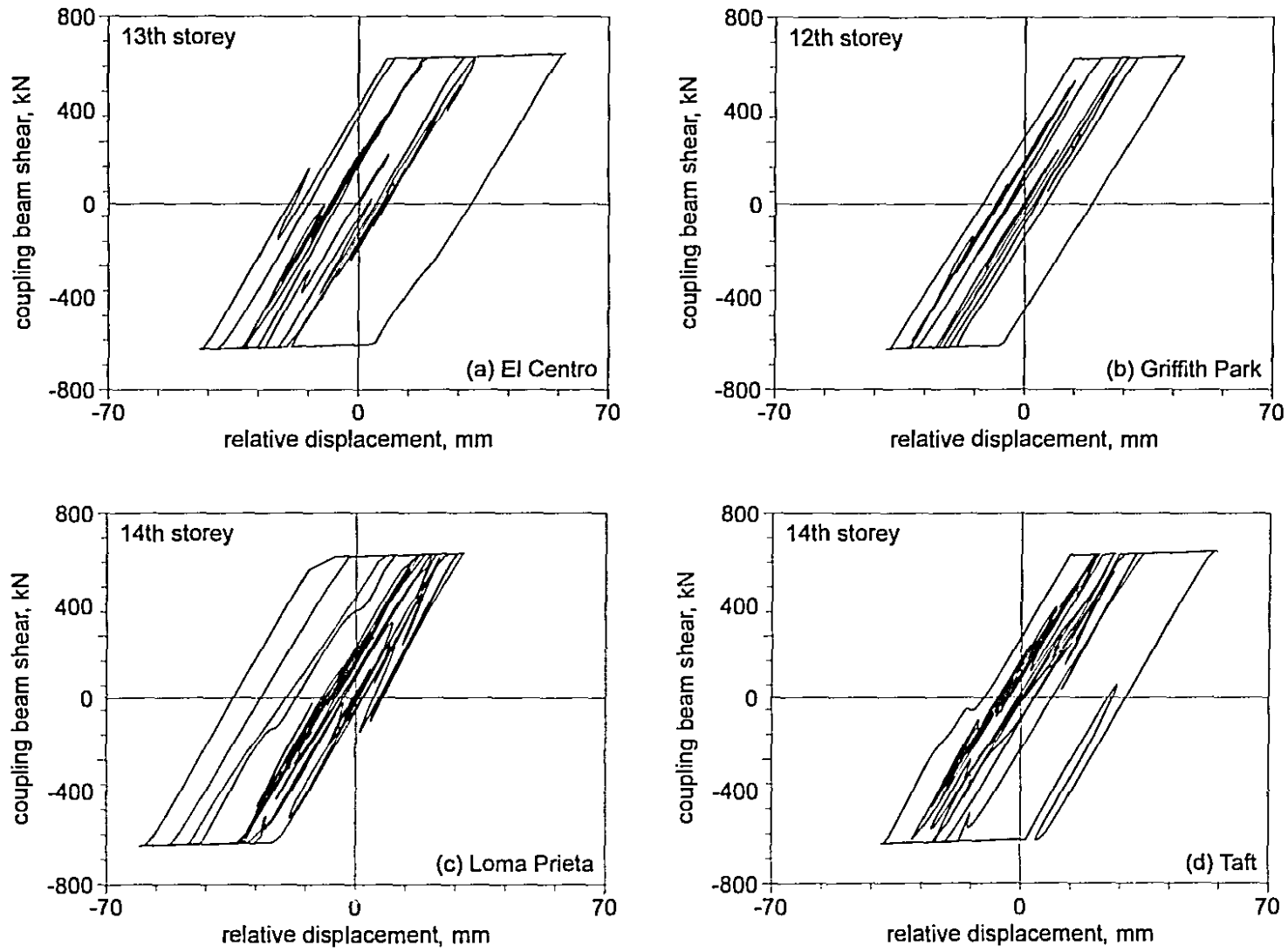


Figure 6.4 Hysteretic behaviour of critical coupling beams of prototype PS

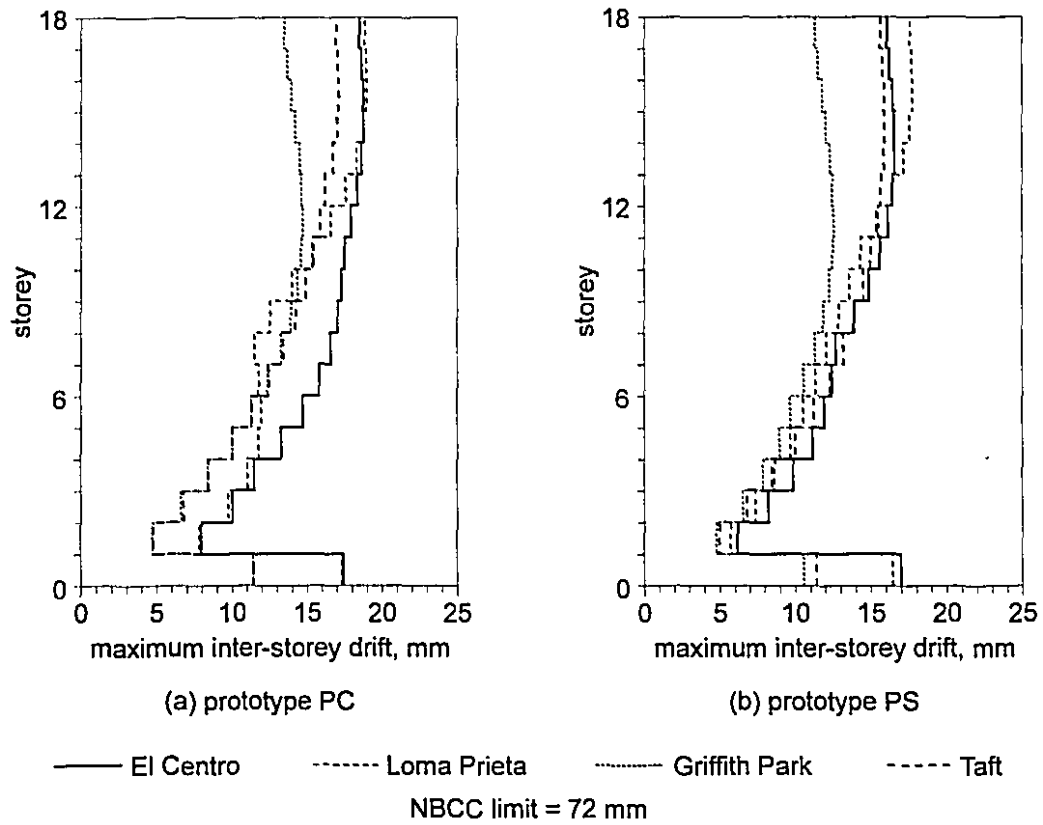
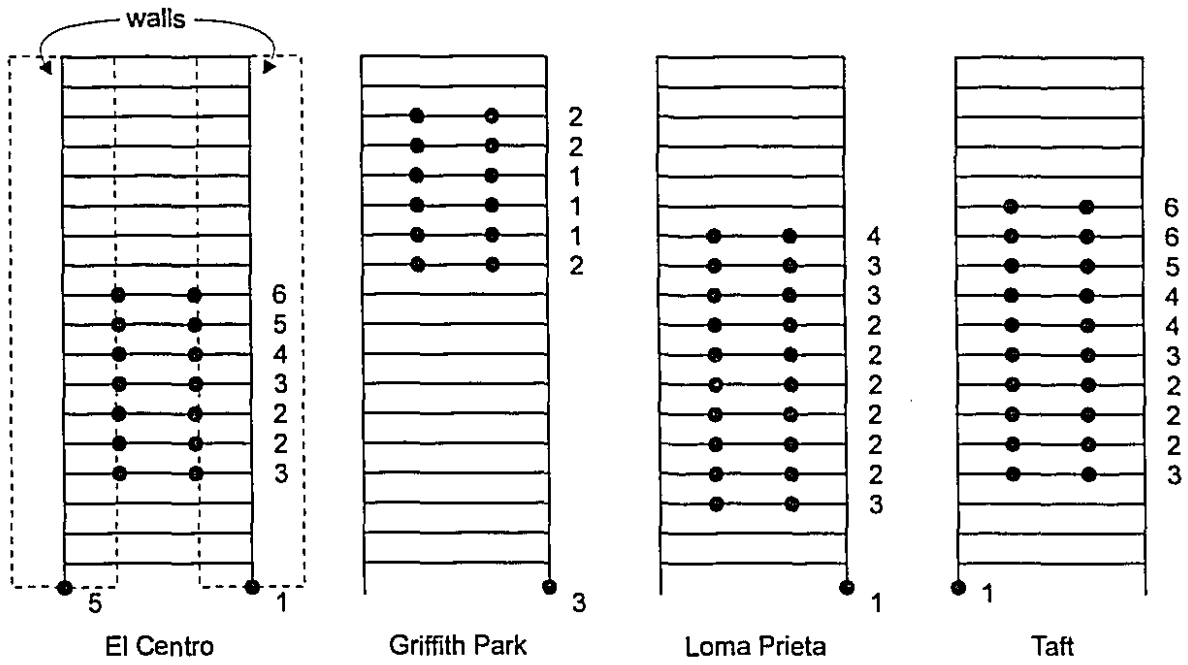
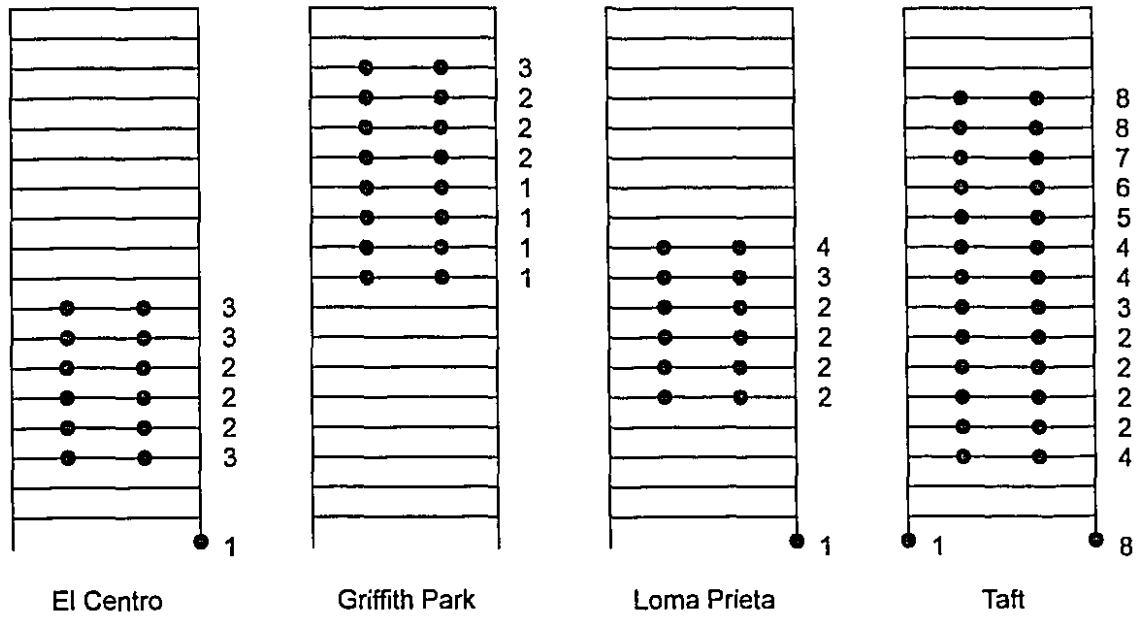


Figure 6.5 Maximum inter-storey drift values for coupled prototypes PC and PS



(a) Sequence of yielding of prototype PC



(b) Sequence of yielding of prototype PS

● flexural hinge

Figure 6.6 Sequence of beam yielding in prototype PC and PS analyses

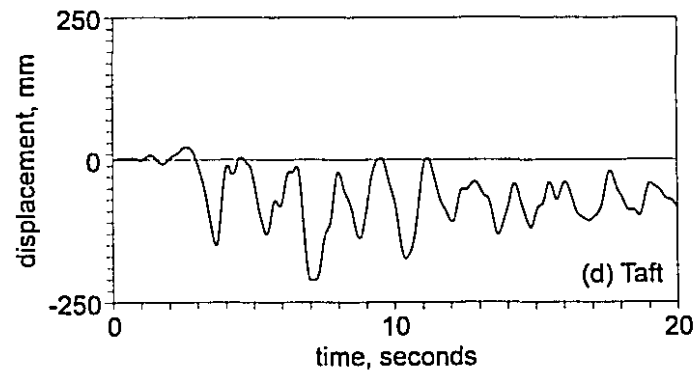
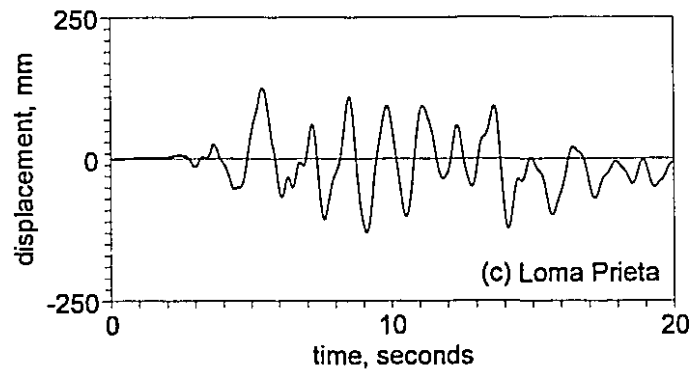
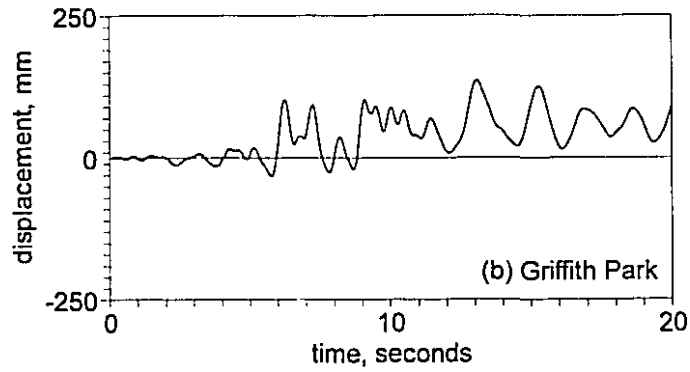
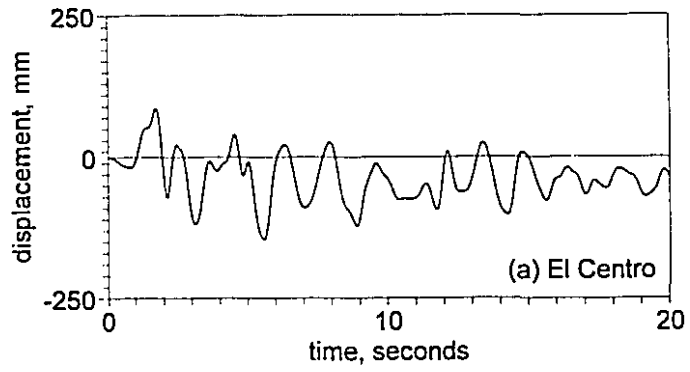


Figure 6.7 Roof displacement - time history for prototype FC

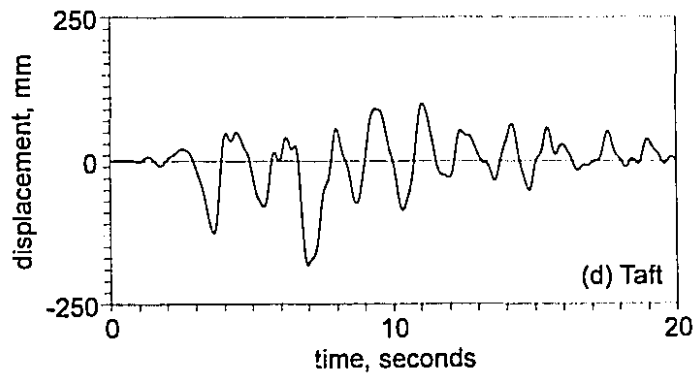
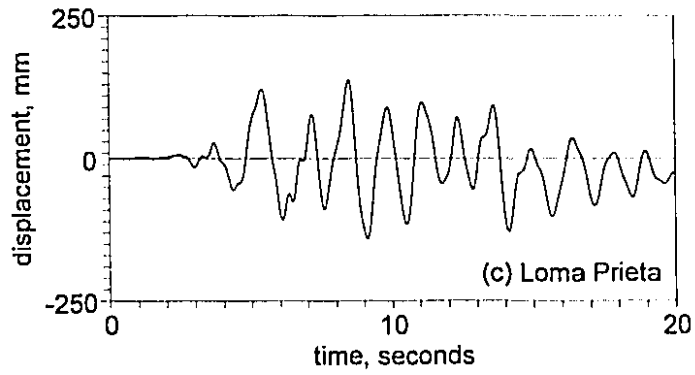
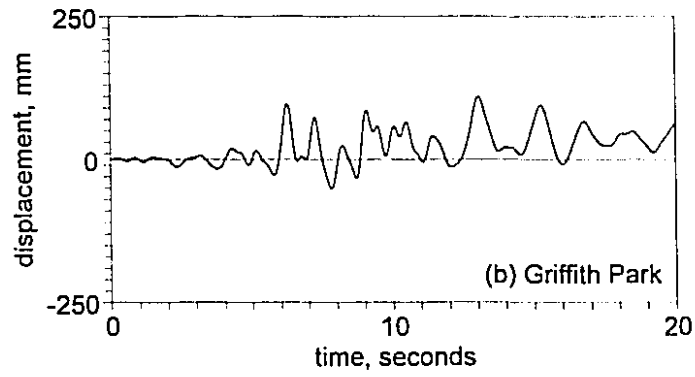
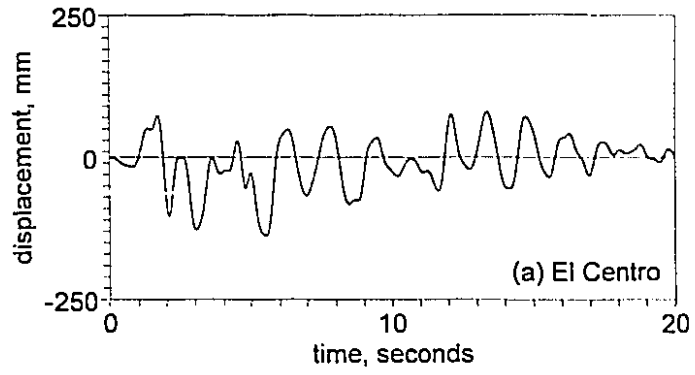


Figure 6.8 Roof displacement - time history of prototype FS

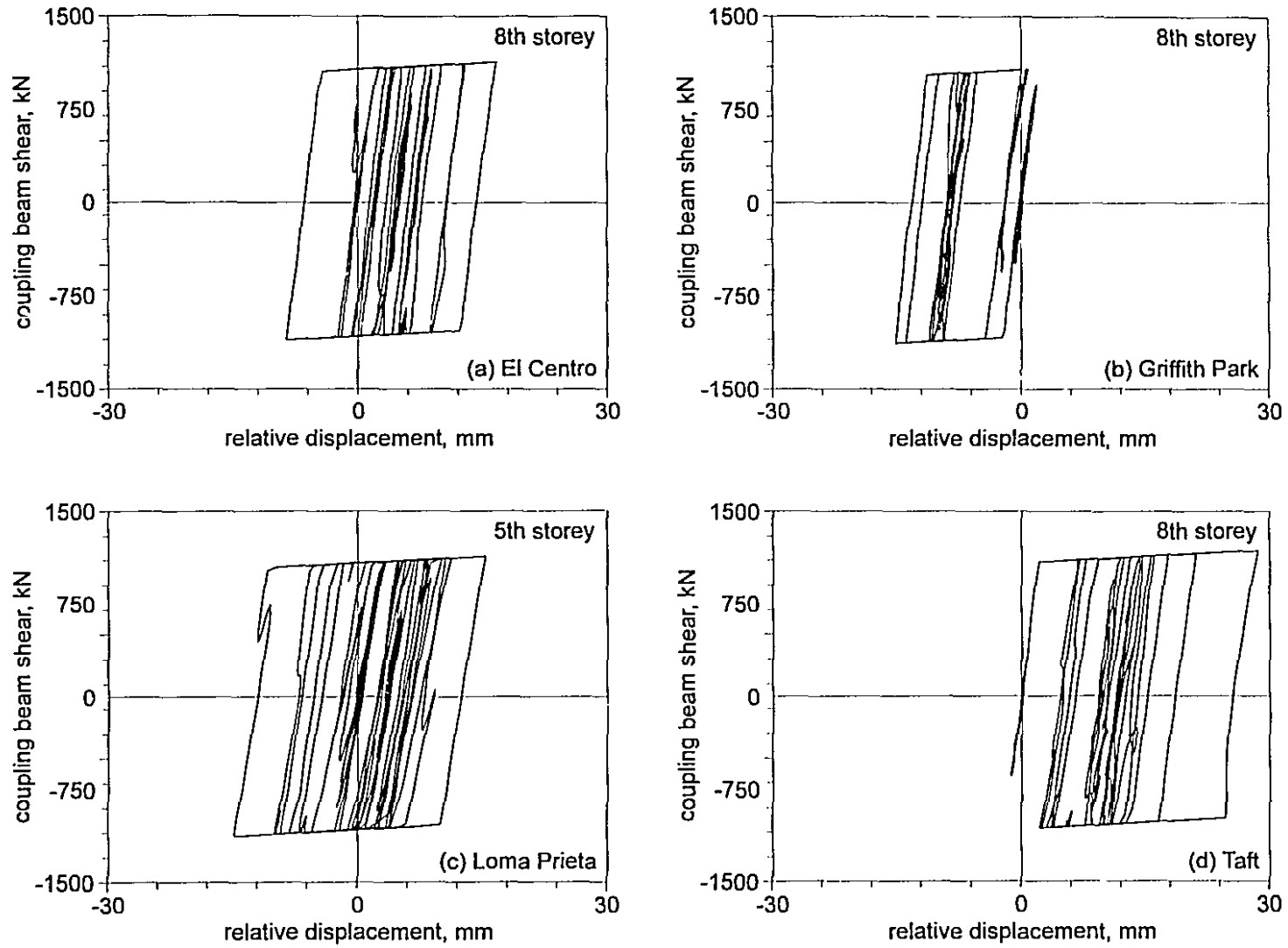


Figure 6.9 Hysteretic behaviour of critical coupling beams of prototype FC

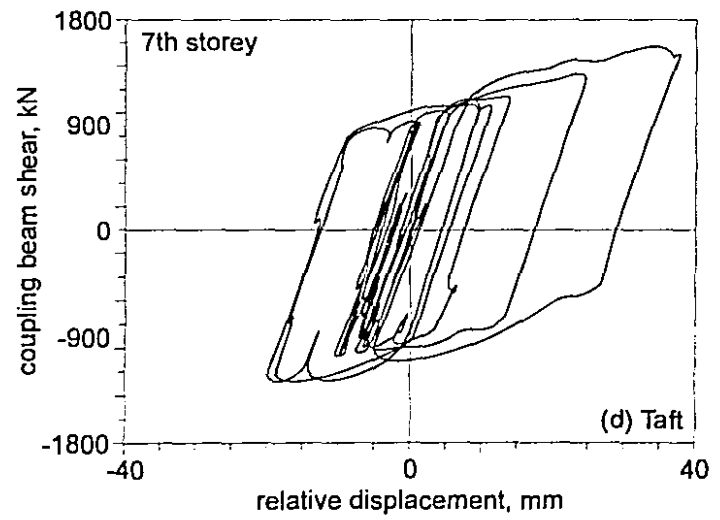
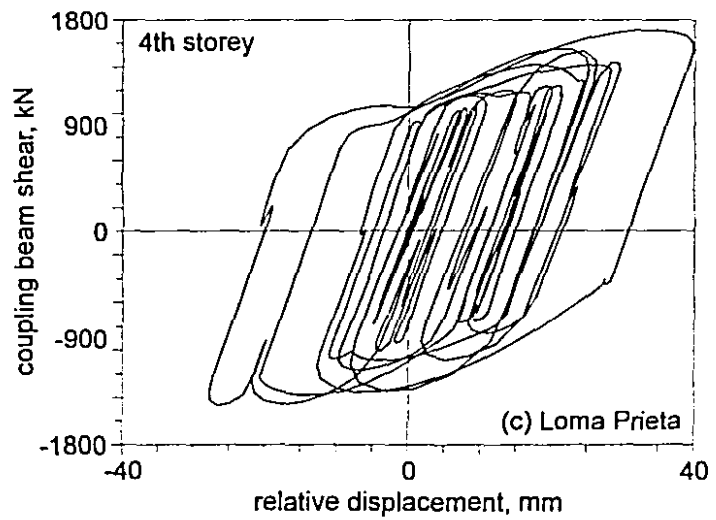
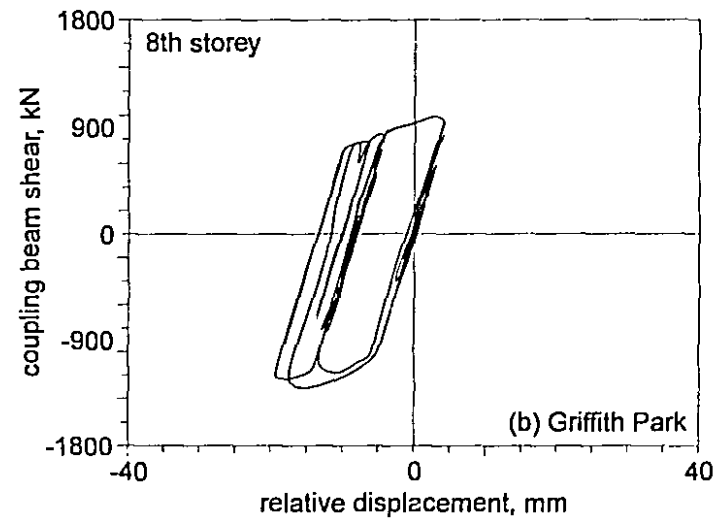
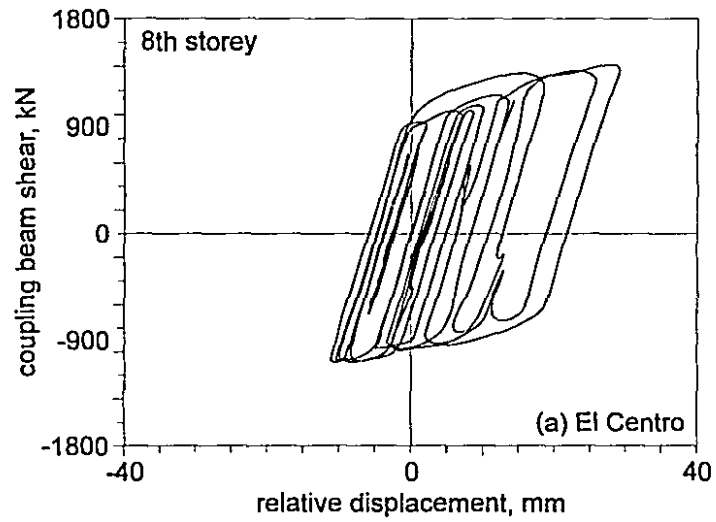


Figure 6.10 Hysteretic behaviour of critical coupling beams of prototype FS

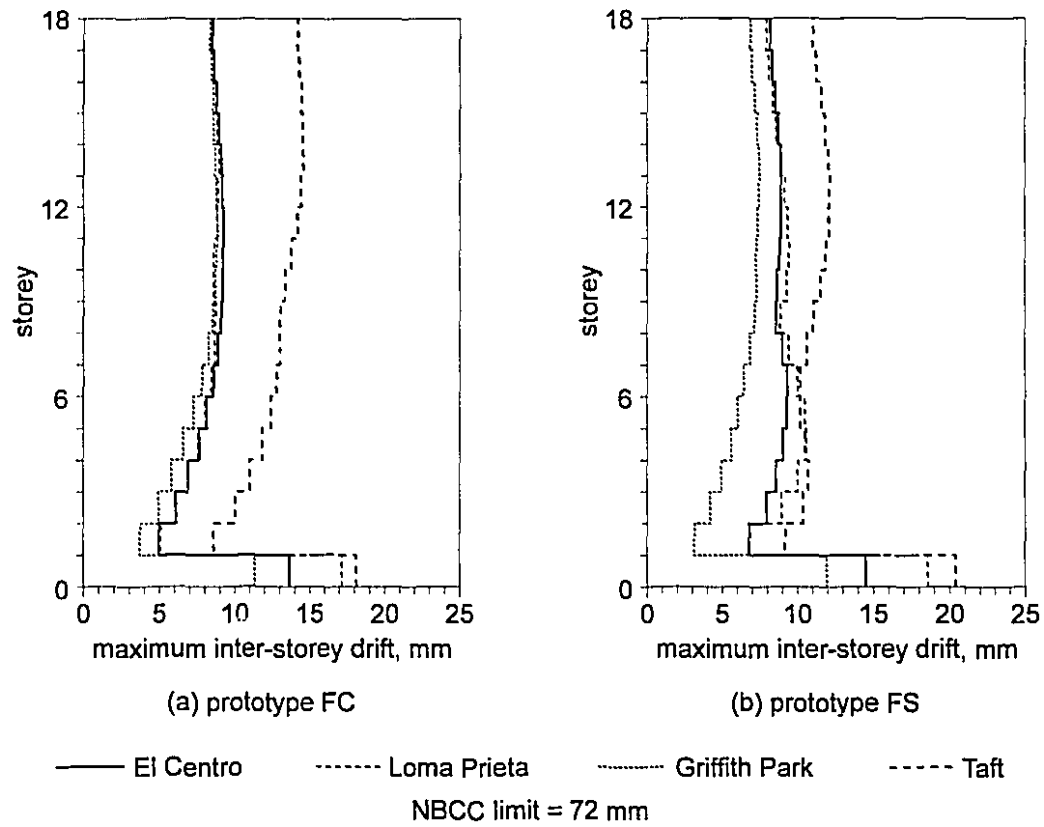
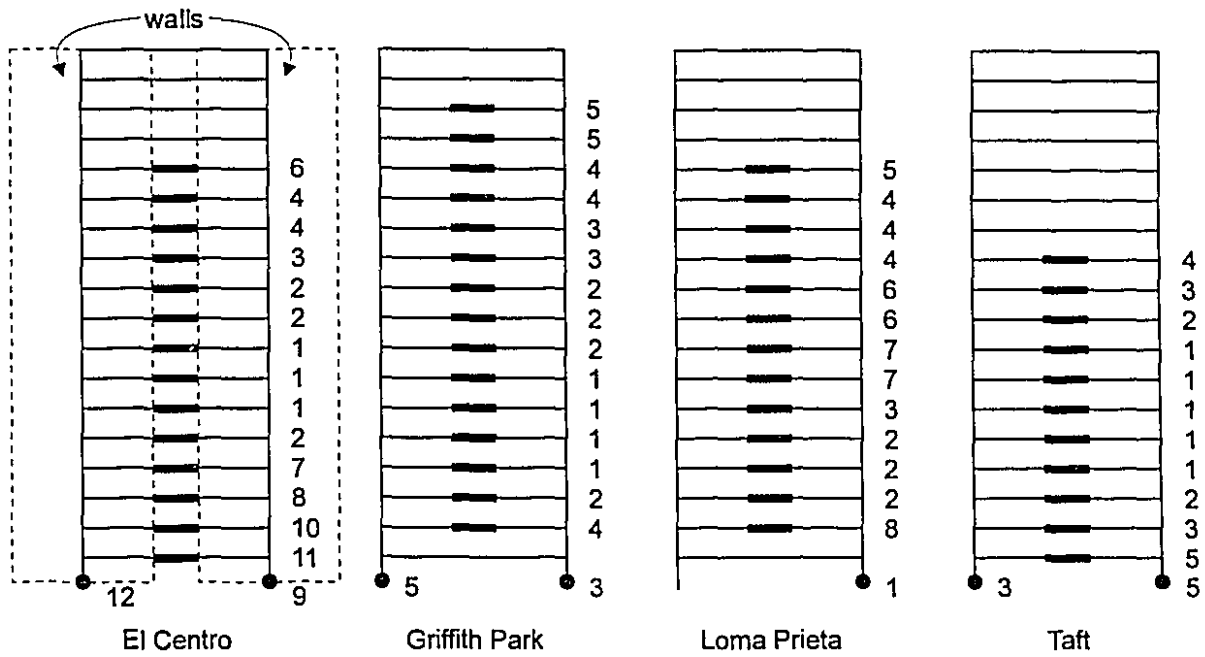
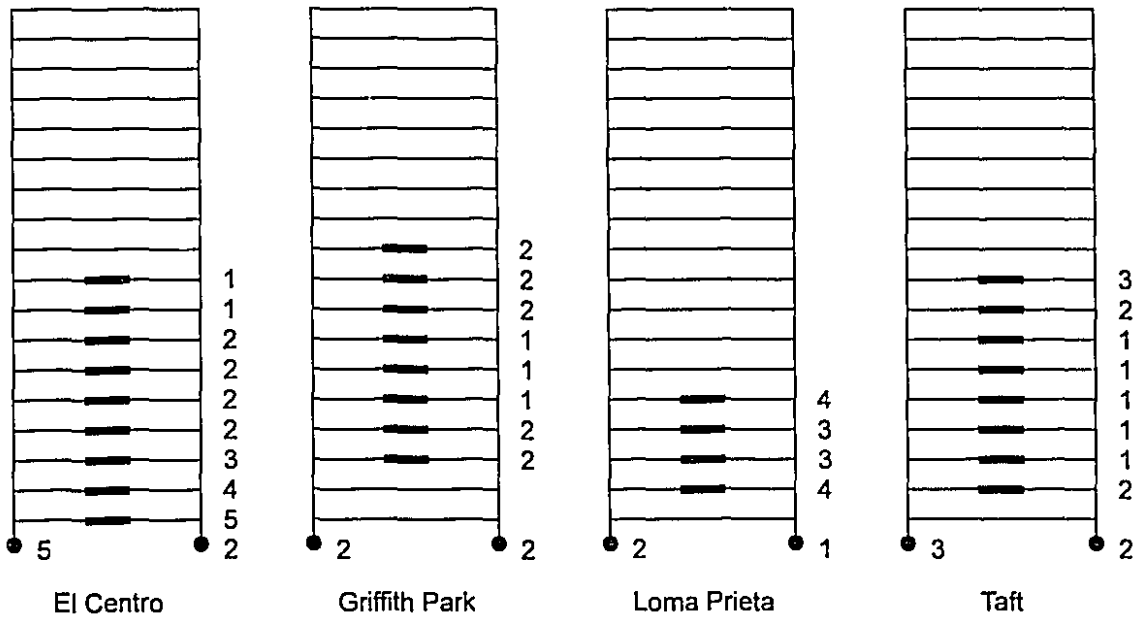


Figure 6.11 Maximum inter-storey drift values for coupled prototypes FC and FS



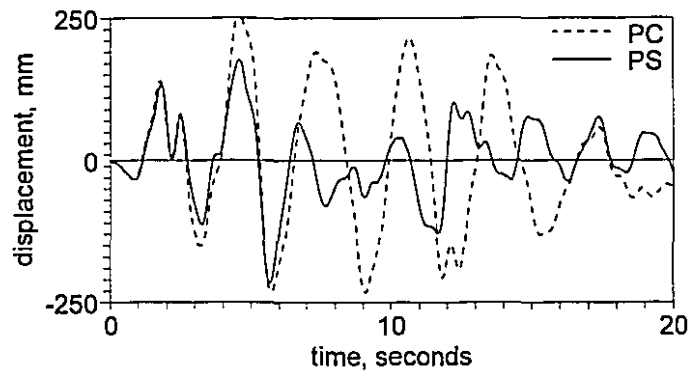
(a) Sequence of yielding of prototype FC



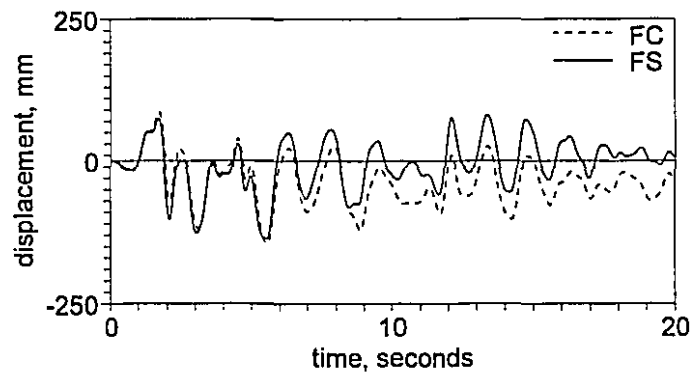
(b) Sequence of yielding of prototype FS

— yield of diagonal reinforcement (FC) ● flexural hinge
 or shear hinge in steel beam (FS)

Figure 6.12 Sequence of yielding in prototype FC and FS analyses



(a) partially coupled prototypes PC and PS



(b) fully coupled prototypes FC and FS

Figure 6.13 Comparisons of roof displacement - time histories for concrete and steel prototypes subjected to El Centro ground motion

Chapter 7

Experimental Programme for Retrofitting Reinforced Concrete Coupling Beams

This chapter describes the details of four reinforced concrete coupling beams, three of which were retrofitted in order to study ways of improving the seismic response.

7.1 Design of the Reinforced Concrete Coupling Beam and Walls

The reinforced concrete coupling beams and wall segments of Specimens R0 through R3, shown in Fig. 7.1 are identical. The coupling beams were intentionally designed to be deficient in shear in order that shear retrofit measures could be investigated. Specimen R0 was the control specimen, without any retrofit. Different retrofit measures were used on Specimens R1, R2 and R3.

The 500 mm deep by 300 mm wide coupling beams were connected to wall segments at each end producing a clear span of 1500 mm. The resulting span-to-depth ratio was 3.0 and the moment-to-shear ratio at the face of the walls was 0.75 m. The coupling beams were designed for a nominal flexural capacity of ± 263 kNm, corresponding to an applied shear of ± 350 kN. The beams have 3 - No. 25 reinforcing bars, top and bottom. Two - No. 10 skin reinforcing bars were located at mid-depth of the beams. To ensure adequate development of the longitudinal beam reinforcement, the bars were provided with an 1100 mm embedment into each wall. Shear reinforcement for the beam consisted of 7 - No. 10 hoops spaced at 225 mm, beginning 75 mm from the face of each wall. This choice of shear reinforcement produced a shear deficient beam, able to develop only 86% of the nominal flexural capacity of the beam. For comparison, a hoop spacing of about 100 mm would be required (see Appendix B) for the beam to conform with the seismic design provisions of CAN/CSA A23.3 Clause 21 (1984).

A region of concentrated reinforcement, consisting of 4 - No. 25 vertical bars enclosed by No. 10 hoops at 300 mm spacing, was provided at the inside face of each wall. The

distributed reinforcement in each wall consisted of vertical and horizontal No. 10 bars spaced at 200 mm in each direction.

7.2 Design of the Steel Plate Retrofit

The retrofit measures investigated involved attaching thin steel plates to the sides of the coupling beams to enhance the shear performance of the beams. Due to the difficulties of access and architectural constraints encountered when retrofitting existing coupling beams, the retrofit plates were applied to only one side of the coupling beam. For example, coupling beams framing across elevator door openings would be accessible for retrofit from only the inside of the elevator shaft.

The intent of the retrofit procedures investigated was to increase the shear capacity of the beam without significantly affecting the flexural capacity. The goal of the retrofit is to allow the beam to develop its nominal flexural capacity. A significant increase in the ultimate capacity of the beam would be undesirable as it would necessitate retrofitting the walls as well.

In order to determine the required retrofit plate thickness, t_p , it is useful to express the influence of the plate in resisting shear by an equivalent stirrup area. The plate is idealized as a series of vertical strips of shear reinforcement, of area A_p , at a spacing equal to the bolt spacing, s_b . The equivalent stirrup area, $A_{v,eq}$ is given as:

$$A_{v,eq} = A_p \frac{s}{s_b} \frac{h_b}{d_v} \frac{F_y}{f_y} \quad (7.1)$$

where: $A_p = 8t_p^2$;
 s = the spacing of existing hoops in the reinforced concrete beam;
 h_b = the vertical distance between anchor bolts attaching the plate to the side of the beam;
 d_v = the shear depth of the reinforced concrete coupling beam (may be taken as $0.9d$); and
 F_y and f_y = the specified yield strengths of the retrofit plate and reinforcing steel, respectively.

The term A_p considers that the plate is effective over a width equal to $4t_p$ on both sides of the anchor bolts (AISC, 1988). The term s/s_b accounts for the difference in spacing between the bolts and existing hoops. The term h_b/d_v accounts for the difference between the height of the portion of the plate considered effective and the height of the existing hoops. In order to determine the shear capacity of the retrofitted beam, the beam can be analyzed with a total equivalent stirrup area of $A_{v,eq} + A_v$ at a spacing of s and having an equivalent yield stress of f_y .

Assuming nominal material properties and plate geometry as shown in Fig. 7.2, the required plate thickness was determined to be 4.0 mm. The plate chosen for this retrofit

investigation was 3/16 inch (4.76 mm) thick and 450 mm deep. The plate was centred on the depth of the beam.

The method of attaching the plate to the coupling beam must be adequate to transmit the shear which the plate is expected to carry across the beam-retrofit plate interface. Specimen R1 was retrofitted with a 4.76 mm thick steel plate attached to one side of the beam with structural epoxy only. The shear capacity of this epoxy was reported by the manufacturer (Sika, 1992) to be 23 MPa, significantly higher than the shear strength of the coupling beam concrete. This would eventually lead to a failure through the concrete cover, as shown in Fig. 7.2(a).

In order to protect against a failure in the concrete cover and to enable shear forces to be transmitted to the retrofit plate after severe cycling has deteriorated the epoxy bond, bolting the retrofit plate to the coupling beam was investigated in Specimens R2 and R3.

In order to ensure that the anchor bolts are strong enough to develop the force of the effective plate area due to both longitudinal and transverse yielding (i.e., due to flexure and shear) the required bolt capacity, V_b , can be expressed as:

$$V_b \geq \sqrt{2} A_p F_y \quad (7.2)$$

where: A_p = effective area of plate in longitudinal and transverse directions = $8t_p^2$;
 F_y = the specified yield strength of the retrofit plate.

Furthermore, the anchor bolts were selected such that their anchorage would be located within the confined core of the coupling beam (see Fig. 7.2(b)). This detail protects against a failure through the concrete cover.

The bolting details provided over the clear span of Specimens R2 and R3 were twelve ½ inch anchor bolts arranged uniformly in two horizontal rows, spaced at 300 mm, centred at the mid height of the beam. The horizontal spacing was 260 mm. The 145 mm long bolts were anchored within the confined core of the coupling beam. In addition to the provision of anchor bolts, the plates were still attached to the beams with structural epoxy.

The critical section for combined moment and shear in the coupling beam is assumed to be at a distance of $d/2$, approximately 220 mm, from the face of each wall. The retrofit plate must be completely developed at this location. In order to ensure the adequate development of the retrofit plate, the plate of Specimen R3 was extended beyond the clear span and epoxied and bolted onto each wall. In order to protect against local plate buckling in the region extending from the face of each wall, through the critical section, additional anchor bolts were also provided in this region.

The procedure used to connect the retrofit plate to the coupling beam, using both structural epoxy and anchor bolts was as follows:

- i) The concrete surface of the beam was ground and wire brushed to remove imperfections and to provide a clean roughened surface. One side of the steel plate was polished with a grinder to improve the epoxy adherence.
- ii) Holes for the anchor bolts were drilled into the beam and matching holes were provided in the retrofit plate.
- iii) A 3 mm layer of epoxy was provided between the entire plate and beam and the plate was clamped in position.
- iv) Before the epoxy had set, the anchor bolts were set to their recommended torque of 80 Nm, resulting in an additional clamping force of about 30 kN per bolt.

7.3 Description of Specimens

The details of the reinforced concrete walls and coupling beams are shown in Fig. 7.1 and described in Section 7.1. The details of the walls and beam of each of the four specimens are identical. The details of the retrofit plates and attachment for Specimens R1 through R3 are shown in Fig. 7.2. The design and detailing of the specimens is given in Appendix B.

In addition to anchor bolt holes, each plate was drilled to accommodate ¼" (6.35 mm) threaded rods used too support the LVDT rosettes (see Section 7.6). These small holes had no effect on the integrity of the plates.

As recommended by the manufacturer, the epoxy was applied to the plates in such a way as to result in an approximately 3 mm thick glue line. The epoxy was applied to the plates in a thicker layer and was allowed to squeeze out of the edges and anchor bolt holes as clamping pressure was applied to bring the glue line to the appropriate thickness.

7.3.1 Specimen R0

Specimen R0 was the control specimen. Specimen R0 was tested without any retrofit in order to determine the response of the specimens before being retrofitted.

7.3.2 Specimen R1

Specimen R1 was retrofitted with a 450 mm deep, 3/16" (4.76 mm) thick retrofit plate extending over the 1500 mm clear span (see Fig. 7.2(a)). The plate was attached to the beam with only structural epoxy.

7.3.3 Specimen R2

Specimen R2 was retrofitted with a 450 mm deep, 3/16" (4.76 mm) thick retrofit plate extending over the 1500 mm clear span. The plate was attached to the beam with structural epoxy and 12 - ½" anchor bolts, spaced at 260 mm, arranged in two rows, spaced at 300 mm.

(see Fig. 7.2(b)). This bolt arrangement results in the last vertical bolt line being located 100 mm from the face of the wall.

7.3.4 Specimen R3

Specimen R3 was retrofitted with a 450 mm deep, 3/16" (4.76 mm) thick retrofit plate extending over the 1500 mm clear span and 450 mm onto each wall. The plate was attached to the beam and walls with structural epoxy and 12 - ½" anchor bolts, spaced at 260 mm, arranged in two rows, spaced at 300 mm over the clear span of the beam. Four anchor bolts on a 300 mm square grid are located on the plate extension 100 mm inside the face of each wall (see Fig. 7.2(c)). Additional anchor bolts are at the beam mid-height on each of the vertical bolt lines adjacent the beam-wall interface. These addition bolts were provided to control buckling of the plate in the joint region.

7.4 Material Properties

Table 7.1 gives the measured material properties for the retrofit plate, reinforcing steel, structural epoxy, anchor bolts and concrete used for Specimens R0 through R3. Anchor bolt and epoxy data were provided by the manufacturers. Figure 7.3 shows the observed material stress-strain curves for the materials used for Specimens R0 through R3.

	R0	R1	R2	R3
Concrete compressive strength, at time of test	35.3 MPa (35 days)	36.3 MPa (78 days)	44.2 MPa (57 days)	44.3 MPa (110 days)
Concrete modulus of rupture, f_r	3.83 MPa		4.27 MPa	
Concrete splitting tensile strength, f_{sp}	2.82 MPa		4.11 MPa	
No. 10 reinforcing bars	$f_y = 447.0$ MPa; $f_u = 660.6$ MPa at 21% elongation			
No. 25 reinforcing bars	$f_y = 437.3$ MPa; $f_u = 658.3$ MPa at 14% elongation			
Retrofit Plate	-	$F_y = 353.3$ MPa $F_u = 498.3$ MPa		$F_y = 365.7$ $F_u = 465.0$
Epoxy shear capacity (reported by Sika, 1992)	-	23 MPa (ASTM D-732)		
Epoxy tensile capacity (reported by Sika, 1992)	-	24 MPa at 0.4% elongation (ASTM D-638)		
Anchor bolt pull-out capacity (reported by Hilti, 1992)	-	-	61.5 kN in 35 MPa concrete	
Anchor bolt shear capacity (reported by Hilti, 1992)	-	-	98.6 kN in 39 MPa concrete	

Table 7.1 Material properties of retrofitted concrete specimens

7.4.1 Retrofit Plate Steel

The retrofit plates of Specimens R1 through R3 were fabricated with Grade 300W plate material conforming to CSA standard G40.21. The initial selection of plate material was based on providing sufficient additional shear capacity without significantly increasing the ultimate capacity of the beams. Three different thicknesses of plate stock were ordered and tested. The results of these tension tests, given in Table 7.2, illustrate the considerable range of tensile strengths likely to be found in the same grade of plate steel. This points out the need to perform tests on potential retrofit material to ensure that it will perform as desired. The tension tests were carried out according to the procedure defined in ASTM Standard E8-85a. Applied load and extension over a 50 mm gauge length were recorded up to the onset of strain hardening, ultimate load and extension were also noted. These tests indicated that the 3/16 inch stock was the most appropriate for these retrofitted specimens. The 3/16 inch plate used for Specimen R3 was from a different heat as those of Specimens R1 and R2 (see Fig. 7.3(c)).

Plate thickness	Yield stress, F_y	Ultimate stress, F_u
1/8" (3.18 mm)	308 MPa	407 MPa
3/16" (4.76 mm)	353 MPa	498 MPa
1/4" (6.35 mm)	472 MPa	549 MPa

Table 7.2 Properties of candidate retrofit plates

7.4.2 Structural Epoxy

The epoxy used to attach the retrofit plates of Specimens R1 through R3 was *Sikadur 31 Hi-Mod Gel* manufactured by Sika Canada Incorporated. *Sikadur 31 Hi-Mod Gel* is a "two-component, solvent-free, moisture-insensitive, high-modulus, high-strength, structural epoxy paste adhesive" (Sika, 1992). The product meets ASTM C-881, Type 1 and 2, Grade 3, Class B and C epoxy resin adhesive standards. The mechanical properties given in Table 5.1, are those reported by Sika Canada Inc. (1992).

7.4.3 Anchor Bolts

The anchor bolts used to attach the retrofit plates of Specimens R2 and R3 were *HSL M12/50* heavy duty mechanical anchors manufactured by Hilti Canada Limited. These 12 mm diameter, high-strength steel bolts have a total length of 145 mm, ensuring that the anchorage will be well within the confined core of the coupling beam. The mechanical properties given in Table 7.1 are those reported by Hilti Canada Ltd (1992).

7.4.4 Reinforcing Steel

In accordance with Clause 21.2.5.1 of CAN/CSA A23.3-M84, the reinforcing steel used conformed to CSA standard G30.18. Tension tests were performed on 300 mm lengths of each bar size. Applied load and extension over a 50 mm gauge length were recorded up to the onset of strain hardening. The results of the tension tests are presented in Table 7.1 and Fig. 7.3 (b).

7.4.5 Concrete

Ready-mix concrete with a minimum specified 28 day compressive strength of 35 MPa was used for each of the four specimens. Table 7.3 gives the composition and properties of the concrete mix as specified by the supplier.

Component or Property	Specified quantity
Cement (Type 10)	450 kg/m ³
Water	170 l/m ³
Sand	685 kg/m ³
Course Aggregate (5 - 20 mm)	1065 kg/m ³
Water reducing agent (PDA 25-XL)	1410 mL/m ³
Air entraining agent (Micro-air)	520 mL/m ³
Superplasticiser (SPN)	n/a
Water-cement ratio	0.38
Slump	100 mm
Entrained air	5 - 8%

Table 7.3 Specified concrete composition and properties

At least 15 150 x 300 mm cylinders and 4 150 x 150 x 600 mm flexural beams were prepared from each concrete batch. Compression, splitting and third point loading flexural tests were conducted to determine the average concrete compressive strength, f'_c , splitting tensile strength, f_{sp} , and the modulus of rupture, f_{cr} . The average concrete strengths at the time of testing are reported in Table 7.1 and the average concrete compressive strengths are shown in Fig. 7.3(a).

7.5 Experimental Set-up

The testing apparatus and procedure used to test Specimens R0 through R3 were identical to those described for Specimens S1 through S4 in Chapter 2. The only difference in the procedure was that for the R-series of specimens, two specimens were cast at once. As such the specimens were cast with 300 mm channels along the bottom of each wall to which the longitudinal steel was welded. The Specimens were then mounted on the testing apparatus. A layer of high strength plaster was placed between the loading beams of the test apparatus and the channels on the base of the walls to ensure a continuous bearing surface between the reaction beams and the specimens. The walls were then clamped into place as in the S-series of specimens. Clamping and tie-down forces were the same as those used for the S-series of specimens. Figure 7.4 shows the coupled wall testing apparatus with a reinforced concrete coupling beam mounted.

7.6 Instrumentation

Figure 7.5 shows the instrumentation used for Specimens R0 through R3. An array of linear voltage differential transformers (LVDTs) measured the vertical displacements of the walls, allowing the differential displacement and rotations of each wall to be determined. Four LVDTs were used to record vertical crack opening and beam joint rotation at the face of each wall. An additional two LVDTs recorded the vertical sliding shear displacements at the face of each wall.

LVDT rosettes (0° - 45° - 90°) were located on the reinforced concrete coupling beam to record shear strains in the beam. These rosettes were located at the mid-height of the beam at the critical sections, $d/2$ from the face of each wall. Electrical resistance strain rosettes (0° - 45° - 90°) were located on the retrofit plates at locations corresponding to the location of the LVDT rosettes on the beams. These rosettes recorded shear strains in the plates and allow a comparison with the strains recorded in the concrete beams.

Strain gauges were located on the top and bottom longitudinal reinforcing steel in the coupling beam in order to determine the flexural strains in the beam.

Positive loads were recorded with two 100 kip (445 kN) load cells located between the hydraulic rams and the loading beam. Negative loads were recorded with 75 kip (334 kN) load cells located on each tension rod. An additional load cell was located at the back of the specimens to record the force required to keep the walls parallel. All recorded load values were post-processed to remove the effect of the dead load of the specimens, leaving only the shear applied shear to the coupling beam.

All readings were recorded with a Doric 245 data acquisition system and simultaneously displayed on a terminal to facilitate ease of test control.

7.7 Load Histories

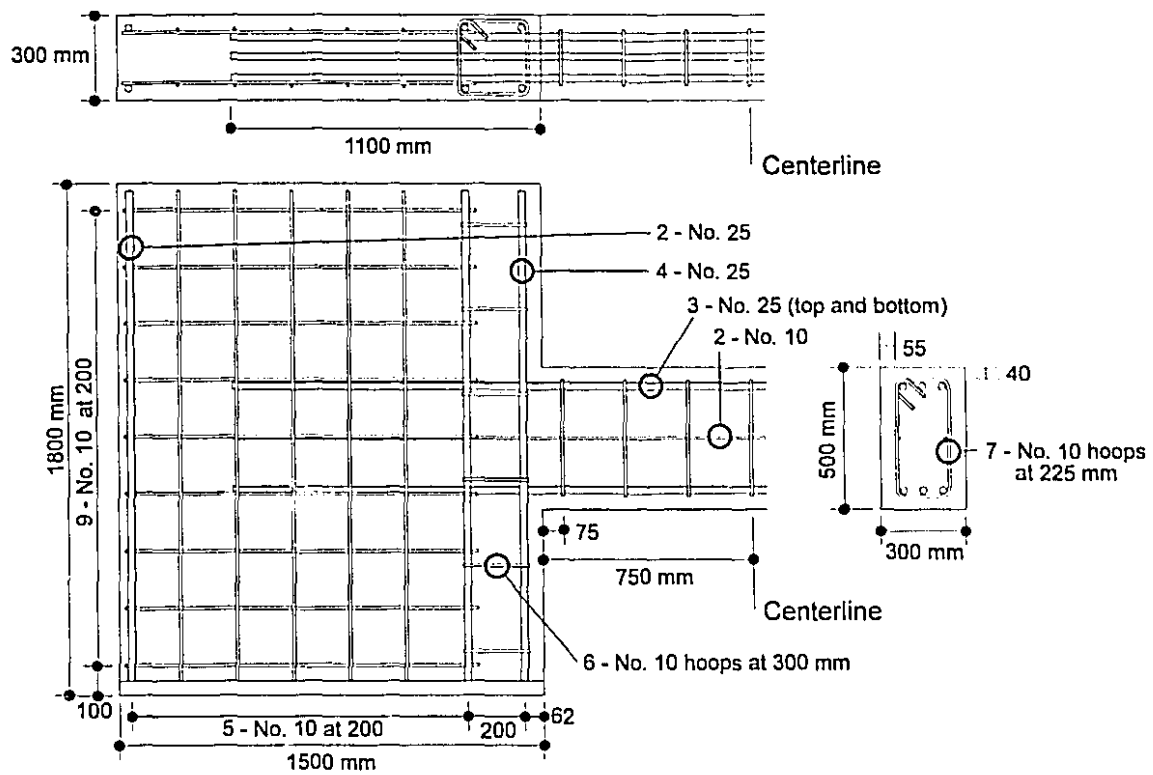
The loading history for each specimen is shown in Fig. 7.6. In order to control testing, load versus deflection of the loaded walls were plotted as testing progressed. Upwards loads and deflections were considered as positive.

The tests were conducted under "load control" up to the point of general yield and "deflection control" thereafter. The specimens were cycled once at each load or deflection level. Each full cycle involved a positive and negative peak. Load control involved cycling the specimens at predetermined load levels until general yield was achieved. Multiples of the deflection at general yield, δ_y , were then used as cycle peaks for deflection control. Table 7.4 gives the load and deflection peaks and the value used for δ_y for each test. It must be noted

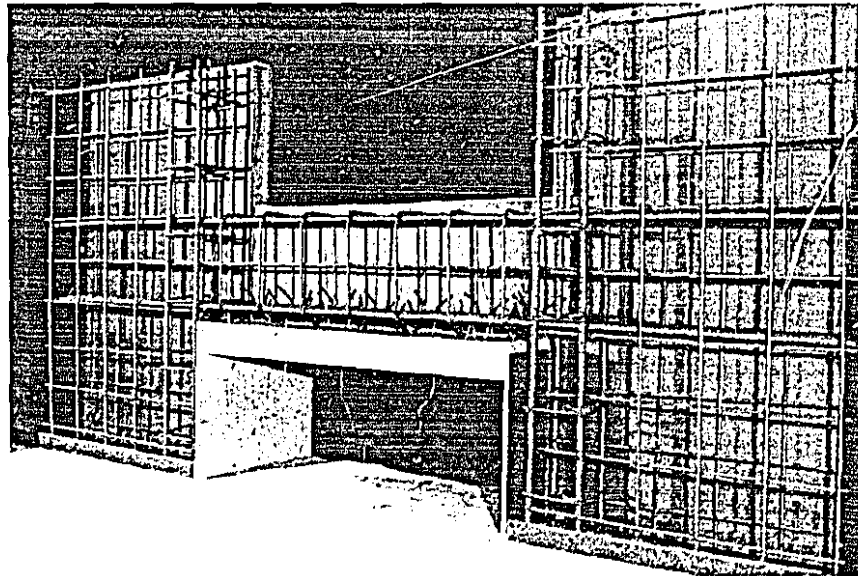
that these values were used for test control, the actual experimental results were determined after post-processing.

	Specimen R0	Specimen R1	Specimen R2	Specimen R3
Load Control	± 95 kN ± 130 kN ± 210 kN	± 100 kN ± 130 kN ± 225 kN	± 110 kN ± 155 kN ± 230 kN	± 100 kN ± 150 kN ± 230 kN
δ_v	± 11 mm	± 15 mm	± 15 mm	± 13 mm
Deflection Control	± 1.5 δ_v ± 2 δ_v ± 2.5 δ_v ± 3 δ_v ± 3.5 δ_v	± 1.5 δ_v ± 2 δ_v ± 2.5 δ_v ± 3 δ_v	± 1.5 δ_v ± 2 δ_v ± 2.5 δ_v ± 3 δ_v ± 3.5 δ_v ± 4 δ_v	± 1.5 δ_v ± 2 δ_v ± 2.5 δ_v ± 3 δ_v ± 3.5 δ_v ± 4 δ_v ± 4.5 δ_v

Table 7.4 Summary of load histories of Specimens R0 through R3

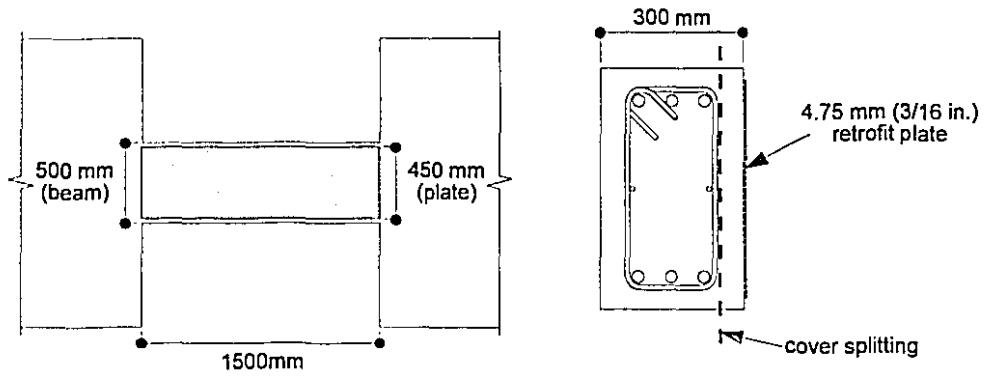


(a) Specimens R0 through R3

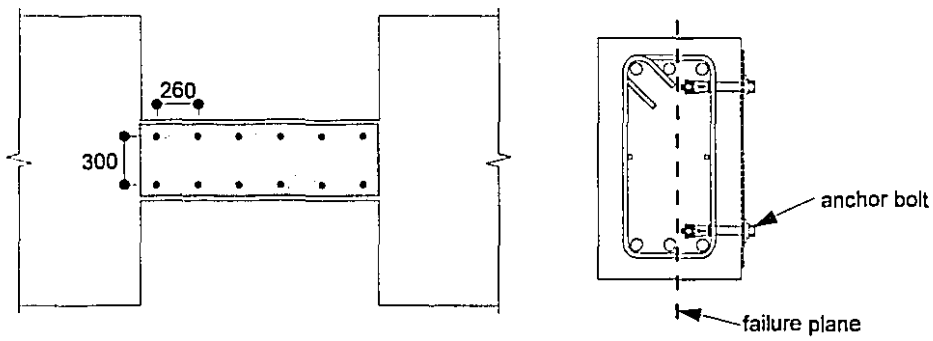


(b) Specimen R0

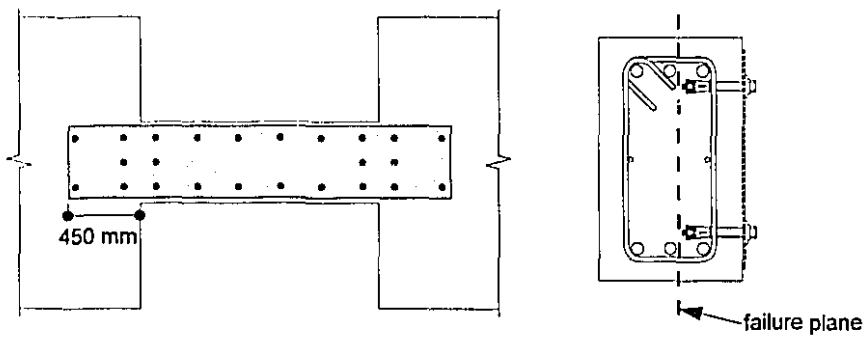
Figure 7.1 Coupling beam and wall reinforcement details for Specimens R0 through R3



(a) Specimen R1 - plate epoxied to beam

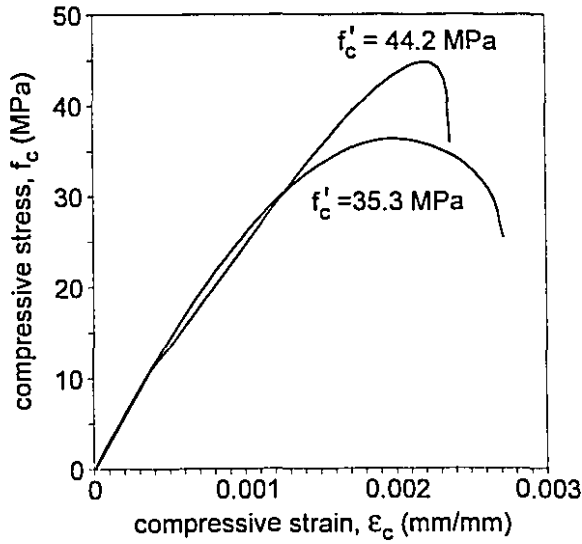


(b) Specimen R2 - plate epoxied and bolted to beam

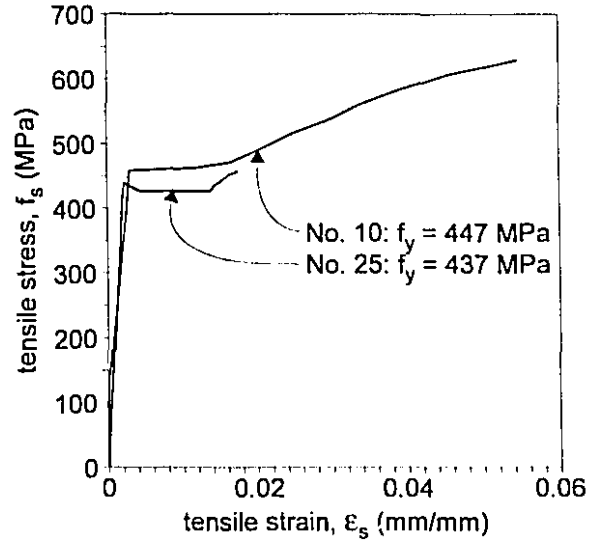


(c) Specimen R3 - plate epoxied and bolted to beam and wall

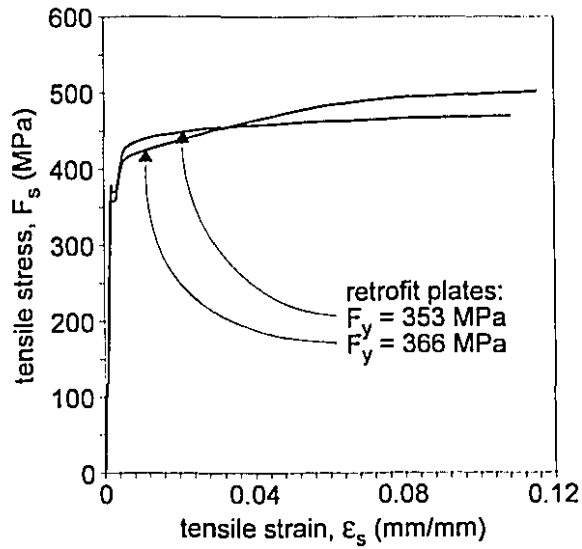
Figure 7.2 Retrofit details for Specimens R1 through R3



(a) concrete



(b) reinforcing steel



(c) 3/16" retrofit plates

Figure 7.3 Material characteristics of retrofitted coupling beam specimens

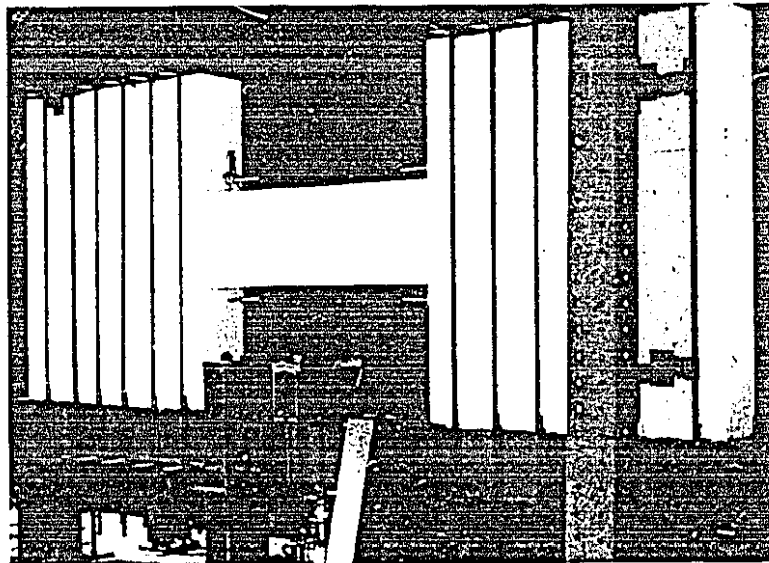
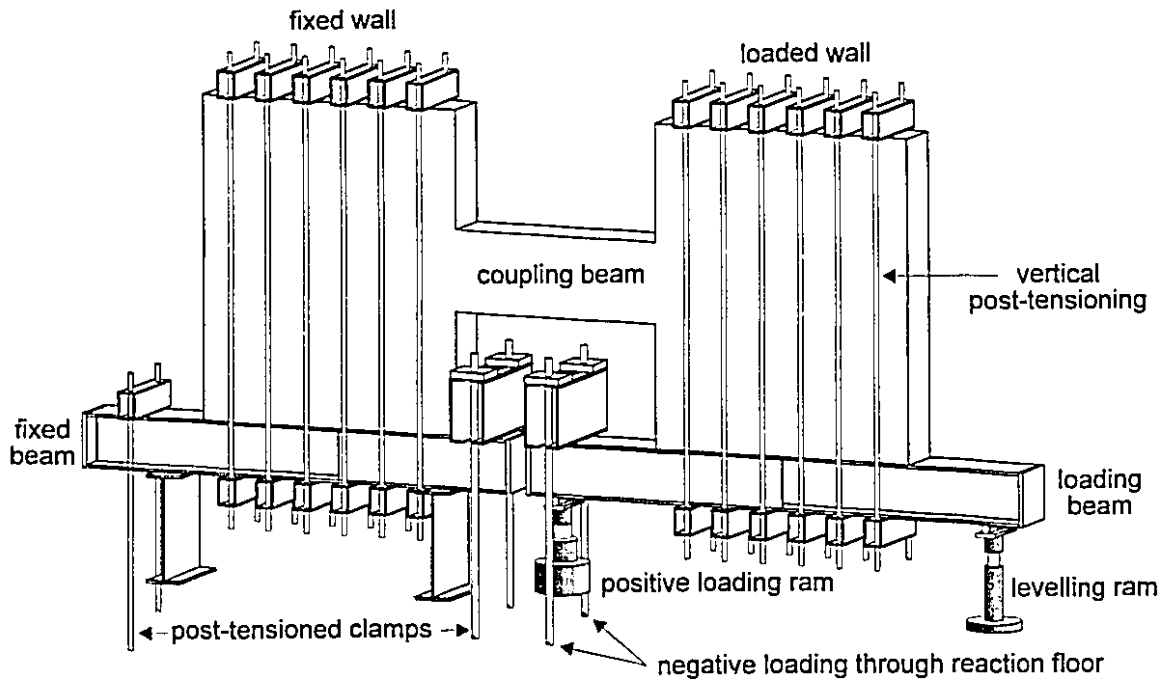
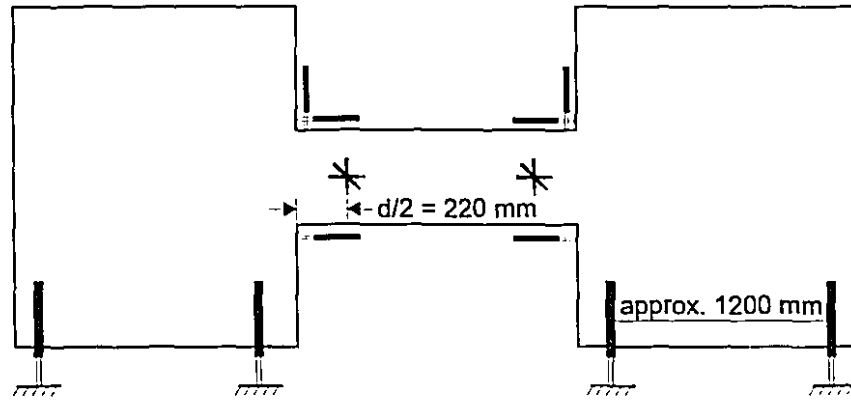
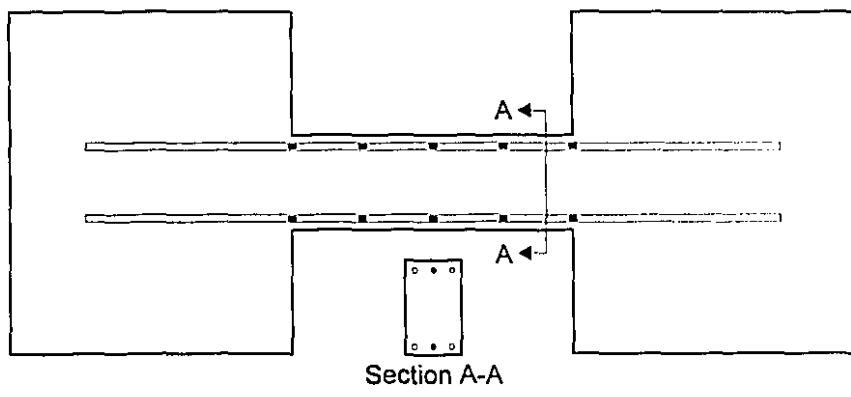


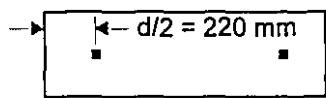
Figure 7.4 Coupled Wall Testing Apparatus with reinforced concrete coupling beam specimen mounted



(a) Coupling beam LVDT locations

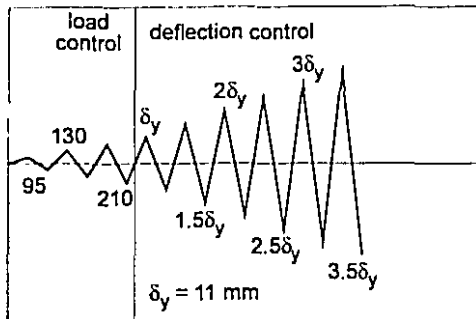


(b) Reinforcing steel strain gauge locations
(located at quarter points of middle reinforcing bar)

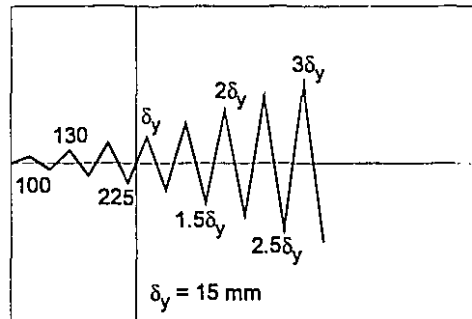


(c) Retrofit plate strain rosette locations (Specimens R1 - R3)

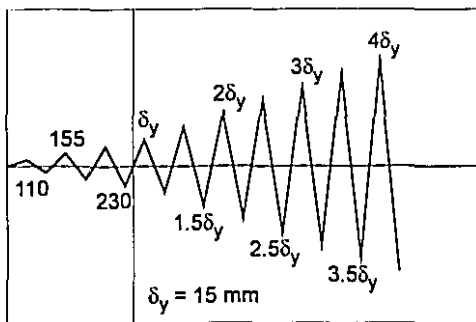
Figure 7.5 Instrumentation of Specimens R0 through R3



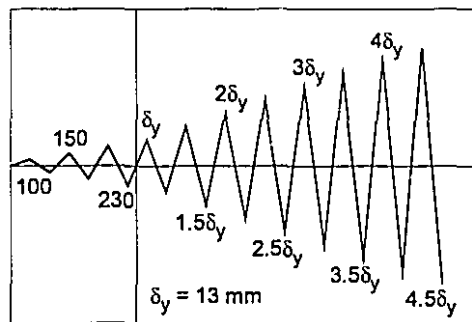
(a) Specimen R0



(b) Specimen R1



(c) Specimen R2



(d) Specimen R3

Figure 7.6 Load histories of Specimens R0 through R3

Chapter 8

Behaviour of Retrofitted Reinforced Concrete Coupling Beams

This chapter presents a detailed description of the observed experimental behaviour of Specimens R0 through R3.

For the load-deflection responses, the load corresponds to the shear transmitted through the coupling beam and the deflection represents the vertical displacement of the loaded (east) wall relative to the fixed (west) wall. The displacements have been corrected to account for measured, differential rotations of the walls. It should be noted that these differential rotations were very small, resulting in only minor corrections to the deflections. Summaries of the load stage peak load and deflections for each specimen are given in Tables 8.1 through 8.4. The load step designations A and B represent positive (upwards) and negative (downwards) loads and deflections, respectively.

8.1 Specimen R0

The applied load versus relative deflection response of Specimen R0 is shown in Fig. 8.1. The load stage, peak applied load and relative deflection values are given in Table 8.1. Specimen R0 was the control specimen for the R-series of tests. The response of R0 is assumed to be the same as the unretrofitted response of Specimens R1 through R3.

Load Stage	Positive (A) Cycle		Negative (B) Cycle		Notes
	Applied Shear (kN)	Relative Deflection (mm)	Applied shear (kN)	Relative Deflection (mm)	
1	97.1	2.03	-98.1	-1.61	
2	126.4	3.02	-137.4	-3.16	
3	214.2	7.39	-236.2	-7.48	
4	263.9	11.23	-296.4	-11.66	general yield, δ_y
5	280.3	17.01	-302.2	-17.57	$1.5\delta_y$
6	238.7	22.77	-242.3	-23.36	$2\delta_y$
7	202.1	29.06	-205.7	-29.10	$2.5\delta_y$
8	169.3	35.28	-169.3	-35.04	$3\delta_y$
9	137.7	41.55	-137.4	-41.00	$3.5\delta_y$

Table 8.1 Load stage peaks for Specimen R0

The first flexural cracking, located at the face of each wall, occurred at an applied load of 61 kN. The predicted applied load to cause flexural cracking was 59 kN. The predicted value of applied load to cause shear cracking was 124 kN. Initial shear cracking occurred at 126 kN at a relative vertical displacement of 3 mm.

The first evidence of yield of shear reinforcement was recorded at load stage 3A, at an applied shear of 214 kN. At this point the stirrup strain near the critical section was 2190 microstrain. There was no noticeable change in the overall stiffness of the specimen however.

General yielding of the coupling beam occurred at load stage 4A, at a load of 264 kN and a relative vertical displacement of 11.2 mm. General yielding in the negative direction occurred at load stage 4B, at a load of -296 kN and a relative displacement of -11.7 mm. The displacement at general yield, δ_y , was taken as ± 11 mm.

The ultimate capacity of the coupling beam was reached at loadstage 5B, at a ductility of $-1.5\delta_y$. The maximum shear reached was -302 kN at a relative displacement of -17.6 mm. The ultimate capacity achieved was only 86% of the nominal flexural capacity of the coupling beam.

By load stage 5 the diagonal crack pattern, typical of shear distress, was well established. Only minor vertical cracks, coinciding with the location of vertical wall reinforcement were evident on the walls. Beyond load stage 5, no further distress was noted in either wall. Figure 8.2 shows the coupling beam at load stage 7B, at a ductility of $-2.5\delta_y$. It

was evident from the intersection of the principal shear cracks that the critical section of this coupling beam was located at about 400 mm from the face of each wall. This value corresponds to a distance from the face of the wall of about $0.9d$, rather than the typically assumed $0.5d$. The moment-to-shear ratio at this location is 0.35 .

Continued cycling resulted in the appearance of many small shear cracks and considerable opening of the principal shear cracks. At load stage 7 (see Fig. 8.2), the principal shear cracks were about 10 mm wide with crack slips of about 7 mm. The cover concrete on all four surfaces of the beam was clearly delaminated from the confined core. The top and bottom cover had loosened to the point of increasing the apparent overall depth of the beam by about 40 mm at the centre of the span. At the end of testing considerable spalling was evident on both sides of the beam and the top and bottom concrete cover could be easily removed. Figure 8.3 shows Specimen R0 at the end of testing.

8.1.1 Hysteretic Response

The pinched hysteretic response of Specimen R0 is shown in Fig. 8.1. The response is typical of longitudinally reinforced concrete beams exhibiting a shear degradation. Specimen R0 exhibited considerable post-peak decay of strength and stiffness, losing 20% of load carrying capacity at a ductility of $2\delta_y$ and exhibiting a 55% loss of capacity when the test had ended at a ductility of $3.5\delta_y$.

8.2 Specimen R1

The applied load versus relative deflection response of Specimen R1 is shown in Fig. 8.4. The load stage, peak applied load and relative deflection values are given in Table 8.2. Specimen R1 was retrofitted with a $3/16$ " (4.76 mm) thick, 450 mm deep steel plate applied to the 1500 mm clear span of the coupling beam. The plate was attached with only structural epoxy (see Fig 7.2(a)).

Load Stage	Positive (A) Cycle		Negative (B) Cycle		Notes
	Applied Shear (kN)	Relative Deflection (mm)	Applied shear (kN)	Relative Deflection (mm)	
1	99.6	1.74	-113.7	-1.51	
2	128.0	2.72	-142.2	-2.05	
3	223.7	6.80	-241.3	-5.69	
4	325.4	14.16	-348.7	-16.93	general yield, δ_y
5	343.0	22.08	-276.0	-24.02	$1.5\delta_y$
6	283.1	29.62	-231.6	-31.46	$2\delta_y$
7	214.7	37.70	-190.0	-39.44	$2.5\delta_y$
8	142.2	45.18	-159.0	-45.38	$3\delta_y$
END	114.4	106.68	-	-	

Table 8.2 Load stage peaks for Specimen R1

The first flexural cracking, located at the face of each wall, occurred at an applied load of 75 kN. The predicted applied load to cause flexural cracking was 60 kN. The predicted value of applied load to cause shear cracking was 127 kN. Initial shear cracking occurred at 128 kN at a relative vertical displacement of 2.7 mm.

General yielding of the coupling beam occurred at load stage 4A, at a load of 325 kN and a relative vertical displacement of 14.1 mm. General yielding in the negative direction occurred at load stage 4B, at a load of -349 kN and a relative displacement of -16.9 mm. The displacement at general yield, δ_y , was taken as ± 15 mm.

The applied shear at the negative yield cycle also corresponded to the maximum capacity of the coupling beam. At a ductility of $-\delta_y$, the ultimate load was -349 kN at a relative displacement of -16.9 mm. The ultimate capacity achieved was 99% of the predicted nominal flexural capacity of the unretrofitted coupling beam.

By load stage 5 the diagonal crack pattern, typical of shear failures, was well established on the exposed, unretrofitted face of the coupling beam. Significant vertical cracks, coinciding with the location of vertical wall reinforcement were evident on the walls. Beyond load stage 5, little further distress was noted in either wall. Figure 8.5 shows the coupling beam at load stage 7B, at a ductility of $-2.5\delta_y$. It was evident, from the intersection of the principal shear cracks, that the critical section of this coupling beam was located at about 270 mm from

the face of each wall. This value corresponds to a distance from the face of the wall of about 0.6d.

Continued cycling resulted in the appearance of many small shear cracks and the considerable opening of the principal shear cracks. At load stage 7 (see Fig. 8.5), the principal shear cracks were observed to be about 6 mm wide. The cover concrete on all three exposed surfaces of the beam was clearly delaminated from the confined core. As was the case with Specimen R0, the top and bottom cover had separated to the point of increasing the apparent overall depth of the beam by about 30 mm at the centre of the span. At the end of testing considerable spalling was evident on the front of the beam and the top and bottom concrete cover could be easily removed. Figure 8.6 shows Specimen R1 at the end of testing.

8.2.1 Response of Retrofit Plate

The retrofit plate of Specimen R1 was attached with only epoxy over the clear span of the beam. Pre-yield response indicated that strain compatibility between the reinforced concrete beam and the retrofit plate was maintained (see Fig. 8.7). Immediately after general yielding, the retrofit plate and attached concrete cover began to separate along a tension failure plane through the concrete cover (see Fig 7.2(a)). The separation initiated at the corners of the plate, where the failure plane began along the concrete-epoxy interface. As the separation progressed toward the centre of the beam, the failure plane went into the concrete cover, essentially following the plane of shear reinforcement.

Significant plate separation had occurred by load stage 6 and the failure plane was completely developed. Beyond a ductility of $2\delta_y$, the retrofit plate was no longer contributing to the response of the beam. Furthermore, it was observed that the retrofit plate was not sufficiently attached to the beam to cycle through the same displacements as the beam. The plate 'pivoted' somewhat on the spalled cover concrete and appeared to rotate relative to the concrete beam.

The maximum vertical strain observed in the retrofit plate was 610 microstrain at a ductility level of $2.5\delta_y$. This maximum strain occurred well into the post peak response of the specimen and likely indicates a local interaction along the failure plane near the location of this strain rosette. The instrument pins holding the LVDT rosettes may also have contributed to this relatively high reading occurring after the plate and cover concrete had apparently spalled.

The maximum vertical strain corresponding to the ultimate applied shear of -349 kN was 302 microstrain. A value of 254 microstrain was observed corresponding to the ultimate applied shear (343 kN) in the positive cycle.

8.2.2 Hysteretic Response

The pinched hysteretic response of Specimen R1 is shown in Fig. 8.4. The response is typical of longitudinally reinforced concrete beams exhibiting a shear mode of behaviour. Specimen R1 exhibited considerable post-peak decay of strength and stiffness, losing 20% of load carrying capacity at a ductility of $2\delta_y$ and 55% of its capacity when the test had ended at a ductility of $3\delta_y$. Final monotonic loading to $7.5\delta_y$ resulted in a final applied load of only 114 kN, 33% of the ultimate capacity of the section.

8.3 Specimen R2

The applied load versus relative deflection response of Specimen R2 is shown in Fig. 8.8. The load stage, peak applied load and relative deflection values are given in Table 8.3. Specimen R2 was retrofitted with a 3/16" (4.76 mm) thick, 450 mm deep steel plate applied to the 1500 mm clear span of the coupling beam. The plate was attached with structural epoxy and anchor bolts (see Fig. 7.2(b)).

Load Stage	Positive (A) Cycle		Negative (B) Cycle		Notes
	Applied Shear (kN)	Relative Deflection (mm)	Applied shear (kN)	Relative Deflection (mm)	
1	103.6	1.16	-119.2	-1.30	
2	159.7	3.05	-175.9	-2.91	
3	234.4	5.94	-257.2	-6.25	
4	352.2	14.15	-406.2	-15.70	general yield, δ_y
5	395.7	21.27	-421.9	-23.35	$1.5\delta_y$
6	385.5	29.08	-325.8	-30.92	$2\delta_y$
7	301.1	37.05	-263.4	-38.11	$2.5\delta_y$
8	246.2	44.65	-211.5	-45.80	$3\delta_y$
9	206.5	52.72	-171.3	-53.16	$3.5\delta_y$
10	169.8	60.49	-145.2	-61.71	$4\delta_y$

Table 8.3 Load stage peaks for Specimen R2

The first flexural cracking, located at the face of each wall, occurred at an applied load of about 75 kN. The predicted applied load to cause flexural cracking was 64 kN. The predicted value of applied load to cause shear cracking was 135 kN. Initial shear cracking occurred at 160 kN at a relative vertical displacement of 3 mm.

General yielding of the coupling beam occurred at load stage 4A, at a load of 352 kN and a relative vertical displacement of 14.1 mm. General yielding in the negative direction occurred at load stage 4B, at a load of -406 kN and a relative displacement of -15.7 mm. The displacement at general yield, δ_y , was taken as ± 15 mm.

The ultimate capacity of the coupling beam was achieved at loadstage 5B, at a ductility of $-1.5\delta_y$. The ultimate load reached was -422 kN at a relative displacement of -23.4 mm. The ultimate capacity achieved was 121% of the predicted nominal flexural capacity of the unretrofitted coupling beam.

By load stage 5 the diagonal crack pattern, typical of shear failures, was well established on the coupling beam. Significant vertical cracks, over the vertical wall reinforcing bars were evident on the walls. Beyond load stage 5, little further distress was noted in either wall. Figure 8.9 shows the coupling beam at load stage 7B, at a ductility of $-2.5\delta_y$. It was evident, from the intersection of the principal shear cracks, that the critical section of this coupling beam was located at about 280 mm from the face of each wall. This value corresponds to a distance from the face of the wall of about $0.6d$.

Continued cycling resulted in the appearance of many small shear cracks and the considerable opening of the principal shear cracks. At load stage 7 (see Fig. 8.9), the principal shear cracks were observed to be about 6 mm wide and to have shifted about 3 mm out-of-plane. The cover concrete on all three exposed surfaces of the beam had delaminated from the confined core. The plane of delamination, particularly at the top of the beam, seemed lower than was observed in Specimen R1 due to the presence of the anchor bolts in the confined core (see Fig. 8.10(a)). Figure 8.10 shows Specimen R2 at the end of testing.

8.3.1 Response of Retrofit Plate

The retrofit plate of Specimen R2 was attached with epoxy and anchor bolts over the clear span of the beam. Pre-yield response indicated that strain compatibility between the reinforced concrete beam and the retrofit plate was maintained (see Fig. 8.11). Immediately after general yielding, the ends of the retrofit plate and attached concrete cover began to separate from the beam along a plane through the concrete cover. As the separation progressed toward the centre of the beam, the failure plane went into the concrete cover, essentially following the plane of shear reinforcement. The presence of the anchor bolts across this plane, effectively arrested the propagation of the failure plane through the cover concrete. The anchor bolts served to tie the retrofit plate and cover concrete to the confined core of the coupling beam. Therefore the retrofit plate continued to contribute to the post-peak response of the specimen.

With continued cycling, the shear reversals on the anchor bolts, began to cause the concrete surrounding the bolts to deteriorate. By load stage 8, at a ductility of $3\delta_y$, the bolts nearest the ends of the retrofit plate could be removed from their deteriorated sockets by hand. Due to the deterioration of bolt sockets, the retrofit plate was observed to be shifting by as much as 12 mm vertically, relative to the concrete beam.

The maximum vertical strain observed in the retrofit plate, corresponding to the maximum applied shear of -422 kN, was 520 microstrain.

8.3.2 Hysteretic Response

The hysteretic response of Specimen R2 is shown in Fig. 8.8. The pinched response is typical of reinforced concrete beams exhibiting significant shear distress. Specimen R2 exhibited considerable post-peak decay of strength and stiffness, losing 20% of load carrying capacity at a ductility of $2.5\delta_y$ and 65% of its capacity when the test had ended at a ductility of $4\delta_y$.

8.4 Specimen R3

The applied load versus relative deflection response of Specimen R3 is shown in Fig. 8.12. The load stage, peak applied load and relative deflection values are given in Table 8.4. Specimen R3 was retrofitted with a 3/16" (4.76 mm) thick, 450 mm deep steel plate applied to the 1500 mm clear span of the coupling beam and extending 450 mm onto each wall. The plate was attached with structural epoxy and anchor bolts to both the beam and wall (see Fig. 7.2(c)).

Load Stage	Positive (A) Cycle		Negative (B) Cycle		Notes
	Applied Shear (kN)	Relative Deflection (mm)	Applied shear (kN)	Relative Deflection (mm)	
1	95.5	1.51	-121.0	-1.39	
2	146.0	2.58	-173.9	-2.45	
3	233.5	5.06	-253.6	-4.78	
4	391.6	11.86	-458.5	-13.64	general yield, δ_y
5	435.6	18.32	-476.0	-20.87	$1.5\delta_y$
6	451.8	24.16	-470.8	-27.24	$2\delta_y$
7	408.3	31.61	-405.8	-33.79	$2.5\delta_y$
8	307.4	38.48	-320.3	-39.53	$3\delta_y$
9	255.0	45.62	-272.3	-46.50	$3.5\delta_y$
10	200.6	51.69	-230.3	-52.14	$4\delta_y$
11	163.8	59.85	-180.9	-60.37	$4.5\delta_y$

Table 8.4 Load stage peaks for Specimen R3

The first flexural cracking, located at the face of each wall, occurred at an applied load of 81 kN. The predicted applied load to cause flexural cracking was 64 kN. The predicted value of applied load to cause shear cracking was 135 kN. Initial shear cracking occurred at 146 kN at a relative vertical displacement of 2.6 mm.

General yielding of the coupling beam occurred at load stage 4A, at a load of 392 kN and a relative vertical displacement of 11.9 mm. General yielding in the negative direction occurred at load stage 4B, at a load of -459 kN and a relative displacement of -13.6 mm. The displacement at general yield, δ_y , was taken as ± 13 mm.

The ultimate capacity of the coupling beam was achieved at loadstage 5B, at a ductility of $-1.5\delta_y$. The ultimate load reached was -476 kN at a relative displacement of -20.9 mm. The ultimate capacity achieved was 136% of the predicted nominal flexural capacity of the unretrofitted coupling beam.

By load stage 5 the diagonal crack pattern was well established on the coupling beam and vertical cracks were evident on the walls over the locations of the vertical wall bars. Unlike the previous specimens, due to the extension of the plate onto the walls, cracking on the walls continued to propagate throughout the course of testing. The cracking on the walls did not effect the integrity of the walls. Figure 8.13 shows the coupling beam at load stage 7B, at a

ductility of $-2.5\delta_y$. It was evident, from the intersection of the principal shear cracks, that the critical sections of this coupling beam were located at about 380 mm from the east wall and 210 mm from the west wall. These values correspond to a distance from the face of the walls of about $0.85d$ and $0.5d$, respectively.

Continued cycling resulted in the appearance of many small shear cracks and the considerable opening of the principal shear cracks. At load stage 7 (Fig 8.13), the principal shear cracks were observed to be about 4 mm wide. By load stage 8, the cover concrete on all three exposed surfaces of the beam was clearly delaminated from the confined core. At the end of testing considerable spalling was evident on the front of the beam and the top and bottom concrete cover could be easily removed. Figure 8.14 shows Specimen R3 at the end of testing.

8.4.1 Response of Retrofit Plate

The retrofit plate of Specimen R3 was attached with epoxy and anchor bolts over the clear span of the beam and extending onto each wall. Pre-yield response indicated that strain compatibility between the reinforced concrete beam and the retrofit plate was maintained (see Fig. 8.15). Immediately after general yielding, there was evidence of the ends of the plate beginning to peel off the wall. In the region of the clear span, however, no distress in the epoxy bond or cover concrete was observed.

With continued cycling, the plate gradually debonded from the walls. The fact that the plate debonded, rather than failed through the cover concrete on the walls, indicates that the epoxy line on the walls was not as good as that on the clear span. This likely resulted from insufficient clamping force of the plate extensions onto the walls. Clamping force on the walls was provided only by the anchor bolts in that region, additional external clamps were used over the clear span.

By load stage 6, the retrofit plate had debonded to the first row of anchor bolts in the clear span. From this location, the failure plane went into the cover concrete as had been previously observed. Despite the debonding, at no point was the plate observed to be separating from the beam or walls. The anchor bolts were effectively maintaining continuity between the retrofit plate and reinforced concrete.

Just prior to the peak of load stage 7B, at a relative displacement of -31 mm and ductility of $2.5\delta_y$, a sudden tensile failure of the epoxy in the compression zone at the east end of the beam caused the retrofit plate to buckle out-of-plane. The buckle extended between the first and second column of anchor bolts, 220 mm from the face of the wall. The buckle extended toward the neutral axis 225 mm, half the depth of the plate, and projected about 10

mm out-of-plane at the centre of its 260 mm span. The following cycle exhibited an identical buckle on the west end of the beam. At load stage 8B and 9A buckles were observed at both compression zones simultaneously.

Once buckling was established, the additional capacity realised by extending the retrofit plates onto the walls was lost. The response deteriorated to that of Specimen R2, where the retrofit plate was only attached to the clear span. Continued cycling loosened the anchor bolts and considerable out-of-plane movement was observed. By load stage 10, the retrofit plate exhibited significant local buckling, exceeding 50 mm out-of-plane movement, in the compression zones. Furthermore, it appeared as though the entire plate was experiencing lateral instability, buckling out, over its entire length, at the top of the plate. The remaining tensile capacity of the bolt anchorages was sufficient to control this instability.

The maximum vertical strain observed in the retrofit plate, corresponding to the ultimate applied shear of -476 kN, was 998 microstrain.

After the completion of testing it was observed that the anchor bolts, located on the clear span, nearest the wall, exhibited evidence of shear distortion. This shearing, located just inside the plane of the retrofit plate, was evident on the bolt and its embedment sleeve.

8.4.2 Hysteretic Response

The response of Specimen R3 shown in Fig. 8.12 exhibits pinching typical of concrete beams failing in shear. Specimen R3 exhibited less significant post-peak decay of strength and stiffness than the previous specimens, attaining a ductility of $3\delta_y$ before losing 20% of its load carrying capacity. After the retrofit plate had buckled, the strength and stiffness decay became more pronounced. By the end of testing, at a ductility of $4.5\delta_y$, the load carrying capacity had decreased to 38% of the beam's ultimate capacity.

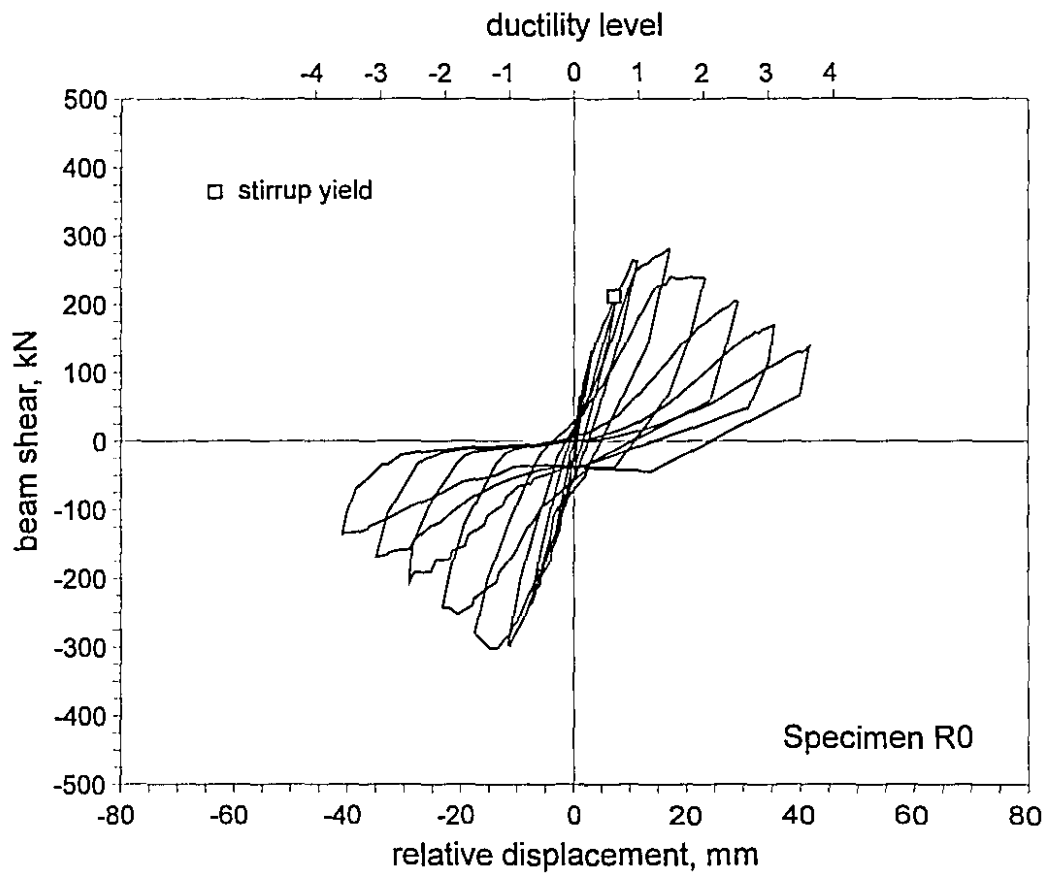


Figure 8.1 Hysteretic response of Specimen R0

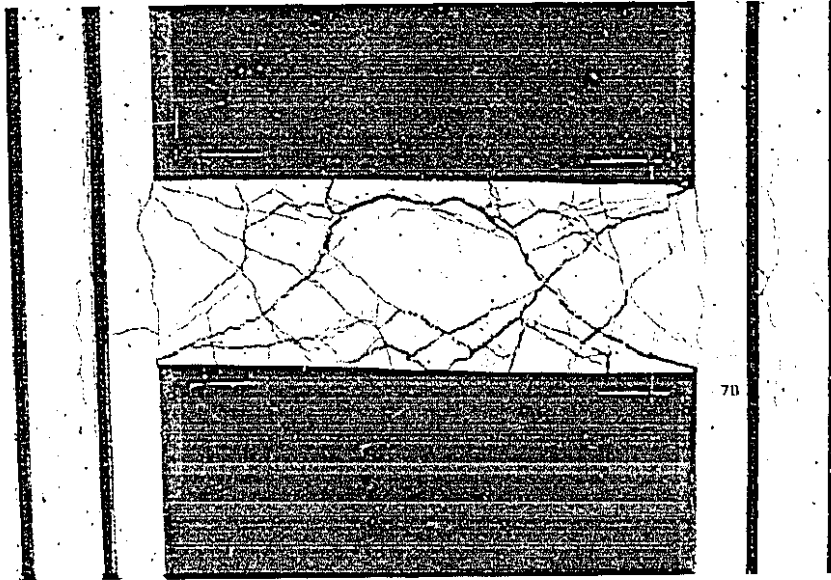


Figure 8.2 Specimen R0 at ductility level $-2.5\delta_y$

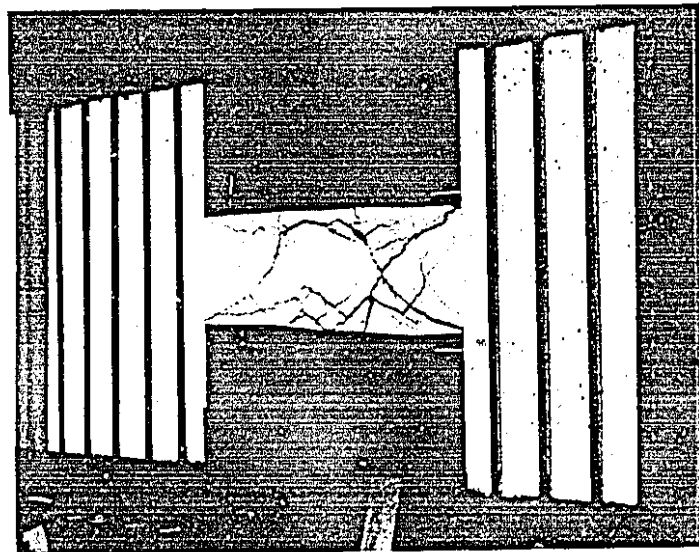


Figure 8.3 Specimen R0 at the end of testing

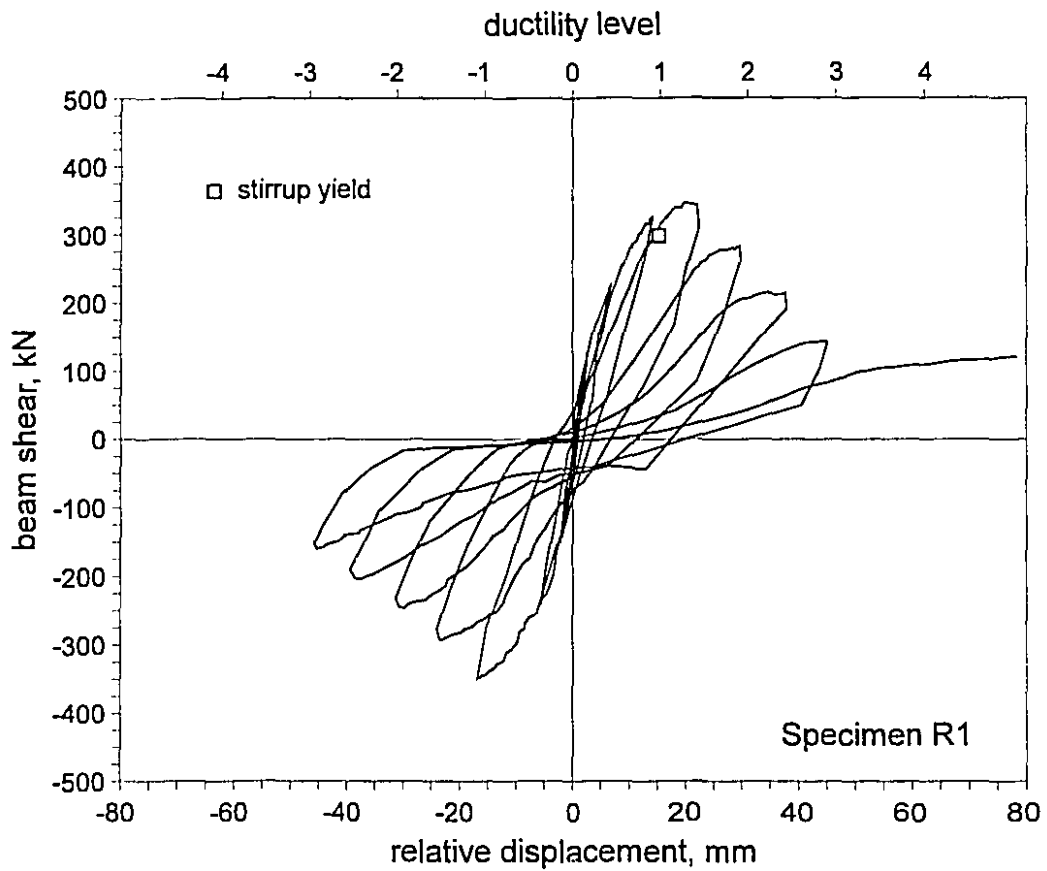


Figure 8.4 Hysteretic response of Specimen R1

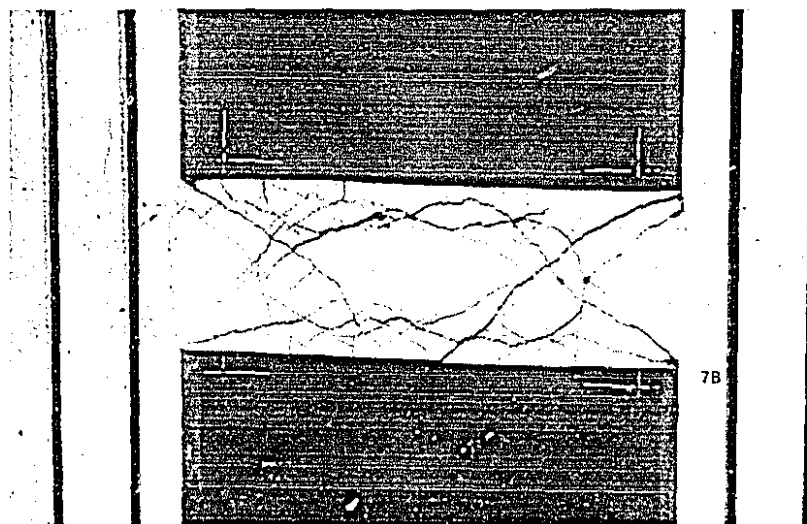
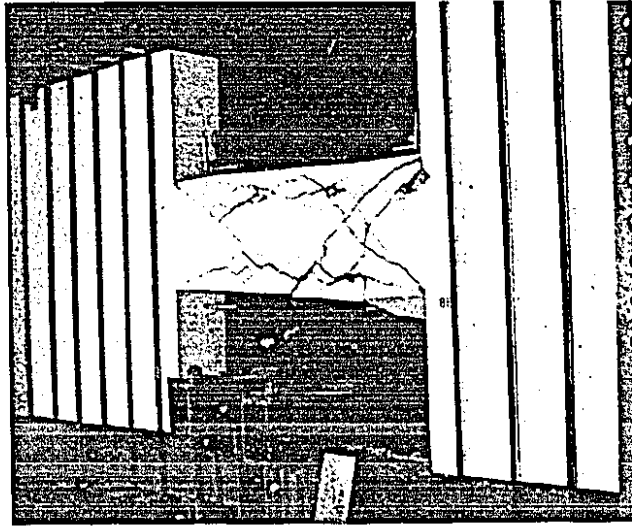
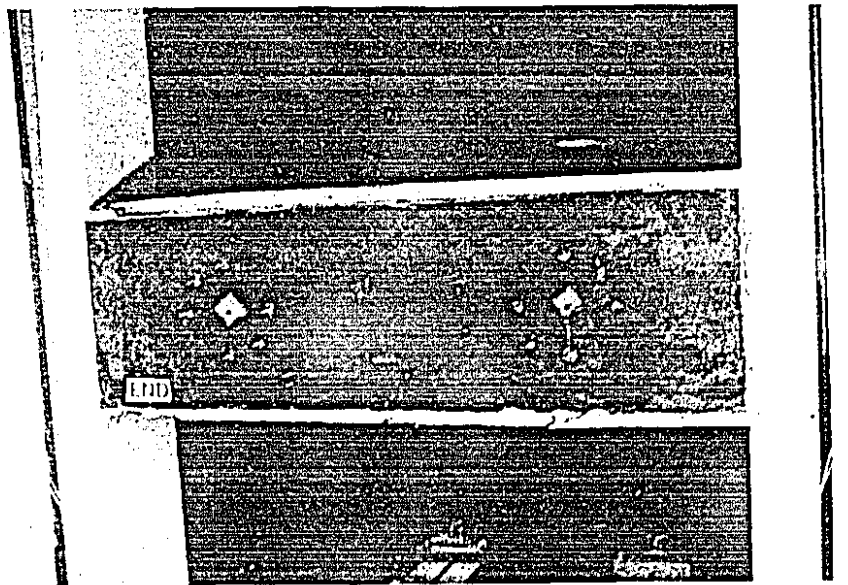


Figure 8.5 Specimen R1 at ductility level $-2.5\delta_y$



(a) Overall view of side without retrofit plate



(b) View of side with retrofit plate

Figure 8.6 Specimen R1 at the completion of testing

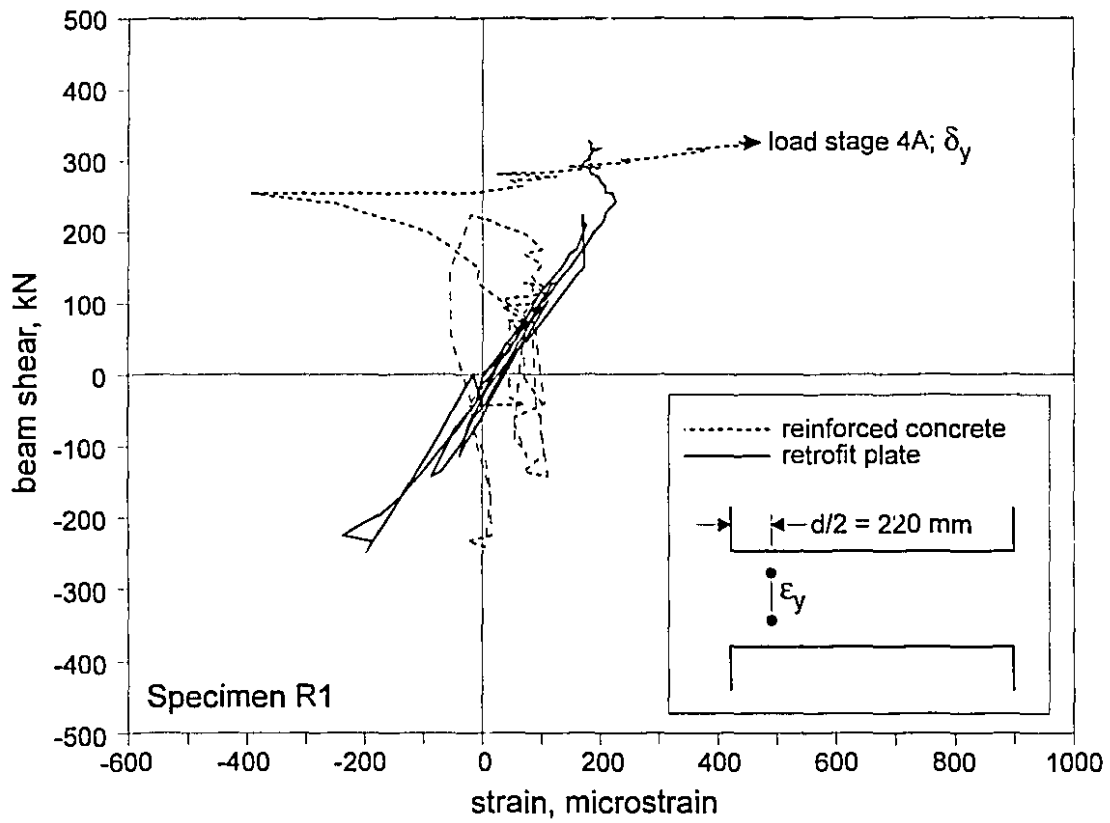


Figure 8.7 Vertical strains in reinforced concrete beam and retrofit plate of Specimen R1

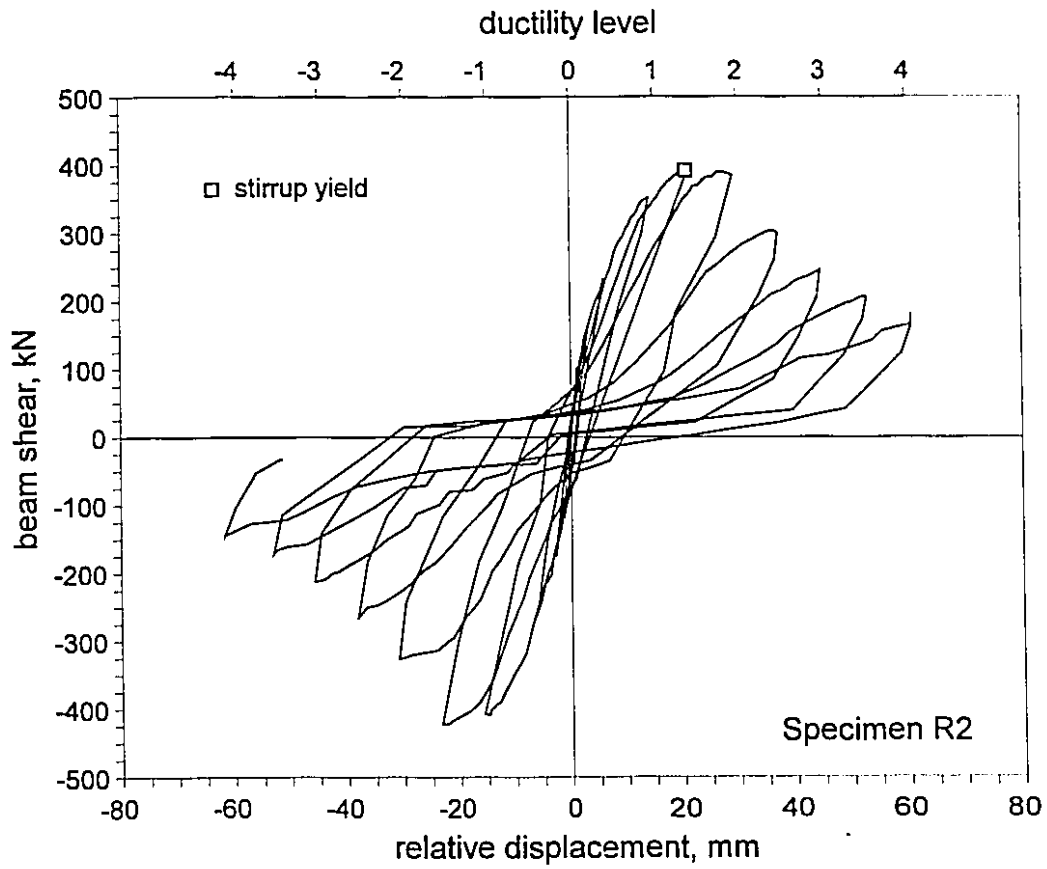


Figure 8.8 Hysteretic response of Specimen R2

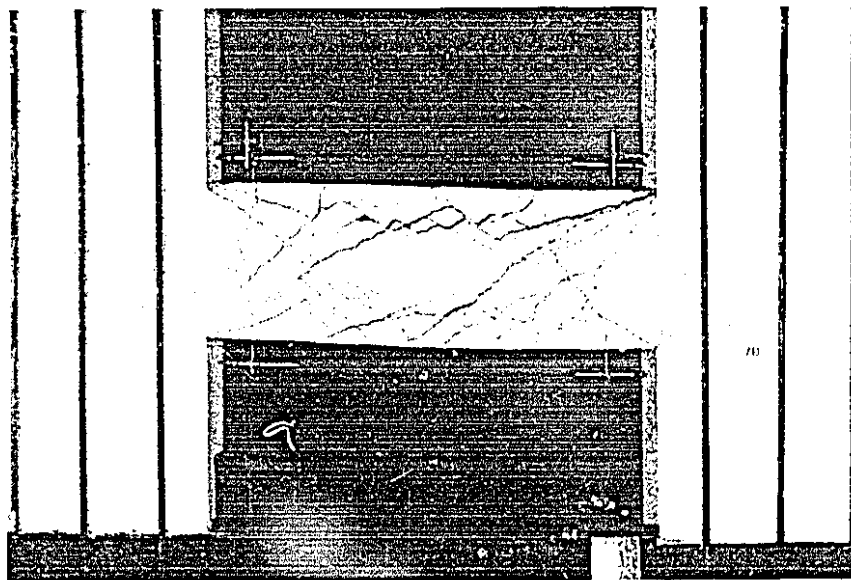
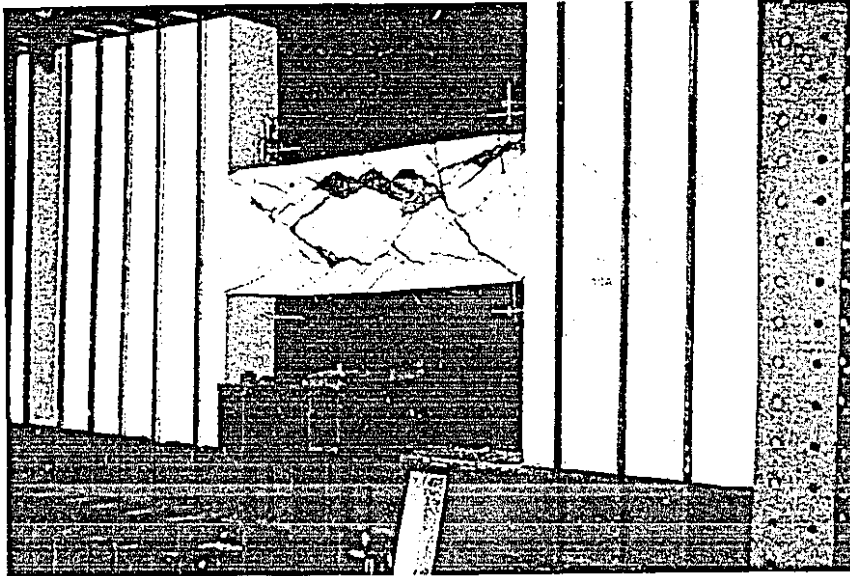
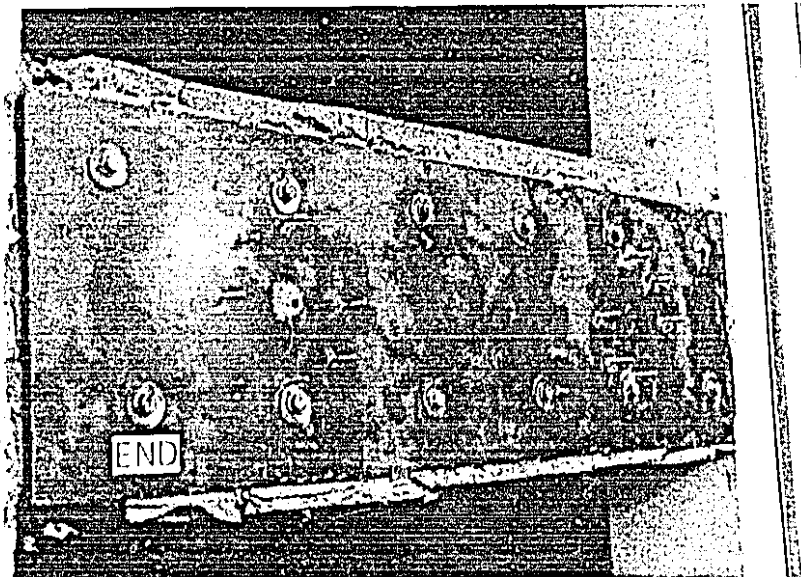


Figure 8.9 Specimen R2 at ductility level $-2.5\delta_y$



(a) Overall view of side without retrofit plate



(b) View of side with retrofit plate

Figure 8.10 Specimen R2 at the completion of testing

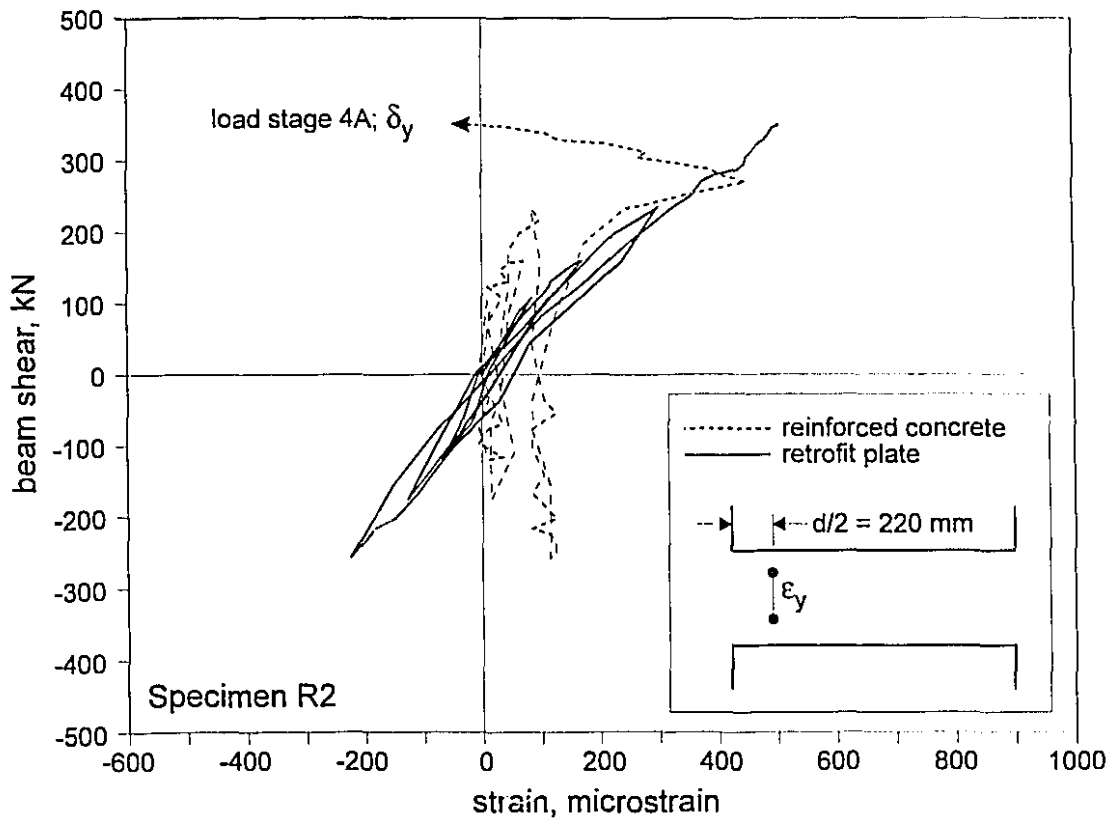


Figure 8.11 Vertical strains in reinforced concrete beam and retrofit plate of Specimen R2

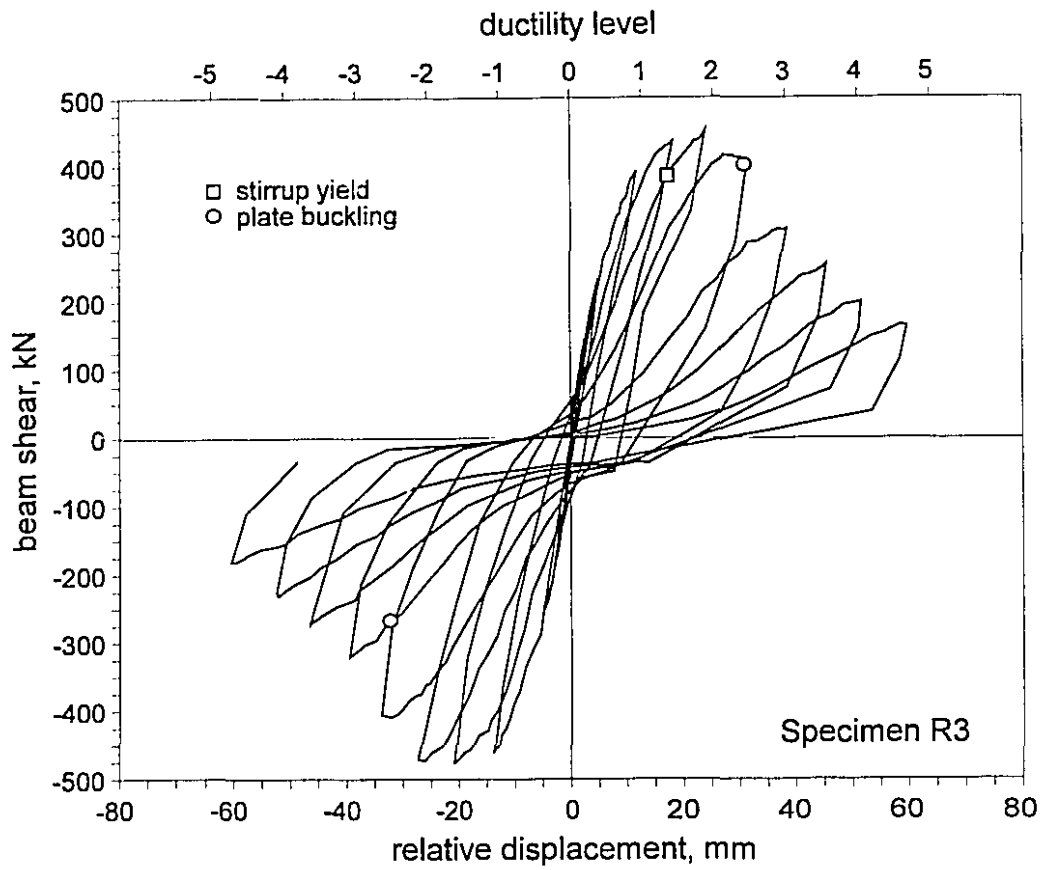


Figure 8.12 Hysteretic response of Specimen R3

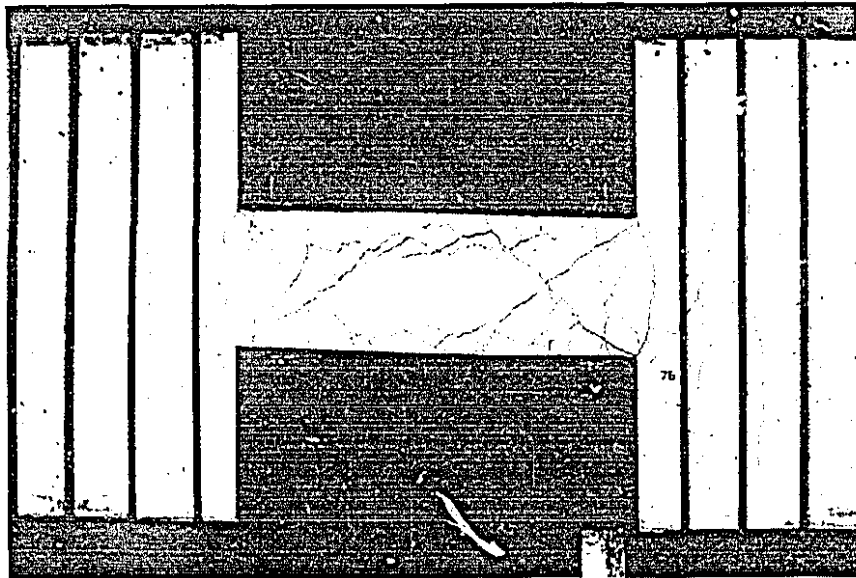
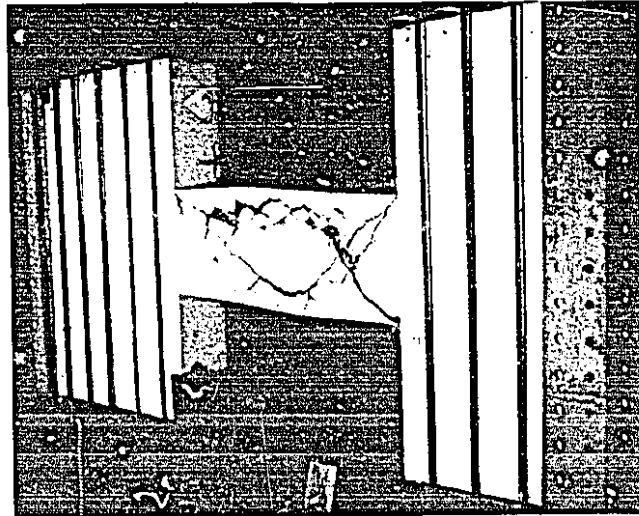
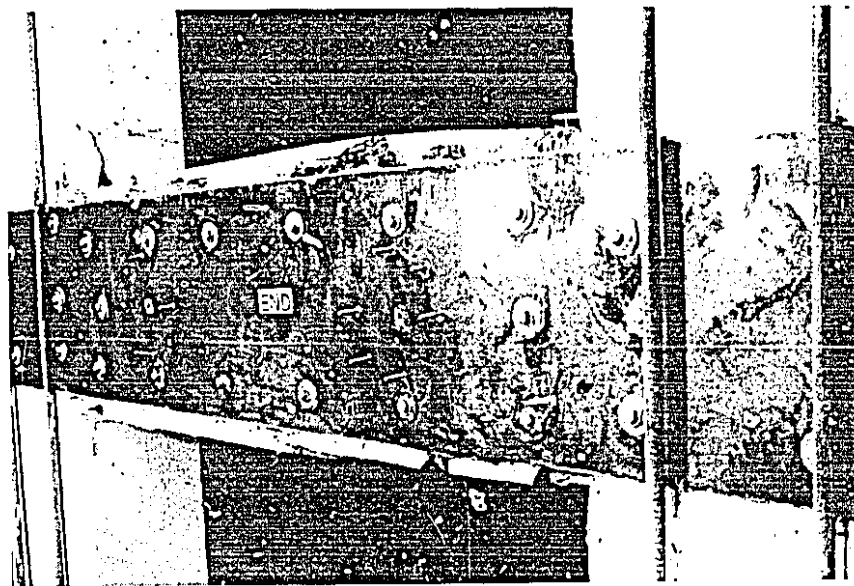


Figure 8.13 Specimen R3 at ductility level $-2.5\delta_y$



(a) Overall view of side without retrofit plate



(b) View of side with retrofit plate

Figure 8.14 Specimen R3 at the completion of testing

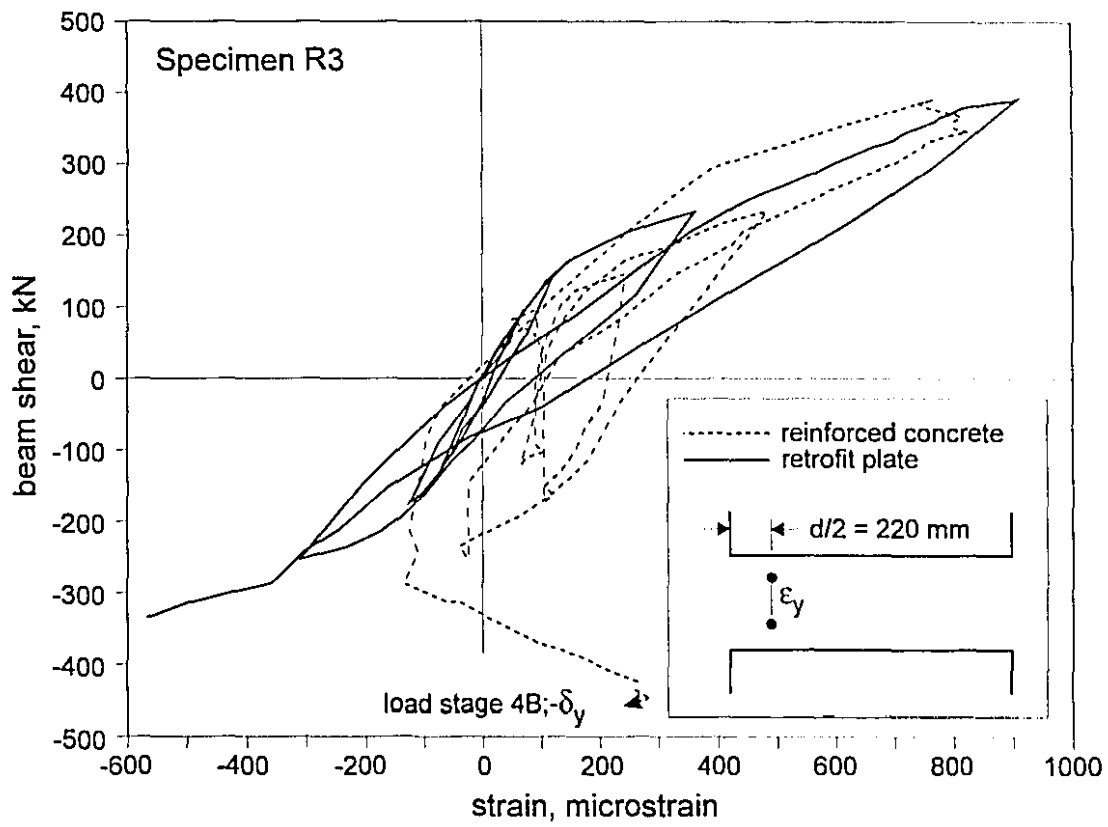


Figure 8.15 Vertical strains in reinforced concrete beam and retrofit plate of Specimen R3

Chapter 9

Response Comparisons of Retrofitted Reinforced Concrete Coupling Beams

9.1 Comparison of Predicted and Experimental Results

Table 9.1 compares the observed and predicted applied shears corresponding to the key behavioural events specimens R0 through R3. Also presented are the values predicted for each behavioural stage. The predicted values were calculated using the computer program RESPONSE (Collins and Mitchell, 1991). The predictions account for the combined effect of moment and shear, using the Modified Compression Field Theory, determined at the critical section, $d/2$ from the face of each wall. Therefore, the moment-to-shear ratio used to predict the capacity of the coupling beams was 0.53 m. Two analyses were performed; one which accounted for the tensile stresses in the concrete (i.e., including V_c), and one which neglected the tensile stresses in the concrete (i.e., $V_c = 0$). Actual material properties and measured dimensions were used in calculating the predicted responses of the specimens.

The RESPONSE model used for the reinforced concrete section is described in Section 9.1.1. The addition of the steel retrofit plate was accounted for by the method described in Section 9.1.2.

	Specimen R0		Specimen R1		Specimen R2		Specimen R3	
(1) Retrofit details	no retrofit		plate epoxied to beam		plate epoxied and bolted to beam		plate epoxied and bolted to beam and walls	
	predicted	observed	predicted	observed	predicted	observed	predicted	observed
(2) First flexural cracking	59 kN	61 kN	60 kN	75 kN	64 kN	≈75 kN	64 kN	81 kN
(3) First shear cracking	124 kN	126 kN	127 kN	128 kN	135 kN	160 kN	135 kN	146 kN
(4) General yield of beam	253 kN	264 kN -296 kN	-	325 kN -349 kN	-	352 kN -406 kN	-	392 kN -459 kN
(5) Predicted ultimate capacity of beam with $V_c = 0$	289 kN	-302 kN at $-1.5\delta_y$	-	-349 kN at $-\delta_y$	372 kN	-422 kN at $-1.5\delta_y$	434 kN	-476 kN at $-1.5\delta_y$
(6) Predicted ultimate capacity of beam including V_c	302 kN		-		430 kN		489 kN	
(7) Peak vertical shear strain in retrofit plate	-	-	-	302 $\mu\epsilon$ at $-\delta_y$ 610 $\mu\epsilon$ at $2.5\delta_y$	-	520 $\mu\epsilon$ at $-1.5\delta_y$	-	998 $\mu\epsilon$ at $-1.5\delta_y$
(8) Deflection at 80% of ultimate capacity	-	23.4 mm at $2\delta_y$	-	29.6 mm at $2\delta_y$	-	37.1 mm at $2.5\delta_y$	-	39.5 mm at $3\delta_y$
(9) Percentage of predicted flexural capacity of Specimen R0	-	86%	-	99%	-	121%	-	136%

Table 9.1 Response of retrofitted reinforced concrete coupling beam specimens

The observed values for both flexural and shear cracking loads were slightly higher than those predicted. The cracking load predictions are based on gross section properties and do not account for the presence of reinforcing steel or, more importantly, the retrofit steel. The externally applied retrofit plate can be expected to increase pre-cracking stiffness somewhat, and to possibly increase the cracking loads. Initial flexural cracking of the retrofitted specimens (R1 - R3) was observed to begin at the front, unretrofitted, face of the beam rather than on the soffit as in Specimen R0.

As can be seen from Table 9.1, the two predictions, with and without V_c , bracket the observed reversed cyclic loading capacities of the specimens. The predictions where V_c is assumed to be equal to zero give conservative strength predictions which are close to the observed shear capacities. As expected, the reversed cyclic loading tends to progressively reduce the tensile stresses with cycling.

9.1.1 RESPONSE Model for Specimen R0

The computer program RESPONSE (Collins and Mitchell, 1991) uses an iterative analysis procedure linking a plane sections analysis for flexure and axial load and the Modified Compression Field Theory (Collins and Mitchell, 1991) for shear.

The reinforced concrete was discretised into ten 50 mm layers and the steel was arranged in two layers at the top and bottom of the section. The RESPONSE model used for the analysis of Specimen R0 is shown in Fig 9.1(a).

The response of the coupling beam was determined with a moment-to-shear ratio of 0.53, corresponding to the applied forces at the critical section, $d/2$ from the face of each wall. Axial loads were neglected since there was minimal longitudinal restraint during testing. As can be seen from Table 9.1 the predicted response was 96% of the observed values.

9.1.2 RESPONSE Model for Retrofitted Specimen R3

In order to predict the response of the retrofitted specimens, the model used to predict the response of Specimen R0 was modified to account for the presence of the retrofit plate. No prediction was made for Specimen R1 since the retrofit plate was only epoxied to the concrete. Although this epoxied plate increases the shear capacity under monotonic loads, it becomes less effective after several reversed loading cycles, and is not a practical retrofit for seismic loading.

The additional shear capacity of the plate was accounted for by increasing the area of stirrups provided in the RESPONSE model. The increased area of stirrups was determined by assuming an effective stirrup width provided within the plate. AISC guidelines for pin

connections allow an area of plate equal to four times the plate thickness on each side of a pin hole to be utilised to carry tension between pin connections (see Fig. 9.1(b)). The equivalent stirrup is therefore a strip of plate eight plate thicknesses wide centred at each vertical pair of anchor bolts. Because RESPONSE only allows one type of stirrup to be specified, the equivalent plate stirrups were scaled to the existing stirrup spacing and material properties. Equation 7.1 was used to scale the retrofit plate "stirrups" to match the existing stirrups in the concrete and determine the equivalent stirrup area provided. The provided area of equivalent stirrups, spaced at 225 mm, used in RESPONSE was 351 mm² and 346 mm² for Specimens R2 and R3, respectively. These values include the existing 200 mm² stirrups at 225 mm spacing in the unretrofitted beam.

The plate also increases the flexural capacity of the coupling beam. The increase in flexural capacity results from the development of the plate at the section being considered. Longitudinally, the plate is developed by the anchor bolts on either side of the critical section. Therefore, the largest tension that can be developed at any section is equal to the shear capacity of the bolts on either side of the section being considered. Therefore, for Specimen R3, the tension that can be developed in the plate is equal to the shear capacity of the three bolts developing the plate at the critical section (see Fig. 9.1(c)). Similarly, Specimen R2, not having an extension of the plate onto the wall, is developed by only a single bolt at the critical section for shear. The shear capacity of the bolts is converted to an equivalent area of longitudinal steel that is located at the level of the rows of anchor bolts (see Fig. 9.1(d)). The area of longitudinal steel provided, $A_{s,eq}$, is determined as:

$$A_{s,eq} = \frac{nV_b}{F_y} \leq n8t_p^2 \quad (9.1)$$

where n = number of bolts developing plate at section being considered, and,
 V_b = shear capacity of an anchor bolt.

Clearly, in these calculations, the tensile capacity of half of the depth of the plate cannot be exceeded.

The RESPONSE predictions assume full strain compatibility between the plate and concrete beam. This condition was respected up to general yield, as discussed in Chapter 8. The RESPONSE model used to determine the yield capacity of the retrofitted specimens is shown in Fig. 9.1(d).

9.2 Hysteretic Responses

The hysteretic responses of Specimens R0 through R3 are presented in Fig. 9.2. The nature of the hysteretic response of each specimen is similar, typical of reinforced concrete members

responding in a shear mode of behaviour. Similar hysteretic "pinching", capacity and stiffness decay are evident in each specimen. The hysteretic responses shown in Fig. 9.2 are plotted to the same scale. The increases in load carrying and displacement capacities are evident with each improved retrofit measure.

Specimen R0 was capable of only achieving 86% of its nominal flexural capacity, corresponding to an applied shear of 350 kN. Each of the retrofit specimens was capable of achieving the nominal flexural capacity of the unretrofitted specimen. Specimen R1 only barely attained an applied shear of 350 kN, and was unable to sustain the load. Specimens R2 and R3 were able to sustain an applied shear of 350 kN through displacements of 30 mm and 33 mm, respectively, corresponding to ductility levels of $2\delta_y$ and $2.5\delta_y$.

Figure 9.3 shows the peak-to-peak hysteretic stiffness plotted against the relative displacement for Specimens R0 through R3. There is an increase in stiffness brought about by the initial retrofit and each successive refinement to the retrofit procedure. The four specimens exhibit similar rates of stiffness decay throughout their load histories. The stiffness of Specimen R3 begins to decay more rapidly, approaching the response of Specimen R2, after the retrofit plate buckled (see Section 8.4).

9.3 Energy Absorption

Figure 9.4(a) shows the cumulative hysteretic energy absorption for Specimens R0 through R3. A steady increase in energy absorption with successive retrofit measures is apparent. Figure 9.4(b) shows the cumulative hysteretic energy absorption normalised by the cumulative energy absorption at general yielding of the coupling beam. It is clear that retrofitted Specimens R1 and R2 showed little increase in energy absorption ability over the unretrofitted Specimen R0. The final retrofit measures used for Specimen R3 show the most significant increase in energy absorption ability.

At a ductility level of $4\delta_y$, Specimens R0 through R2 were capable of absorbing about 10 times their energy absorbed at yield. Specimen R3 was able to absorb about 15 times its absorbed energy at yield.

9.4 Response of Retrofit Plates

As was discussed in Chapter 8, strain compatibility between the retrofit plates and reinforced concrete coupling beams was observed up to general yielding. Beyond yield, delamination of the cover concrete began to effect the compatibility between the elements.

The maximum shear strains observed in the retrofit plates corresponded to the maximum applied shears (with the exception of one of the strain rosettes on Specimen R1, as discussed

in Section 8.2.1). The post-peak strains observed in the retrofit plates of Specimens R2 and R3 had similar decay patterns as the applied shear. This would indicate that the presence of anchor bolts allowed continued continuity across the delaminated concrete cover as desired. Post-yield strains in the plate of Specimen R1 appeared to be dependent on conditions in the immediate vicinity of the strain rosettes. Post-yield continuity was not in evidence in Specimen R1.

Figure 9.5 shows the principal shear strains, determined from the rosettes, in the retrofit plates of Specimens R1 through R3. It is apparent that each of the retrofit plates remained elastic throughout testing. The controlled, elastic response is evident in the responses of Specimens R2 and R3. Specimen R1 exhibits some hysteretic behaviour although the strains are very low, not exceeding 350 microstrain.

9.5 Assessment of Retrofit Performance

Each of the retrofit procedures investigated exhibited an improvement in response over that of the unretrofitted Specimen R0. Table 9.2 presents the ratio of each of the retrofitted specimens' responses to those of Specimen R0.

	Specimen R1	Specimen R2	Specimen R3
applied shear at flexural cracking	1.21	1.13	1.22
applied shear at shear cracking	0.99	1.17	1.06
applied shear at general yield	1.23	1.33	1.48
positive	1.18	1.37	1.55
negative			
displacement at general yield	1.26	1.26	1.06
positive	1.45	1.35	1.17
negative			
applied shear at ultimate capacity	1.16	1.40	1.58
displacement at ultimate capacity	0.96	1.33	1.19
deflection at 80% of ultimate capacity	1.26	1.59	1.69
initial peak-to-peak stiffness (load stage 1)	1.22	1.69	1.39
yield peak-to-peak stiffness (load stage 4)	0.88	1.04	1.36

Table 9.2 Ratio of response parameters of retrofitted specimens to those of Specimen R0

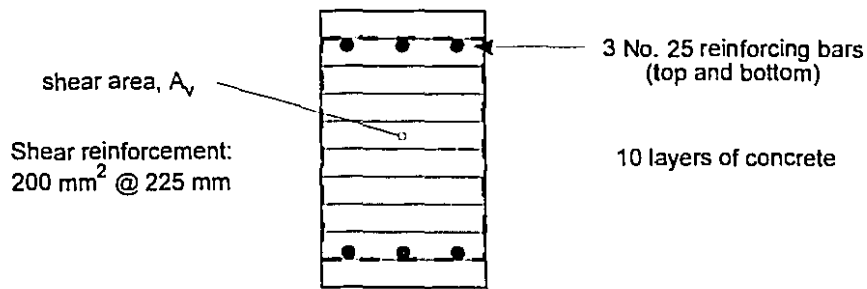
Improvement of response over Specimen R0 is evident in every response parameter for Specimens R2 and R3. Shear and flexural cracking loads were increased, primarily due to the presence of the steel plates. Significant improvement in yield capacity and displacement was evident. Stiffness at general yield was significantly increased by the extension of the retrofit

plates onto the walls, as may be expected. The improved stiffness of Specimen R3 was not detrimental to the ductility achievable.

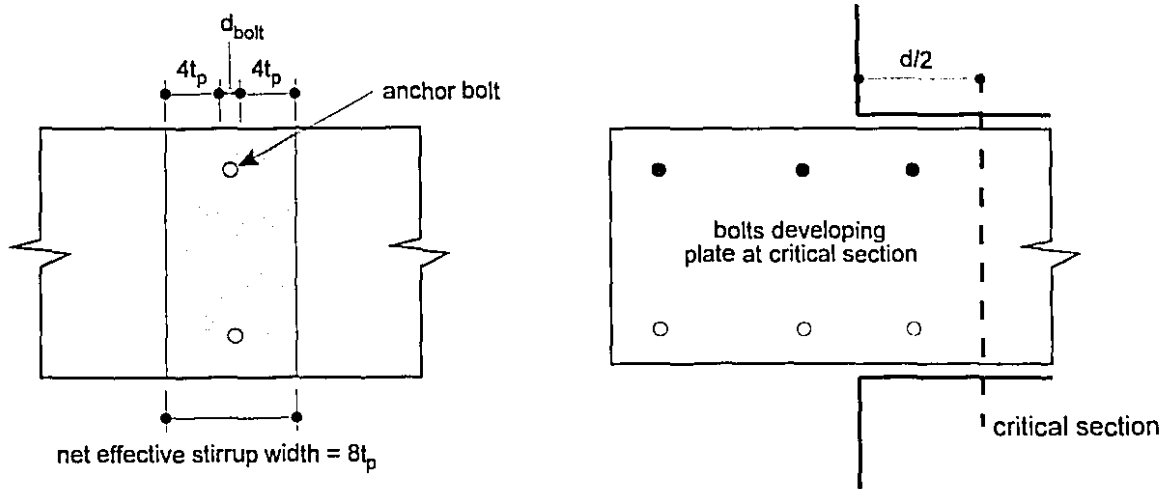
The improvement in ultimate capacities and displacements is similar to the improvement in yield capacities. Significant improvement in the ability to sustain post-peak capacity was also exhibited with successive retrofit measures.

Figure 9.6 shows the hysteretic response envelopes for Specimens R0 through R3. With each successive retrofit, increases in stiffness, yield and ultimate applied shears, post-peak load sustainability, ductility and energy absorption are evident.

An assessment of the retrofit procedures investigated reveals that the retrofit of Specimen R3 was the most efficient and resulted in the most significant improvements in response. This is most evident in the normalised cumulative energy absorption shown in Fig 9.4(b), where the extension of the retrofit plate onto the walls results in a 37% increase in energy absorption ability.

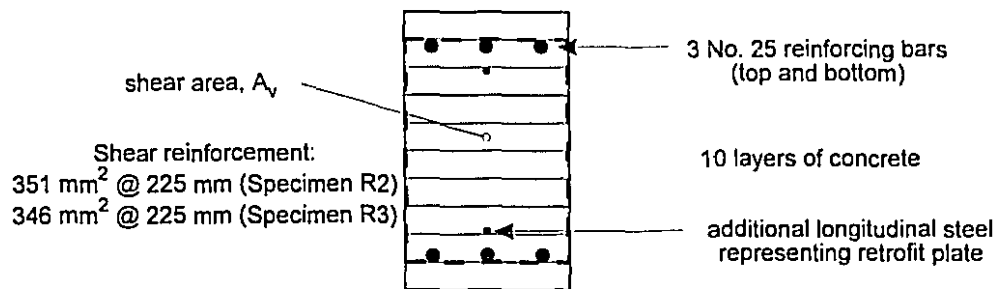


(a) RESPONSE model of Specimen R0



(b) additional shear contribution of retrofit plate

(c) additional flexural contribution of retrofit plate



(d) RESPONSE model of retrofitted specimens

Figure 9.1 RESPONSE models for predicting behaviour of Specimens R0 through R3

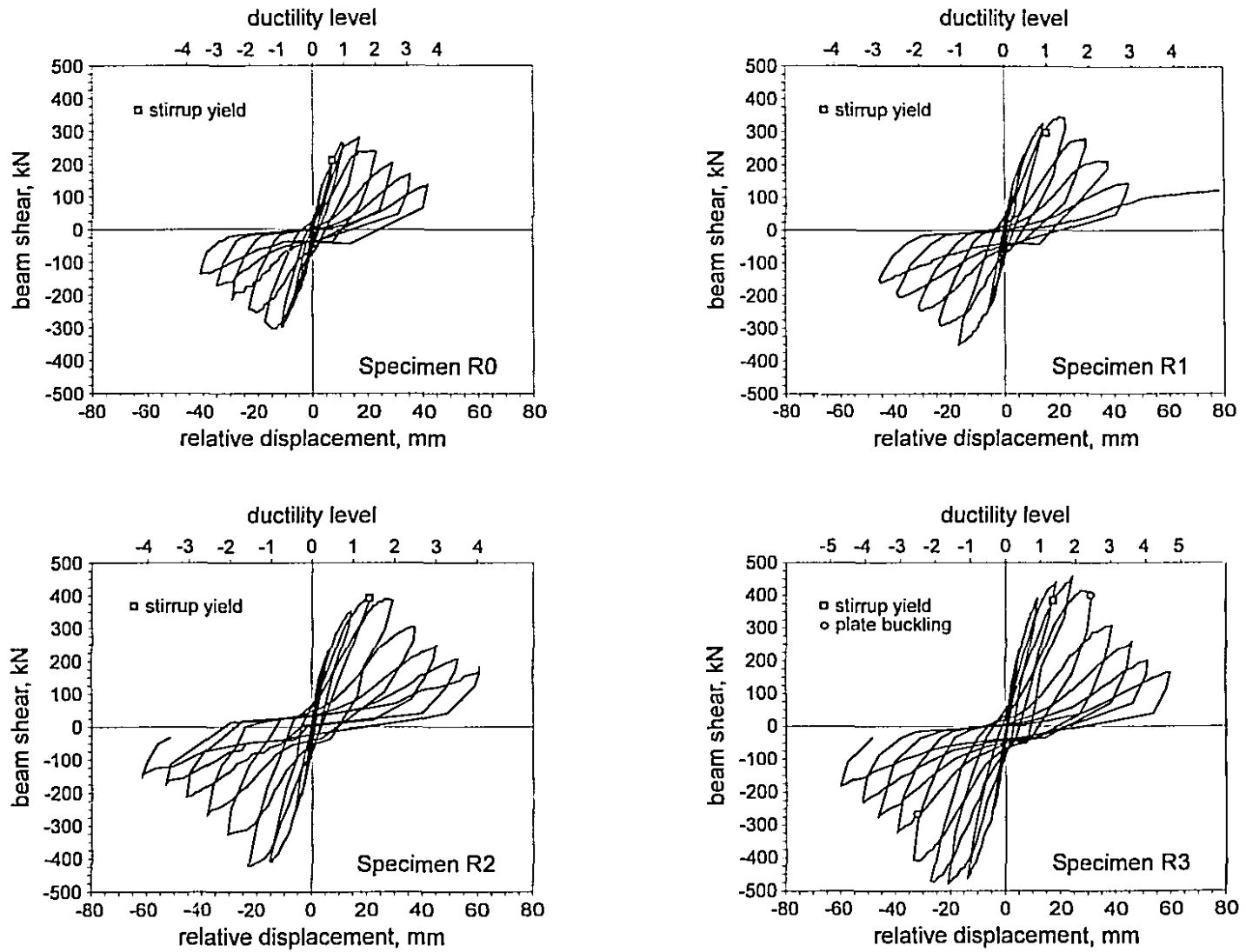


Figure 9.2 Hysteretic responses of Specimens R0 through R3

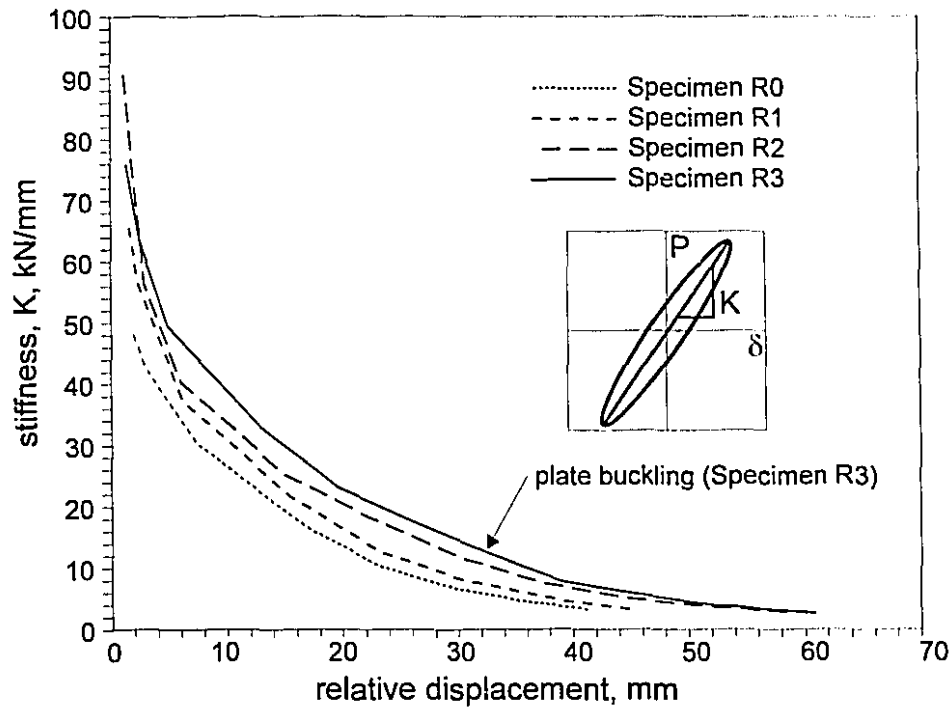


Figure 9.3 Peak-to-peak stiffnesses of Specimens R0 through R3

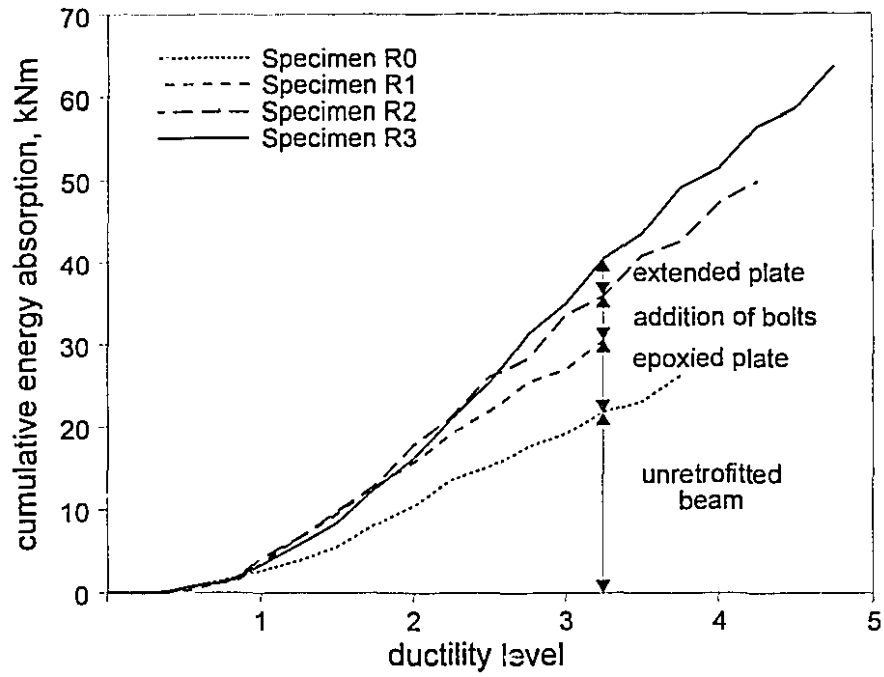


Figure 9.4(a) Cumulative hysteretic energy absorption of Specimens R0 through R3

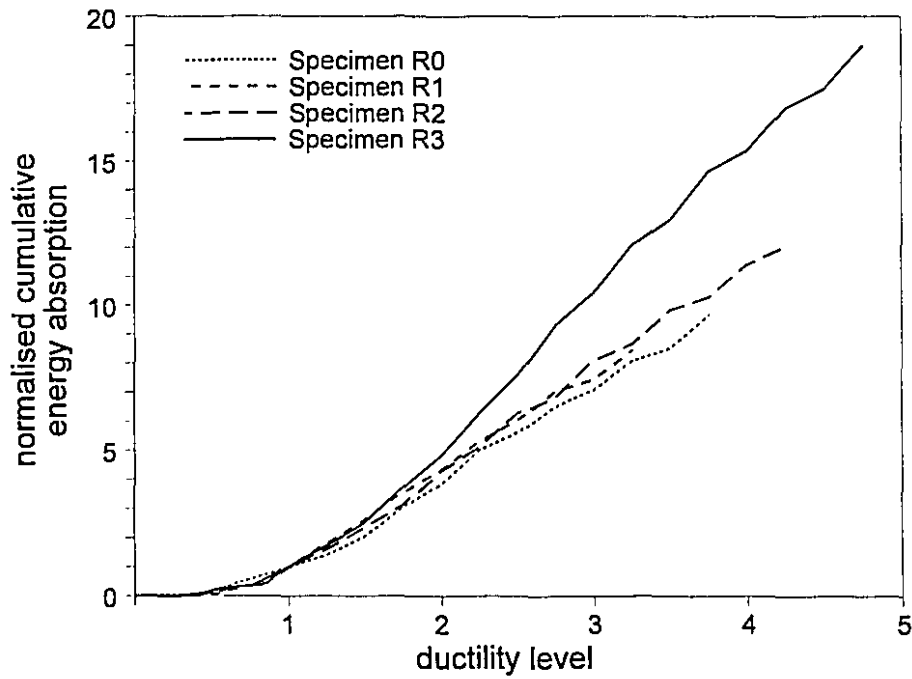


Figure 9.4(b) Normalised cumulative energy absorption of Specimens R0 through R3

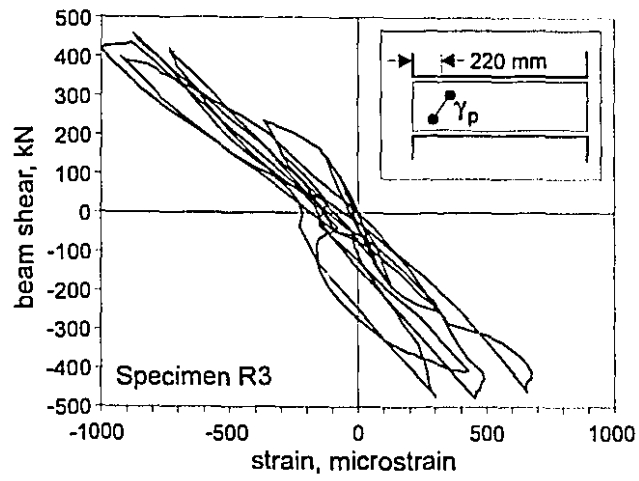
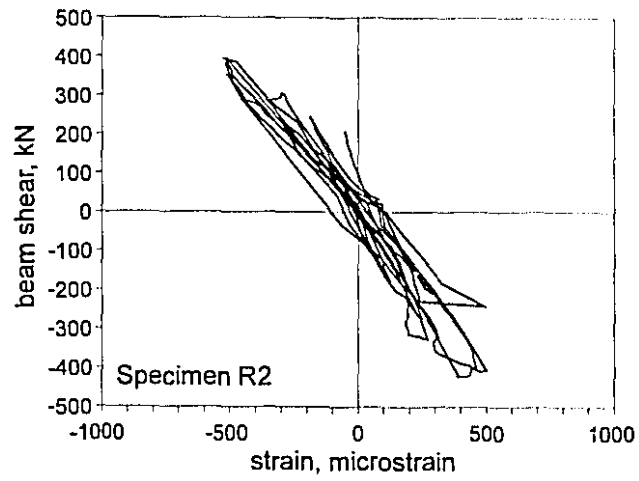
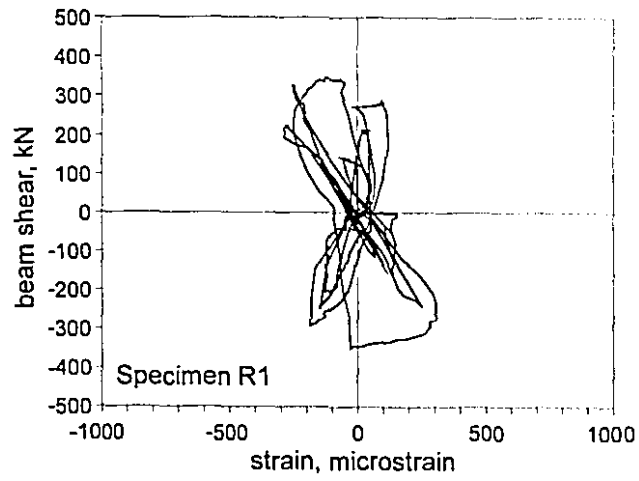


Figure 9.5 Principal shear strains in retrofit plates of Specimens R1 through R3

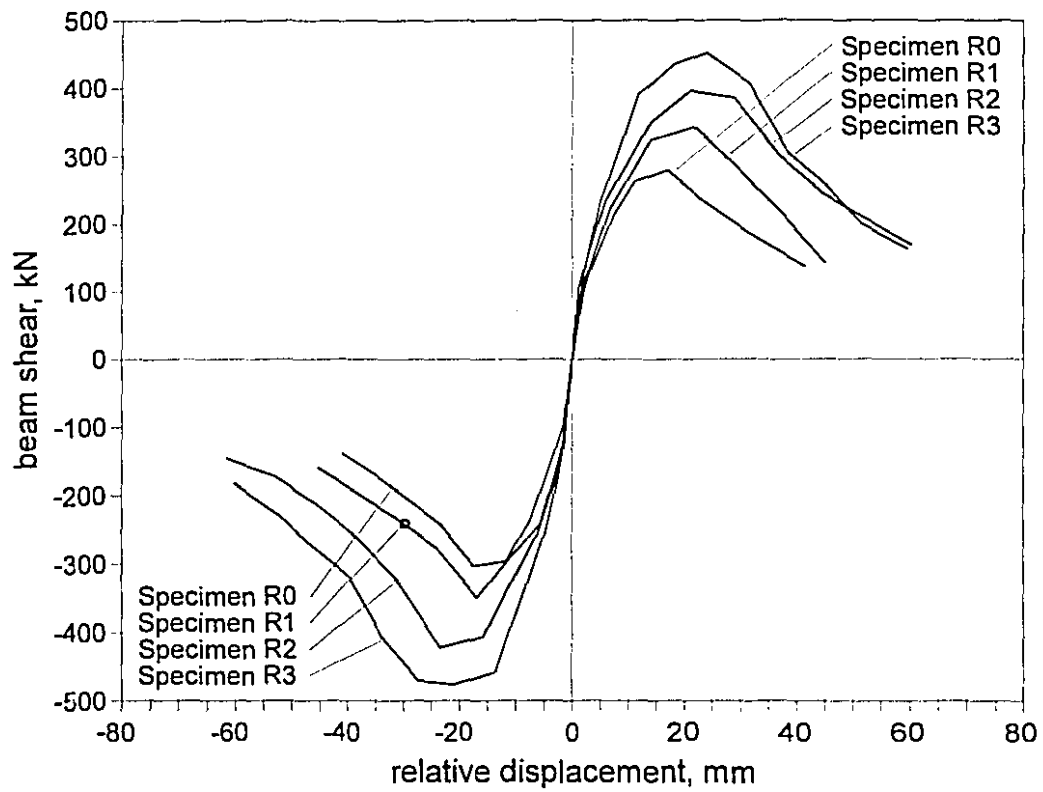


Figure 9.6 Hysteretic envelopes of Specimens R0 through R3

Chapter 10

Non-Linear Dynamic Analyses of Unretrofitted and Retrofitted Prototype Structures

In order to determine the appropriateness of using steel plates to retrofit shear deficient coupling beams, a shear deficient prototype structure was designed. The same prototype was then retrofit using the procedure developed in Section 7.2. Both the unretrofitted and retrofitted prototypes were subject to identical non-linear dynamic analyses using DRAIN-2DX (1992). The development of the prototype and the results of the analysis are presented in this Chapter.

10.1 Shear Deficient Prototype Structure

Prototype PC, developed in Chapter 5 was chosen as the basis for the shear deficient prototype structure. In order to render the coupling beams deficient in shear, the spacing of the transverse reinforcement, s , was increased from 90 mm in prototype PC (see Fig. 5.2(a)) to 300 mm for the unretrofitted prototype (see Fig. 10.1(a)). The 300 mm hoop spacing corresponds to a spacing of $d/2$. Table 10.1 gives an indication of the transverse reinforcement details that may be expected in similar coupling beams designed to older Canadian concrete design standards. The detail given in the right column assumes the same design shears, material properties and geometry (i.e.: double legged No. 10 hoops or stirrups) as was used in prototype PC. That is to say, changes in NBCC prescribed loading levels, from one year to the next, have not been accounted for. Furthermore, the detail given in the right column corresponds to that required at the critical section for shear (i.e.: $d/2$ from the face of the wall). In the older standards (Table 10.1, bottom row), the spacing may be increased toward the midspan of the coupling beam. The older standards, not having specific guidelines for seismic design, allow both a concrete and steel contribution to be considered in design for shear. The seismic design provisions of newer standards, do not permit a concrete contribution to be considered (e.g.: CSA A23.3-94 Clause 21.7.3). It should also be noted that it is only in the recent standards (Table 10.1, top row) that closed hoops, rather than stirrups, are required. In addition, when

metric bar sizes were introduced in 1977, the smallest bar size was a No. 10 ($A_s = 100 \text{ mm}^2$) while previous practice utilised smaller #3 bars ($A_s = 71 \text{ mm}^2$).

The smaller spacing of hoops in the more recent standards serve to improve the shear capacity, improve the confinement of the concrete and prevent premature buckling of the longitudinal bars. The retrofit procedure developed in this research programme serves to increase the shear capacity, however the retrofit does not enhance the confinement of the concrete and therefore the post-yield response continues to exhibit hysteretic pinching. Furthermore, the plate does not provide additional restraint for the buckling of the longitudinal bars. The buckling of longitudinal bars probably contributes to the observed "bulging" of the centre portion of the coupling beam observed in later stages of loading.

Standard	Year	Maximum Spacing Requirements ¹	Required Detail at Critical Section ²
CSA A23.3-94 and CSA A23.3-M84 Clause 21.3	1994 1984	$d/4 = 150 \text{ mm}$ $8d_{bl} = 240 \text{ mm}$ $24d_{bh} = 240 \text{ mm}$ 300 mm	$s \leq \frac{A_v \phi_s f_y d_v}{V_r \tan \theta}$ seismic hoops at 90 mm
CSA A23.3-M77 and CSA A23.3-1973 Clause 19.6	1977 1973	$d/2 = 300 \text{ mm}$ $16d_{bl} = 480 \text{ mm}$ 300 mm	$s \leq \frac{A_v d}{0.15 A_s}$ stirrups at 285 mm
CSA A23.3-1970 Clause 6.3 NBCC 1965 & 1953 Section 4	1970 1965 1953	$d/2 = 300 \text{ mm}$	$s \leq \frac{A_v \phi f_y d}{V_s}$ stirrups at 275 mm

Table 10.1 Transverse reinforcement spacing requirements of older Canadian concrete design standards

¹ where d = distance from the extreme compression fibre to the centroid of the tension steel;
 d_{bl} = diameter of longitudinal reinforcement; and
 d_{bh} = diameter of transverse reinforcement.

² where A_v = area of transverse reinforcement;
 A_s = area of longitudinal reinforcement;
 d_v = effective shear depth of beam, taken as $0.9d$;
 V_f = factored shear force;
 V_s = factored shear force to be provided by transverse steel;
 f_y = specified yield stress of reinforcing steel;
 ϕ_s = material resistance factor for reinforcing bars = 0.85; and
 ϕ = capacity reduction factor = 0.85 for shear.

Apart from the change in hoop spacing, the details of the unretrofitted specimen remain identical to those of prototype PC. The shear capacity of the unretrofitted prototype was determined using the computer program RESPONSE (see Section 9.1.1) to be 505 kN at the critical section. For comparison, the shear capacity of prototype PC at the critical section is 630 kN and the shear corresponding to the nominal flexural capacity is 615 kN. The shear capacity of the unretrofitted prototype corresponds to about 82% of the nominal design flexural capacity of the coupling beam.

10.2 Retrofitted Prototype Structure

The retrofit procedure described in Section 7.2 was used to determine the required retrofit for the shear deficient coupling beams described in Section 10.1. The required area of transverse reinforcement, $A_{v,req}$, assuming a spacing, s , of 300 mm was determined to be 1065 mm². The equivalent stirrup area, $A_{v,eq}$, to be provided by the retrofit plate is therefore 1065 - 400 = 665 mm², assuming that four legs of No. 10 hoops are present in the retrofit beam (see Fig. 10.1(a)). Using Equation 7.1 the required retrofit plate thickness can be determined as:

$$t_p^2 = \frac{A_{v,eq}}{8} \frac{s_b}{s} \frac{d_v}{h_b} \frac{f_y}{F_y} \quad (10.1)$$

for this prototype, the values assumed in Equation 10.1 are as follows:

- $A_{v,eq} = 665 \text{ mm}^2$;
- $s_b =$ spacing of bolts = 100 mm;
- $s =$ spacing of existing hoops = 300 mm;
- $d_v =$ shear depth of coupling beam = 539 mm;
- $h_b =$ vertical distance between bolts = 360 mm;
- $f_y =$ specified yield strength of existing transverse reinforcement = 400 MPa;
- and
- $F_y =$ specified yield strength of retrofit plate = 300 MPa

The required retrofit plate thickness is determined to be 7.5 mm. A 9.5 mm (3/8") plate was selected. The 500 mm deep plate was considered to be attached along the beam and 500 mm onto each wall (see Fig. 10.1(b) and (c)). The required bolt capacity was determined from Equation 7.2 to be 307 kN. *HSL M24/60* mechanical anchors, manufactured by Hilti Canada Limited (see Section 7.4.3), were determined to be adequate for the required capacity. The retrofit details and anchor bolt arrangement are shown in Fig. 10.1.

The shear capacity of the retrofitted coupling beam was determined using RESPONSE. The addition of the plate was accounted for in the manner described in Section 9.1.2. The retrofitted shear capacity was determined to exceed the shear corresponding to the

development of the beam's flexural capacity (615 kN). As such the beam was no longer shear deficient and the response of the original prototype PC was recovered.

10.3 Modelling Unretrofitted and Retrofitted Prototypes

Both the unretrofitted and retrofitted prototypes were modelled in the same manner as prototype PC (see Section 5.4.1). It is difficult to accurately model the significant strength and stiffness degradation exhibited in the post peak behaviour of shear critical reinforced concrete members. In lieu of modelling this complex behaviour, it was felt that halting the analysis at the point where the first coupling beam experiences shear failure would illustrate the appropriateness of this form of retrofit.

As had been seen in the analysis of prototype PC (see Section 6.1), a number of coupling beams are predicted to yield virtually simultaneously (see Fig. 6.6(a)). Redistribution of forces, from this yielding, progresses rapidly upwards and downwards in the structure. In terms of the shear deficient unretrofitted prototype, this would suggest that more than one coupling beam would exhibit severe shear distress at the same time resulting in severe distress in a number of adjacent members as well as increasing the demands on the walls. This could lead to significant damage or, in fact, failure. It was therefore felt that halting the analyses when the beams achieve a predetermined shear failure criteria would adequately represent the useful service conditions of the coupled structural system.

As was shown with Specimen R3 (see Section 8.4), the steel plate retrofit has a limit to its improved response, based on separation of the plate from the concrete beam and buckling of the plate. Once this limit has been exceeded, the response decays rapidly as it would in the unretrofitted case.

Both the unretrofitted and retrofitted models, therefore have a limiting criteria beyond which the analysis will be halted. This limiting criteria is imposed on the DRAIN-2DX model as a spring rotation corresponding to the shear deformation beyond which the coupling beam can no longer contribute to the structural system. The rotation limits were applied to the springs at the ends of the coupling beams (see Fig. 5.3(b)). The rotations corresponding to the initial strength decay (ϕ_u , on Fig. 10.2) were determined from RESPONSE to be 0.0076 rad and 0.02 rad for the unretrofitted and retrofitted coupling beams, respectively. For comparison, the limiting value for the unretrofitted Specimen R0 was observed to be about 0.008 rad while that of the retrofitted Specimen R3 was observed to be about 0.018 rad.

The hysteretic response used to model the shear deficient coupling beams in DRAIN-2DX is shown in Fig. 10.2. As was seen in Chapter 7, the capacity predicted by RESPONSE for the coupling beams underestimates the actual capacity of the member, V_n . The predicted

capacity is in the range of $0.9V_n$ (see Table 7.1). In order to more accurately model the energy absorbing ability of the coupling beams, the predicted capacity, $0.9V_u$, was used while the limiting rotation was increased one third to $1.33\phi_u$ (see Fig. 10.2). The resulting shear capacity and limiting rotation for the unretrofitted prototype were 2020 kN and 0.0101 rad. The shear capacity corresponding to yield of the retrofitted prototype was 2353 kN. A limiting rotation of 0.0267 rad was applied to the retrofitted prototype, although at no time in the analyses did any coupling beam rotation exceed 0.02 rad (corresponding to ϕ_u).

10.3.1 Ground Acceleration Records

Both prototypes were subjected to the El Centro, Griffith Park, Loma Prieta and Taft ground acceleration records scaled to 1.5 times the PHV for Vancouver (see Table 5.6).

10.4 Non-linear Dynamic Response of Unretrofitted and Retrofitted Prototypes

The displacement-time histories of both prototypes are shown in Fig. 10.3. Figure 10.4 shows the shear versus relative displacement of the critical coupling beams for each analysis. Table 10.2 summarises the displacement and ductility demands of both the unretrofitted and retrofitted prototype structures. The analyses of the unretrofitted prototype structure were halted when the rotation at the end of a coupling beam exceeded 0.0101 rad. Beyond this point, response of the structure becomes increasingly uncontrolled and unpredictable. As the coupling beams fail in shear, the overturning moment, originally resisted by the coupling action, is redistributed to the walls. The response of the system then begins to approach that of the walls acting as individual, relatively slender, cantilevers. The time into the record at which each analysis was halted is given in Table 10.2. The rotation limit for the retrofitted prototype was not exceeded at any time in the analyses.

acceleration record	time of first yield	time halted	Δ_y (mm)	Δ_{ult} (mm)	δ_y (mm)	δ_{ult} (mm)	μ_{global}	μ_{local}
unretrofitted prototype analyses halted when beam rotation exceeds 0.0101 rad								
El Centro	1.54 s	1.92 s	75.1	209.1	13.03	41.06	2.8	3.2
Griffith Park	6.28 s	14.7 s	74.6	186.2	13.55	40.18	2.5	3.0
Loma Prieta	4.66 s	8.32 s	79.6	163.9	13.99	41.07	2.1	2.9
Taft	3.40 s	3.64 s	79.3	194.9	12.72	38.16	2.5	3.0
retrofitted prototype								
El Centro	1.54 s	20.0 s not halted	75.1	263.3	15.36	55.47	3.5	3.6
Griffith Park	6.32 s		78.3	212.0	16.53	46.18	2.7	2.8
Loma Prieta	4.62 s		79.6	210.2	15.02	40.00	2.6	2.7
Taft	3.36 s		79.3	206.8	16.36	47.66	2.6	2.9

Table 10.2 Summary of global and local ductility demands for unretrofitted and retrofitted prototypes subject to the maximum credible ground motion

The values for Δ_{ult} and δ_{ult} given for the unretrofitted prototype are those observed when the analysis was halted (with the exception of Δ_{ult} for the Loma Prieta record). In all cases these values correspond to global ductility levels between 2.1 and 2.8 and local ductility levels of 2.9 to 3.2. Beyond this point it would be expected that ductility demand would increase significantly in a short period of time. Furthermore, the values given in the top section of Table 10.2, reflect a limiting rotation value increased to reflect energy absorbing ability. Where there a number of displacement excursions approaching this value (eg: Griffith Park record), the energy dissipating ability would decay and a limiting value of ϕ_u (see Section 10.2) would be more appropriate. That is, the values shown on the top of Table 10.2 likely represent the practical limit of the controlled response of this unretrofitted prototype structure.

The ratio of global to local ductility demand for all eight analyses is consistent with the analyses of prototype PC and PS reported in Section 6.1.

The roof displacement-time histories (see Fig. 10.3) for each structure are essentially the same up to the point were the unretrofitted analysis is halted. The retrofit allows the structure to continue to behave in a controlled manner to the end of the analysis. As was the case previously, all analyses exhibited their maximum response within the 20 second time frame considered and the response was beginning to be damped out at the end of the analysis. Based on the predicted limiting rotations, the retrofitted prototype still possessed considerable reserve

capacity. A local deformation, δ_{ult} , exceeding 80 mm (rotation of 0.02 rad), corresponding to a local ductility level, μ_{local} , of about 5, would likely be achievable using this retrofit procedure. The corresponding global ductility demand, μ_{global} , would be slightly less than this.

The predicted hysteretic responses of the coupling beams, shown in Fig. 10.4, clearly illustrate the greater local ductility and energy absorption ability available in the retrofitted structure. At the predicted ductility levels, strength and stiffness decay are not yet a factor in the response of the coupling beams. If the unretrofitted beams were cycled beyond their predicted limiting rotation values, it is likely that significant strength and stiffness decay would be observed and the degree of pinching (see Section 5.4.1) would become greater.

The external energy absorbed by each prototype is shown in Fig. 10.5. The total external energy observed at the end of the analysis time period represents the energy content of the imposed ground motion. In each analysis, the coupling beams began failing before significant amounts of energy could be absorbed. Certainly, the unretrofitted prototypes would continue to absorb energy beyond this point, however they would do so by developing significant hinging at the base of the walls which the structure may not be detailed to attain.

10.5 Evaluation of Retrofit Procedure

It is apparent from the analyses conducted that the procedure for retrofitting shear deficient coupling beams can considerably enhance the overall structural response of the system. The retrofit is specifically designed not to increase the overall design capacity of the coupling beams, but rather to allow this capacity to be attained while the beam exhibits flexural yielding. The significant effect of the retrofit is therefore to allow larger ductility levels to be achieved without significant strength or stiffness decay. However, because the retrofit method does not significantly improve the confinement of the concrete, nor does it significantly restrain the buckling of the longitudinal bars in beams with large hoop spacings, its improvement is limited. The increased strength and energy dissipation does however significantly improve the response of the coupling beam. This retrofit technique provides a simple and economical method for improving the response of shear deficient coupling beams in moderate seismic zones.

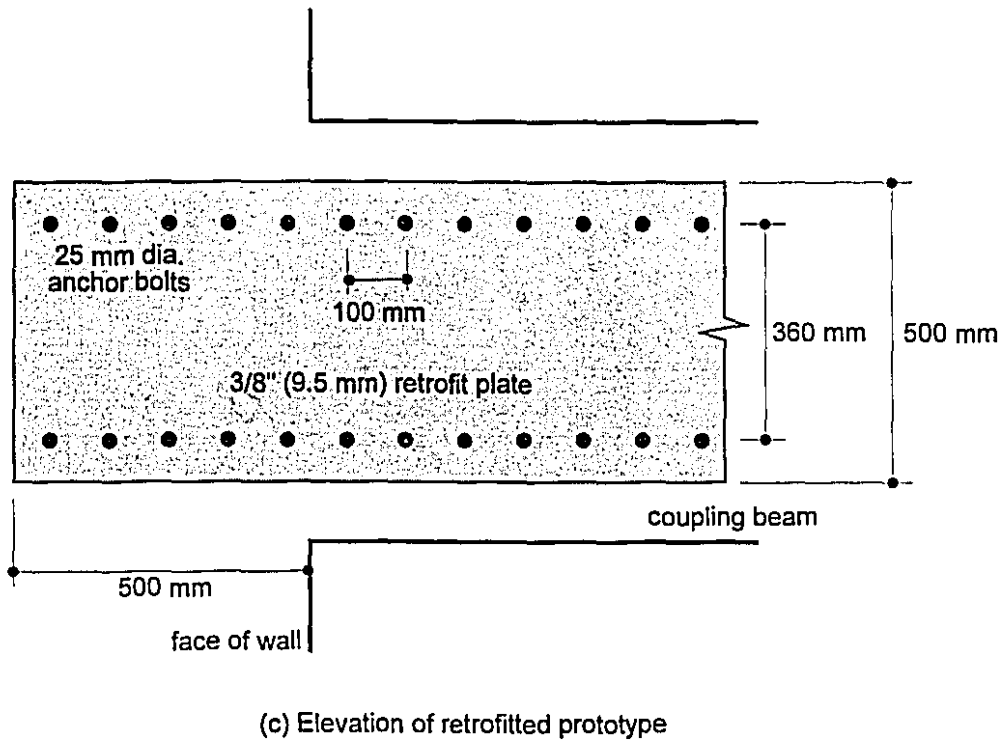
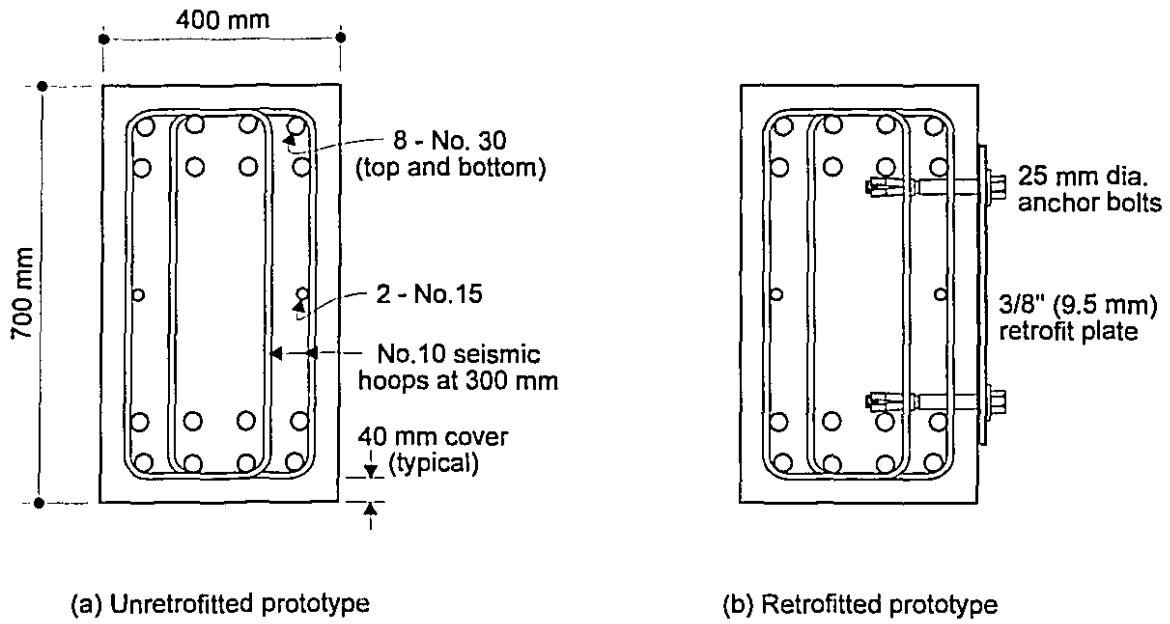
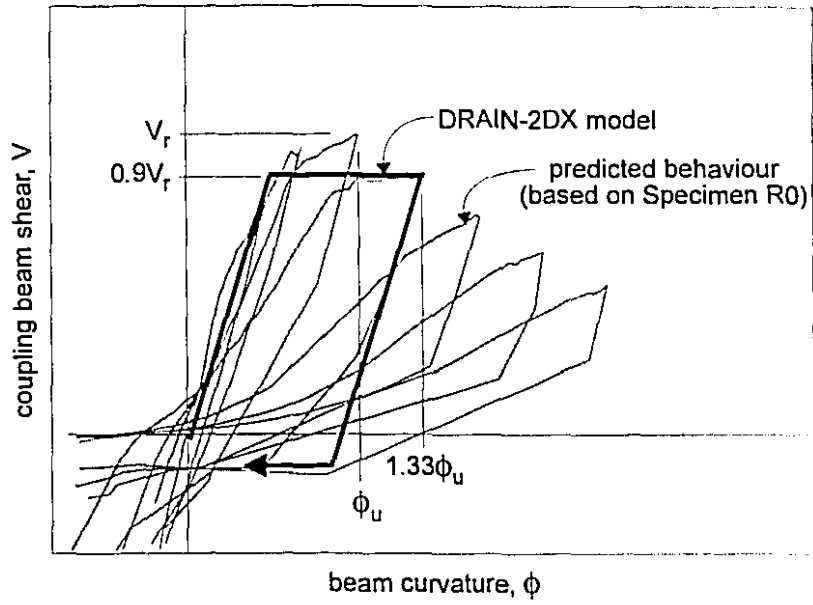
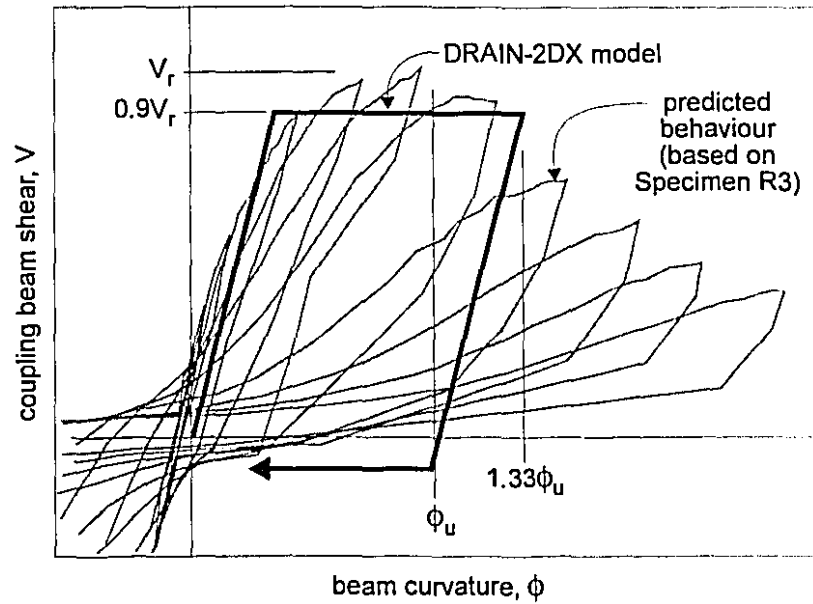


Figure 10.1 Unretrofitted and retrofitted prototype coupling beam details



(a) unretrofitted coupling beam



(b) retrofitted coupling beam

Figure 10.2 Determination of coupling beam response for DRAIN-2DX models of unretrofitted and retrofitted coupling beams

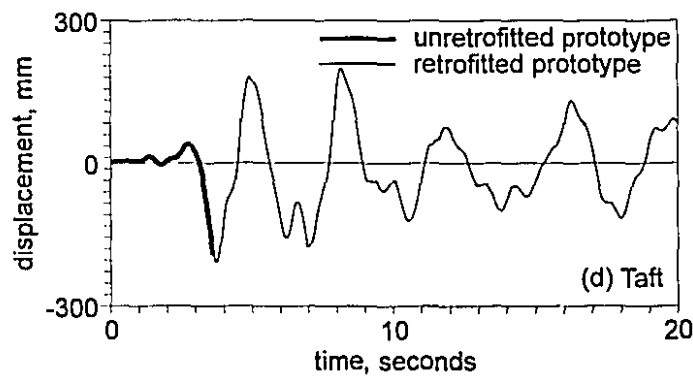
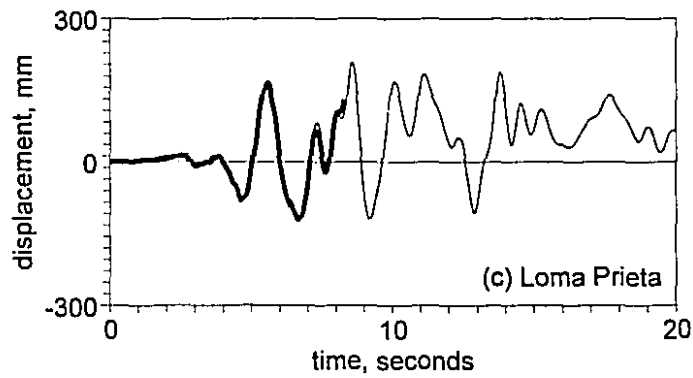
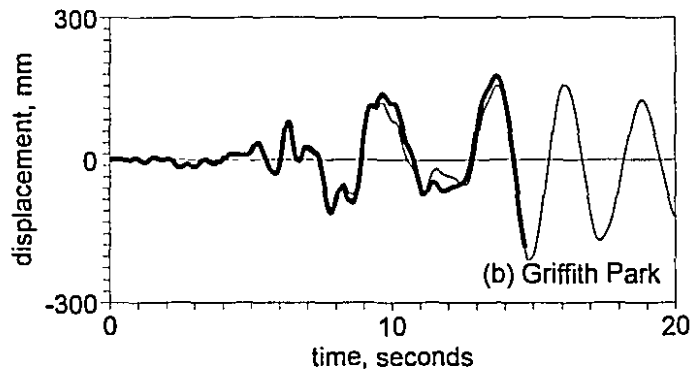
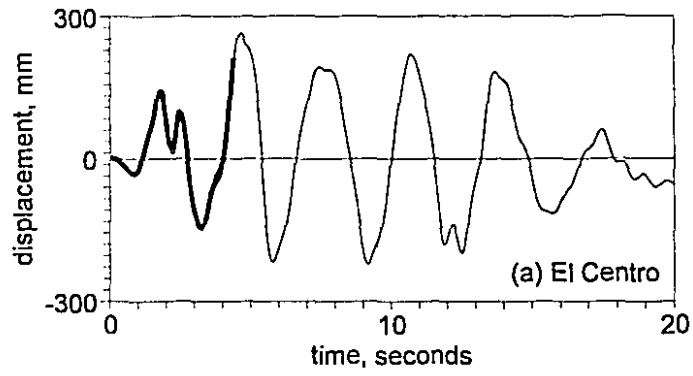


Figure 10.3 Top storey displacement - time history of unretrofitted and retrofitted prototypes

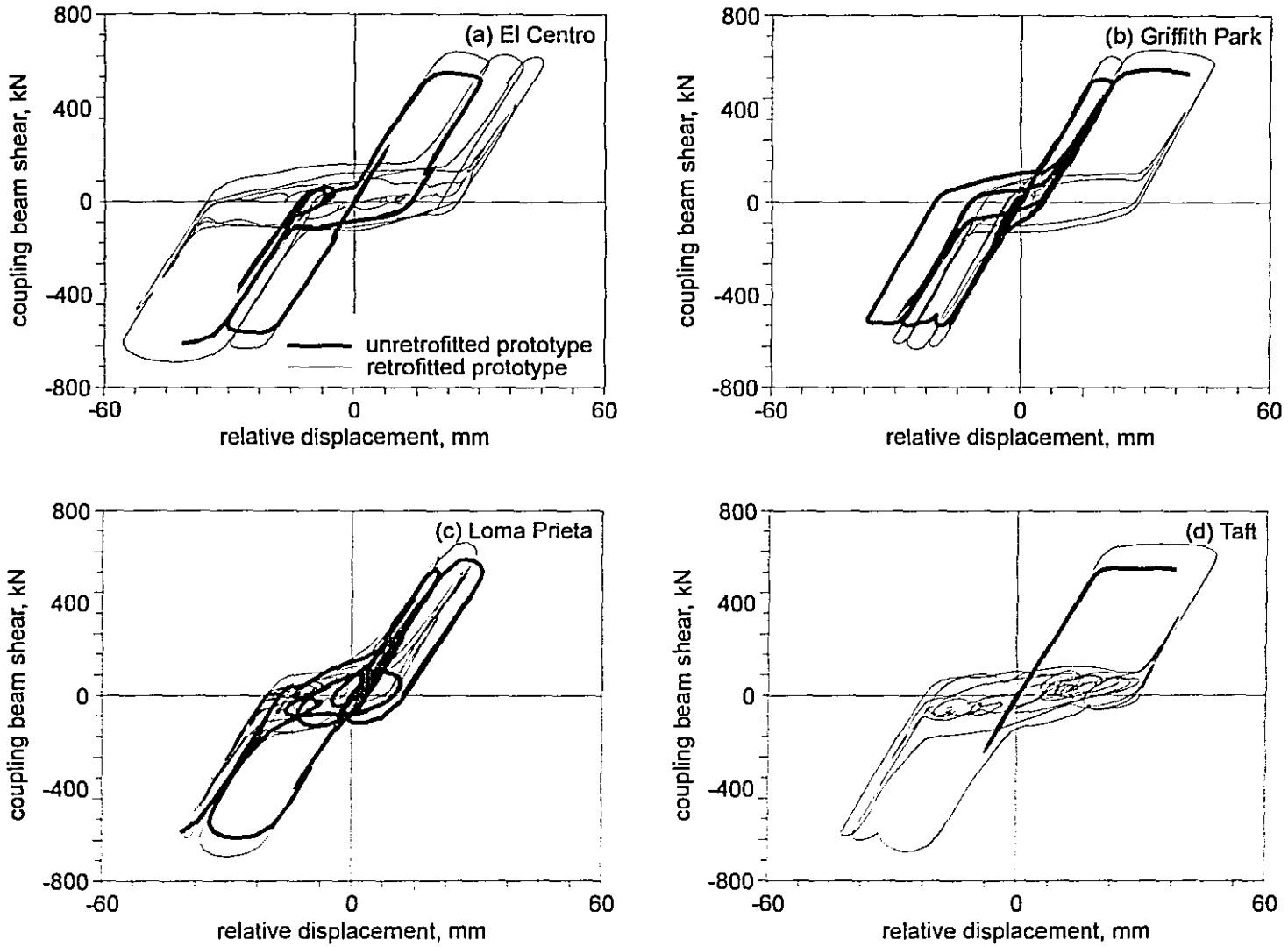


Figure 10.4 Hysteretic behaviour of critical coupling beams of unretrofitted and retrofitted prototypes

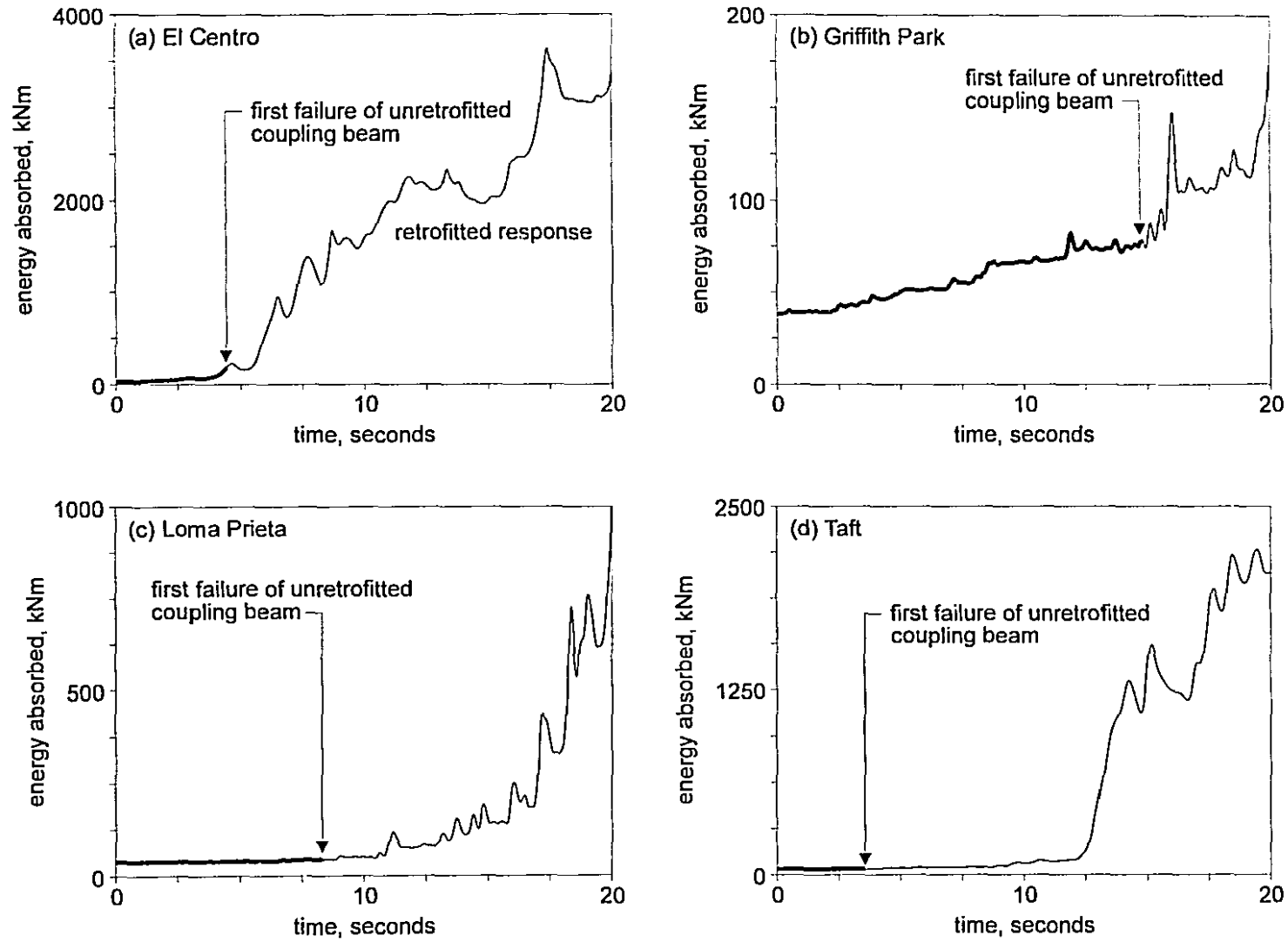


Figure 10.5 External energy absorbed by unretrofitted and retrofitted prototypes

Chapter 11

Design Recommendations and Conclusions

The recommendations and conclusions given below have been developed in the context of the current Canadian structural design standards: 1995 NBCC, CSA A23.3-94 and CAN/CSA S16.1-94.

11.1 Behaviour and Design of Steel Beams Coupling Reinforced Concrete Walls

The use of steel beams to couple reinforced concrete walls has been shown to be a viable alternative to either conventionally or diagonally reinforced concrete coupling beams. Design and detailing requirements for "shear critical" and "flexure critical" steel coupling beams are presented. These requirements ensure that adequate energy absorbing capability and ductility are provided, consistent with the force modification factor recommended for this new form of construction. Since the embedded portion of the coupling beam is designed and detailed to ensure that hinging is confined to the clearspan, special care is required in designing the region of embedment in the walls. In order to provide sufficient over-strength in the embedment:

- i) a thicker web or intermediate stiffeners must be provided over the embedment region in order that the embedded portion of the steel beam remains elastic, and
- ii) the reinforced concrete embedment region must be designed to transmit the required shear and moment from the plastic hinging of the beam in the clearspan. This design must include the effects of cover spalling and additional vertical reinforcement must be provided in the walls to control the crack at the flange-concrete interface.

It is proposed that "flexural critical" steel coupling beams offer a practical alternative to conventionally reinforced concrete coupling beams. Full-scale reversed cyclic loading tests have shown that "flexure critical" steel coupling beams have the following advantages:

- i) "Flexure critical" steel coupling beams offer greater energy absorbing capabilities than conventionally reinforced concrete coupling beams.
- ii) "Flexure critical" steel coupling beams are able to attain ductility levels at least as high as their conventionally reinforced counterparts without exhibiting strength or stiffness decay
- iii) "Flexure critical" steel coupling beams, fabricated from rolled sections can greatly simplify the construction of the coupling beams.

"Shear critical" steel coupling beams are proposed as an alternative to the more complex diagonally reinforced concrete coupling beams. Tests indicated that "shear critical" steel coupling beams have the following advantages:

- i) "Shear critical" steel coupling beams exhibit excellent ductility and energy absorption characteristics, exceeding that of diagonally reinforced concrete coupling beams.
- ii) Although often requiring stiffened built-up sections, "shear critical" steel coupling beams offer a simpler alternative to diagonally reinforced concrete coupling beams, eliminating a considerable amount of on-site labour.

Non-linear dynamic analyses, for different acceleration-time histories, were carried out for partially and fully coupled prototype structures located in Vancouver. These analyses allowed comparisons to be made between the behaviour of structures with steel coupling beams ("shear critical" or "flexure critical") and structures with reinforced concrete coupling beams (conventionally or diagonally reinforced). These analyses indicated that steel coupling beams offer the following advantages:

- i) Due to their greater energy absorption ability, steel coupling beams reduce the energy absorption and ductility demand on the walls, and hence reduce lateral displacements of the structure.
- ii) The larger ductilities, without significant strength or stiffness decay, exhibited by steel coupling beams offer significantly improved response. Hence, they would be better able to withstand seismic events of long duration or events with numerous peaks of strong ground motion.

Design and detailing criteria are proposed for the selection of steel coupling beams and are compared with those for reinforced concrete coupling beams in Table 11.1 It is important to note that reinforced concrete coupling beams have limiting shear stress levels which may result in larger sections, particularly in shorter span coupling beams. It is likely that steel coupling beams will be more compact than their reinforced concrete counterparts. The decision to use either a "shear critical" or "flexure critical" coupling beam will depend on the degree of coupling as well as the span-to-depth ratio. In general, for span-to-depth ratios less than about 2, "shear critical" beams will be more practical.

Span-to-depth ratio (ℓ_u/d)	Reinforced Concrete Coupling Beams		Steel Coupling Beams
	Concrete shear stress level (v_f)	Reinforced concrete coupling beam shear design criteria	Steel coupling beam capacity design criteria
$\ell_u/d > 4$	$v_f < 0.1(\ell_u/d)\sqrt{f'_c}$	conventional reinforcement $V_r = \phi_s A_v f_y d/s$	"flexure-critical" $V_r > 1.27 \times 2M_r/\ell$
$\ell_u/d > 4$	$v_f > 0.1(\ell_u/d)\sqrt{f'_c}$	diagonal reinforcement $V_r = 2\phi_s A_s f_y \sin\alpha$	"flexure-critical" $V_r > 1.27 \times 2M_r/\ell$
$\ell_u/d < 4$	$v_f < \sqrt{f'_c}$	diagonal reinforcement $V_r = 2\phi_s A_s f_y \sin\alpha$	"shear-critical" or "flexure-critical"
$\ell_u/d < -2$	$v_f < \sqrt{f'_c}$	diagonal reinforcement $V_r = 2\phi_s A_s f_y \sin\alpha$	"shear-critical" $M_r > 1.27V_r \ell/2$
$\ell_u/d < -2$	$v_f > \sqrt{f'_c}$	not permitted	"shear-critical" $M_r > 1.27V_r \ell/2$

Table 11.1 Design and detailing criteria for reinforced concrete and steel coupling beams

11.2 Retrofitting Reinforced Concrete Coupling Beams with Steel Plates

In the evaluation of existing structures, coupling beams designed using older standards are often found to have insufficient shear capacity and hence there is a need to develop simple retrofit techniques. Full-scale reversed cyclic loading tests were carried out on shear deficient reinforced concrete coupling beams retrofitted with steel plates. The steel plates were attached, using structural epoxy and anchor bolts, to one side of the web of shear deficient beams. Different connection details were examined and the responses of the coupling beams, before and after retrofit were compared. Design and detailing requirements were developed for the selection of the steel plate and its connection to the concrete. It is recommended that the steel plate be attached over the clearspan and extended onto each wall when possible. Where this is not possible (e.g., the wall is thicker than the coupling beam), attaching the plate over only the clear span still provides significant response improvement. The intent of this retrofit procedure is to improve the shear response of the member such that its nominal flexural capacity may be achieved. The full-scale experiments indicated that the steel plate retrofit has the following benefits:

- i) The addition of the retrofit plate makes it possible to significantly improve the strength, stiffness, displacement capacity and energy absorption of shear deficient reinforced concrete coupling beams.
- ii) The thin steel plate, attached to one side of the coupling beam, is a practical means of retrofitting deficient coupling beams with minimum disruption to architectural finishes and to the occupants of the building. For example, the retrofit may be applied to the inside of a shear wall core.

Non-linear dynamic analyses were carried out on a structure having shear deficient coupling beams, both before and after retrofitting the coupling beams. These analyses showed that the larger shear capacity, together with the greater energy absorption and slightly improved ductility, resulted in significantly improved responses of the overall structure. Although the response of the beams has been improved with this simple retrofit technique, significant plastic hinging cannot develop due to the lack of confinement and the inability to control longitudinal bar buckling. Therefore, this retrofit method is limited to structures in low or moderate seismic zones.

11.3 Areas for Future Investigation

Some areas requiring further investigation are:

- i) Providing steel, in lieu of reinforced concrete, coupling beams appears to be an inexpensive and less labour intensive alternative. The design and construction of a actual structure with steel coupling beams would allow a proper economic assessment.
- ii) The application of steel plates to one side of shear deficient coupling beams offers an efficient retrofit technique compared to other retrofit methods. A proper economic assessment of this new technique is required.
- iii) Alternative methods of retrofitting shear deficient reinforced concrete coupling beams, which address the need to improve confinement and limit longitudinal bar buckling requires investigation. This would permit the retrofit of shear deficient coupling beams in severe seismic regions.

Statement of Originality

Original contributions described in this thesis include:

- i) Four full-scale segments of coupled walls having steel coupling beams with their ends embedded in the reinforced concrete walls were built and tested under reversed cyclic loading. Two of these specimens were reported by the author in his Master's thesis.
- ii) Design and detailing guidelines for the steel coupling beam clear span, the embedded portion of the beam and the reinforced concrete embedment region were proposed.
- iii) Methods of modelling both steel and reinforced concrete coupling beam hysteretic behaviour were developed for use with the non-linear dynamic analysis program DRAIN-2DX.
- iv) Four 18-storey prototype structures, two fully coupled and two partially coupled, were designed with different degrees of coupling and different coupling beam details. A total of sixteen non-linear dynamic analyses were performed on these coupled wall structures. A study of these responses enabled the performance of reinforced concrete and steel coupling beams to be compared for both fully and partially coupled structures.
- v) Four full-scale segments of coupled walls having shear deficient reinforced concrete coupling beams, retrofitted with steel plates, were built and tested under reversed cyclic loading. One specimen, used as a control specimen, was not retrofitted.
- vi) A method was developed for designing and analysing the steel plate retrofit measures presented.
- vii) Four non-linear dynamic analyses were performed on each of an unretrofitted and retrofitted 18-storey prototype structure in order to assess the performance of the proposed retrofit technique.
- viii) Recommendations are made for the design and detailing of steel beams coupling reinforced concrete walls and for the use of steel plates as a retrofit measure for shear deficient reinforced concrete coupling beams.

References

- Al-Sulaimani, G.J., Sharif, A., Basunbul, I.A., Baluch, M.H. and Ghaleb, B.N., 1994, *Shear Repair for Reinforced Concrete by Fibreglass Plate Bonding*, American Concrete Institute Structural Journal, Vol. 91, No. 3, pp 458-464.
- American Institute of Steel Construction (AISC), 1988, Manual of Steel Construction: Load and Resistance Factor Design, First Edition, AISC, Chicago, Ill.
- American Society of Civil Engineers (ASCE) Task Committee on Design Criteria for Composite Structures in Steel and Concrete, 1993, *Guidelines for Design of Joints Between Steel Beams and Reinforced Concrete Columns*, Journal of Structural Engineering, ASCE, to be published.
- Beck, H., 1962, *Contribution to the Analysis of Coupled Shear Walls*, American Concrete Institute Journal, Vol. 59, August 1962, pp 1055-1069.
- Berg, V.B. and Stratta, J.L., 1964, Anchorage and the Alaska Earthquake of March 27, 1964, American Iron and Steel Institute, New York, 63 pp.
- Bhatt, P., 1973, *Effect of Beam-Shear Wall Junction Deformation on the Flexibility of the Connecting Beams*, Building Science, Vol. 8, pp 149-151.
- Bolander, J. and Wight, J.K., 1991, *Finite Element Modelling of Shear Wall Dominant Buildings*, Journal of the Structural Division, ASCE, Vol. 117, No. 6, June 1991, pp 1719-1739.
- Canadian Prestressed Concrete Institute (CPCI), 1987, Metric Design Manual, CPCI, Ottawa, Ont.
- Canadian Standards Association (CSA), 1989, CAN/CSA S16.1-M89, Limit States Design for Steel Structures, CSA, Rexdale, Ont.
- Canadian Standards Association (CSA), 1994, CAN/CSA S16.1-M94, Limit States Design for Steel Buildings, CSA, Rexdale, Ont.
- Canadian Standards Association (CSA), 1984, CSA CAN3 A23.3-M84, Design of Concrete Structures for Buildings, CSA, Rexdale, Ont.
- Canadian Standards Association (CSA), 1994, CSA A23.3-94, Design of Concrete Structures, CSA, Rexdale, Ont.
- Candy, C.F., 1964, *Analysis of Shear Wall Frames by Computer*, Engineering (New Zealand), Vol. 19, No. 9.
- Chitty, L., 1947, *On the Cantilever Composed of a Number of Parallel Beams Interconnected by Cross Bars*, London, Edinburgh and Dublin Philosophical Magazine and Journal of Science, Vol. 38, October 1947, pp 685-699.
- Chitty, L. and Wan, W.J., 1948, *Tall Building Structures under Wind Load*, 7th International Conference for Applied Mechanics, Vol. 1, Paper 22, pp. 254-268.

- Collins, M.P. and Mitchell, D., 1991, Prestressed Concrete Structures, Prentice Hall, 766 pp.
- Coull, A. and Bensmail, L., 1991, Stiffened, Coupled Shear Walls, Journal of the Structural Division, ASCE, Vol. 117, No. 8, August 1991, pp 2205-2223.
- Coull, A. and Stafford-Smith, B., 1967, Analysis of Shear Wall Structures, Symposium on Tall Buildings, Pergamon Press, Oxford, pp 139-155.
- Coull, A. and Wong, Y.C., 1981, Bending Stiffness of Floor Slabs in Cross Wall Structures, Proceedings, ICE, Vol. 71, Part 2, pp. 17-35.
- Cusens, A.R. and Smith, D.W., 1980, A Study of Epoxy Resin Adhesive Joints in Shear, The Structural Engineer, Vol. 58A, No. 1, January 1980. pp 13-18.
- DRAIN-2DX, 1992, Base Program Users Guide and Preliminary Element Users Guide Version 1.03, December 1992, Berkeley.
- Engelhardt, M.D. and Popov, E.P., 1989, Behavior of Long Links in Eccentrically Braced Frames, Earthquake Engineering Research Center, Berkeley, Report No. UCB/EERC-89/01, 406 pp.
- Eriksson, O., 1961, Analysis of Wind Bracing Walls in Multistorey Housing, Inenoren, International Edition, Vol. 5, No. 4, pp. 115-124.
- ETABS, 1992, Three dimensional analysis of building systems computer program, Computers and Structures, Inc. Berkeley.
- Harries, K.A., 1992, Seismic Response of Steel Beams Coupling Concrete Walls, Masters' Thesis, McGill University, May 1992, 95 pp.
- Harries, K.A., Cook, W.D., Redwood, R.G. and Mitchell, D., 1992, Concrete walls coupled by ductile steel link beams, Proceedings of Tenth World Earthquake Engineering Conference, Vol. 6, Madrid, July 1992, pp 3205-3211.
- Harries, K.A., Mitchell, D, Cook, W.D. and Redwood, R.G., 1993, Seismic Response of Steel Beams Coupling Concrete Walls, Journal of the Structural Division, ASCE, Vol. 119, No. 12, pp 3611-3629.
- Harries, K.A., Cook, W.D. and Mitchell, D., 1994, Seismic Retrofit of Reinforced Concrete Coupling Beams Using Steel Plates, submitted to ACI Seismic Rehabilitation Proceedings, ACI Annual Convention, San Francisco, March 1994.
- Hasselmann, T.K. and Wiggins, J.H., 1982, Earthquake Damage to High-Rise Buildings as a Function of Interstory Drift, Proceedings of the Third International Earthquake Microzonation Conference, University of Washington, Seattle, June 1982, 12 p.
- Hilti (Canada) Limited, 1992, Product Catalogue (includes technical data), 72 pp.
- Jones, R., Swamy, R.N. and Ang, T.H., 1982, Under- and Over-reinforced concrete beams with glued steel plates, International Journal of Cement Composites and Lightweight Concrete, Vol. 4, No. 1, pp 19-32.

- Kanno, R., 1993, Strength, Deformation and Seismic Resistance of Joints Between Steel Beams and Reinforced Concrete Columns, Volumes 1 and 2, Doctoral Thesis, Cornell University, New York, 617 pp.
- Kasai, K. and Popov, E.P., 1986, A Study of Seismically Resistant Eccentrically Braced Frames, Earthquake Engineering Research Center, Berkeley, Report No. UCB/EERC-86/01, 215 pp.
- Khan, M.J., 1989, The nonlinear response of reinforced concrete coupling members in earthquake resisting shearwall structures, M.Eng. Thesis, McGill University.
- L'Hermite, R., 1967, *Use of Bonding Techniques for Reinforced Concrete and Masonry Structures*, Materiaux et Constructions (RILEM), Vol. 10, No. 56, pp 85-89.
- Lim, A.K.W., 1989, The nonlinear response of reinforced concrete coupling slabs with drop panels in earthquake resisting shearwall structures, M.Eng. Thesis, McGill University, July 1989, 166 pp.
- MacLeod, I.A., 1967, *Lateral Stiffness of Shear Walls with Openings in Tall Buildings*, Symposium on Tall Buildings, Pergamon Press, Oxford, pp 223-244.
- Maley, R., Acosta, A., Ellis, F., Foote, L., Johnson, D., Porcella, R., Salsman, M. and Switzer, J., 1989. U.S. Geological Survey strong motion records from the Northern California (Loma Prieta) earthquake of October 17, 1989, U.S.G.S. Open-file Report 89-568.
- Malley, J.O. and Popov, E.P., 1983a, Design of Links and Beams to Column Connections for Eccentrically Braced Steel Frames, Earthquake Engineering Research Center, Berkeley, Report No. UCB/EERC-83/03, 62 pp.
- Malley, J.O. and Popov, E.P., 1983b, Design Considerations for Shear Links in Eccentrically Braced Frames, Earthquake Engineering Research Center, Berkeley, Report No. UCB/EERC-83/24, 117 pp.
- Malyszko, T.E., 1986, The nonlinear response of reinforced concrete coupling slabs in earthquake resisting shearwall structures, M.Eng. Thesis, McGill University, August 1986, 130 pp.
- Magnus, D., 1968, Analysis and Design of Pierced Shear-Walls, Concrete Publications Limited, London. 28 pp.
- Marcakis, K. and Mitchell, D., 1980, *Precast concrete connections with embedded steel members*, PCI Journal, Vol. 25, No. 4, July/August 1980, pp 88-116.
- Mattock A.H. and Gaafar, G.H., 1982, *Strength of Embedded Steel Sections as Brackets*, American Concrete Institute Journal, Vol. 79, No. 2, March/April 1982, pp 83-93.
- McKenna, J.K. and Erki, M.A., 1994, *Strengthening of reinforced concrete flexural members using externally applied steel plates and fibre composite sheets - a survey*, Canadian Journal of Civil Engineering, Vol. 21, February 1994, pp 16-24.
- McMaster University Seismological Executive (MUSE) Database System, 1987. database of strong motion records.

- Michael, D., 1967, *The Effect of Local Wall Deformations on the Elastic Interaction of Cross Walls Coupled by Beams*, Symposium on Tall Buildings, Pergamon Press, Oxford, pp 253-270.
- Minami, K., 1984, *Beam to Column Stress Transfer in Composite Structures*, Composite and Mixed Construction, Proceedings of the U.S./Japan Joint Seminar, Seattle, July, 1984. ASCE, New York, pp 215-226.
- Mitchell, D. and Cook, W.D., 1989, Testing of Half-Scale Reinforced Concrete Link Beam - Bell Canada Office Building, 160 Elgin Street, Ottawa, Internal report prepared for Mr. R. Slattery, Houser, Henry, Louden and Syron, Toronto. 19pp.
- Munro, P.S. and Weichert, D., 1989, The Saquenay earthquake of November 25, 1988 - processed strong motion records, Geological Survey of Canada, Open File Report 1996.
- Naeim, F. (editor), 1989, Seismic Design Handbook, Van Nostrand Reinhold, New York, 450 pp.
- National Research Council of Canada, 1990 and 1995, National Building Code of Canada, NRC, Ottawa, Ont.
- New Zealand Standards Association (NZS), 1984, Code of Practice for General Structural Design and Design Loadings for Buildings, NZS 4203:1984
- Newmark, N.M. and Hall, W.J., 1982, *Earthquake Spectra and Design*, Engineering Monographs on Earthquake Criteria, Structural Design and Strong Motion Records, Vol. 3, Earthquake Engineering Research Institute, Berkeley, 140 pp.
- Paparoni, M., 1972, *Model Studies of Coupling Beams*, Proceedings of the International Conference on Tall Concrete and Masonry Buildings, August, 1972, Vol. 3, pp 671-681.
- Park, R. and Paulay, T., 1975, Reinforced Concrete Structures, John Wiley and Sons, New York. (particularly: Chapter 12 - Shear Walls of Multistory Buildings.)
- Paulay, T., 1969, The Coupling of shear walls, Volumes 1 and 2, Doctoral thesis, University of Canterbury, New Zealand. 432 pp.
- Paulay, T., 1970, *An Elasto-Plastic Analysis of Coupled Shear Walls*, American Concrete Institute Journal, Vol. 67, No. 11, November 1970, pp 915-922.
- Paulay, T., 1971a, *Coupling Beams of Reinforced Concrete Shear Walls*, Journal of Structural Division, ASCE, Vol. 97, ST3, March 1971, pp 843-862.
- Paulay, T., 1971b, *Simulated Seismic Loading of Spandrel Beams*, Journal of Structural Division, ASCE, Vol. 97, ST9, September 1971, pp 2407-2419.
- Paulay, T. and Binney, J.R., 1974, *Diagonally reinforced coupling beams of shear walls*, Shear in Reinforced Concrete, Publication No. SP-42, American Concrete Institute, Detroit. pp 579-598.
- Paulay, T. and Taylor, R.G., 1981, *Slab Coupling of Earthquake Resisting Shearwalls*, American Concrete Institute Journal, Vol. 78, No. 2, March/April 1971, pp 130-140.

- Paulay, T., 1986, *The design of ductile reinforced concrete structural walls for earthquake resistance*, Earthquake Spectra, Vol. 2, No. 4, 1986, pp 783-823.
- Paulay, T. and Priestley, 1992, Seismic Design of Reinforced Concrete and Masonry Buildings, John Wiley and Sons, New York. 744 pp.
- Paultre, P., 1987, Evaluation of Seismic Performance of Concrete Frame Structures in Canada, Ph.D. thesis, McGill University, July 1987, 213 pp.
- Prestressed Concrete Institute (PCI), 1985, PCI Design Handbook, PCI, Chicago, Ill.
- Priestly, N.M.J. and Seible, F., 1991, Seismic Assessment and Retrofit of Bridges, University of California at San Diego Structural System Research Project No. SSRP-91/03, 426 pp.
- Raths, C.H., 1974, *Embedded Structural Steel Connections*, PCI Journal, Vol. 19, No. 3, May/June 1974, pp 104-112.
- Remmetter, M., Qin, F. and Shahrooz, B., 1992, Seismic Resistance of Composite Coupled Structural Walls, Report UC-CII-92/01, Cincinnati Infrastructure Institute, University of Cincinnati, 174 pp.
- Ricles, J.M. and Popov, E.P., 1994, *Seismic Analysis*, Journal of Structural Engineering, ASCE, Vol. 120, No. 2, February 1994, pp 441-463.
- Roeder, C.W. and Popov, E.P., 1978, *Eccentrically Braced Steel Frames for Earthquakes*, Journal of the Structural Division, ASCE, Vol. 104, No. ST3, March 1978, pp 391-411.
- Roeder, C.W. and Hawkins, N.M., 1981, *Connections Between Steel Frames and Concrete Walls*, Engineering Journal, AISC, Vol. 18, No. 1, pp 22-29.
- Rosman, R., 1964, *Approximate Analysis of Shear Walls Subject to Lateral Loads*, American Concrete Institute Journal, Vol. 61, No. 6, June 1964, pp 717-732.
- Saatcioglu, M., Derecho, A.T. and Corely, W.G., 1980, Coupled Walls in Earthquake Resistant Buildings - Modelling Techniques and Dynamic Analysis, Report to the National Science Foundation, Construction Technology Laboratories, Portland Cement Association, Skokie, Ill. 117 pp.
- Saatcioglu, M., Derecho, A.T. and Corely, W.G., 1981, Coupled Walls in Earthquake Resistant Buildings - Parametric Investigation and Design Procedure, Report to the National Science Foundation, Construction Technology Laboratories, Portland Cement Association, Skokie, Ill. 117 pp.
- Saatcioglu, M., Derecho, A.T. and Corley, W.G., 1983, *Modelling Hysteretic Behaviour of Coupled Walls for Dynamic Analysis*, Earthquake Engineering and Structural Dynamics, Vol. 11, pp 711-726.
- Santhakumar, A.R., 1974, Ductility of coupled shear walls, Doctoral thesis, University of Canterbury, New Zealand. 385 pp.
- Schultz, M., 1961, *Analysis of Reinforced Concrete Walls with Openings*, Indian Concrete Journal, Vol. 35, pp 432-433.

- Schwaighofer, J., 1969, Analysis of Shear Wall Structures using Standard Computer Programs, ACI Proceedings, Vol. 66, No. 12, December, 1969
- SEAOC, 1988, Recommended Lateral Force Requirements, Seismology Committee, Structural Engineers Association of California (SEAOC), Seismology Committee.
- Sheikh, T.M., Deierlein, G.G., Yura, J.A. and Jirsa, J.O., 1989, Beam-Column Moment Connections for Composite Frames: Parts 1 and 2, Journal of the Structural Division, ASCE, Vol. 115, No. 11, November 1989, pp 2858-2896.
- Shiu, K.N., Barney, G.B., Fiorato, A.E. and Corley, W.G., 1978, Reversed load tests of reinforced concrete coupling beams, Central American Conference on Earthquake Engineering, El Salvador, January 1978, pp 239-249.
- Shiu, K.N., Takayangi, T. and Corley, W.G., 1984, Seismic Behavior of Coupled Wall Systems, Journal of the Structural Division, ASCE, Vol. 110, No. 5, May 1984, pp 1051-1066.
- Sika Canada Inc., 1992, Sikadur 31 Hi-Mod Gel Technical Data Sheet, 4 pp.
- Stafford-Smith, B. and Coull, A., 1991, Tall Building Structures, John Wiley and Sons, 537 pp.
- Subedi, N.K., 1989, Reinforced concrete beams with plate reinforcement for shear, Proceedings of the Institution of Civil Engineers (Great Britain), part 2, Vol. 87, September 1989, pp 377-399.
- Subedi, N.K., 1991a, RC-Coupled Shear Wall Structures. I: Analysis of Coupling Beams, Journal of the Structural Division, ASCE, Vol. 117, No. 3, March 1991, pp 667-680.
- Subedi, N.K., 1991b, RC-Coupled Shear Wall Structures. II: Ultimate Strength Calculations, Journal of the Structural Division, ASCE, Vol. 117, No. 3, March 1991, pp 681-698.
- Swamy, R.M., Jones R. and Bloxham, J.W., 1987, Structural Behaviour of Reinforced Concrete Beams Strengthened with Epoxy-Bonded Steel Plates, Structural Engineer, Vol. 65, No. 2, pp 59-68.
- Swamy, R.M., Jones R. and Sharif, A., 1989, Effect of External Reinforcement on the Strengthening of Structurally Damaged RC Beam, Structural Engineer, Vol. 67, No. 3.
- Taranath, B.S., 1982, Composite design of First City Tower, Houston, Texas, The Structural Engineer, Vol. 60A, No. 9, September 1982. pp 271-281.
- Taranath, B.S., 1988, Structural Analysis and Design of Tall Buildings, McGraw Hill, 739 pp.
- Trieu, B., 1986, Strengthening Concrete Slabs and Beams Using Epoxy Bonded Steel Sheets, Masters' Thesis, McGill University, August 1986, 95 pp.
- Wakabayashi, M., 1985, Recent Developments for composite buildings in Japan, Composite and Mixed Construction, C. Roeder, editor, ASCE, New York, pp 241-253.
- Wakabayashi, M., 1986, Design of Earthquake Resistant Buildings, McGraw Hill, 309 pp.

Winokur, A and Gluck, J, 1968a, *Lateral Loads in Asymmetric Multistorey Structures*, Journal of Structural Division, ASCE, Vol. 94, ST3, March 1968, pp 645-656.

Winokur, A and Gluck, J, 1968b, *Ultimate Strength Analysis of Coupled Shear Walls*, American Concrete Institute Journal, Vol. 65, No. 12, December 1968, pp 1029-1036.

APPENDIX A

Design of Steel Coupling Beam Specimens (Specimens S1 - S4)

A.1 Design of Steel Coupling Beams S1

Trial Section

Shear Critical Section:

clear span, $\ell = 1200$ mm
concrete cover, $c = 40$ mm

Design Criteria:

$$V_f = 260 \text{ kN}$$

$$M_r > 1.27V_r \ell_{\text{eff}}/2$$

Trial Section:

Flange: $b = 134$ mm; $t = 18$ mm
web: $w = 5$ mm
overall depth, $d = 350$ mm
 $F_y = 300$ MPa

Verification of Section: Capacities

$$V_r = 0.55A_w F_y$$

$$V_r = 0.55 \times 350 \times 5 \times 0.3$$

$$V_r = 289 \text{ kN} \dots\dots\dots \text{OK}$$

$$M_r > 1.27 \times 289 \times 1200/2 = 221 \text{ kNm}$$

$$M_r = ZF_y \text{ (neglect contribution of web)}$$

$$M_r = 760 \ 345 \times 0.3$$

$$M_r = 228 \text{ kNm} \dots\dots\dots \text{OK}$$

Verification of Section: Stability

Class of Flange: $\dots\dots\dots$ Class 1

$$\frac{b}{2t} = \frac{134}{36} = 3.72 < \frac{145}{\sqrt{F_y}} = 8.37$$

Class of Web: $\dots\dots\dots$ Class 1

$$\frac{h}{w} = \frac{350 - 36}{5} = 62.8 < \frac{1100}{\sqrt{F_y}} = 63.5$$

Maximum unsupported length, ℓ_{cr} . OK

$$\ell_{\text{cr}} = \frac{200b}{\sqrt{F_y}} = \frac{200 \times 134}{\sqrt{300}} = 1547 \text{ mm}$$

Actual Section

Shear Critical Section:

effective clear span, $\ell_{\text{eff}} = 1280$ mm
concrete cover, $c = 40$ mm

Design Criteria:

$$V_f = 260 \text{ kN}$$

$$M_r > 1.27V_r \ell_{\text{eff}}/2$$

Actual Section: as built

Flange: $b = 135$ mm; $t = 19$ mm
web: $w = 5$ mm
overall depth, $d = 347$ mm
 $F_{y, \text{web}} = 320$ MPa
 $F_{y, \text{flange}} = 372$ MPa

Verification of Section: Capacities

$$V_r = 0.55 \times 347 \times 5 \times 0.32$$

$$V_r = 305 \text{ kN} \dots\dots\dots \text{OK}$$

$$M_r > 1.27 \times 305 \times 1280/2 = 248 \text{ kNm}$$

$$M_r = 796 \ 143 \times 0.372$$

$$M_r = 296 \text{ kNm} \dots\dots\dots \text{OK}$$

Verification of Section: Stability

Class of Flange: $\dots\dots\dots$ Class 1

$$\frac{b}{2t} = \frac{135}{38} = 3.55 < \frac{145}{\sqrt{F_y}} = 7.52$$

Class of Web: $\dots\dots\dots$ Class 1

$$\frac{h}{w} = \frac{347 - 38}{5} = 61.8 \approx \frac{1100}{\sqrt{F_y}} = 61.5$$

Maximum unsupported length, ℓ_{cr} . OK

$$\ell_{\text{cr}} = \frac{200b}{\sqrt{F_y}} = \frac{200 \times 135}{\sqrt{372}} = 1400 \text{ mm}$$

Web to flange welds: built-up section

must develop yield stress of web: $\omega 0.67F_y = \text{say } 1 \text{ kN/mm}$

capacity of 2 - 5 mm welds: $2 \times 5 \sin(45^\circ) \times 0.67 \times 0.67 \times 0.48 = 1.53 \text{ kN/mm} \dots \text{OK}$

Web Stiffeners:

Provide full depth, 65 x 10 mm stiffeners on both sides of web at end of clear span.

Provide full depth, 65 x 10 mm stiffeners on one side of the web over clear span

Intermediate stiffener spacing: $s \leq 38w - 0.2d = 38(5) - 0.2(350) = 120 \text{ mm}$

Stiffener weld to web must transfer: $A_s F_y = 65 \times 10 \times 0.3 = 195 \text{ kN}$

capacity of 5 mm weld on one side: $0.762 \times 314 = 239 \text{ kN} \dots \dots \dots \text{OK}$

Stiffener weld to flange must transfer: $0.25A_s F_y = 0.25 \times 195 = 49 \text{ kN}$

capacity of 5 mm on one side, top and bottom: $0.762 \times 130 = 99 \text{ kN} \dots \dots \dots \text{OK}$

A.2 Design of Steel Coupling Beams S2

Trial Section

Shear Critical Section:

clear span, $l = 1200$ mm
concrete cover, $c = 40$ mm

Design Criteria:

$$V_f = 260 \text{ kN}$$

$$M_r > 1.27V_r l_{\text{eff}}/2$$

Trial Section:

Flange: $b = 134$ mm; $t = 18$ mm
web: $w = 5$ mm
overall depth, $d = 350$ mm
 $F_y = 300$ MPa

Verification of Section: Capacities

$$V_r = 0.55A_w F_y$$

$$V_r = 0.55 \times 350 \times 5 \times 0.3$$

$$V_r = 289 \text{ kN} \dots\dots\dots \text{OK}$$

$$M_r > 1.27 \times 289 \times 1200/2 = 221 \text{ kNm}$$

$$M_r = ZF_y \text{ (neglect contribution of web)}$$

$$M_r = 760 \ 345 \times 0.3$$

$$M_r = 228 \text{ kNm} \dots\dots\dots \text{OK}$$

Verification of Section: Stability

Class of Flange: $\dots\dots\dots$ Class 1

$$\frac{b}{2t} = \frac{134}{36} = 3.72 < \frac{145}{\sqrt{F_y}} = 8.37$$

Class of Web: $\dots\dots\dots$ Class 1

$$\frac{h}{w} = \frac{350 - 36}{5} = 62.8 < \frac{1100}{\sqrt{F_y}} = 63.5$$

Maximum unsupported length, l_{cr} . OK

$$l_{\text{cr}} = \frac{200b}{\sqrt{F_y}} = \frac{200 \times 134}{\sqrt{300}} = 1547 \text{ mm}$$

Actual Section

Shear Critical Section:

effective clear span, $l_{\text{eff}} = 1280$ mm
concrete cover, $c = 40$ mm

Design Criteria:

$$V_f = 260 \text{ kN}$$

$$M_r > 1.27V_r l_{\text{eff}}/2$$

Actual Section: as built

Flange: $b = 135$ mm; $t = 19$ mm
web: $w = 5$ mm
overall depth, $d = 347$ mm
 $F_{y, \text{ web}} = 309$ MPa
 $F_{y, \text{ flange}} = 295$ MPa

Verification of Section: Capacities

$$V_r = 0.55 \times 347 \times 5 \times 0.309$$

$$V_r = 295 \text{ kN} \dots\dots\dots \text{OK}$$

$$M_r > 1.27 \times 295 \times 1280/2 = 240 \text{ kNm}$$

$$M_r = 796 \ 143 \times 0.295$$

$$M_r = 235 \text{ kNm} \dots\dots\dots \text{accepted}$$

Verification of Section: Stability

Class of Flange: $\dots\dots\dots$ Class 1

$$\frac{b}{2t} = \frac{135}{38} = 3.55 < \frac{145}{\sqrt{F_y}} = 8.44$$

Class of Web: $\dots\dots\dots$ Class 1

$$\frac{h}{w} = \frac{347 - 38}{5} = 61.8 < \frac{1100}{\sqrt{F_y}} = 62.6$$

Maximum unsupported length, l_{cr} . OK

$$l_{\text{cr}} = \frac{200b}{\sqrt{F_y}} = \frac{200 \times 135}{\sqrt{295}} = 1572 \text{ mm}$$

Embedded region of web:

$$V_f = 2M_r/l'$$

$$V_f = 2 \times 228/1200 = 380 \text{ kN}$$

Trial Section:

$$\text{web} = 8 \text{ mm thick}$$

$$F_y = 300 \text{ MPa}$$

Verification of Section: Capacity

$$V_r = 0.55A_w F_y$$

$$V_r = 0.55 \times 350 \times 8 \times 0.3$$

$$V_r = 462 \text{ kN} \dots\dots\dots \text{OK}$$

Embedded region of web:

$$V_f = 2M_r/l'$$

$$V_f = 2 \times 235/1200 = 392 \text{ kN}$$

Actual Section:

$$\text{web} = 8 \text{ mm thick}$$

$$F_y = 276 \text{ MPa}$$

Verification of Section: Capacity

$$V_r = 0.55A_w F_y$$

$$V_r = 0.55 \times 347 \times 8 \times 0.276$$

$$V_r = 421 \text{ kN} \dots\dots\dots \text{OK}$$

Web to flange welds: built-up section

must develop yield stress of web: $\omega 0.67F_y = \text{say } 1 \text{ kN/mm}$

capacity of 2 - 5 mm welds: $2 \times 5 \sin(45^\circ) \times 0.67 \times 0.67 \times 0.48 = 1.53 \text{ kN/mm} \dots \text{OK}$

Clear span web to embedded web butt weld:

required joint resistance is smaller of:

$$V_r = 0.67\phi F_y A_m = 0.67 \times 0.9 \times 0.3 \times 350 \times 5 = 317 \text{ kN}$$

$$V_r = 0.67\phi_w X_u A_w = 0.67 \times 0.67 \times 0.48 \times 314 \times 5 = 338 \text{ kN}$$

therefore, a full depth, double bevel groove weld, butt welding the 5 mm and 8 mm web plates will be sufficient to carry the applied shear, V_r .

Web Stiffeners:

Provide full depth, 65 x 10 mm stiffeners on both sides of web at end of clear span.

Provide full depth, 65 x 10 mm stiffeners on one side of the web over clear span

Intermediate stiffener spacing: $s \leq 38w - 0.2d = 38(5) - 0.2(350) = 120 \text{ mm}$

Stiffener weld to web must transfer: $A_s F_y = 65 \times 10 \times 0.3 = 195 \text{ kN}$

capacity of 5 mm weld on one side: $0.762 \times 314 = 239 \text{ kN} \dots\dots\dots \text{OK}$

Stiffener weld to flange must transfer: $0.25A_s F_y = 0.25 \times 195 = 49 \text{ kN}$

capacity of 5 mm on one side, top and bottom: $0.762 \times 130 = 99 \text{ kN} \dots\dots\dots \text{OK}$

A.3 Design of Steel Coupling Beams S3

Trial Section	Actual Section
Shear Critical Section:	Shear Critical Section:
clear span, $\ell = 500$ mm concrete cover, $c = 40$ mm	effective clear span, $\ell_{\text{eff}} = 530$ mm concrete cover, $c = 40$ mm
Design Criteria:	Design Criteria:
$V_f = 360$ kN $M_r > 1.27V_f \ell_{\text{eff}}/2$	$V_f = 360$ kN $M_r > 1.27V_f \ell_{\text{eff}}/2$
Trial Section: W360 x 33	Actual Section: W360 x 33
Class 1 rolled section	$F_{y, \text{web}} = 403$ MPa $F_{y, \text{flange}} = 378$ MPa
$V_r = 361$ kN OK	$V_r = 485$ kN OK
$M_r > 1.27 \times 361 \times 500/2 = 115$ kNm	$M_r > 1.27 \times 485 \times 530/2 = 163$ kNm
$M_r = 146$ kNm OK	$M_r = 184$ kNm OK
$\ell_{\text{cr}} = 1466$ mm OK	
determined from CISC, 1985	
in order to reduce ℓ/d , clear span was reduced to 450 mm:	
Web Stiffeners:	
Provide full depth, 60 x 10 mm stiffeners on both sides of web at end of clear span.	
Provide full depth, 60 x 10 mm stiffeners on one side of the web over clear span and embedments.	
Intermediate stiffener spacing: $s \leq 38w - 0.2d = 38(6) - 0.2(349) = 158.2$ mm	
Stiffener weld to web must transfer: $A_s F_y = 60 \times 10 \times 0.3 = 180$ kN	
capacity of 5 mm weld on one side: $0.762 \times 333 = 254$ kN OK	
Stiffener weld to flange must transfer: $0.25A_s F_y = 0.25 \times 180 = 45$ kN	
capacity of 5 mm on one side, top and bottom: $0.762 \times 120 = 91$ kN OK	

A.4 Design of Steel Coupling Beams S4

Trial Section	Actual Section
Shear Critical Section:	Shear Critical Section:
clear span, $\ell = 1200$ mm concrete cover, $c = 40$ mm	effective clear span, $\ell_{\text{eff}} = 1280$ mm concrete cover, $c = 40$ mm
Design Criteria:	Design Criteria:
$M_f = 156$ kNm ($V_f = 260$ kN) $V_r > 1.27 \times 2M_r/\ell_{\text{eff}}$	$M_f = 156$ kNm $V_r > 1.27 \times 2M_r/\ell_{\text{eff}}$
Trial Section: W360 x 33	Actual Section: W360 x 33
Class 1 rolled section	$F_{y, \text{web}} = 403$ MPa $F_{y, \text{flange}} = 378$ MPa
$M_r = 162$ kNm OK	$M_r = 204$ kNm OK
$V_r > 1.27 \times 2 \times 162 / 1200 = 343$ kN	$V_r > 1.27 \times 2 \times 204 / 1200 = 432$ kNm
$V_r = 361$ kN OK	$V_r = 485$ kN OK
$\ell_{\text{cr}} = 1466$ mm OK	
determined from CISC, 1985	
Web stiffeners:	
Provide full depth, 60 x 10 mm stiffeners on both sides of web at end of clear span.	
Stiffener weld to web must transfer: $A_s F_y = 60 \times 10 \times 0.3 = 180$ kN	
capacity of 5 mm weld on one side: $0.762 \times 333 = 254$ kN OK	
Stiffener weld to flange must transfer: $0.25 A_s F_y = 0.25 \times 180 = 45$ kN	
capacity of 5 mm on one side, top and bottom: $0.762 \times 120 = 91$ kN OK	
no further stiffeners provided.	
Embedded Flange Cover Plates:	
flexural capacity of embedment must exceed: $V_r \ell_{\text{eff}}/2 = 361 \times 1200 / 2 = 217$ kNm	
capacity of section with 5 mm cover plate on each flange: 229 kNm OK	

Lateral Instability due to Flexural Hinges

determine critical buckling length of hinge:

$$\alpha l = 1.42b \left(\frac{t}{w} \right) \left(\frac{A_w}{A_f} \right)^{0.25} = 1.42 \times 127 \left(\frac{8}{6} \right) \left(\frac{1926}{1080} \right)^{0.25} = 278 \text{ mm}$$

length of hinge corresponding to development of shear capacity of beam: 152 mm . . . OK

allowable beam rotation:

$$\frac{lV_r}{M_r} = \frac{1200 \times 361}{162000} = 2.67 > 2.6 \therefore \theta_{\text{allowable}} = 0.030 \text{ rad}$$

hinge rotation corresponding to $\alpha l = 152$ mm:

$$\theta_H = \frac{2\epsilon_y (s - 1)}{d} \alpha l = \frac{2 \times 0.002 (11.25 - 1)}{349} 152 = 0.018 \text{ rad} \quad \dots \text{OK}$$

A.5 Design of Reinforced Concrete Embedment Regions

Capacity of Embedment:

$$V_c = \frac{0.85\phi_c f'_c b' (\ell_e - c)}{1 + \frac{3.6e}{(\ell_e - c)}} \geq 1.27V_r$$

	Specimen S1 (as designed)	Specimen S1 (following revised design criteria)	Specimen S2	Specimen S3	Specimen S4
$1.27V_r$	367 kN	367 kN	367 kN	459 kN	459 kN
f'_c	25.9 MPa	25.9 MPa	43.1 MPa	32.9 MPa	35.0 MPa
b'	200 mm	200 mm	200 mm	200 mm	200 mm
ℓ_e	600 mm	600 mm	600 mm	500 mm	600 mm
c	not considered	40 mm	40 mm	40 mm	40 mm
e	900 mm	920 mm	920 mm	495 mm	920 mm
V_c	413 kN	357 kN	593 kN	528 kN	482 kN
$V_c > 1.27V_r$	OK	not OK, hence design revisions	OK	OK	OK

Vertical Reinforcement Across Flange-Concrete Interface:

$$A_{sc} \geq \frac{1.27V_r}{f_y}$$

six No. 25 reinforcing bars were provided in each specimen:

$$V_r = \frac{A_{sc} f_y}{1.27} = \frac{3000 \times 0.4}{1.27} = 945 \text{ kN}$$

the capacity provided clearly exceeds the demand.

concentrated vertical reinforcement is located over the entire embedment region with at least two thirds of the steel in the front half of the embedment. In this case, the four bars nearest the front of the embedment are adequate to carry the applied shear.

APPENDIX B

Design of Retrofitted Reinforced Concrete Coupling Beam Specimens (Specimens R0 - R3)

B.1 Design of Reinforced Concrete Coupling Beams R0 - R3

$l = 1500$ mm; overall depth = 500 mm; $b = 300$ mm; $f'_c = 35$ MPa
 assume one layer of No. 25 longitudinal bars and No. 10 closed ties and 40 mm cover
 therefore, $d = 500 - 40 - 10 - 12.5 = 437$ mm
 $V_f = 260$ kN; $M_r > 260 \times 1500/2 = 195$ kNm

Design of Longitudinal Steel:

in order that beam may be designed with longitudinal reinforcement:

$$\frac{V_f}{db} < 0.1 \frac{l}{d} \sqrt{f'_c}$$

$$\frac{260000}{437 \times 300} < 0.1 \frac{1500}{437} \sqrt{35}$$

$$1.98 < 2.03$$

select 3 No. 25 bars, top and bottom, resulting in a flexural capacity of:

$$M_r = 0.85 A_s f_y \left[d - \frac{A_s f_y}{2 \times 0.85 \beta f'_c b} \right] = 0.85 \times 1500 \times 400 \left[437 - \frac{1500 \times 400}{2 \times 0.85 \times 0.81 \times 35 \times 300} \right] = 202 \text{ kNm}$$

from RESPONSE, considering measured properties the flexural capacity is 263 kNm

Transverse Reinforcement Requirements:

in order that the beam be deficient in shear, only 7 No. 10 closed hoops, spaced at 225 mm are provided over the clear span.

for comparison, assuming No. 10 hoops are used, the following spacing requirements would apply to the coupling beams (CAN/CSA A23.3 - M84):

- Clause 21.3.3.3 (a) $d/4 = 437/4 = 109$ mm controls
 (b) $8d_{lb} = 8 \times 25 = 200$ mm
 (c) $24d_{sb} = 24 \times 10 = 240$ mm
 (d) 300 mm

Clause 11.3 (with $V_c = 0$)

$$s = \frac{d A_v f_y}{V_f} = \frac{437 \times 200 \times 400}{260000} = 134 \text{ mm}$$

Clause 11.4 (with $\theta = 30^\circ$)

$$s = \frac{d_v A_v f_y}{V_f \tan \theta} = \frac{0.9 \times 437 \times 200 \times 400}{260000 \times \tan 30^\circ} = 210 \text{ mm}$$

B.2 Design of Retrofit Plates

Selection of Plate Thickness

required to select from available plate material (ie: 1/8" or larger at 1/16" increments)

consider Grade 300 ($F_y = 300$ MPa), 450 mm deep plate:

determine $A_{v,required}$, assuming spacing of 225 mm, to resist $V_f = 2M_r/\ell = 350$ kN:

$$A_{v,required} = \frac{sV_f}{\frac{d_v}{\tan\theta} f_y} = \frac{225 \times 350000}{\frac{394}{\tan 32^\circ} 400} = 313 \text{ mm}^2$$

the plate thickness is determined from:

$$A_{v,required} - A_v = A_{v,eq} = A_p \frac{s}{s_b} \frac{h_b F_y}{d_v f_y} = 313 - 200 = 8t_p \frac{225}{260} \frac{300}{393} \frac{300}{400}$$

solving: $t_p = 5.34$ mm

a 3/16" thick (4.76 mm) plate was selected after material properties of available plate stock were considered ($f_{y,stirrups} = 447$ MPa):

	1/8" plate	3/16" plate	1/4" plate
t_p	3.18 mm	4.76 mm	6.35 mm
F_y	308 MPa	353 MPa	472 MPa
A_v (including plate)	237 mm ²	295 mm ²	425 mm ²